UNIVERSITAT POLITÈCNICA DE VALÈNCIA

Doctoral Thesis

EFFECTS OF EGR TRANSIENT OPERATION ON EMISSIONS AND PERFORMANCE OF AUTOMOTIVE ENGINES DURING RDE CYCLES

PRESENTED BY:

Mr. Chaitanya Yashvant Patil

SUPERVISED BY:

Dr. José Galindo Lucas

June 2020

Departamento de Máquinas y Motores Térmicos

UNIVERSITAT POLITÈCNICA DE VALÈNCIA

Departamento de Máquinas y Motores Térmicos

DOCTORAL THESIS:

"Effects of EGR transient operation on emissions and performance of automotive engines during RDE cycles"

Presented by: D. Chaitanya Yashvant Patil
Supervised by: Dr. D. José Galindo Lucas

Valencia, June 2020

Doctoral Thesis

"Effects of EGR transient operation on emissions and performance of automotive engines during RDE cycles"

Presented by: D. Chaitanya Yashvant Patil
Supervised by: Dr. D. José Galindo Lucas

THESIS EXAMINERS

Dr. D. Octavio Armas Vergel
Dr. D. David Chalet
Dr. D. Pascal Higelin

DEFENSE COMMITTEE

Chairman: Dr. D. Vicente Remigio Bermúdez Tamarit
Secretary: Dr. D. Francisco Vera García
Member: Dr. D. David Chalet

Valencia, June 2020

Abstract

The emission regulations are getting more stringent. New methods of homologation are being considered other than standard cycles considering the real driving behavior on road. EGR is one of the proven and well tested strategies in steady state which can be used on those dynamic real driving conditions.

This dissertation focuses on implementation of different EGR systems during dynamic operations of turbocharged diesel engine. Firstly, a driving cycle analysis is carried out to identify the specific and frequent transient operations on dynamic cycles like WLTC and RDE. The results showed frequency of harsh load transients is higher than speed transients. Number of Tip-Out operations outnumber Tip-Ins with higher density in 1250-2000 RPM range. These harsh transients are repeated separately on the dynamic test bench equipped with high frequency gas analyzers to track the instantaneous CO_2 and NO_x concentration. A parametric study is carried out with EGR valve actuation during various type of transients, quantifying the transportation delays, NO_x concentration and particulate matter. The LPEGR is found to be more effective at the full load as well as during transient operations compared to HPEGR. The best suited LPEGR valve control is proposed, which can be helpful for transient calibration of a turbocharged diesel engine. The trade-off between the performance and emission during EGR transients is also pointed out. The implementation of EGR all over the engine map minimizes the unexpected NO_x peaks during transients. Specifically, LPEGR strategies manages to reduce around 20-60% of NO_x in first few seconds with less than 5% of penalty in performance.

Additionally, 1D model simulation results of load transient operations are presented in the document. Moreover, the EGR split optimization on various steady points is carried out by simulations through the trade-off of performance and emissions. An algorithm to search the optimum split is proposed further reducing around 80% of the calculation time consumed by DOE or genetic algorithm method. Finally, a simple 3D quasi steady NO_x model is created to predict the transient emissions in real driving conditions. EGR rate, as 3^{rd} input in model shows significant improvement in prediction of transient NO_x over the 2D model.

Keywords: Transient EGR; Hybrid/dual EGR; RDE; WLTC; NO_x; Soot

Resumen

Hoy en día, las regulaciones sobre emisiones de los automóviles se están haciendo más estrictas. Además de los ciclos de homologación estándar, actualmente se están empezando a considerar nuevos métodos de homologación que tienen en cuenta las condiciones reales que se dan en la carretera. Los sistemas de Recirculación de Gases de Escape (*EGR*) son estrategias que han demostrado ser efectivas durante estacionarios y que también pueden ser usadas en ese tipo de ciclos dinámicos que corresponden a condiciones reales de conducción.

Esta tesis se centra en la implementación de diferentes sistemas *EGR* para su uso en condiciones dinámicas en motores diésel turbosobrealimentados. En primer lugar, se lleva a cabo un análisis del ciclo de conducción para identificar las operaciones específicas de tipo transitorio más frecuentes en los ciclos dinámicos como *WLTC* y *RDE*. Los resultados muestran que la frecuencia en la que se producen fuertes transitorios en carga es mayor que en la que se producen transitorios de velocidad. Entre ellos, el número de operaciones de tipo *Tip-out* es superior a las de tipo *Tip-Ins*, especialmente en el rango de 1250-2000 rpm. Estos fuertes transitorios se repiten en el banco de ensayos de motor equipado con analizadores de gas de alta frecuencia, de forma que se registran la concentración instantánea de CO_2 y NO_x. También se ha realizado un estudio paramétrico de la actuación de la válvula de *EGR* durante la operación de varios transitorios fuertes, cuantificando el retraso en el transporte, la concentración de NO_x y las partículas. El lazo de *EGR* de baja presión, *LPEGR*, ha resultado ser más efectivo cuando se operaba a plena carga, así como durante los transitorios, comparado con el lazo de *EGR* de alta presión, *HPEGR*. De esta forma, se propone la válvula de control más adecuada para *LPEGR*, lo que puede ser útil para la calibración de los transitorios de los motores diésel turbosobrealimentados. Además de ello, se señala el compromiso entre rendimiento y emisiones durante los transitorios de *EGR*. Al implementar la recirculación de los gases de escape a lo largo de todo el mapa del motor se minimiza la aparición de picos inesperados de emisión de NO_x. Concretamente, las estrategias *LPEGR* consiguen reducir alrededor de un 20-60 % los NO_x emitidos durante los primeros pocos segundos con menos de un 5 % de penalización en el rendimiento.

Adicionalmente, en el documento también se presentan las simulaciones que se han realizado de los modelos unidimensionales de los transitorios. El

control de la turbina de geometría variable juega un papel importante a la hora de calibrar el modelo para transitorios de *EGR*. Además de ello, se lleva a cabo una optimización de la separación de *EGR* para varios puntos estacionarios por medio de simulaciones que están basadas en el compromiso entre rendimiento y emisiones. Además, se propone un algoritmo para optimizar la separación de *EGR*, reduciendo en alrededor de un 80 % el tiempo de cálculo de un *DOE* o un método de algoritmo genético. Finalmente, se crea un modelo simple de NO_x 3D cuasi-estacionario para predecir las emisiones durante el transitorio en condiciones de conducción reales. La tasa de *EGR*, como tercera entrada del modelo, muestra una mejora significativa a la hora de predecir el transitorio de NO_x con respecto al modelo 2D.

Resum

En els darrers temps, les regulacions sobre emissions contaminants dels vehicles s'han fet més estrictes. A més dels cicles d'homologació estàndards, actualment s'estan començant a considerar nous mètodes d'homologació que tinguen en compte les condicions reals que es donen en la carretera. Els sistemes de Recirculació de Gasos d'Escapament (*EGR*) són estratègies que s'han demostrat com a efectives durant condicions estacionàries i que també poden ser emprades en aquest tipus de cicles dinàmics, que corresponen a condicions reals de conducció.

Aquesta tesi està centrada en la implementació de diferents sistemes *EGR* per al seu ús en condicions dinàmiques en motors dièsel turbosobrealimentats. En primer lloc, es du a terme un anàlisi del cicle de conducció per a identificar les operacions específiques de tipus transitori més freqüents en els cicles dinàmics *WLTC* i *RDE*. Els resultats mostren que la freqüència a la que s'obtenen forts transitoris de càrrega és major que en aquella en la que es produeixen transitoris de velocitat. Entre aquestos, el nombre d'operacions de tipus *Tip-out* és superior a les del tipus *Tip-ins*, especialment en l'interval de 1250-2000 rpm. Aquestos forts transitoris es repeteixen en el banc d'assajos de motor equipat amb analitzadors de gasos d'alta freqüència, de manera que es registren les concentracions de CO_2 i NO_x. També s'ha realitzat un estudi paramètric de l'actuació de la vàlvula d'*EGR* durant l'operació de diversos transitoris forts, quantificant el retard en el transport, la concentració de NO_x i les partícules. El llaç d'*EGR* de baixa pressió, *LPEGR*, ha resultat ser més efectiu quan s'operava a plena càrrega, així com durant els transitoris, comparat amb el llaç d'*EGR* d'alta pressió, *HPEGR*. D'aquesta forma, es proposa la vàlvula de control més adequada per a *LPEGR*, el que pot resultar útil per a la calibratge dels transitoris dels motors dièsel turbosobrealimentats. A banda d'això, s'ha assenyalat el compromís entre rendiment i emissions durant els transitoris d'*EGR*. Al implementar la recirculació dels gasos d'escapament a tot arreu del mapa del motor es minimitza l'aparició de pics inesperats d'emissió de NO_x. Més concretament, les estratègies *LPEGR* aconsegueixen reduir al voltant d'un 20-60% els NO_x emesos durant els primers pocs segons amb menys d'un 5% de penalització en el rendiment.

Addicionalment, en el document també es presenten les simulacions que s'han realitzat dels models unidimensionals dels transitoris. El control de la turbina de geometria variable juga un paper important a l'hora de calibrar

el model per a transitoris d'*EGR*. A més d'això, s'ha dut a terme una optimització de la separació d'*EGR* en diversos punts estacionaris per mitjà de simulacions que estan basades en el compromís entre rendiment i emissions. També es proposa un algoritme per a optimitzar la separació d'*EGR*, reduint al voltant d'un 80% el temps de càlcul d'un *DOE* o un mètode d'algoritme genètic. Finalment, es crea un model simple de NO_x 3D quasi-estacionari per a predir les emissions durant el transitori en condicions de conducció real. La taxa d'*EGR*, com a tercera entrada del model, mostra una millora significativa a l'hora de predir el transitori de NO_x respecte al model 2D.

Acknowledgments

Firstly, I would like to express my sincere gratitude to my advisor Prof. José Galindo for the continuous support of my Ph.D study and related research, for his patience, motivation, and immense knowledge. His guidance helped me in all the time of research and writing of the research articles and this thesis. I could not have imagined having a better advisor and mentor for my Ph.D studies. Besides my advisor, I would like to thank the rest of my thesis committee: Dr. Armas Vergal Octavio, Dr. Chalet David and Dr. Higelin Pascal, for their insightful comments and encouragement, but also for the hard question which incented me to widen my research from various perspectives.

My sincere thanks also goes to Dr. Pyri Francisco and Dr. Desantes, who provided me an opportunity to join their department, and who gave access to the laboratory and research facilities. Without their precious support it would not be possible to conduct this research. Additionally, I would like to thank Mr. Devising Rathod and Mr. Emran Ashraf for giving me the opportunity to work at FEV India ltd. and allowed me to get the industrial experience related to my research that leaded to acquire the international title for my thesis.

Specially, I want to thank Dr. Climent Héctor and Dr. Pla Benjamín for the stimulating discussions and guidance allowing me to keep motivated towards my research and making it more interesting. I would like to thank all those technicians specially Vicente and Sergio who helped me to setup the experiments and give the practical edge to my knowledge.

I can't miss to thank my fellow lab mates Auñon, Fran, Julian, Pablo and Tarí for the discussions and for all the fun we had in the last four years at our desks. Without you it wouldn't have been possible to stay and work away from my home. Also I thank my motherland friends Varun and Vishnu for their support in their unique way. It's really difficult to acknowledge all, but I would like to thank each and every one who directly or indirectly helped me to carry out this work. Last but not the least, I would like to thank my family: Aai, Pappa and Nandita for supporting me spiritually throughout writing this thesis and my my life in general.

Valencia, June 2020.

नेहमी नवीन शोधाचे कारण बनण्यापेक्षा,
वैज्ञानिक ज्ञानातील भर, ही देखील एका नवीन शोधाचे
कारण ठरू शकते.

Instead of becoming always the reason for the ground breaking invention,
an added scientific knowledge also could become a reason for the one.

Contents

List of Tables

List of Figures

List of symbols

Latin characters

c_p	specific heat capacity at constant pressure	$J \cdot kg^{-1} \cdot K^{-1}$
c_v	specific heat capacity at constant volume	$J \cdot kg^{-1} \cdot K^{-1}$
$\dot{m}$	mass flow rate	$kg \cdot s^{-1}$
p	pressure	Pa
t	time	s
T	temperature	K

Acronyms

0D	zero dimensional
1D	one dimensional
2D	two dimensional
3D	three dimensional
AFR	Air to Fuel Ratio
BSFC	Brake Specific Fuel Consumption
CFD	computational fluid dynamics
CLD	Chemi-Luminescence Detection
DOC	Diesel Oxidation Catalyst
DOE	Design of Experiment
DPF	Diesel Particulate Filter
ECU	Engine Control Unit
EGR	exhaust gas recirculation
EMS	Engine Management Strategy
UNECE	United Nations Economic Commission for Europe
ESI	EGR Split Index
ET	Exhaust Throttle
EUDC	Extra Urban Driving Cycle
GA	Genetic Algorithm
GT	Gamma Technologies
ICE	internal combustion engine
INCA	Integrated Calibration and Application Tool
MEP	Mean Effective Pressure

MK	Modulated Kinetics
MOEA	Multi-objective Evolutionary Algorithm
MOGA	Multi Objective Genetic Algorithm
MPC	Model Predictive Control
MVEG	Motor Vehicle Emission Group
NDIR	Non Dispersive Infra-Red Technique
NEDC	New European Driving Cycle
NSGA	Non-dominated Sorting Genetic Algorithm
PAH	Polycyclic Aromatic Hydrocarbons
PCCI	Premixed Compression Charge Ignition
PEMS	Portable Emission Measurement System
PMEP	Pumping Mean Effective Pressure
RANS	Reynolds-averaged Navier-Stokes
RCCI	Reactivity Controlled Compression Ignition
RDE	Real Driving Emissions
RPM	Revolutions Per Minute
RPA	Relative Positive Acceleration
SCR	Selective Catalytic Reduction
SOI	Start Of Injection
TNO	Toegepast Natuurwetenschappelijk Onderzoek (organization in Netherlands)
UEGO	Universal Exhaust Gas Oxygen sensor
UN	United Nation
WLTC	World-wide harmonized Light vehicle Test Cycle

Chapter 1

Introduction

Contents

1.1 Motivation

Environment is the biggest concern these days due to various climatic changes that are taking place and getting even worse day by day. It has a direct effect on the humans who are a vital part of this ecosystem. Looking at the reasons behind the upsetting of this environment, humans are most responsible entities and are required to take some steps to recover the condition. Various scientific evidences are published proving the human influences on the climatic conditions [1]. The emissions from different sectors are causing the problems like greenhouse effect. Figure 1.1 shows the sectorial contributions of carbon dioxide emissions from all over the world. The transportation is always been the prominent and consistent sector among them. The share of total CO_2 emitted by these sector is more or less remained constant for almost 54 years. In response to this, various efforts has been taken by the UN to mitigate the adverse effects of human activities to save the environment.

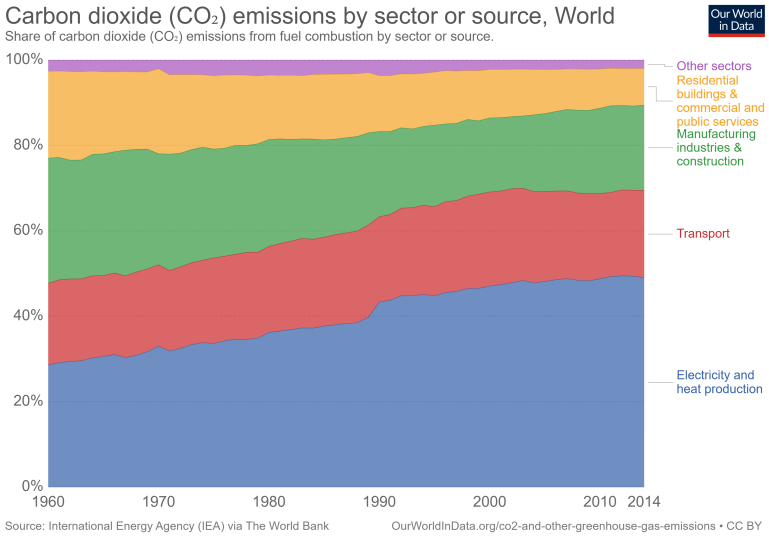

Figure 1.1: Sector wise contribution of CO_2 emissions all over the world.[2]

Being the important part of this environment humans are also getting affected by the harmful pollutant emissions due to combustion of fuel from the transportation industry which is referred as primary pollution. The products such as carbon monoxide (CO), nitrogen oxides (NO_x), hydrocarbons (HC), sulfur oxides (SOx) and particulate matter (PM) cause harmful effects to hu-

man bodies. Moreover, the combustion products from the ICE transform into toxic compounds causing secondary pollution of air like photochemical smog which is produced by the reaction of NO_x and HC in presence of sunlight [3, 4]. NO_x particles are harmful for the lungs with too much concentration. They are the important accomplice in the acid rain and smog. The soot particles are suspected to be carcinogenic. They are cause of symptoms in respiratory system and increase mortality in cardiovascular and respiratory diseases. Therefore it is a high priority to reduce these dreadful pollutant emission from different means in transportation sector [5].

Considering the transportation industry, road transportation is responsible of 83% of the total transport energy consumption [6]. Motorization indices of vehicles per inhabitant are rapidly growing in developing economies and the expectations of those numbers is keep on rising. Countries such as China are experiencing a significant increase in vehicle registration as a consequence of the expanding economy, showing motorization rates of 20–40%/year [7, 8]. As shown in Figure 1.2, developed countries' present passenger car densities are close to 0.5 cars per inhabitant [9, 10], while developing countries, such as China or India are around at 0.03. The economic development is expected to make this average grow even further in future.

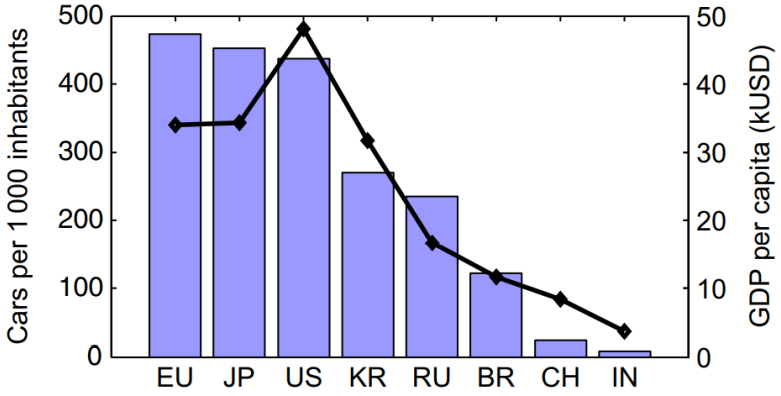

Figure 1.2: Cars per person (bars) and GDP per capita (line) in some selected countries.[11]

1.1.1 Pollutant Formation

During the combustion, the fuel and air react together to form water and other gases as byproducts of the combustion inside the chamber. Equation 1.1 represents the balanced common combustion reaction of fuel ($C_xH_yO_z$) with air ($O_2 + a{\cdot}N_2 + b \cdot CO_2 + c \cdot Ar + d \cdot H_2O$). But as the combustion is not perfect always, the other intermediate products such as HC, CO, NO_x and soot particles are formed in the process. The pollutants are harmful for the human body and the environment. Therefore, the formation and emission of these pollutants is required to be reduced. The HC and $CO$are comparatively in less in proportion and can be reduced further by after-treatment system. However, the NO_x and soot are more problematic pollutants. Moreover, the CO_2 from the perfect combustion is cause of the global warming and needed to be reduced. This is possible by reducing the fuel consumption.

$$C_xH_yO_z + B \cdot (O_2 + a{\cdot}N_2 + b \cdot CO_2 + c \cdot Ar + d \cdot H_2O) \longrightarrow (x + B \cdot b){\cdot}CO_2 + (\frac{y}{2} + B \cdot d)H_2O + k \cdot O_2 + B \cdot a \cdot N_2 + B \cdot c \cdot Ar \tag{1.1}$$

From the equation 1.1, B represents the number of moles of air reacting to the fuel. If the combustion. The perfect combustion (stoichiometric) requires a particular proportion of air to react with the fuel which is also called as stoichiometric air (B_{st}). The ratio of B to the (B_{st}) is called lambda which is equivalent to the ratio of air to fuel ratio with stoichiometric air to fuel ratio. λ less than 1 referred as the 'rich' mixture while greater than 1 is called 'lean' mixture.

$$\lambda = \frac{B}{B_{st}} = \quad \frac{AFR}{AFR_{st}} \tag{1.2}$$

The formation of pollutants depend upon the composition of gas inside the combustion chamber. Figure 1.3 shows the concentration of CO, HC, CO_2 and NO_x with different air to fuel ratios. where 14.7 is the stoichiometric air to fuel ratio.

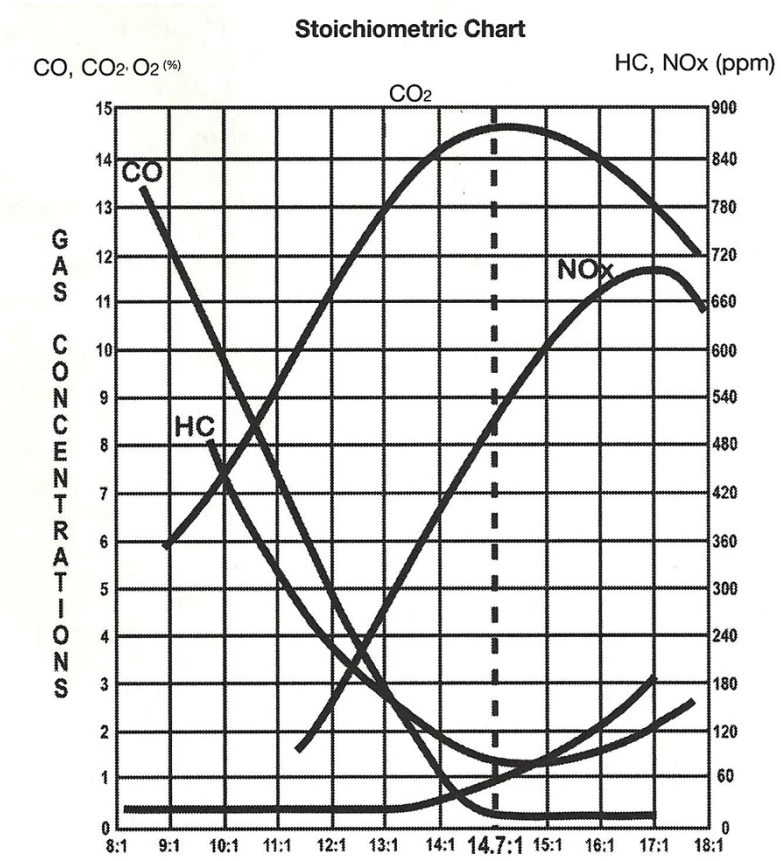

Figure 1.3: Pollutant concentration with the air to fuel ratio

1.1.1.1 NO_x

Normally NO_x formation takes place at higher temperature and high oxygen concentration. The concentration of NO_x in Figure 1.3 increases with the higher air to fuel ratio up to a point where the temperature of the combustion is high and decreases further with increase in air. There are two important types of NO_x formation mechanisms in internal combustion engines, prompt NO_x and thermal NO_x. The thermal NO_x formation is can be explained by the extended 'Zeldovich' mechanism. It consists of 3 chemical reactions [12].

$$\begin{aligned} O^* &+ N_2 \leftrightarrow NO + N^* \\ N^* &+ O_2 \leftrightarrow NO + O^* \\ N^* &+ OH \leftrightarrow NO + H^* \end{aligned} \tag{1.3}$$

The chemical rate of these reactions is high only at the high temperature above 2200K [13]. Therefore equilibrium is not achieved in this reactions as the temperature is not always high enough for long time during the compression stroke. It reduces during the expansion stroke. On the other hand, the prompt NO_x (also called as Fenimore NO_x) is formed by rapid reaction of CH^- radicals with molecular nitrogen to build amines or cyano compounds, where the subsequent reactions form the NO [14]. The quantity of this prompt NO_x is much lesser than the thermal NO_x in diesel engines [15].

1.1.1.2 Particulate Matter

Diesel particulate matter mainly consists of carbonaceous material (a.k.a. soot generated from the combustion) on which some organic compounds from unburnt fuel and oil have been absorbed. The size of particulate material varies from 20nm to 10μm. The soot is formed from th unburned fuel that nucleates from the vapor phase to a solid phase in fuel-rich regions at elevated temperatures. The evolution of liquid or vapor phase hydrocarbons to solid soot particles, and possibly back to gas-phase products, involves six commonly identified processes, schematically depicted in the Figure 1.4

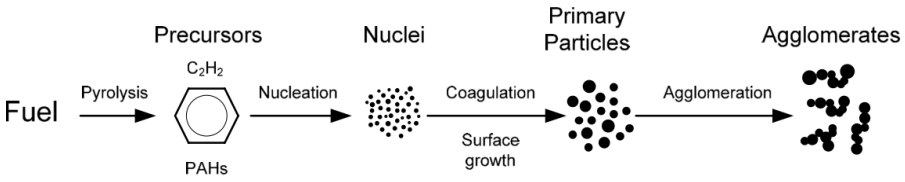

Figure 1.4: Schematic diagram showing the steps of the soot formation process from gas phase to solid agglomerated particles.[16]

Pyrolysis consists of endothermic process altering the molecular structure of fuel in the presence of high temperature and producing species such as

polycyclic aromatic hydrocarbons (PAHs), considered as soot precursors. afterwords in nucleation occurs spontaneous formation of a nucleus or nanoparticles from volatile materials such as hydrocarbons. Thereafter, process of adding mass to the surface of a nucleated soot particle termed as surface growth. When roughly spherical particles collide and coalesce to form bigger spherical particles, coagulations happens. This is followed by agglomeration, where particles stick together to form large groups of primary particles in chain-like structure. Typically, at temperatures higher than 1300 K, soot is burned in the presence of oxidizing species to form gaseous products such as CO, CO_2 and H_2O. This process is called oxidation and it can happen anytime in between the above processes. [17]

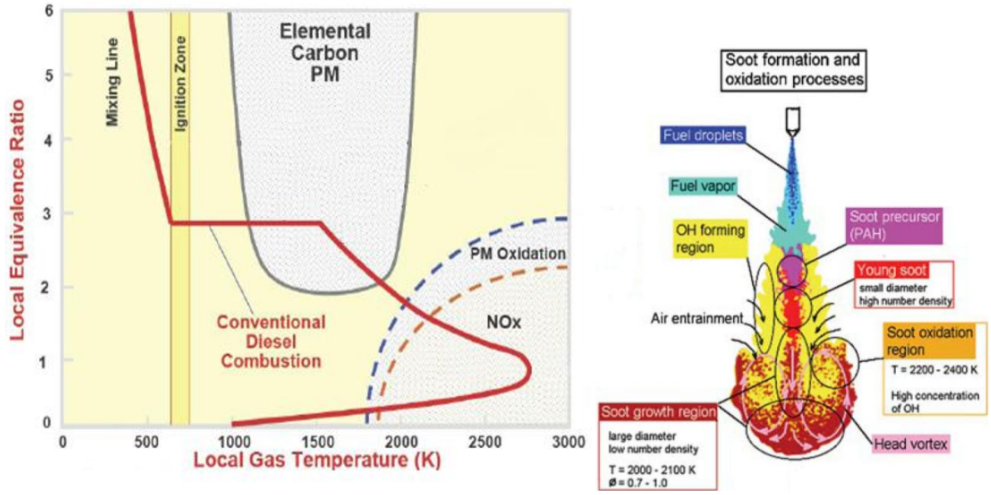

Figure 1.5: Emission formation in conventional diesel combustion.[18]

The path of conventional diesel combustion is represented on the ϕ-T map in Figure 1.5. The ϕ is called an equivalence ratio which is inverse of λ from the equation1.2. The soot is formed in the parts of the spray where the oxygen concentration is low. Most of the formed soot gets oxidized in the later part of the combustion when the oxygen concentration gets higher.

1.2 Environmental Regulations

Increasing risk of health from pollutants has stir up the human mind since few decades. Various regulations on these pollutant emission have been enforced on various industries by the governments of different countries. Transportation industry, not being an exception, is consciously taking steps to improve the situation since 1970 when the first Landmark clean air act is passed by the state of california, USA. It was a first national effort to reduce the pollution from cars by adopting standard regulations [19]. The vehicle emissions are variable and depend on the surrounding, therefore, standard laboratory conditions are specified to reproduce the standard tests [20]. A fixed schedule of operations also called as a driving cycle is designed to test the vehicles on test bench under reproducible conditions [21]. Various driving cycles have been designed representing respective driving conditions by US Federal and california regulations (FTP75, Highway fuel economy cycle, SC03 air conditioning, US06 high speed) and European Union (ECE-15/UDC, NEDC, WLTC). The wide comparative study of US and Europe legislation for emission in automotive sector has been made by [22]. The emission regulation strategy and after-treatment system are designed to maintain the emissions below the stringent emission limits on these driving cycles measured on the test bench. Past and current limits of Euro standards for NO_x and PM are shown in figure 1.6, illustrating the swift movement to cleaner technologies.

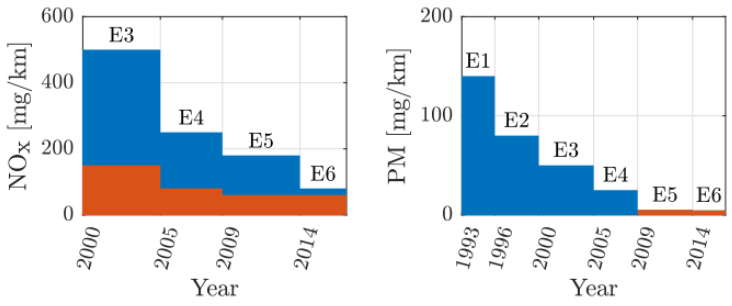

Figure 1.6: Pollutant limits of past and current Euro standards for CI (blue) and SI (red) vehicles. (NO_x limits were introduced with Euro 3, before it was combined NO_x+HC emissions and PM are regulated since Euro 5 for SI engines.[23]

From few years before, The new portable emission measurement system (PEMS) has brought changes in the legislation as it involves measurement of

pollutant emissions while the vehicle is driving on road [24, 25]. It is also called as Real Driving Emission testing (RDE). It disclosed various loop holes from the old homologation procedure with the driving cycles performed on the test bench as wide range of engine loads, vehicle speeds and ambient temperature and pressure differences have to be meet by a real driving route. Therefore, the need for new dynamic driving cycles representing real driving conditions has came up [26, 27]. Additionally, the emission measurement tests with PEMS are supported by the various studies [28, 29, 30]. The specific constraints have ben designed by the european union to be followed for the route of RDE measurement which are discussed in detail in the next Chapter.

1.3 EGR Systems

Exhaust Gas Recirculation is nothing but the recirculating certain percentage of exhaust gas mass flow from the exhaust to the intake line controlled by the valve. Reduction of NO_x formation is the main reason behind the mixing of exhaust gases with the intake air. The exhaust gases mainly consist of CO_2, water vapour and the inert gases. Mixing of exhaust gases in the intake charge reduces the oxygen concentration. Because of the reduction in the number of oxygen molecules, the fuel has to find them through large amount of gas for the combustion reaction. The fuel energy is used to heat up this amount of gas resulting into lowering the temperature of the combustion. Moreover, specific heat capacity of the exhaust gases is very high due to presence of free CO_2 molecules and the gas requires more heat to increase the temperature. Therefore the temperature of the combustion is less as compared to the pure air. The lower temperature leads to reduction in the formation of NO_x by freezing the the 'Zeldovich' mechanism.

The EGR rate is represented by the ratio of the mass flow rate of exhaust gas circulated to the intake with the total mass flow of gases and air going inside the combustion chamber. The EGR can be extracted from any point of the exhaust line depending on the requirement. It has different types according to the point of extraction. Internal EGR, LPEGR and HPEGR are the types of EGR that are used on diesel and gasoline engines.

Advanced development in the field of after-treatment system lead to competition in the high EGR rate and after-treatment strategies. However, future combustion technologies with low temperature combustion rely on the high

EGR rates if they are used in broader operating range [31].

1.3.1 HPEGR

The high pressure EGR (also referred as short route EGR) is common in passenger cars and heavy duty vehicles. The high pressure exhaust gases are extracted from exhaust line upstream of the turbocharger. The system usually contains cooler to cool down the exhaust gases before entering into the intake manifold. The EGR valve is used to regulate the quantity of the EGR mass flow. The placement of EGR valve on the hot side of EGR cooler is advantageous for transient response [32] as the exhaust pulses are damped by the smaller volume before the valve on the hot side. This gives more energy to the turbine. The pressure difference across the EGR valve is required to drive exhaust gases through. Sometimes, it is not possible to obtain the required pressure difference. The VGT is used in this case. closing of VGT creates the pressure upstream of turbine increasing the positive pressure difference to drive the HPEGR.

HPEGR system is simple and fast to provide required EGR flow. However, it requires throttling often and it has risk of soot deposition in the intake line. While, fouling of EGR cooler is another issue with HPEGR [33]. The ability of turbocharger is also affected due to reduction of pressure upstream of turbine. Extraction of the gases through HPEGR line reduces the enthalpy of gas before turbine.

1.3.2 LPEGR

The low pressure EGR (also referred as long route EGR) extracts the exhaust gases downstream of the turbocharger and recirculates upstream of the compressor. Therefore, the length of the EGR line is tend to be longer than HPEGR line. Addition to this, there are other problem with the LPEGR. One of them is the flow of exhaust gases through compressor. It could be dangerous due to clogging by soot particles. This can be removed by placing EGR loop downstream of particulate filter. However, it increases the length of LPEGR line. Additionally, the pressure downstream of particulate filter and upstream of compressor is close to ambient pressure. That means, the lack of natural pressure drop makes it difficult to drive the EGR flow. This can

also be rectified by creating a forced pressure drop using intake and exhaust throttling. Out of this two, throttling of exhaust gases is preferred over the other [32], as it is useful for driving high EGR mass flow rates at low load points.

In addition to above problem, condensation of water in the LPEGR cooler is also problematic issue, as the water droplets going inside the compressor can damage the compressor wheel. While, LPEGR also increases the compressor outlet temperature. Therefore special attention is required during designing of EGR cooler. Fouling of inter-cooler is still remains as a problem even though the gases are drawn after DPF. From transient point of view, due to long length of the EGR system, it takes time to change the EGR composition in the intake line as compared to fast HPEGR. The 2 stage boosting with EGR can increase more the risk of reaching thermal limitations [34, 35].

Despite of above drawbacks, there are various advantages of the LPEGR system. At low load points, where the flow of air is very less, the LPEGR can improve the efficiency of the turbocharger with increased mass flow. This leads to increase in fuel economy. The cooling capacity requirements is less in LPEGR as the gases are cooled twice in LPEGR cooler and inter-cooler of the air. It reduces the intake temperature and thus the heat losses inside the cylinder [36]. Considering the dispersion and mixing of exhaust gases, LPEGR has time to mix well with the air and therefore, the distribution of EGR is more even in LPEGR than HPEGR system [37, 38, 39].

1.3.3 Hybrid EGR

Hybrid EGR system is the combination of both HP and LPEGR system. It is a profitable attempt to get the advantages of both types of EGR systems according to the driving situations [40]. Even the combination of both is useful to attain the optimum engine efficiency at certain load points [41, 42]. The optimum combination can be found to give the quickest response and reduce emission for the particular engine operation. The hybrid system can also be used with un-cooled HPEGR to increase the temperature of recirculated exhaust gases in cold conditions and low load points [43, 44]. This thesis document has given special attention tho this kind of EGR system during steady state and transient operation to improve the performance with reduced emission.

1.4 Transient operation

'Transient operation' is an engine operation when the engine undergoes sudden change in load or speed, altering the dynamics of air and fuel flow [45]. It could also called as 'unsteady operation'. The change should be either in engine load or speed or both. The change in engine load at constant speed is called 'load transient', while the change in engine speed at similar load is called 'speed transient'. The reasons behind this kind of operations could be as follows,

- Sudden acceleration by step change in the pedal position;
- Engaging of clutch after gear change;
- Vehicle climbing a hill;
- Cold or hot start of vehicle;
- Roundabout maneuver on road;

There are some other engine operations which can loosely be termed as 'transient' operations like cyclic variation, warm-up, DPF regeneration etc [17]. The transient operation, where the acceleration is increased by pushing the pedal is also called as 'Tip-In' operation while the one with releasing the pedal to drop the torque is called as 'Tip-Out' operation.

There are two important types of variables during transient operations. The 'fast' variables, which change their values rapidly as per the requirement during transients. While the 'slow' variables show hysteresis during the change or require more time for control. The fuel path variables like mass of fuel, start of injection fuel rail pressure etc. are the examples of fast variables. While, the air mass flow, EGR rate, VGT positions etc. are some examples of slow variables which depend on the response of fast variables and the dynamics of the air path system [46, 47, 48].

So far, the transient performance was the most important part of the investigations related to the ICE. There are various experimental and simulation studies done to improve the transient performance of an engine. [49] has done the systematic review of all the transient simulation studies to improve the performance with various modelling techniques in the chronological order. [35] has studied the effect of thermo-mechanical limits of the engine during

transient operations. [50] has compared the transients with different types of EGR. However, the improvement of transient operation in a diesel engine from the emission perspective has become important these days. Effect of different parameters like manifold volume, valve timing, oil temperature, and turbocharger moment of inertia on the emissions during transient operation are studied by Rakopoulos with modelling [51]. But the experimental study is required with the high response emission measurement system to observe the exact evolution of pollutants in the exhaust line.

1.5 Background

This section explains the background behind the formation of main objectives of this dissertation. The base for the studies, related to the EGR control, is presented to see the effect on the performance and emission during the transient operations. Keeping in mind the drawbacks and constraints of current engine control strategies, further potential of EGR transient operation is studied, focussing on reducing the instantaneous pollutant formation.

1.5.1 EGR calibration

The current calibration consists a particular zone on the engine map for controlling the flow of exhaust gases in the intake line. It is also called as EGR zone. When engine operates in that particular range of operating condition, the ECU activates the EGR system. However, when the operating point of the engine lies outside of this EGR zone, all the EGR valves present on the engine are closed by the ECU. This removes all the exhaust gases in the intake line and as a consequence, the NO_x emissions get increased.

Firstly, the new driving cycles like WLTC cover almost all the part of engine map. RDE cycles also have no fix defined trajectory or zone of working to follow all the time. That means, the engine can operate randomly at any torque and engine speed. Therefore, the need to expand the boundaries of EGR zone is essential to control overall NO_x emission on the new driving cycles. Secondly, during the transient operations, where the engine load is shifted from low load to full load, this EGR zone plays vital role. As soon as, the ECU senses the transient operation due to rapid change in fuel require-

ments, it closes the EGR valves and opens the exhaust throttle fully. This removes the exhaust gases from the circuit increasing air to comply with the demanded torque and fuel quantities. This improves the torque evolution of the engine. However, sudden closure of EGR valves increases the temperature inside the combustion chamber and thus the NO_x formation. Therefore, sudden peaks of NO_x are seen during these transient operations. As described in the Chapter 2, the number of transient operations during WLTC and RDE cycles is very high. Therefore, the cumulative NO_x emission on the driving cycle increases due to these transients. Taking into account those harsh transient operations, the EGR zone range should be increased till the full load.

1.5.2 EGR control

Engine control has been mostly performed with a set of PID controller that track factory calibrated set points to perform adequately. Those set points are normally mapped by measurable quantities like engine speed and torque/fuel flow. Conventionally, The EGR rate is regulated by controlling the steady state air mass flow measured just after the air filter. The boost pressure is also regulated steady state maps available in ECU. However, The control of EGR at full load and during harsh load transients going outside of EGR zone is remain a challenging task. The availability of air at full load is very less as compared to low load operation. So there is a chance of high soot formation at low engine speeds. Moreover during the transient operations, unexpected delays (like mechanical, fluid dynamic, thermal [52]) associated with the turbocharger inertia, manifold volume [53], cylinder wall temperature [54] result not only in emission spikes higher than the steady state operation but also make the EGR control difficult.[55, 56]. Due to turbo lag, the air responds very slowly as compared to the change in fuel requirement, especially at low speed and loads [57]. This also increases the possibility of soot increase in the exhaust line. Another challenge lies in the control is the type of EGR to be used in those operating conditions. As discussed before and further in chapter 4, the HP and LPEGR have various advantages, if used separately as well as combined together. HPEGR is very sensitive to the VGT movements (also called as EGR/VGT coupling) and can reduce the turbocharger power while LPEGR is delayed due to longer circuit. So combining these two different EGR systems makes the air path control more complex. That is why, a simple method of choosing only one type of EGR is used in previous calibrations according to the engine operating condition and switching in between them.

There are some other air path control strategies suggested in the literature like the EGR/ VGT control. In which, the air is controlled by the actuation of EGR valve while in closed loop while the boost pressure is controlled by the actuation of VGT positions in open loop. this strategy avoids the coupling of HPEGR and VGT. But it is still stays complicated for hybrid EGR, which consists of usage of both HP and LPEGR types. In the dual loop/hybrid EGR strategy, the total EGR rate is calculated by the sum of mass flows of both EGR types. The control is similar to the single EGR/VGT control, however requires an appropriate algorithm for defining the EGR split [58]. The 'fast' variables or fuel path variables explained in the last section strongly affect the engine performance by changing the combustion process. Some authors have proposed the joint control of fast and slow variables at the same time to optimize the transient performance and emissions. The explicit off-line model is used to control the NO_x and soot by controlling 'fast' variables while the performance by 'slow' variables. However, this requires real time measurements of exhaust concentration [59, 60]. Another model based control strategies are also proposed by building virtual sensors and physical model of the system by constantly monitoring the exhaust concentration and the performance of the system. The MPC using the EGR/VGT control strategy [61][62][60] and the dual loop EGR strategy [44, 63, 64] are few of them. The optimization of actuator trajectories like VGT, fuel and EGR valves is performed and applied for specific mild load transients to reduce the soot and NO_x [48, 65].

1.6 Objectives

The transient operations play important role in the newly developed dynamic cycles like WLTC and RDE. They actually represent the dynamic real driving behavior on road. Due to various delays and mismatch between fuel and air path variables, unexpected emission spikes appear during these transient operations. The objective is to find the solution to reduce those emission spikes without hampering the performance of the engine. The solution includes use of EGR systems (HP/LPEGR/both) which are proved to be effective during steady state but mostly neglected in engine calibration for transients. Therefore, the application of both HP and LPEGR systems on diesel transients, identifying the trends of the pollutant formation using instantaneous emission measurement systems, is the main goal of this work. Moreover, it involves, pointing out the subsiding trade-off between performance and emission using

proposed solution to see the potential of improvement in a transient operation.

Additionally, the objectives focus on studying the effects of both EGR types on engine subsystems improving the overall efficiency of the engine for all operating ranges. They asses the full potential of the EGR systems during steady and transient operation considering the modern driving cycle operations. This study is useful for engine calibration and designing a control during the transients taking into account the dynamics of actuators and their effect on engine components.

1.6.1 Specific objectives

The main objectives of the thesis are accomplished with the achievement of certain specific objectives supporting the global goals. These underlying specific objectives are classified into experimental and simulation parts. Some of the important ones are mentioned as following,

Experimental

- Identification and classification of most peculiar and frequent transient operations on different driving cycles like NEDC, WLTC and RDE. Find the importance of those transient operations in regard to the pollutant emissions.(Chapter 2);
- Detailed experimental analysis of the selected transient operations focusing on the pollutant emissions and temporal performance. Measurement and comparison of the the fast and slow emission measurement systems during the these transients.(Chapter 5):
- Experimental analysis to find out the impact of hybrid EGR on pollutant emissions and performance during the harsh transient operations.(Chapter 5)

Modelling and Simulation

- 1D modelling of transient operations to find the potential factors to improve the performance with parametric study of actuator movements like VGT and EGR valves.(Chapter 3);

- 1D simulations to see the impact of different ratios between HP and LPEGR on engine components considering the thermo-mechanical limits. See the potential of cooled HPEGR and compare with its counterpart.(Chapter 4);
- Propose an algorithm to speed up the process of optimization of the split between HP and LPEGR on various operating points on the engine map.(Chapter 4);
- Prepare a simple quasi-steady NO_x model to predict the NO_x emission during the real driving conditions using the 2D and 3D NO_x maps as a function of engine torque, engine speed and EGR rate.(Chapter 6)

1.7 Thesis outline

Chapter 2.1 has introduced the current situation of the automotive industry and the importance of the pollutant emission from the transportation sector. The pollutant formation in ICE are discussed in details along with their adverse effects on the environment and the human bodies. The developing environmental regulations to avoid the bad impacts on the ecosystem are presented with the developments in last few years. Furthermore, the EGR system and its types assessing the state of art types is explained briefly. Definition of possible transient operations faced by the engine on a vehicle is discussed along with their origin and types. Their importance for the new emission regulations is mentioned with the previous work associated with them. The background of the thesis objective is discussed with the state of art knowledge in the field of calibration and control for transient operations. The main objectives are coined following the local experimental and simulations goals achieved throughout the research work.

The Chapter 2 introduces the dynamic analysis of driving cycle like NEDC, WLTC and RDE. These cycles are performed on the dynamic engine test bench with the same engine and vehicle model. The vehicle model is explained in details following with the introduction of each driving cycle and their characteristics as per regulations. The derivative analysis of engine torque and speed for each second is performed to see the distribution of the load change on on engine map. The most frequent zones for the transients are identified with the magnitude and direction of load change. An extended analysis is performed on

a RDE cycles generated from the external algorithm following the constraints of the RDE regulations to support the previous analysis. Finally, the three driving cycles are compared with each other on the basis of dynamic nature and emissions.

Chapter 3 presents the experimental and simulation tools used in the investigation for this thesis work. The experimental methods pollutant measurement systems are explained which are required for the study. The data analysis and correction factors used to present the data is also mentioned for the ease of the reader.

Chapter 4 speaks about the hybrid/dual EGR for steady state operations. A parametric study with different split between the HP and LPEGR is carried out with the calibrated 1D model of a turbocharged diesel engine. The ESI index is defined representing the split in the range of 0 to 1. The impact of ESI on various engine parameters is presented with exhaustive parametric study for operating condition covering full engine map. The optimization of this ESI is carried out using the genetic algorithm. An alternative algorithm is generated in GT Power to optimize the ESI for the same engine operating points with 80% reduction of time than traditional DOE and genetic algorithm approach.

Chapter 5 focuses on the effect of different EGR actuator dynamics on the transient emission and performance. Firstly, implementation of HP and LPEGR on full load is done determining the EGR valve situations to provide the EGR at full load. Furthermore, comparison of both EGR types is done on the harsh transient operations selected from the Chapter 2 on a dynamic engine test bench. The impact on emission is captured with the high response emission measurement system. Moreover, a different trajectories of LPEGR valve actuation are performed to quantify the tradeoff between emission and performance during a load transient operation. Specific roundabout transient operations are also performed on the dynamic test bench to see the effect of transportation of exhaust gases on the performance and instantaneous emissions. finally, the comparison has been made on full driving cycle between old calibration and the new developed control strategy.

The last Chapter 6 presents the simple quasi-steady NO_x model to predict the pollutant formation during harsh transient operations and full real driving cycle. A 2D and 3D model is created based on the input argument to predict the NO_x by interpolating between steady state maps prepared on

the test bench. The accuracy and error difference between the two models are presented at the end of the chapter with full cycle prediction.

Chapter 1 Bibliography

[1] R. S. J. Tol. "Comment on 'Quantifying the consensus on anthropogenic global warming in the scientific literature'." *Environmental Research Letters* 11(4) (2016). ISSN: 1748-9326. DOI: 10.1088/1748-9326/11/4/048001. URL: http://stacks.iop.org/1748-9326/11/i=4/a=048001?key=crossref.0b692e0e30f61886b8cfc6904d5e2cbe (cit. on p. 2).

[2] R. S. J. Tol. "CO2 and Greenhouse Gas Emissions." *Our World in Data* (2019) (cit. on p. 2).

[3] R. R. Dickerson. "The Impact of Aerosols on Solar Ultraviolet Radiation and Photochemical Smog." *Science* 278(5339) (1997), pp. 827–830. ISSN: 00368075. DOI: 10.1126/science.278.5339.827. URL: http://www.sciencemag.org/cgi/doi/10.1126/science.278.5339.827 (cit. on p. 3).

[4] R. Atkinson and A. C. Lloyd. "Evaluation of Kinetic and Mechanistic Data for Modeling of Photochemical Smog." *Journal of Physical and Chemical Reference Data* 13(2) (1984), pp. 315–444. ISSN: 0047-2689. DOI: 10.1063/1.555710. URL: http://aip.scitation.org/doi/10.1063/1.555710 (cit. on p. 3).

[5] S. Jungnelius and M. Svartengren. *Hälsoeffekter av trafikavgaser*. Yrkesmedicinska enheten, Karolinska sjukhuset, 2000 (cit. on p. 3).

[6] *Energy, transport and environment indicators*. 2016. ISBN: 978-92-79-60137-8. DOI: 10.2785/138586 (cit. on p. 3).

[7] N. B. o. S. of China. "China statistical yearbook." *Beijing: Chinese Statistical Bureau* (2017) (cit. on p. 3).

[8] S. C. Davis, S. E. Williams, and R. G. Boundy. *Transportation Energy Data Book: Edition 36.1*. 2018. ISBN: 1800553684 (cit. on p. 3).

[9] U.S. Department of Transportation. *Summary of Travel Trends 2001 National Household Travel Survey*. 2001. ISBN: 1800553684 (cit. on p. 3).

[10] Eurostat - Statistical Office of the European Communities. *Energy, transport and environment indicators 2011 edition*. 2011. ISBN: 9789279213847. DOI: DOI10.2785/17571 (cit. on p. 3).

[11] F Payri, J. Luján, C Guardiola, and B Pla. "A Challenging Future for the IC Engine: New Technologies and the Control Role." *Oil & Gas Science and Technology – Revue d'IFP Energies nouvelles* (2015). ISSN: 1294-4475. DOI: 10.2516/ogst/2014002 (cit. on p. 3).

[12] J. B. Heywood. *Internal Combustion Engine Fundementals*. Vol. 21. 1988, p. 930. ISBN: 007028637X. DOI: 10987654 (cit. on p. 5).

[13] J Kahrstedt, A Blechstein, O Maiwald, and J Kabitzke. "Grundlegende Untersuchungen zu Low-NOX-Brennverfahren für PKW-Dieselmotoren unter Nutzung zusätzlicher Variabilitäten, 6." In: *Internationales Stuttgarter Symposium*. 2005 (cit. on p. 6).

[14] J. A. Miller and C. T. Bowman. "Mechanism and modeling of nitrogen chemistry in combustion." *Progress in Energy and Combustion Science* 15(4) (1989), pp. 287–338. ISSN: 03601285. DOI: 10.1016/0360-1285(89)90017-8. URL: https://linkinghub.elsevier.com/retrieve/pii/0360128589900178 (cit. on p. 6).

[15] U. Gärtner. *Die Simulation der Stickoxid-Bildung in Nutzfahrzeug-Dieselmotoren*. na, 2001 (cit. on p. 6).

[16] R. Stone. *Introduction to Internal Combustion Engines*. London: Macmillan Education UK, 1992. ISBN: 978-0-333-55084-7. DOI: 10.1007/978-1-349-22147-9. URL: http://link.springer.com/10.1007/978-1-349-22147-9 (cit. on p. 6).

[17] C. D.Rakopoulos and E. G.Giakoumis. *Diesel Engine Transient Operation*. Vol. 53. 9. 2013, pp. 1689–1699. ISBN: 9788578110796. DOI: 10.1017/CBO9781107415324.004. arXiv: arXiv:1011.1669v3 (cit. on pp. 7, 12).

[18] M. Hirsch, K. Oppenauer, and L. del Re. "Dynamic Engine Emission Models." In: *Lecture Notes in Control and Information Sciences*. 2010, pp. 73–87. DOI: 10.1007/978-1-84996-071-7_5. URL: http://link.springer.com/10.1007/978-1-84996-071-7{_}5 (cit. on p. 7).

[19] O. Park. "Citizens to Preserve Overton Park." *Inc. v. Volpe* 401 (1971) (cit. on p. 8).

[20] A. Faiz, C. S. Weaver, and M. P. Walsh. *Air pollution from motor vehicles: standards and technologies for controlling emissions*. The World Bank, 1996 (cit. on p. 8).

[21] T. J. BARLOW, S Latham, I. McCrae, and P. Boulter. "A reference book of driving cycles for use in the measurement of road vehicle emissions." *TRL Published Project Report* (2009) (cit. on p. 8).

[22] M. Nesbeit, M. Fergusson, A. Colsa, J. Ohlendorf, C. Hayes, K. Paquel, and J.-P. Schweitzer. *Comparative Study on the Differences Between the EU and US Legislation on Emissions in the Automotive Sector: Study*. European Parliament, 2016 (cit. on p. 8).

[23] A. Reig Bernad. "Optimal Control for Automotive Powertrain Applications." PhD thesis. Valencia (Spain): Universitat Politècnica de València, 2017. DOI: 10.4995/Thesis/10251/90624. URL: https://riunet.upv.es/handle/10251/90624 (cit. on pp. 8, 136).

[24] M. Kousoulidou, G. Fontaras, L. Ntziachristos, P. Bonnel, Z. Samaras, and P. Dilara. "Use of portable emissions measurement system (PEMS) for the development and validation of passenger car emission factors." *Atmospheric Environment* 64(x) (2013), pp. 329–338. ISSN: 13522310. DOI: 10.1016/j.atmosenv.2012.09.062. URL: http://dx.doi.org/10.1016/j.atmosenv.2012.09.062 (cit. on p. 9).

[25] J. M. Luján, V. Bermúdez, V. Dolz, and J. Monsalve-Serrano. "An assessment of the real-world driving gaseous emissions from a Euro 6 light-duty diesel vehicle using a portable emissions measurement system (PEMS)." *Atmospheric Environment* 174 (2018), pp. 112–121. ISSN: 18732844. DOI: 10.1016/j.atmosenv.2017.11.056 (cit. on pp. 9, 135).

[26] B. Degraeuwe and M. Weiss. "Does the New European Driving Cycle (NEDC) really fail to capture the NOx emissions of diesel cars in Europe?" *Environmental Pollution* 222 (2017), pp. 234–241. ISSN: 18736424. DOI: 10.1016/j.envpol.2016.12.050 (cit. on p. 9).

[27] N. Hooftman, M. Messagie, J. Van Mierlo, and T. Coosemans. "A review of the European passenger car regulations – Real driving emissions vs local air quality." *Renewable and Sustainable Energy Reviews* 86(March 2017) (2018), pp. 1–21. ISSN: 18790690. DOI: 10.1016/j.rser.2018.01.012. URL: https://doi.org/10.1016/j.rser.2018.01.012 (cit. on p. 9).

[28] J. Merkisz, P. Lijewski, P. Fuć, Ł. Rymaniak, and A. Ziółkowski. "Measurement of Exhaust Emissions under Actual Operating Conditions with the Use of PEMS: Review of Selected Vehicles." In: *Improvement Trends for Internal Combustion Engines*. InTech, 2018. DOI: 10.5772/intechopen.70442. URL: http://www.intechopen.com/books/improvement-trends-for-internal-combustion-engines/measurement-of-exhaust-emissions-under-actual-operating-conditions-with-the-use-of-pems-review-of-se (cit. on p. 9).

[29] J. Gallus, U. Kirchner, R. Vogt, C. Börensen, and T. Benter. "On-road particle number measurements using a portable emission measurement system (PEMS)." *Atmospheric Environment* 124 (2016). ISSN: 18732844. DOI: 10.1016/j.atmosenv.2015.11.012 (cit. on p. 9).

[30] R. A. Varella, M. V. Faria, P. Mendoza-Villafuerte, P. C. Baptista, L. Sousa, and G. O. Duarte. "Assessing the influence of boundary conditions, driving behavior and data analysis methods on real driving CO2 and NOx emissions." *Science of the Total Environment* 658 (2019), pp. 879–894. ISSN: 18791026. DOI: 10.1016/j.scitotenv.2018.12.053. URL: https://doi.org/10.1016/j.scitotenv.2018.12.053 (cit. on pp. 9, 43).

[31] M. K. Khair and W. A. Majewski. *Diesel Emissions and Their Control*. Warrendale, PA: SAE International, 2006. ISBN: 978-0-7680-0674-2. DOI: 10.4271/R-303. URL: http://books.sae.org/book-r-303 (cit. on p. 10).

[32] S. Reifarth and H.-E. Angstrom. "Transient EGR in a long-route and short-route EGR system." In: *ASME Internal Combustion Engine Division Spring Technical Conference*. 2009, pp. 761–770. ISBN: 978-0-7918-4340-6. DOI: 10.1115/ICES2009-76107 (cit. on pp. 10, 11, 135, 138).

[33] R. Zhang, F. Charles, D. Ewing, J.-S. Chang, and J. S. Cotton. "Effect of Diesel Soot Deposition on the Performance of Exhaust Gas Recirculation Cooling Devices." In: *SAE Technical Papers*. 2004. ISBN: 0768013194. DOI: 10.4271/2004-01-0122. URL: https://www.sae.org/content/2004-01-0122/ (cit. on p. 10).

[34] J. Galindo, H. Climent, O. Varnier, and C. Patil. "Effect of boosting system architecture and thermomechanical limits on diesel engine performance: Part-I—Steady-state operation." *International Journal*

of Engine Research 19(8) (2017), pp. 854–872. ISSN: 20413149. DOI: 10.1177/1468087417731654 (cit. on p. 11).

[35] J. Galindo, H. Climent, O. Varnier, and C. Patil. "Effect of boosting system architecture and thermomechanical limits on diesel engine performance: Part-II—Transient operation." *International Journal of Engine Research* 19(8) (2018), pp. 854–872. ISSN: 1468-0874. DOI: 10.1177/1468087417731654. URL: http://journals.sagepub.com/doi/10.1177/1468087417731654 (cit. on pp. 11, 12).

[36] F. Millo, C. V. Ferraro, M. G. Bernardi, S. Barbero, and P. Pasero. "Experimental and Computational Analysis of Different EGR Systems for a Common Rail Passenger Car Diesel Engine." *SAE International Journal of Engines* 2(1) (2009), pp. 527–538. ISSN: 1946-3944. DOI: 10.4271/2009-01-0672. URL: https://www.sae.org/content/2009-01-0672/ (cit. on p. 11).

[37] F. Payri, J. Lujan, H. Climent, and B. Pla. "Effects of the Intake Charge Distribution in HSDI Engines." In: *SAE Technical Papers*. 2010. DOI: 10.4271/2010-01-1119. URL: https://www.sae.org/content/2010-01-1119/ (cit. on p. 11).

[38] G. Lim, Y. Choi, C. Park, and J. Park. "Effects of HPL and LPL EGR Gas Mixed Supply on Combustion and Emissions in Automotive Diesel Engine." In: *SAE Technical Papers*. 2011. DOI: 10.4271/2011-01-1831. URL: https://www.sae.org/content/2011-01-1831/ (cit. on p. 11).

[39] M. Van Aken, F. Willems, and D. J. De Jong. "Appliance of high EGR rates with a short and long route EGR system on a heavy duty diesel engine." In: *SAE Technical Papers*. 2007. DOI: 10.4271/2007-01-0906 (cit. on pp. 11, 89).

[40] J. M. Luján, C. Guardiola, B. Pla, and A. Reig. "Switching strategy between HP (high pressure)- and LPEGR (low pressure exhaust gas recirculation) systems for reduced fuel consumption and emissions." *Energy* 90 (2015), pp. 1790–1798. ISSN: 03605442. DOI: 10.1016/j.energy.2015.06.138 (cit. on pp. 11, 134).

[41] S. Reifarth and H.-E. Ångström. "Transient EGR in a High-Speed DI Diesel Engine for a set of different EGR-routings." *SAE International Journal of Engines* 3(1) (2010), pp. 1071–1078. ISSN: 19463936. DOI: 10.4271/2010-01-1271 (cit. on pp. 11, 73).

[42] P. S. Keller, V. Joergl, O. Weber, and R. Czarnowski. "Enabling Components for Future Clean Diesel Engines." In: *SAE Technical Papers*. 2008. DOI: 10.4271/2008-01-1530. URL: https://www.sae.org/content/2008-01-1530/ (cit. on p. 11).

[43] H.-J. Neusser, J. Kahrstedt, R. Dorenkamp, and H. Jelden. "The EURO 6 engines in the modular diesel engine system of Volkswagen." *MTZ worldwide* 74(6) (2013), pp. 4–10 (cit. on p. 11).

[44] J. M. Desantes, J. M. Luján, B. Pla, and J. A. Soler. "On the combination of high-pressure and low-pressure exhaust gas recirculation loops for improved fuel economy and reduced emissions in high-speed direct-injection engines." *International Journal of Engine Research* 14(1) (2013), pp. 3–11. ISSN: 1468-0874. DOI: 10.1177/1468087412437623. URL: http://journals.sagepub.com/doi/10.1177/1468087412437623 (cit. on pp. 11, 15).

[45] D Jain. "Using and electronically controlled VGT to improve engine transient performance." In: *Proceedings of the IMechE Seminar on Engine Transient Performance*. 1990, pp. 27–30 (cit. on p. 12).

[46] A. Uzun. "Air mass flow estimation of diesel engines using neural network." *Fuel* 117(PART A) (2014), pp. 833–838. ISSN: 00162361. DOI: 10.1016/j.fuel.2013.09.078. URL: http://dx.doi.org/10.1016/j.fuel.2013.09.078 (cit. on p. 12).

[47] K. Min, D. Jung, and M. Sunwoo. "Air system modeling of light-duty diesel engines with dual-loop EGR and VGT systems." *IFAC Proceedings Volumes (IFAC-PapersOnline)* 48(15) (2015), pp. 38–44. ISSN: 14746670. DOI: 10.1016/j.ifacol.2015.10.006. URL: http://dx.doi.org/10.1016/j.ifacol.2015.10.006 (cit. on p. 12).

[48] D. Alberer and L. del Re. "Fast Oxygen Based Transient Diesel Engine Operation." *SAE International Journal of Engines* 2(1) (2009), pp. 2009–01–0622. ISSN: 1946-3944. DOI: 10.4271/2009-01-0622. URL: https://www.sae.org/content/2009-01-0622/ (cit. on pp. 12, 15).

[49] C. D. Rakopoulos and E. G. Giakoumis. "Review of Thermodynamic Diesel Engine Simulations under Transient Operating Conditions." *SAE Technical Paper Series* (2006). ISSN: 0148-7191. DOI: 10.4271/2006-01-0884. URL: http://papers.sae.org/2006-01-0884/https://www.sae.org/content/2006-01-0884/ (cit. on pp. 12, 68).

[50] L. Cornolti, A. Onorati, T. Cerri, G. Montenegro, and F. Piscaglia. "1D simulation of a turbocharged Diesel engine with comparison of short and long EGR route solutions." *Applied Energy* 111 (2013), pp. 1–15. ISSN: 03062619. DOI: 10.1016/j.apenergy.2013.04.016. URL: http://dx.doi.org/10.1016/j.apenergy.2013.04.016 (cit. on pp. 13, 89).

[51] C. D. Rakopoulos, A. M. Dimaratos, E. G. Giakoumis, and D. C. Rakopoulos. "Evaluation of the effect of engine, load and turbocharger parameters on transient emissions of diesel engine." *Energy Conversion and Management* 50(9) (2009), pp. 2381–2393. ISSN: 01968904. DOI: 10.1016/j.enconman.2009.05.022. URL: http://dx.doi.org/10.1016/j.enconman.2009.05.022 (cit. on p. 13).

[52] J. Galindo, J. Luján, J. Serrano, V. Dolz, and S. Guilain. "Description of a heat transfer model suitable to calculate transient processes of turbocharged diesel engines with one-dimensional gas-dynamic codes." *Applied Thermal Engineering* 26(1) (2006), pp. 66–76. ISSN: 13594311. DOI: 10.1016/j.applthermaleng.2005.04.010. URL: https://linkinghub.elsevier.com/retrieve/pii/S1359431105001353 (cit. on p. 14).

[53] C. D. Rakopoulos, E. G. Giakoumis, D. T. Hountalas, and D. Rakopoulos. "The Effect of Various Dynamic , Thermodynamic and Design Parameters on the Performance of a Turbocharged Diesel Engine Operating under Transient Load Conditions." *SAE International* (724) (2004). DOI: 10.4271/2004-01-0926 (cit. on p. 14).

[54] C. Rakopoulos, E. Giakoumis, and D. Rakopoulos. "Cylinder wall temperature effects on the transient performance of a turbocharged Diesel engine." *Energy Conversion and Management* 45(17) (2004), pp. 2627–2638. ISSN: 01968904. DOI: 10.1016/j.enconman.2003.12.014. URL: https://linkinghub.elsevier.com/retrieve/pii/S0196890404000111 (cit. on p. 14).

[55] C. Rakopoulos, A. Dimaratos, E. Giakoumis, and M. Peckham. "Experimental Assessment of Turbocharged Diesel Engine Transient Emissions during Acceleration, Load Change and Starting." *SAE Technical Paper Series* 1 (2010). DOI: 10.4271/2010-01-1287 (cit. on pp. 14, 55).

[56] H. Kang and P. V. Farrell. "Experimental investigation of transient emissions (HC and NOx) in a High Speed Direct Injection (HSDI) diesel engine." *SAE Technical Papers* (724) (2005). ISSN: 26883627. DOI: 10.4271/2005-01-3883 (cit. on p. 14).

[57] S. Park, T. Matsumoto, and N. Oda. *Numerical analysis of turbocharger response delay mechanism*. Tech. rep. SAE Technical Paper, 2010 (cit. on p. 14).

[58] J. Shutty, H. Benali, L. Daeubler, and M. Traver. "Air System Control for Advanced Diesel Engines." In: *Numerical Analysis - Theory and Application*. 2007. DOI: 10.4271/2007-01-0970. URL: https://www.sae.org/content/2007-01-0970/ (cit. on p. 15).

[59] J. Deng, R. Stobart, C. Liu, and E. Winward. "Explicit Model Predictive Control of the Diesel Engine Fuel Path." In: *SAE Technical Papers*. 2012. DOI: 10.4271/2012-01-0893. URL: https://www.sae.org/content/2012-01-0893/ (cit. on p. 15).

[60] F. Tschanz, A. Amstutz, C. H. Onder, and L. Guzzella. "Feedback control of particulate matter and nitrogen oxide emissions in diesel engines." *Control Engineering Practice* 21(12) (2013), pp. 1809–1820. ISSN: 09670661. DOI: 10.1016/j.conengprac.2012.09.014. URL: https://linkinghub.elsevier.com/retrieve/pii/S0967066112001979 (cit. on p. 15).

[61] A. G. Stefanopoulou, I. Kolmanovsky, and J. S. Freudenberg. "Control of variable geometry turbocharged diesel engines for reduced emissions." *Proceedings of the American Control Conference* 3(4) (1998), pp. 1383–1388. ISSN: 07431619. DOI: 10.1109/ACC.1998.707043 (cit. on p. 15).

[62] P. Ortner and L. del Re. "Predictive control of a diesel engine air path." *IEEE Transactions on Control Systems Technology* 15(3) (2007), pp. 449–456. ISSN: 10636536. DOI: 10.1109/TCST.2007.894638 (cit. on p. 15).

[63] B. Haber and J. Wang. "Robust control approach on diesel engines with dual-loop exhaust gas recirculation systems." In: *ASME 2010 Dynamic Systems and Control Conference*. American Society of Mechanical Engineers Digital Collection. 2010, pp. 711–718 (cit. on p. 15).

[64] J. Chauvin, O. Grondin, and P. Moulin. "Control Oriented Model of a Variable Geometry Turbocharger in an Engine with Two EGR Loops." *Oil & Gas Science and Technology – Revue d'IFP Energies nouvelles* 66(4) (2011), pp. 563–571. ISSN: 1294-4475. DOI: 10.2516/ogst/2011103. URL: http://ogst.ifpenergiesnouvelles.fr/10.2516/ogst/2011103 (cit. on p. 15).

[65] D. Alberer and L. del Re. "Optimization of the transient Diesel engine operation." In: *SAE Technical Paper Series*. Vol. 1. 2009. DOI: 10.4271/2009-24-0113. URL: https://www.sae.org/content/2009-24-0113/ (cit. on p. 15).

Chapter 2

Analysis of driving cycles

Contents

2.1 Introduction

For a type approval process, different countries use different cycles to test an engine for the performance and emission measurements. Driving cycles like NEDC, FTP, EPA are one of them. The cycle which was designed to represent the typical driving behavior of a car in Europe, is composed by four repetitions of the Urban Driving Cycle (UDC) and an Extra Urban Driving Cycle (EUDC). The first Urban Driving Cycle (UDC) was introduced in 1970 under the United Nations Economic Commission for Europe (UNECE) vehicle regulation program. The Extra-Urban Driving Cycle EUDC was introduced by ECE in 1990 to represent more aggressive, high speed driving modes. This combination of UDC and EUDC was known as MVEG-A cycle that was used for EU type approval testing of emissions and fuel consumption in light duty vehicles until 2000. After 2000, the cycle was modified by removing the initial idling period at the engine start by including cold start emission sampling from the beginning of the cycle. This modified cold-start procedure is referred to as the New European Driving Cycle (NEDC) or as the MVEG-B test cycle.[66].

The WLTC is a World-wide harmonized Light duty Test Cycle which was developed under the working party on pollution and energy (GRPE) by countries playing a crucial part in automotive industry. The main objective was to design the harmonized driving cycle from unified 'real world' driving database collected from different regions around the world [67]. Although, the standardization of this cycle for homologation process is still under discussion, it is acknowledged as well representative of on road real driving conditions. These cycles are used for standard procedure and predefined surrounding conditions. The operating range was fixed with standard driving behavior for respective country. But in recent years, new concepts regarding driving cycles are becoming popular. Unlike the old cycles, their driving behavior is close to real driving conditions with dynamic nature.

Apart from WLTC, the successful validation of portable emission measurement system (PEMS) enabled the measurement of the tailpipe emission while driving a vehicle on road. This leaded the way to develop new procedure for measurement and validation of a vehicle emissions on actual road with certain constraints which is also called as Real Driving Emissions (RDE). Retrospectively, a new emerging driving procedures are demanding modern engines to go through wide operating range unlike in NEDC cycle.

This chapter introduces the three main driving cycles governing the automotive industry these days. It focuses on statistical analysis of those old and new driving cycles on the basis of their dynamics and operating ranges on an engine. It acts as the preparation for the further studies in this thesis. It encompasses the identification and classification of different transient operations and their trends over the whole cycle. The pollutant formation (NO_x) and variation for each cycle is assessed, finding a correlation with the type of operation (Tip-In and Tip-Out). A vehicle model is used to calculate the torque demands at particular speeds which were used as targets to the test bench control system. A full test cycle run has been made on various driving cycles like NEDC, WLTC, RDE. Engine out emissions like NO_x, CO_2, HC etc. were measured with Horiba gas analyzer downstream of the turbine. The comparison of those three driving cycles is presented at the end of the chapter highlighting the potential of representing real driving conditions.

2.2 Driving cycles

The characteristics of the each driving cycle used in this chapter are as follow,

2.2.1 NEDC

The well known New European Driving Cycle also known as MVEG-B is used since EURO 3 regulations with deletion of idle 40s at the beginning of the cycle. The total duration of this cycles is 1180s covering 10.9 km length on the road. The average speed of this cycle is 43.1 km/h. It has two parts which are called as 'Urban' and 'Extra Urban' part. As name suggests, the 'Urban' part represents the city driving conditions while the 'Extra Urban' part represents the driving situation outside of the city. Figure 2.1 represents the vehicle velocity profile for the whole NEDC cycle.

2.2.2 WLTC

The newly developed Worldwide Harmonized Light duty cycle is the new cycle developed to represent the driving conditions all over the world. This cycle lasts for 1800s covering 23.25 km on road. The average speed of the WLTC

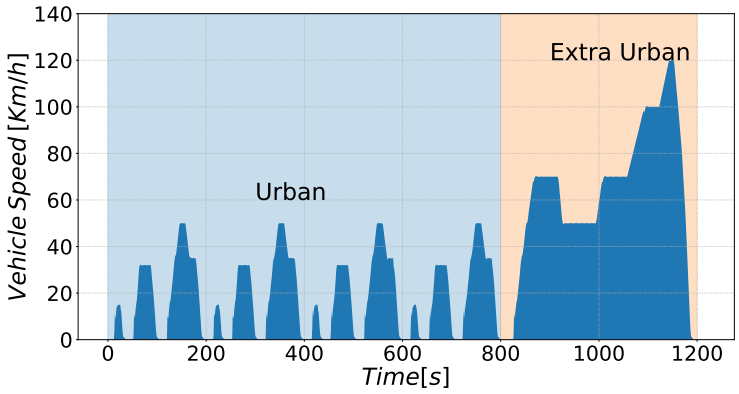

Figure 2.1: Vehicle speed profile for NEDC cycle.

cycle is 53.76 km/h. It consists 4 different parts classified as per the vehicle speed. They are called as 'Low', 'Medium', 'High' and 'Extra High'. Figure 2.2 represents the vehicle speed profile in km/h. Visually, it can be seen that this cycle has some sudden acceleration as compared to NEDC.

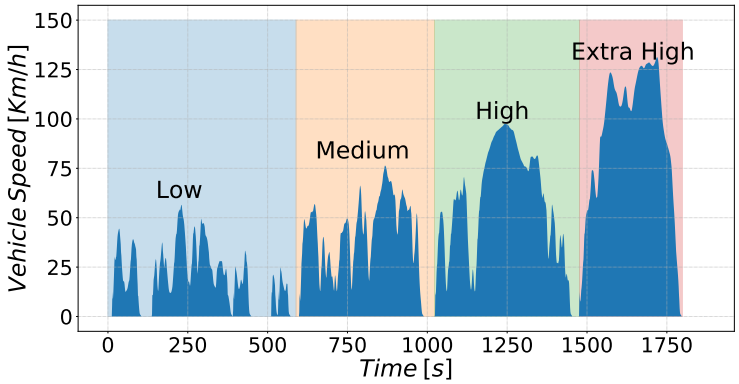

Figure 2.2: Vehicle speed profile for class 3b WLTC cycle cycle.

2.2.3 RDE

As discussed earlier, Real Driving Emissions (RDE) are not measured on a vehicle test bed with specific driving cycle. The emission measurement is done on road with portable emission measurement system (PEMS). A wide

range of engine loads, vehicle speeds and ambient temperature and pressure differences have to be covered by a real driving route to validate the trip. The trip requirements required for the valid RDE tests are shown in the Table 2.1. For this reason, an actual vehicle speed demand was measured on a vehicle for different routes in Valencia (Spain) in a test campaign, complying with the real driving constraints framed by European Union. Figure 2.3 displays the selected driving cycle with urban, rural motorway part. The collected data is processed and validated in the next sections by average and dynamic conditions of the cycle.

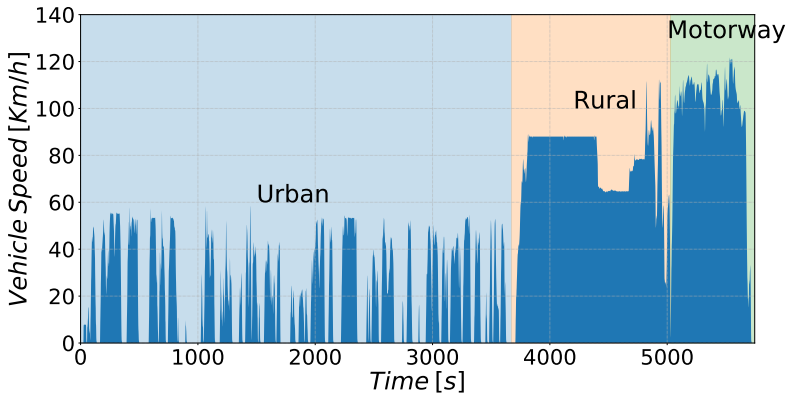

Figure 2.3: The vehicle speed profile in km/h for a real driving road trip measurements done on road with urban, rural and motorway parts.

2.2.3.1 Trip measurements validation

The analysis and validation of the trip data measurement is done as per the guidelines in [68]. The total time duration of the selected trip is around 5746s ($\sim 96min$), while the total distance travelled is calculated by velocity measurements with 1Hz resolution from 1s to t_t (last second) and number of samples (N_t). For each Δt (here 1s), the distance covered d_i is calculated by

$$d_i = \frac{v_i}{3.6}; \quad i = 1 \quad to \quad N_t \tag{2.1}$$

Where v_i is vehicle speed in km/h. This vehicle speed data is used to divide the measured data into different part like urban, rural and motorway operation. Table 2.1 represents the classification and requirements of these different

operations. The total distance travelled by the vehicle during the selected trip is 69.186 km, while distance covered during each part is calculated by velocities and number of samples for the corresponding portion of trip. Therefore, distance travelled during urban, rural and motorway part trip is equal to 23.586, 25.347 and 20.251 km with share of 34.09%, 36.63% and 29.27% respectively.

Trip Requirements for valid RDE Test			
Driving Portion	Urban ($Speed \leq 60km/h$)	Rural ($60 < Speed \leq 90km/h$)	Motorway ($90km/h < Speed$)
Minimum Distance	16km	16km	16km
Distance Share	29-44%	23-43%	23-43%
Total trip duration		(90-120 min)	
Average speed including stops	15<Avg<40km/h	-	-
Total stop time[1]	6-30% of urban time	-	-
individual stop time	$\leq 300sec$	-	-
v>100km/h	-	-	$\geq 5min$
v>145km/h	-	-	<3% motorway time
Cumulative positive elevation gain		(<1200m/100km)	
Start/end test elevation diff.		($\leq 100m$)	

[1] velocity <1km/h, urban operations may contain several stop periods of 10s or longer.

Table 2.1: The trip requirements for the validation of an RDE cycle.[69]

The acceleration for a i^{th} sample is calculated by the velocities of the next and previous point of the sample by equation 2.2,

$$a_i = \frac{v_{i+1} - v_{i-1}}{2 \cdot 3.6}; \quad i = 1 \quad to \quad N_t \tag{2.2}$$

As mentioned before, the classification of data is done in different bins with respect to velocity. All data sets with $v_i \leq 60km/h$ go to the 'urban' speeds, points with $60km/h < v_i < 90km/h$ belong to the 'rural' while, data sets with $v_i > 90km/h$ are termed as motorway speeds. This is also called as binning of the results. For every bin, the average speed ($\bar{v_k}$) is calculated as follows,

$$\bar{v_k} = \frac{\left(\sum_i^{N_k} v_{i,k}\right)}{N_k}; \quad k = u, r, m \tag{2.3}$$

Where, N_k is the total number of samples of the urban (u), rural (r) and motorway (m) shares. The average vehicle speeds for urban, rural and motorway parts of the selected real driving trip are 21.678, 79.764 and 106.431 km/h respectively.

2.2.3.2 Verification of trip dynamics

Apart from validating global parameters, the measured data should also pass some dynamic constraints. The driving dynamics of the real driving measurements should be within following limits.[68]

1. Excessive driving dynamics using the $v.a+$ (velocity times positive acceleration):

   The 95^{th} percentile ($(v.a+)_{[95]}$) for urban, rural and motorway portion of the trip should not exceed limiting maximum $v.a+$ values which are calculated by,

   $$max(v.a+) = 0.136 \cdot v + 14.44 \quad for \quad v \leq 74.6 \quad km/h \tag{2.4}$$

   $$max(v.a+) = 0.136 \cdot v + 14.44 \quad for \quad v > 74.6 \quad km/h \tag{2.5}$$

2. Insufficient driving dynamics using the RPA (Relative Positive Acceleration):

   Relative positive acceleration values for each portion of the trip should not be below than limiting minimum RPA values which are calculated by,

   $$min(RPA) = -0.0016 \cdot v + 0.1755 \quad for \quad v \leq 94.05 \quad km/h \tag{2.6}$$

   $$min(RPA) = 0.025 \quad for \quad v > 94.05 \quad km/h \tag{2.7}$$

Where $(v.a+_i)$ values are the products of velocity and acceleration of i^{th} sample who has the acceleration greater than $0.1m/s^2$ for urban, rural and motorway share. $(v.a+)_{[95]}$ is the 95^{th} percentile of the $v.a+$ values for each portion of the trip, calculated from the data set obtained by the vehicle speeds and the positive accelerations. The total number of samples (M_k) for each bin with positive acceleration is determined, to compute the 95^{th} percentile for respective bins. The process of calculating this 95^{th} percentile involves, ranking the $v.a+$ values in ascending order and then assigning the percentile values from $1/M_k$ (lowest value) to M_k/M_k (Highest value). The highest value has percentile of 100%. Henceforth, the $v.a+$ value having percentile of 95% is extracted with $i/M_k = 95\%$. If $i/M_k = 95\%$ cannot be met, $(v.a+)_{[95]}$ should be calculated by linear interpolation between consecutive samples i and i + 1 with $i/M_k < 95\%$ and $(i+1)/M_k > 95\%$. Figure 2.4 represents the

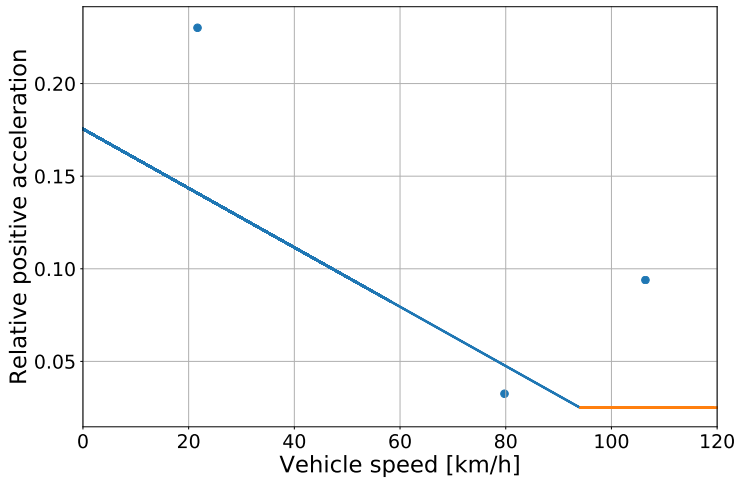

Figure 2.4: 95^{th} percentile of the v.a+ or urban, rural and motorway speeds from real driving cycle with excessive dynamic requirements.

95^{th} percentile of 3 parts of the trip with maximum limitation. The lines are nothing but the maximum not to exceed limit for $(v.a+)_{[95]}$ depending on the velocity of the vehicle described in the equation 2.4 and 2.5.

The second condition of dynamic validation of the data involves relative positive acceleration for each zone of the cycle. The RPA values for each portion of the trip are calculated by following equation,

$$RPA_k = \frac{\sum_{i=1}^{M_k} (\Delta t \cdot (v \cdot a+)_{i,k})}{\sum_{i=1}^{N_k} d_{i,k}} \quad k = u, r, m \tag{2.8}$$

Figure 2.5 represents the calculated RPA for different portions of the RDE cycle with the minimum limit which should be followed to validate the real driving trip. The RPA from urban and motorway portions are higher than the minimum limit except the rural part. i.e. this cycle is not that dynamic for the rural part of the trip. However, it could be analysed for other 2 parts as they are in limits.

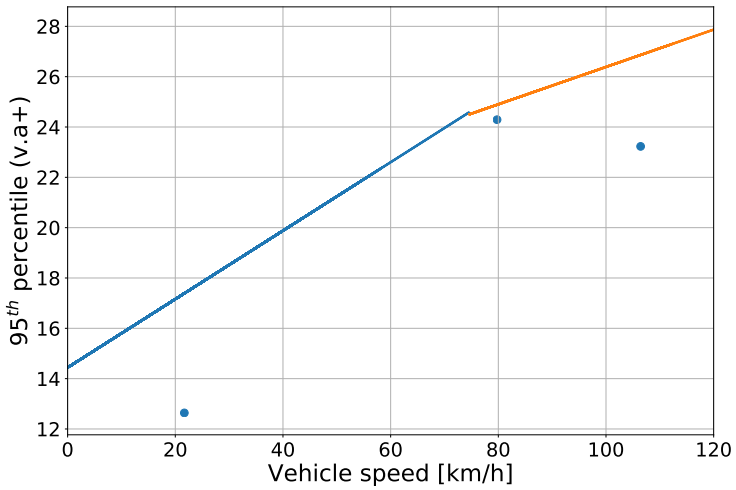

Figure 2.5: RPA of urban, rural and motorway section of real driving cycle with sufficient trip dynamic requirements.

2.3 Vehicle Model

The vehicle moving on road experiences different forces apart from the driving force to propagate the vehicle. The resultant traction force (F_b) is calculated by the equation 2.9.

$$F_b = F_r + F_{st} + F_L + F_B \tag{2.9}$$

Where F_r, F_{st}, F_L and F_B are the the rolling, slope, aerodynamic and acceleration resistance forces respectively. The free body diagram of a vehicle of mass (m) moving with acceleration $\ddot{x}$ on a road with slope α is shown in 2.6, with vectorial representation of forces acting on it. The rolling resistance is the force exerted by road on vehicle and is calculated by rolling coefficient (f_r) and the *cosine* component of vehicle weight by equation 2.10. The slope resistance is the force component exerted by the weight of vehicle in the direction opposite to the motion of vehicle. This resistance is calculated with the mass and sine component of slope angle α (2.11). The aerodynamic resistance is the important force dependant on the relative velocity of vehicle w.r.t. wind. This force is calculated by the equation 2.12 by density of air (ρ), the coefficient of drag (c_w) and the frontal area of vehicle (A) multiplied by square of a relative velocity of the vehicle. The vehicle velocity is $\dot{x}$ and wind velocity is $\dot{x}_w$.

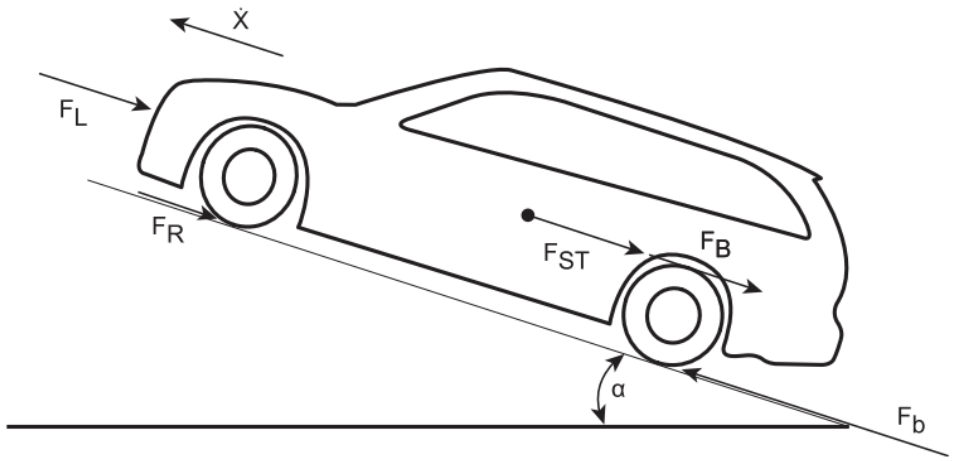

Figure 2.6: Force diagram of vehicle moving with acceleration.

Finally, the acceleration resistance force F_B represents d'Alembert's principle of inertial force on the vehicle. This is calculated by the acceleration and the inertia factor λ by the equation 2.13.[70]

$$F_r = mgcos(\alpha) \tag{2.10}$$

$$F_{st} = mgsin(\alpha) \tag{2.11}$$

$$F_L = \frac{1}{2} c_w A \rho_L (\dot{x} - \dot{x}_w)^2 \tag{2.12}$$

$$F_B = m\lambda\ddot{x} \tag{2.13}$$

The vehicle speed and gear ratios along with vehicle parameters are used as inputs to calculate the engine torque demand at particular engine speed. This torque demands were fed to the engine dynamometer control as targets. The main characteristics of vehicle model regarding aerodynamic coefficients and power train ratios are given in the table 2.2. The detailed information about the experimental setup used for the tests is presented in the chapter 3.

Parameter	Value
Vehicle Mass [kg]	1430
C_w	0.3
$\rho[kg/m^3]$	1.2
$A[m^2]$	2.8

Table 2.2: Vehicle specifications used for the vehicle model with given diesel engine.

2.4 Analysis

This section consists analysis of different driving cycles (NEDC, WLTC and RDE), performed on dynamic engine test bench. Vehicle model described in the previous section is used to input the engine torque and speed target for the dynamometer control. Various engine parameters like torque, speed, gear ratios along with emissions and actuator movements like EGR valves and VGT were recorded during the tests. The derivatives of engine torque and speed with respect to every second in the driving cycle are calculated for each driving cycle. This derivative arrays are used to analyse and compare the dynamics of these cycles.

$$\frac{\delta(Torque)}{\delta(Time)} \; and \quad \frac{\delta(Speed)}{\delta(Time)}, \quad where \quad \delta(Time) = 1s \tag{2.14}$$

The positive load change (torque change) is called as the Tip-In operation while the negative one is termed as Tip-Out operation. The frequency of occurrence and location on the engine map for these operations is identified for particular driving cycle. Moreover, the probability of 'load' and 'speed' transients is also assessed for given cycles. Apart from classification and identification of the different transient types, the driving cycles are compared at the end on the basis of newly calculated parameters representing dynamic behavior of the driving cycle.

2.4.1 NEDC

Figure 2.7 represents the measured engine parameters for NEDC cycle. The blue fill plot is the vehicle speed profile during the test run. The top gray plot is the engine torque measured on engine dynamometer throughout the cycle,

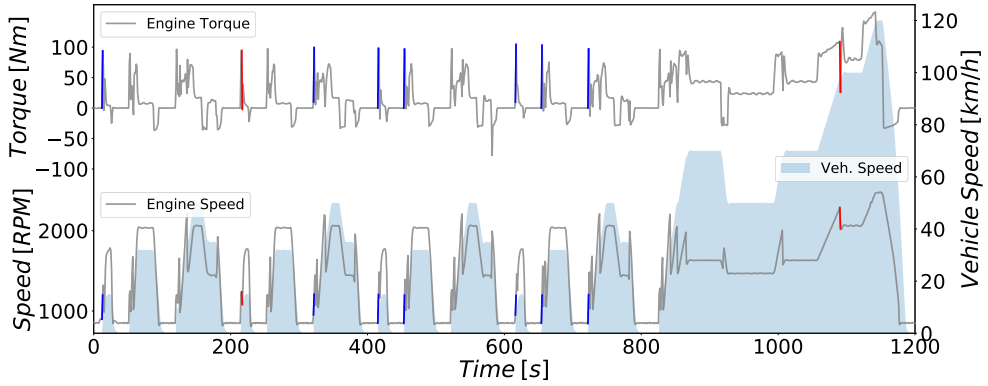

Figure 2.7: NEDC Cycle profile with torque and speed of turbocharged 2 lit. diesel engine and representation of harsh transient Tip-In (blue) and Tip-Out (red) operations with absolute torque change of more than 80Nm. The time interval for this change in torque in 1s.

while the bottom gray plot is engine speed in RPM. The discreet changes in engine torque for every 1 second are calculated separately in the successive operating points on the driving cycle. The engine torque transitions higher than absolute 80 Nm are plotted along with the change in engine speed for the same. The lines in red color represent transients with negative torque change while the lines in blue color are positive change. As it can be seen,

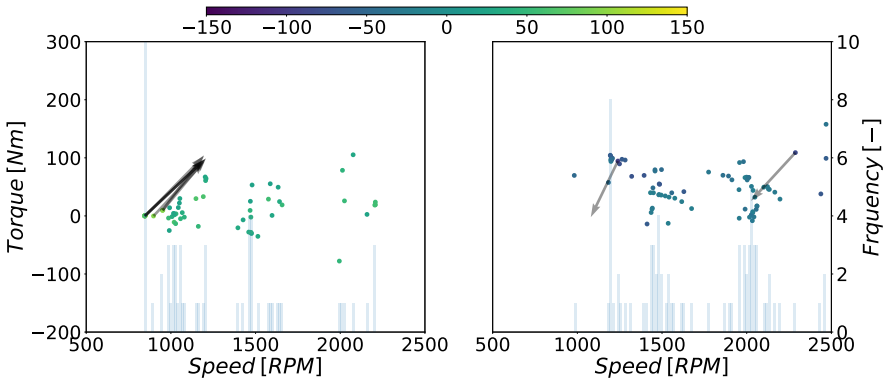

Figure 2.8: Harsh transient operation Tip-In (left) and Tip-Out (right) in NEDC cycle with torque change more than 20 Nm (points) and the harsh transients with torque change more than 80 Nm. (arrows)

there are very few transient operations consisting positive torque change higher than absolute 80 Nm. Only 7 positive torque change higher than 80 Nm are seen on urban driving zone. The respective change in engine speed is also reasonable which signifies the change in gear for those particular transitions. On the other hand, only 2 Tip-Out transients are seen with torque change less than -80Nm. Their vertical nature signifies that they are very close to load transient with very less change in engine speed.

The same few harsh engine transient on the NEDC cycle are plotted on the engine map in the figure 2.8. The nature of this As per the analysis, the NEDC cycle is not that dynamic owing to the very less number of transient operations across whole driving cycle considering EUDC zone too.

2.4.2 WLTC

Figure 2.9 shows a test run of typical class 3 WLTC cycle with urban and extra Urban part. The blue fill in portion in the plot represents vehicle speed in kilometers per hour while gray curves shows an engine torque and engine speed across the cycle. The portions marked in red and blue lines on each variable plot are actually the changes in discreet values of respective variables in 1 second with exceptional torque change greater than 80 Nm (blue) or less than -80 Nm (red). As you can imagine, with a change in absolute torque more than 80 Nm (which is equal to change in MEP of around 4 bar) is surely a harsh change of state for a steady running engine but the interesting fact that could be seen is the engine speed doesn't responds with the similar amount of changes like torque. The red lines (for Tip-In) and blue line (Tip-Out) from the top plot are seems to be points in the bottom plot of engine speed.

To identify the engine speed ranges where these transient operations are frequent, all the operating points of the WLTC cycle undergoing change in absolute torque more than 20 Nm are plotted on the engine map.(see Figure 2.10) The colour scheme of the points represents a change in engine torque between current and the successive operating point on the cycle. The transients mentioned above with absolute torque change more than 80 Nm are represented with arrows pointing towards the direction of change in torque or MEP of the engine. The frequency of Tip-In operations is higher than Tip-Out operations. The vertical nature of arrows confirms the behavior of these transients as load transients. Although most of the transients are spread

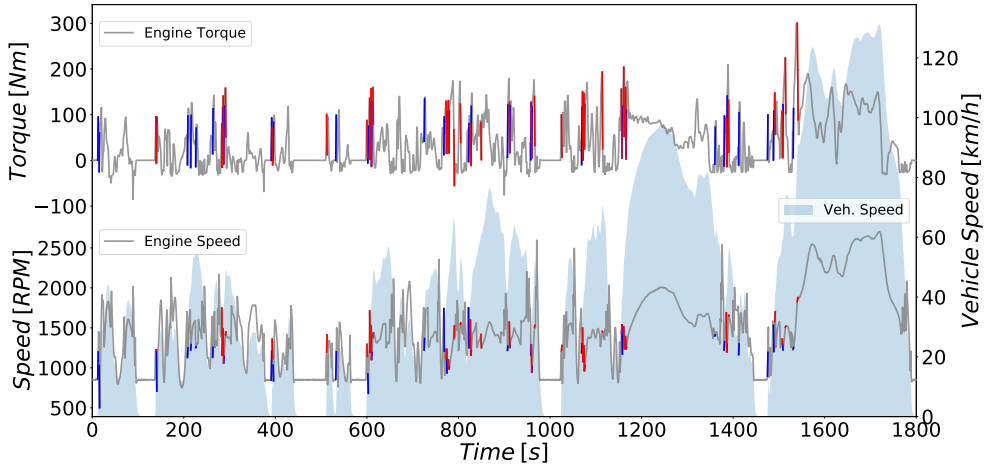

Figure 2.9: WLTC Cycle profile with torque and speed of turbocharged 2 lit. diesel engine and representation of harsh transient Tip-In (blue) and Tip-Out (red) operations with absolute torque change of more than 80Nm. The time interval for this change in torque in 1s.

over the range from 800 to 2250 RPM, the frequency of typical harsh Tip-In transients on WLTC cycles is higher at 1250 RPM while the harsh Tip-Out operations are spread over the higher engine RPM. The normal Tip-In oper-

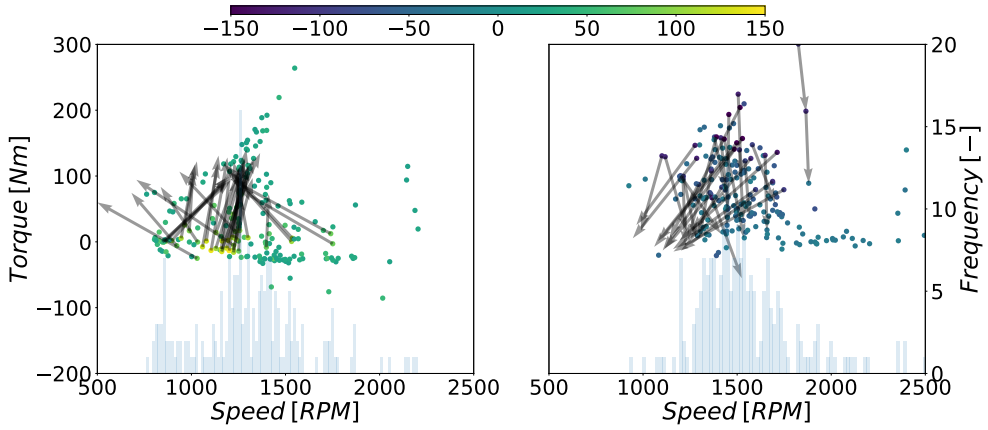

Figure 2.10: Harsh transient operation Tip-In (left) and Tip-Out (right) in WLTC cycle with torque change more than 20 Nm (points) and the harsh transients with torque change more than 80 Nm. (arrows)

ation points are accumulated in the range from 1000 to 2000 RPM. No harsh Tip-In transients detected in the negative torque zone, while only one of them is present among Tip-Out operations.

As compared to NEDC cycle analysis, WLTC cycle seems more dynamic with various transient operations across whole driving cycle. Most of the harsh transients operations are load transients at particular constant engine speeds.

2.4.3 RDE

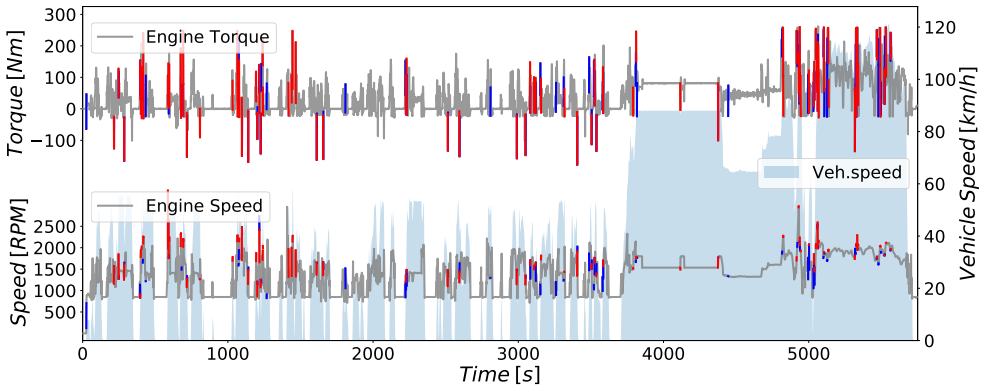

Figure 2.11: Real driving cycle profile with torque and speed of turbocharged 2 lit. diesel engine and representation of harsh transient Tip-In (blue) and Tip-Out (red) operations with absolute torque change of more than 80Nm. The time interval for this change in torque in 1s.

The engine torque and engine speed measured on above RDE cycle are plotted in Figure 2.11 with similar methods used for WLTC analysis. The harsh transients represented by the red and blue lines here have absolute values more than 100 Nm as the time between successive operating point is 1 second. The number of harsh load transients is more than the WLTC cycle. The big change in engine torque is accompanied by the small change in engine speed, as the time between the successive operating points is greater than 0.1 s unlike WLTC and NEDC.

The frequency of occurrence of these transients can bee seen on the engine map in Figure 2.12. The high frequency range for Tip-in and Tip-Out operations is from 1000 to 2000 RPM. The inclined arrows represent the transient

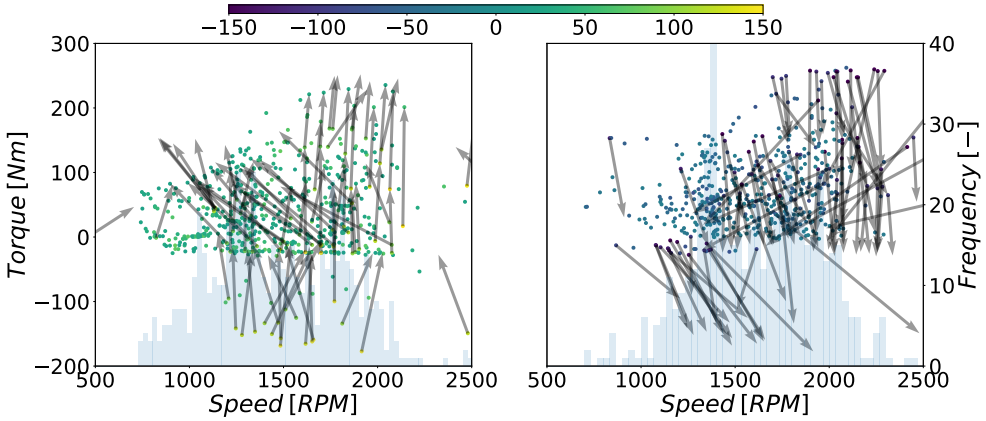

Figure 2.12: Harsh transient operation Tip-In (left) and Tip-Out (right) during real driving cycle with torque change more than 20 Nm (points) and the harsh transients with torque change more than 80 Nm. (arrows)

from gear change, while vertical arrows represent the load transient operation at the same gear. Unlike WLTC, the frequency of Tip-Out operations is higher than Tip-Ins. Moreover, there are harsh transient present in the negative torque zone too. Most of them are starting point of harsh change in engine torque.

2.4.3.1 Extended analysis of RDE

As the process of measurement of data on road is costly and time taking, additional mathematical approach has been used to analyse the engine behavior in dynamic cycles. An algorithm (using probability) generated by TNO (Netherlands) using *Markov chains* has been used to create a virtual real driving speed profile with different driving behaviors.[71][72] Around 90 real driving cycles fulfilling the requirements of Regulations 2016/646 was generated for the transient analysis. A 2-D histogram in Figure 2.13 shows the frequency of those 90 real driving cycles on a engine map with bin size of 100 RPM and 2 bar BMEP. Most of the operating points lie between 1200 to 2000 RPM. For every cycle, the change in BMEP w.r.t. change in engine speed is calculated for every dt of 0.1 seconds like WLTC cycle. Evidently, during transients, if there is a gear change, the speed of engine also changes with considerable amount till $\pm$ 1500 RPM. These type of transient operations are termed as speed transients. The

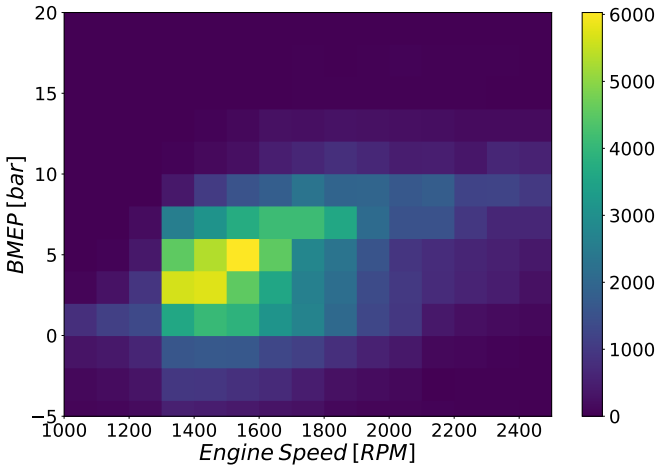

Figure 2.13: 2-D histogram of engine operating points from the randomly generated 90 real driving cycles from TNO algorithm.

frequency of these load transient operations is 1000 times higher than to speed transients.

2.5 Comparison of the cycles

The change in engine torque and speed per second across the driving cycles gives an idea about the dynamics of the driving conditions. Actually these values depend on different driving behaviors of vehicle drivers. For example, the aggressive driving can create severe dynamics and have different emissions than steady and calm driving.[30] The number and the timing of gear change also affects the engine operating conditions as discussed in the real driving cycle section. However, this kind of analysis can give the basic idea about the transients occurred by road condition not considering the driving behavior. Table 2.3 shows the tabular comparison of the variables like total duration and distance of the driving cycles. Average and maximum change in engine torque and speed in one second can portray the engine transient behavior. According to the table, the maximum change in torque and engine speed values are greater in WLTC than the NEDC cycle. They are even more for

RDE cycles. Average absolute change in torque also shows the similar traits among the 3 cycles. However this average change in torque value for WLTP cycle is falls in the negative side, while average for NEDC and RDE cycles is inclined to the positive side. i.e. there could be many ascending transient operations in RDE and NEDC cycles compared to WLTC.

Performance	NEDC	WLTC	RDE
Duration [s]	1200	1844	5746
Distance [km]	11.12	23.106	69.186
Max Speed [km/h]	120	131.2	121.76
Max. dT (TipIn) [Nm/s]	103.15	154.33	184.42
No. Harsh TipIn/TipOut per km	0.63/0.18	1.64/1.43	1.1/1.2

Table 2.3: Comparison of different features of NEDC, WLTC and RDE cycles.

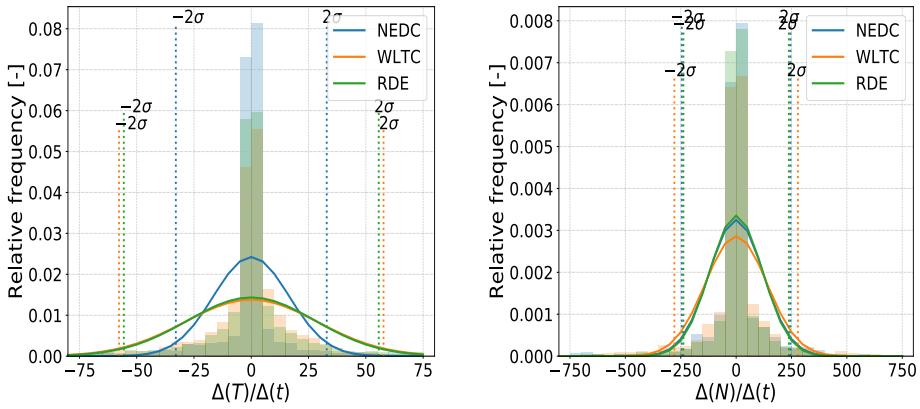

(a) Engine torque (b) Engine speed

Figure 2.14: Comparison of different driving cycles on the basis of change in engine speed with respective to time.

Figure 2.14 represent the graphical comparison of dynamics of the above driving cycles. The histogram of relative frequencies of each cycle transient operations (with change in torque and speed with respect to time (1s)) shows the large amount of operations involves changes in torque and speed close to 0. The relative frequency is calculated by dividing counts by the number of observations times the bin width of histogram. The bin width for all cycles

is kept same for comparison[1]. The curves represent the probability density function (Normal distribution) derived from the number of bins, average and standard deviation of the cycle data. The Σ denotes the standard deviation of the variable.

The 2σ limit for the operations representing the 95% confidence for each cycle to fall in the respective limits is shown as the dotted line. According to the Figure 2.14(a), 95% of NEDC cycle operations involve torque change of around 34 Nm in a second while the WLTP and RDE cycles have more points with higher torque change up to 60-70 Nm. The spectrum of changes in engine torque is widely spread for dynamic cycles unlike NEDC who's bell curve is observed with high frequency at the center than other cycles. Naturally the WLTP and RDE cycles are more dynamic and seem to be having almost similar 2σ limits. On the other hand, the change in engine speed in Figure 2.14(b) does not show noticeable difference between cycles. As per the given vehicle model, the NEDC and RDE cycles have very similar curve of normal distribution with higher frequency close to zero. The steady rural part in the giver RDE cycle must be the reason behind the higher frequency of no change in engine speed. Although the WLTP cycle spectrum is little wider than the other two, the 2σ limit is not higher than change in 50 rpm.

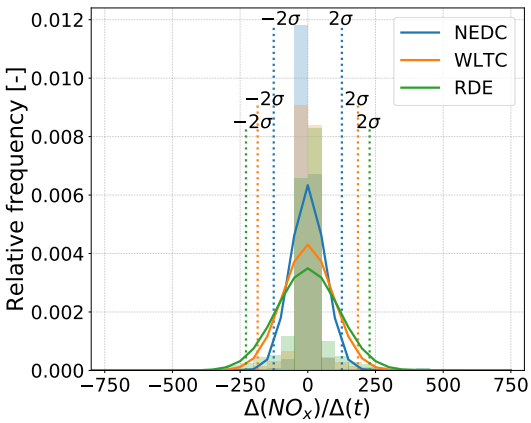

Figure 2.15: Comparison of different driving cycles on the basis of change in NO_x measurements with respective to time.

The NO_x measurements are also analysed with the same method. The

[1]bin width for torque change histogram is 5 Nm and the bin width for speed change histogram is 50 rpm

changes in the NO_x measurements are not related to above load transient operation as the measurements involves the time delays (explained in chapter 3). Macroscopically the change in the NO_x measurements for each second with different driving cycle (see Figure 2.15) correspond with the dynamics. NEDC cycle involves the 95% change in NO_x values till 13ppm per second while WLTP and RDE cycles have up to 200 and 250 ppm. The RDE spectrum is widely spread for the change in NO_x measurements.

The rough origin of the high NO_x values from these transient can be found by plotting the change in torque and change in speed giving the NO_x change more than 100 ppm in Figure 2.16. The number of points succeeding this criteria are very few in the NEDC case. The vertical nature of dense points shows that most of the responsible transient for the higher NO_x change are load transients with minimum change in engine speed. The change in NO_x for WLTP and RDE cycles are higher than 800-900 ppm at some points which are not found in the NEDC plot.

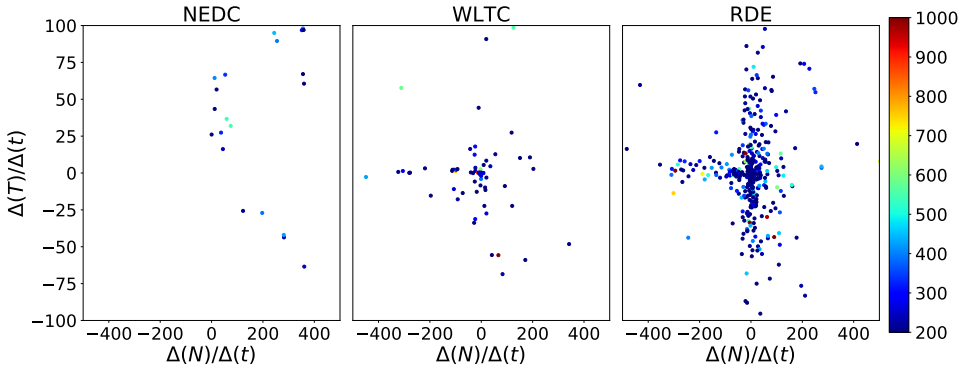

Figure 2.16: Change in NO_x concentration in the exhaust line roughly related to change in engine speed and torque for different driving cycles.

2.6 Conclusion

Highly dynamic driving cycles like WLTC and RDE have been performed on same vehicle and engine to analyse the engine operating condition from a view of transient operations. The load transient operation with a load change at particular engine speed are found to be frequent on these dynamic driv-

ing cycles. The WLTC cycle consists of more harsh transient operations per kilometer than the specified RDE cycle in this study. Although engine operating condition during real driving cycles depends on the driving behavior and other road characteristics, it can be seen that load transient operations at same gear/engine speed are way higher than the speed transient operation due to gear change as per the TNO based real driving speed profiles and gear patterns. The number of harsh Tip-Out operations with are always higher than harsh Tip-In transients on RDE cycles. Around 85% load transient Tip-In operations occur in the range of 1000-2000 rpm. While the same range includes almost 80% of all the Tip-Out operations sharing 60% of them in 1500-2000 rpm. In general Tip-Out operations are more spread over the higher engine speed range than the Tip-Ins. During WLTC, the large number of harsh Tip-Ins/transients occur around 1250 rpm. The similar trend is observed in real driving cycle too, however considerable amount of load-increasing transients cover the range from 1000 to 2000 rpm compared to WLTC cycle.

Chapter 2 Bibliography

[30] R. A. Varella, M. V. Faria, P. Mendoza-Villafuerte, P. C. Baptista, L. Sousa, and G. O. Duarte. "Assessing the influence of boundary conditions, driving behavior and data analysis methods on real driving CO2 and NOx emissions." *Science of the Total Environment* 658 (2019), pp. 879–894. ISSN: 18791026. DOI: 10.1016/j.scitotenv.2018.12.053. URL: https://doi.org/10.1016/j.scitotenv.2018.12.053 (cit. on pp. 9, 43).

[66] E. Directive. "90/C81/01,"Emission Test Cycles for the Certification of light duty vehicles in Europe", EEC Emission Cycles, 1999" (). URL: https://dieselnet.com/standards/cycles/index.php (cit. on p. 28).

[67] M. Tutuianu, P. Bonnel, B. Ciuffo, T. Haniu, N. Ichikawa, A. Marotta, J. Pavlovic, and H. Steven. "Development of the World-wide harmonized Light duty Test Cycle (WLTC) and a possible pathway for its introduction in the European legislation." *Transportation Research Part D: Transport and Environment* 40 (2015), pp. 61–75. ISSN: 13619209. DOI: 10.1016/j.trd.2015.07.011. URL: http://dx.doi.org/10.1016/j.trd.2015.07.011 (cit. on p. 28).

[68] European Parliament and Council of the European Union. "Commission Regulation (EU) 2016/427 of 10 March 2016 amending Regulation (EC) No 692/2008 as regards emissions from light passenger and commercial vehicles (Euro 6) (Text with EEA relevance)." *Official journal of the European Union* 82(31/03/2016) (2016), pp. 1–98. URL: http://data.europa.eu/eli/reg/2016/427/oj (cit. on pp. 31, 33).

[69] J. Merkisz and J. Pielecha. "Selected remarks about RDE test." *Cobustion Engines* 166(3) (2017), pp. 54–61. DOI: 10.19206/CE-2016-340 (cit. on p. 32).

[70] R. Fischer, F. Küçükay, G. Jürgens, R. Najork, and B. Pollak. *The Automotive Transmission Book*. Springer Cham Heidelberg New York Dordrecht London, 2015. ISBN: 10.1007/978-3-319-05263-2 (cit. on p. 36).

[71] Q. Gong, S. Midlam-Mohler, V. Marano, G. Rizzoni, and Y. Guezennec. "Statistical analysis of PHEV fleet data." *2010 IEEE Vehicle Power and Propulsion Conference, VPPC* (2010), pp. 1–6. ISSN: 1938-8756. DOI: 10.1109/VPPC.2010.5729224 (cit. on p. 42).

[72] T. Donateo and M. Giovinazzi. "Building a cycle for Real Driving Emissions." *Energy Procedia* 126 (2017), pp. 891–898. ISSN: 18766102. DOI: 10.1016/j.egypro.2017.08.307. URL: https://doi.org/10.1016/j.egypro.2017.08.307 (cit. on pp. 42, 135).

Chapter 3

Tools and modelling

Contents

3.1 Introduction

This chapter includes, the description of experimental facility, the engine, test benches and other laboratory measurement devices. Moreover, the test procedure for different steady and transient engine operations and analytic tools used for data analysis are explained briefly. The tools used for simulation of transient operations are presented along with the results and studies at the end.

3.2 Engine and test cell

The experimental part of this thesis is carried out on two inline 4 cylinder turbocharged HSDi engines. The main characteristics of the engines are listed in Table 3.1. Both engines are from Renault with the EURO 6 and EURO6d calibrations. The steady state EGR percentages for both the engines are presented on a engine map in the Figure 3.1. The EGR maps of engine 2 is modified as per the requirement for different type of studies in the following chapters.

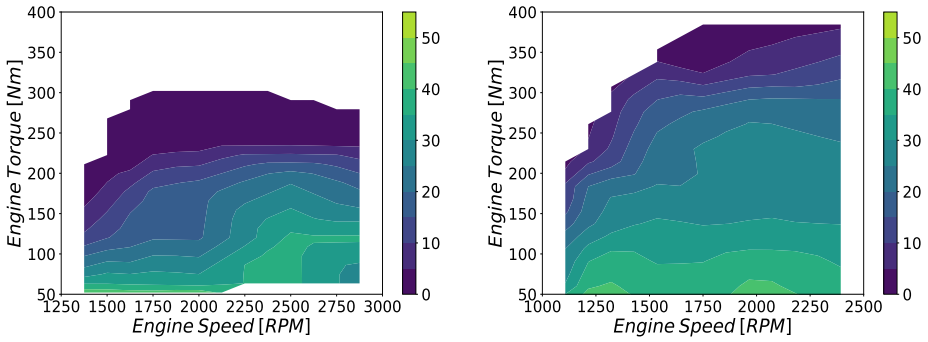

(a) Engine 1 (b) Engine 2

Figure 3.1: EGR percentage for Engine 1 and Engine 2 as per the calibration.

Engine 1 (with old calibration) is used for comparing operating conditions on different driving cycles with a same vehicle model. The charging air is cooled with WCAC, provided with the external water bath to cool the air with longer intake line. The after treatment system includes DOC and DPF.

It consists both HP and LPEGR lines. The HPEGR line was extended with extra heat exchanger to cool the high pressure EGR for certain experiments. The LPEGR is drawn from exhaust line down stream of DPF. Exhaust throttle is also provided to generate a pressure difference across the LPEGR valve and provide high mass flow rates of LPEGR.

Parameter	Engine 1	Engine 2
Cylinder number	4	4
Bore [mm]	85	84
Stroke [mm]	88	90
Displacement [cm^3]	1997	1994
Compression ratio	17.6	15.8
Maximum power [kW/rpm]	120/3750	140/3750
Maximum torque [Nm/rpm]	340/2000	400/1750
Torque at maximum power [Nm]	300	350
Valve number	16	16
Valve train	Double camshaft over head	
Fuel delivery system	Common rail direct injection	
EGR system	HP and LP (cooled)	
Intake boosting	Turbocharger with VGT	
Intake cooling system	Water charged air cooler (WCAC)	

Table 3.1: Engine Specifications

The engine 2 was used to implement different EGR strategies for specific operations due to the flexibility in calibration. It bears the water charged air cooler (WCAC), as integrated part of the intake manifold. The after-treatment system of this engine includes DOC, DPF in addition of an urea circuit. Although, both engines consist the HP and LPEGR line, the length of the LP line is shorter in the second one. The HPEGR line is also designed through cylinder head to reduce the length. Moreover, the HPEGR is injected directly into the intake valves through an external dedicated duct attached to the intake manifold. The LPEGR line is also supported with the exhaust throttle similar to engine 1. This type of architectures are good for packaging of the engine and it makes the transportation of exhaust gases faster.

An electrical dynamometer test bench is used for testing on above described engines. The test bench was equipped with sensors for pressure and temperature measurements. The fuel mass flow measurements were carried

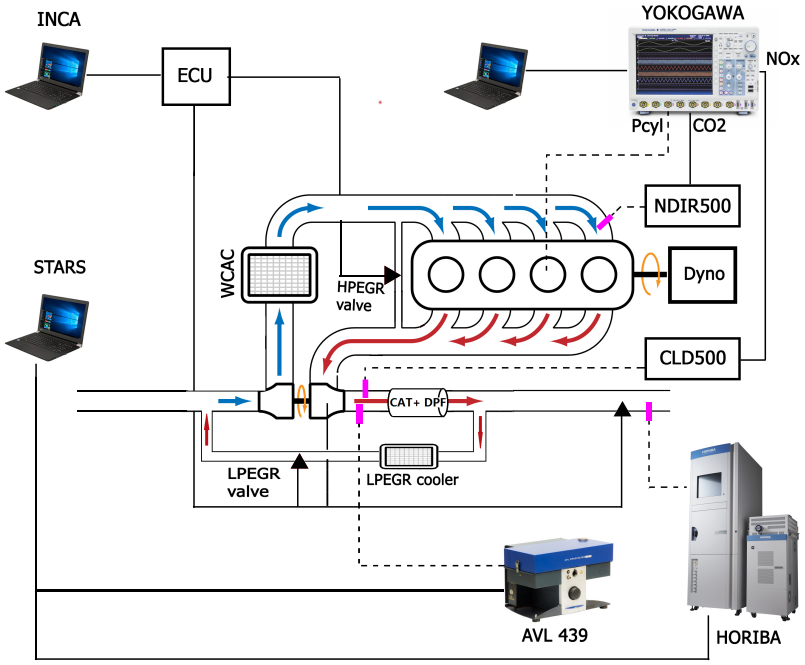

Figure 3.2: Engine test bench layout.

by the fuel balance based on gravimetric measurement[1]. Air mass flow measurements are done by ABB Sensy-flow FMT700-P meter based on hot-film anemometry. The locations of the sensors of different measuring devices are presented in the Figure 3.2. The recording of this test bench sensor data is done with the software called STARS and YOKOGAWA. The data acquisition frequencies are mentioned in the coming section in this chapter.

Additionally, the engine onboard sensor measurements for temperature, pressure, fuel injected quantity, air mass flow, actuator positions etc. were recorded with a software called INCA. The instantaneous data from these sensors is used with corrections described further in this chapter. Moreover, various actuators like EGR valves, exhaust throttle and VGT positions are

[1]The built-in calibration unit is standard scope of supply and allows calibration and accuracy check according to ISO 9001. The determined fuel consumption has an uncertainty of 0.12%.

controlled through the INCA software manually or by modifying the engine maps present inside the ECU.

3.3 Performance measurement

As said earlier, the engine is controlled by electrical dynamometer through a software called STARS from Horiba. The engine load and speed is applied through this software in the form of pedal signal to the ECU. The fuelling parameters are changed as per the signal. To perform a load transient operation, the target engine speed is maintained constant by the dynamometer brake. Figure 3.3 provides the typical response of a electrical dynamometer during such a load transient performed by shifting a pedal from around 13% to 100% at 1250 RPM. The change in engine speed as soon as pedal is pushed can be seen during first part of a second. This increase in speed is restricted by a dynamometer brake to maintain the constant speed. This action also gets reflected on the torque curve distorting it during progression before reaching to final value. Time response (τ) of the engine is the time taken to reach 90% of final torque value after the pedal is pushed. It is the quantity used to rate the performance of engine during transient events and is useful to compare different transient strategies.

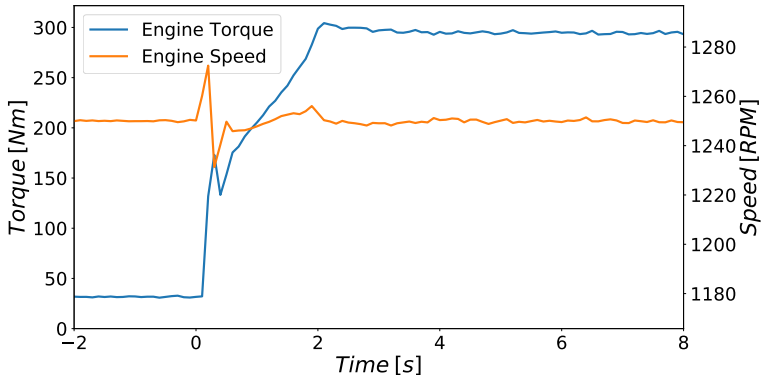

Figure 3.3: Electrical dynamometer response during a typical load transient operation on 1250 RPM.

3.4 Emission measurement

Transient emissions develop in a completely different manner compared with their steady state counterparts, owing to the off-design phenomena experienced during dynamic engine operations [73]. As the main objective of this thesis is to capture and measure the accurate real time pollutant emission during the transient operations, the emission measurement has given a special attention. Various traditional and new generation emission measurement methods used during the experiments are briefly presented in this section. Nitrogen oxide and smoke opacity are the most critical pollutants playing paramount important role in the transient operations and studied widely. Conventional gas analyzers are usually characterized by the response time of the order of few seconds. The dynamics distort the measurements and requires comprehensive reconstruction techniques like [74, 75, 76, 77, 78]. Moreover, the long length of sampling conduits from the sensor to gas analyzers induce delay in the measurements. The dilution and diffusion of sampled gas change the composition of the pollutant to be measured till it reaches the analyzer. Therefore, to capture the emission peaks accurately during Tip-In and Tip-Out operations, a high response time system is needed [79].

3.4.1 NO_x measurement

Fast response system

The advanced CLD500 f-NO_x system from Cambustion, uses Chemi-luminescence detection (CLD) with gas analyzers located very close to sensor (sampling point). The sampled gas is oxidized to NO_2 by ozone (O_3) in the reactor. The reaction produces approx. 10% of excited $NO_2^{\bullet}$ which further decays to its ground state by emitting energy in the form of photons ($h\nu$). The intensity of luminescence is proportional to the amount of NO reacted with ozone. CLD can be used to measure NO_x by using a converter to convert NO_2 in to NO before with carbon. Therefore, the output is combined for NO and NO_2 which is also termed as NO_x. The response time for CLD500 analyzer is 2 ms ($\sim 10ms$ with NO_2 converter fitted) only.[2]. Figure 3.4 represents the

[2]Overall time response here, is the 90–10% 'response time' of the system output to a step input at the source plus the 'transit time' ($\sim 4ms$), which depends on the sample entering into the sampling system.

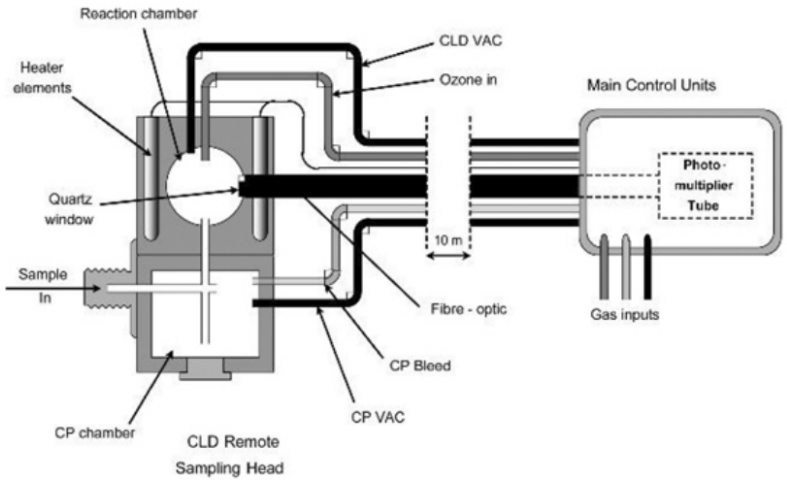

Figure 3.4: Schematic diagram of fast CLD500 operating principle (NO_x measurement). [55]

schematic of a typical fast CLD500 detector controlled by a main control unit away from the actual gas analyzer. To avoid the chemical reaction with the sampled gas, the inert material (eg. Teflon) is used for the parts exposed to the gas.

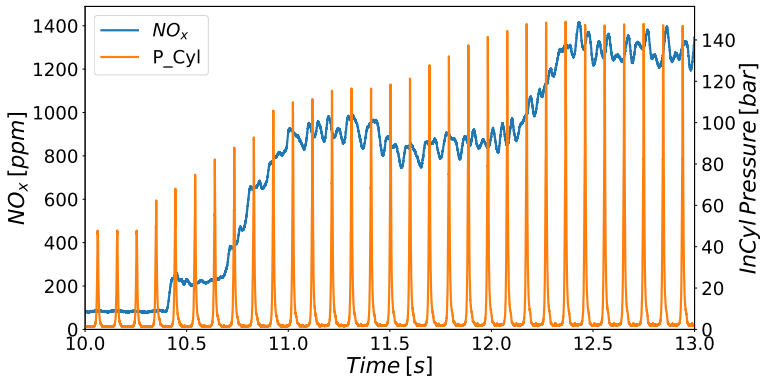

Figure 3.5: NO_x measurement by CLD500 and the in-cylinder pressure measurement.

The CLD500 sensor is placed downstream of turbine in the engine setup to

avoid to avoid repetitive cleaning of the probe. Figure 3.5 shows the instantaneous measurement of NO_x along with the in-cylinder pressure measurement during a load transient operation at 1250 RPM. The in-cylinder pressure measurements are done with the piezoelectric pressure transducer. The temporal response of the CLD500 reacts well with the change in cylinder pressure. To calibrate the CLD500 system all over the NO_x range, steady state operations with various pedal positions from low load to full load are performed simultaneously with another traditional (Horiba) NO_x measurement system. The Horiba sensor is also installed downstream of turbine close to CLD500 sensor. Figure 3.6(a) shows the measured values by both emission measurement system with the correlation between them.

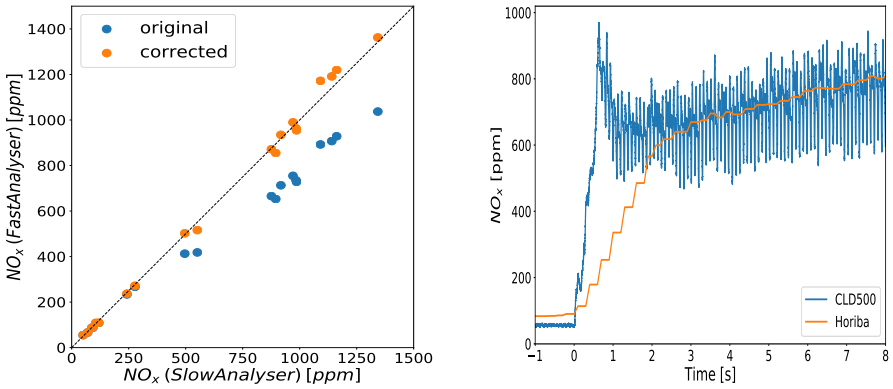

(a) Steady (b) Transient

Figure 3.6: Calibration of NO_x measurement system in 3.6(a)steady-state and 3.6(b) transient operation.

The steady state measurements by CLD500 up to 400 ppm match with the measurements of Horiba but as the NO_x concentration increases further, CLD500 is found to be underestimating the real value. This could be due to the change in pressure at the point where measurement has been done at the exhaust line. This under measurements are corrected by a multiplication factor depending on the measured NO_x values by CLD500. The linear correlation 3.1 used for this purpose is as follows,

$$NO_{x(Corrected)} = NO_{x(CLD500)} \cdot 1.32 - 27.72 \tag{3.1}$$

On the other hand, Figure 3.6(b) confirms the temporal response of the above

mentioned two gas analyzers. The steady state signal at the beginning and end of the transient matches well after the correction. However, Horiba measurements are slow (they are also delayed due to length of insulated pipe from the engine to the sensor device but it is corrected in the figure) compared to the other. Therefore, it is evident that, CLD500 is fast enough to measure the instantaneous pollutant concentration in the exhaust line during transients. It is able to detect the abrupt peaks which slow measurement system fails to detect.

Slow response system

Although, fast measurement is useful for recording instantaneous pollutant concentration at the exhaust during a transient operations, it is difficult to measure on long driving cycles due to the larger time duration and size of the data saved with high acquisition frequency. Therefore, traditional emission measurement system is used for full driving cycle emission recording. In case of these traditional emission measurement system with gas analyzers located far away from the measuring point on the engine, it is necessary to process the data in order to ensure the right time span and avoid the mismatch between pollutant emissions and the other engine variables, such as air and fuel mass flow. The delay in pollutant measurement is due to two reasons, first could be an internal delay incorporated while analyzing the sample depending on the type of pollutant [80]. On the other hand, the distance between the sample point and the gas analyzer forces the existence of a delay defined by the gas velocity and the length of the sample pipes. The gas speed through the sample pipes is produced by the vacuum pressure generated by the gas analyzer pump, which remains equal during the whole cycle. In this case, the delays are corrected by correlation methods comparing the pollutants with other related variables like engine speed [81, 82, 83, 84]

The correction in the NO_x measurements have been made for individual transient operation just to compare with fast CLD500 system. The potential of traditional emission measurement device for transient operation emission measurement can be observed with the certain correction regarding the response time. The corrected NO_x measurement can be obtained by the equation 3.2

$$x_{corr} = x_{meas} + \zeta \cdot \frac{d(x_{meas})}{dt} \tag{3.2}$$

Where x_{corr} and x_{meas} are the corrected and measured NO_x measurements

while ζ is the response time of traditional horiba CLD system with the gas analyzer located far away from the engine measurement point at the exhaust line.

3.4.2 CO_2 Measurement

NDIR500 is the another analyzer from Cambustion systems used for measurement of CO and CO_2 concentration. It uses the miniaturized Non Dispersive Infra-Red technique (NDIR) measuring the volumetric concentration of CO and CO_2 in the given sample. The sample gas is transported to the detector through heated capillaries thereby minimizing the mixing of the sample gas and yielding a very fast response time. The infra red light with particular frequency is sent through the chamber with sampled gas which will be absorbed by certain constituent in the gas. Therefore, measuring the amount of infra-red absorbed by sample at the necessary wavelength, the NDIR detector is able to measure the volumetric concentration of each species. Figure 3.7 represents the schematic of a NDIR500 system with a chopper wheel mounted in front of the detector which corrects continually the offset gain and allows a single sampling head to measure the concentration of 2 different gases. The response time of NDIR500 system is 7 ms.[3]

The location of the NDIR500 sensor is chosen very close to the intake valve of the cylinder. Because, the HPEGR injection ports in the engine 2 were very close to the intake valves. Hence, from the point of view of detecting the arrival of burned gases to the combustion chamber during transient operations under EGR conditions, the location of NDIR500 sensor was very important [85].

3.4.3 Opacity measurement

Soot is formed from unburned fuel that nucleates from the vapour phase to a solid phase in fuel rich regions at elevated temperatures. This evolution of vapour phase to solid soot particles gets through different processes like pyrolysis and nucleation to agglomeration gradually [86]. This soot formation further gets oxidized at higher temperatures (around 1300K) to gaseous

[3]Overall time response here, is the 90–10% 'response time' of the system output to a step input at the source plus the 'transit time' ($\sim 15ms$), which depends on the sample entering into the sampling system.

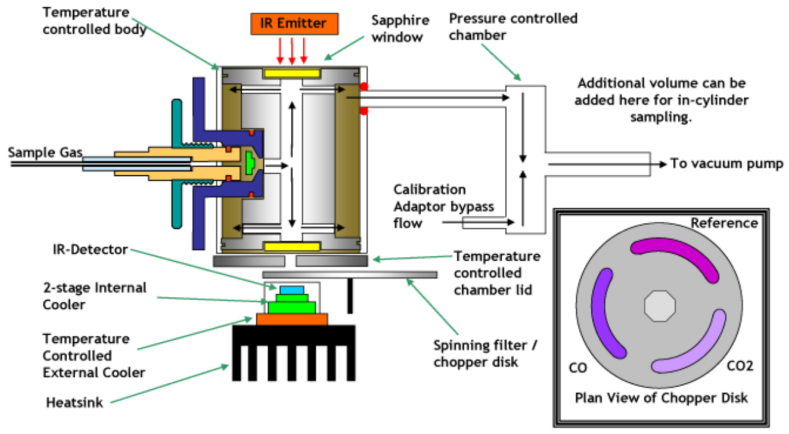

Figure 3.7: Schematic diagram of fast NDIR operating principle (CO and CO_2 measurement).

products like CO, CO_2 and H_2O. But in the absence of good combustion and oxygen, which is the normal condition during transients, favors the soot formation. Similar results are found out within various compression ignition engines in [87, 88, 89].

The soot formation is normally measured by two popular methods using filter smoke meter and opacity meter [90, 91]. The filter smoke methods consists of passing a sample of exhaust gas through a filter. The filter is further analysed in the controlled intensity light to determine the blackness of the that filter paper which is quantified to a number from 0 to 10. This number is also called as Filter Smoke Number (FSN), the unit of smoke measurement by this method. The opacity method on the other hand measures the intensity of the light passed through a tube containing sampled exhaust gas. The relative intensity with the original controlled light intensity is measured in percentage also called as opacity as a unit for the smoke measurement. Traditional smoke meters like AVL 415 measure the opacity in FSN while the AVL 439 measures in percentage adsorption. The first method is good for the steady state measurement of the smoke formation as it relies on the accumulated soot on the filter paper in certain time and gives the average value. Therefore the second method giving opacity measurement along with specific interval of time is advantageous for observing transient smoke formation.

There is a strong correlation between these soot concentration and FSN

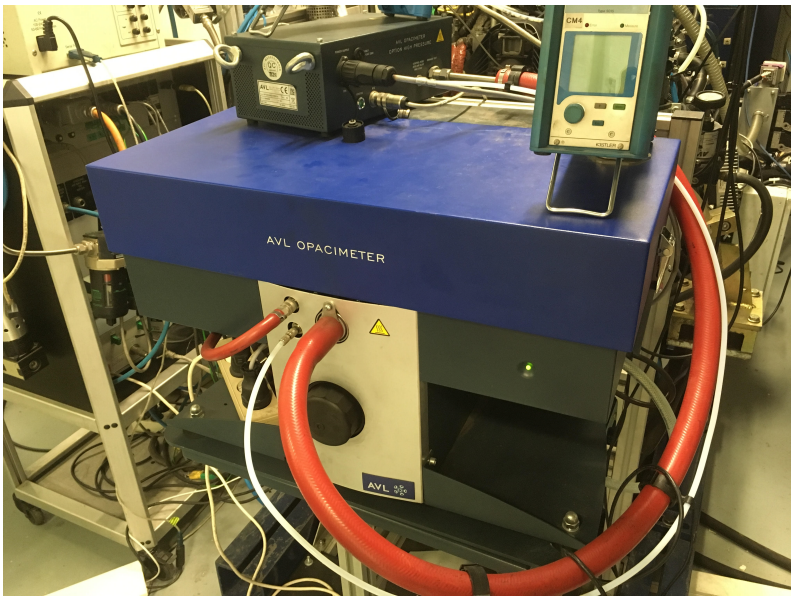

Figure 3.8: Opacity meter with pressure reducing device

values [92]. The opacity measurements in percentage can be converted to the FSN values as a preference. The empirical relation between the percentage opacity and FSN values for smoke measurements is developed and stated by equation 3.3 [93]. Efforts has been done to find the precise correlation by measurements in different labs. Equation 3.4 represents the most recent reference for the empirical relation.

$$Opacity[\%] = 0.12 \cdot (FSN)^3 + 0.62 \cdot (FSN)^2 + 3.96 \cdot (FSN) \tag{3.3}$$

$$Soot[mg/m^3]. = \frac{1}{0.405} \cdot 4.95 \cdot (FSN) \cdot e^{0.38 \cdot (FSN)} \tag{3.4}$$

The opacity was measured with AVL439 opacity meter downstream of turbine in the exhaust line for the transient and steady state operations. A pressure reducing device was installed between the sensor and the AVL439 as the location of a gas sampling was at the high pressure point in the exhaust line. (See Figure 3.8). The recorded measurements in terms of percentage values have the resolution of 0.01%.

3.4.4 EGR measurement

EGR rate is the ratio of mass flow rate of recirculated exhaust gases to total mass flow rate of gases going inside the cylinder. It is an important parameter during transient operations as it determines the composition of the combustion chamber and thus the formation of emissions. Different studies regarding the implementation of HP and LPEGR strategies during transient and steady operations are presented in the coming chapters. Therefore, exact EGR rate estimation/measurement going inside the cylinder is important. EGR rate measurement during transient operations is very critical as well as difficult as compared to steady state operation. This is due to certain delays occurred by turbocharging, transportation of gases and errors in the measurement of engine parameters. Various experimental and model based efforts has been done to assess this estimation of EGR rate in the literature. Some of the methods are mentioned here,

1. Characterizing EGR valve positions with mass flow and pressure difference across the EGR valve during steady state operations. But this method does not take into account the dynamics of gases and pressure wave effects as it is just a interpolation of steady state data. Moreover, the volumetric efficiency is assumed same even at high temperature due to presence of EGR. The pressure ratio correction factor considered is very sensitive for low pressure difference across the valve [94].
2. Using two high response CO_2 gas analyzer probes at intake and exhaust to measure the CO_2 concentration and estimate the instantaneous EGR rate going inside the cylinder [85].
3. 'Volume filling' effect using ideal gas law and conservation of mass used to estimate the transient EGR by a physical model based approach throughout the low pressure EGR circuit [95].
4. Model based EGR rate observer design [96].
5. Intake oxygen measurement (UEGO) sensor is used to measure the change in partial pressure of oxygen in the presence of EGR and humidity in the intake line of an engine. for EGR measurement [97, 98].
6. As EGR rate affects both the temperature of combustion and the composition of the in-cylinder gases. Without any sensor in the exhaust line the EGR rate can be calculated by in-cylinder pressure measurements [99].

For the given engine, due to complexity of intake manifold design and compactness, it was difficult to measure the HPEGR rate even at steady state. Hence, conventional Horiba system is used to measure the LPEGR with a CO_2 sensor after the WCAC. The corresponding valve positions giving iso-torque values at particular steady state operation were used during transient testing to provide same rate of exhaust gas recirculation. The low pressure EGR rate (fraction) inside intake manifold is calculated with conventional method of species continuity conservation equation in terms of CO_2 concentration measured at the intake and exhaust of the engine. The calculation of LPEGR rate is done by the equation 3.5. It considers the equal molecular masses for exhaust and fresh air, as the influence of assuming the same molecular mass gives maximum error below 0.3% [100].

$$EGR = \frac{\dot{m}_{EGR}}{\dot{m}_{air} + \dot{m}_{EGR}} = \frac{[CO_2]_{in} - [CO_2]_{amb}}{[CO_2]_{exh} - [CO_2]_{amb}} \tag{3.5}$$

Where, $[CO_2]_{in}$ and $[CO_2]_{exh}$ represent the CO_2 concentration measured at intake and exhaust respectively. While $[CO_2]_{amb}$ represent the concentration in ambient air. As the propagation of error is important when certain quantity is calculated from the measured variables. Neglecting the uncertainties in the ambient CO_2 measurements, the relative error for the EGR is estimated as the twice the measurement by gas analyser [101].

3.5 Transient tests

Normal load transient operations can be performed on the engine on test bench with the help of electric dynamometer. The dynamometer can be used in modes like 'speed-torque mode' or 'speed-pedal mode'. In first mode, the engine speed is maintained constant by a brake in dynamometer, while the target value for engine torque is provided as a step function. The PID control actuates the pedal accordingly to achieve the final torque. On the other hand, the second mode allows the user to change the pedal manually with custom time step. The second mode is quiet similar to the real road driving scenario where the pedal signal is sent through the driver as per the requirement of power. Therefore, second mode is used mostly to perform the load transient operation. The selected engine speeds for executing this operations are 1250, 1500, 1750 and 2000 RPM referenced from the last chapter.

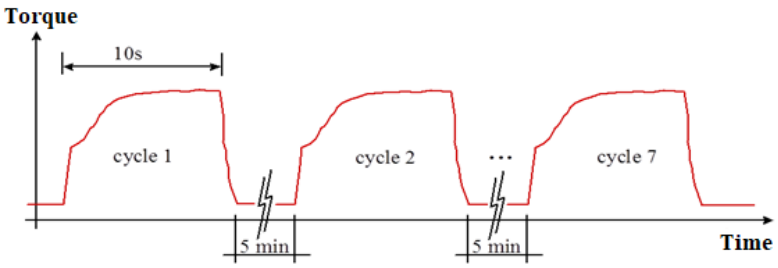

Figure 3.9: Load transient test procedure on the dynamic test bench.

As a part of test procedure, The engine is heated to 80°C of coolant temperature. To observe the transient behavior for increment and decrement in load (Tip-In and Tip-Out operation), the preheated engine is controlled with pedal. The pedal is shifted from low load (2 bar BMEP) to full load (100% pedal position) for around 10 seconds until the engine torque gets stabilized. Consequently, it is further shifted back to its initial position as shown in Figure 3.9. To verify the repeatability in the different transient measurements, every transient operation is repeated for 6-7 times successively for a particular engine speed. Every repetition is separated by 5 minutes gap to stabilize the parameters like exhaust temperature and compressor outlet temperature after every load change operation.

3.5.1 Air mass flow measurement

The air mass flow measurement going inside the combustion chamber is very important for knowing the composition of intake charge during transient operation. The correct instantaneous measurement required to simulate the transient performance and emissions [102, 103]. The signal registered by the hot-wire anemometer (sensy-flow) after air filter is slow and delayed. It has to be corrected due to the effect of pressure waves travelling and the effect of air mass storage inside the intake system [104]. Considering the compressible behavior of air, it causes a time delay in air mass flow measuring device and the actual air mass entering through intake valve. The new corrected air mass flow can be corrected by the equation 3.6 which can be obtained by considering

the ideal gas equation ($pV = mRT$) and conservation of mass.

$$m_{out} = m_{in} + \frac{dm}{dt}$$
$$\frac{dm}{dt} = \frac{V}{R} * \frac{\Delta(\frac{P}{T})}{\Delta(t)} \tag{3.6}$$

Where V is the volume between the hot wire anemometer and the intake manifold of the engine. m_{out} is the air mass flow at the intake valve while m_{in} is the mass flow measurement at the anemometer. Figure 3.10 shows the difference between measured and corrected air mass flow during a transient operation from low load to full load.

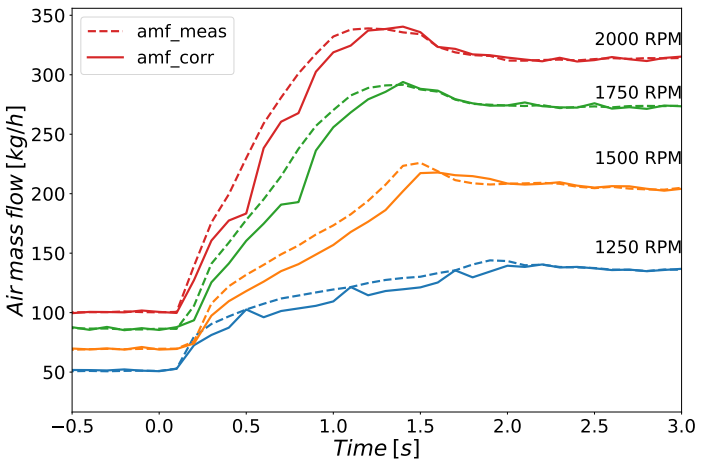

Figure 3.10: Measured and corrected air mass flow at the intake manifold during a typical transient operation from low load to full load.

3.6 Driving cycle tests

Different driving cycles used for the type approval process, are analyzed and explained in chapter 2. Performing these driving cycle on the engine test bench involves programing of a control system. The vehicle speed profile is recreated

along with the road load forces by providing an engine load and speed as a target to the control. The control model used for the purpose is called 'Road-Load-Speed model'. The power requirement on the whole driving cycles are calculated using vehicle model explained in 2.3. This requirements are further translated to target engine speed and torque. The engine speed is calculated by equation 3.7

$$N = \frac{v}{\pi \cdot D \cdot g_r} \tag{3.7}$$

Where, N is the engine speed, v is the vehicle speed, D is the vehicle diameter and g_r is the gear ratio for driving. The engine torque requirements are calculated by the power requirements by the equation 3.8.

$$\tau = \frac{60 \cdot P}{\pi \cdot 2 \cdot N} \tag{3.8}$$

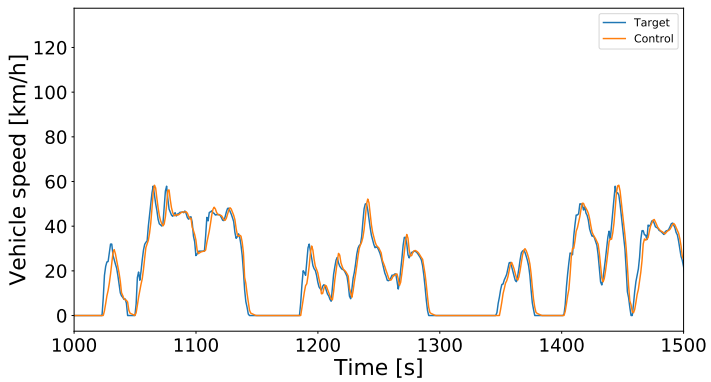

Figure 3.11: Road-Load-Speed control on engine dynamometer for a real driving cycle.

Where P is power and τ is the engine torque. A PID controller controls the pedal position for attaining the required engine speed. A part of driving cycle is shown in Figure 3.11 with the vehicle speed demand and output vehicle speed by PID control. For a given gear ratio, when load torque is increased in dynamometer (by acceleration) the engine speed goes down which has to be compensated by shifting the pedal. The control moves the pedal until the target vehicle speed is achieved. Therefore the output vehicle speed is slower than vehicle speed input demand.

3.7 Data analysis procedure

As discussed before in Section 3.2, the test data acquisition is done with three different systems with frequencies stated in the Table 3.2. Engine dynamometer measurements are done through the software called 'STARS' from 'Horiba'. It consisted pressure, temperature and emission sensors instrumented at various points on the air path. The engine sensors' data was recorded with 'INCA' software from ETAS. The fast emission measurement data was acquired with 'YOKOGAWA' with highest frequency among the other systems. Due to the fact that, 3 different computing machines independent to each other are used during tests, the sampled time for data logging was not synchronized for all the variables. Therefore the synchronization of the signals is necessary in order to compare the performance and emission during a transient operation.

System	Parameters	Acquisition frequency
STARS	Pressure Temperature Fuel Flow Air flow	10Hz
INCA	Engine Sensors	100Hz
YOKOGAWA	CLD500 NDIR500 P_{cyl}	10000Hz

Table 3.2: Data acquisition system with the measuring variables and acquisition frequencies.

For load transient operation. pedal shift is the prime signal. Therefore, variables within a particular acquisition system are synchronized with the pedal signal. However, the 'YOKOGAWA' doesn't contain the pedal measurements. In that case, the synchronization was done with the NO_x, being the fastest measurement among the variables recorded with 'YOKOGAWA'.

For during a driving cycles, slow response gas analyser measurements are needed to be corrected to avoid the mismatch between emission and other engine variables. It is important to compare the pollutants with fast response gas analyser measurements. Moreover, to convert the pollutant concentration from ppm to g/l, the mass flow and emissions should be well synchronized. It

is required to get rid of the delays incorporated due to different sources [105]. This mismatch depends on the internal delay depending on the type of pollutant. Likewise, it depends on the distance between the sample point and the gas analyser inducing a lag. This lag confides to the gas velocity and a length of the pipe carrying the sample to analyser. There are some behavioral models presented by [80] to identify the delays. The correlation methods described by [84, 82] consists of finding a correlation with the variable with which the signal is needed to be synchronized (eg. pedal signal). The highest correlated index represents the array elements by which the signal should be shifted to match with the reference. Another method based on the 'convolution' principal in 'signal processing' is used by changing the time domain to frequency domain by fourier transform. Later, the signal can be reconstructed by 'de-convolution' method [75]. Equation 3.9 represents this principal.

$$y(t) = x(t) * g(t) \tag{3.9}$$

Where, $x(t)$ is the original signal while the $y(t)$ is the measured signal with the induced delay represented by $g(t)$ in time domain. The $*$ represent the convolution of the signals. The original signal can be reconstructed from the de-convolution theorem. The $\hat{y(s)}$ denotes the fourier transform of the function converting from time domain to frequency domain. While, the $\mathcal{F}^{-1}$ represents the inverse fourier transform changing the frequency domain back to time domain. The 's' is called as a cyclic frequency. The new signal is the one synchronized with the reference variable.

$$x(t) = \mathcal{F}^{-1}\left(\frac{\hat{y(s)}}{\hat{g(s)}}\right) \tag{3.10}$$

The concentration of some pollutants are required to be converted into other. This can be done by synchronized signal of the air and fuel mass flow. Equation 3.11 gives the conversion of , in order to know how much pollutants are released to the atmosphere.

$$\dot{m}_{pollutant} = \frac{M_{pollutant}}{M_{air}} \cdot [C_{pollutant}] \cdot (\dot{m}_{air} + \dot{m}_{fuel}) \tag{3.11}$$

where $M_{pollutant}$ and M_{air} are the molecular weights of pollutant and air respectively. $C_{pollutant}$ is the measured pollutant concentration and m_{air} and m_{fuel} are the mass flow of fresh air and fuel respectively.

3.8 Simulation

Simulation is an important tool for engine analysis. It is a fast and low cost method available to see the effects on the large systems compared to real engine testing. It is also helpful to perform various parametric studies with design parameters of the engine. Furthermore, engine simulation results contains more information about the gas flows that can be measured. Therefore they are convenient to understand the flow phenomena.

Apart from successful modelling of steady state operations, various efforts have been made over the decades to model the transient operations too. Rakopoulos and Giakoumis have performed an intensive review on the history of engine transient simulations [49]. Numerous models following the filling and emptying [106, 107, 108, 109, 110] or quasi-linear [111, 112, 113, 114] approach have been developed. In recent years, the 1D simulation tools are used frequently to model transient operations giving detailed information about the flows [115, 116]. It is more accurate than quasi steady. All of the steady state and transient simulations in this work have been done on the commercial software called GT-Power.

3.8.1 GT-Power

It is one of the calculating softwares used for modelling flows in a engine components based on mass, momentum and energy conservation equations(also known as Navier-Stokes equations). These equations are solved in one direction only making all models called as 1D models. The whole system is discretized into many volumes connected by boundaries on the basis of 'staggered-grid discretization'. The scalar variables (pressure, temperature, density, internal energy, enthalpy, species concentrations, etc.) are assumed to be uniform over each volume. The vector variables (mass flux, velocity, mass fraction fluxes, etc.) are calculated for each boundary [117]. Supplementary to the flow calculations the version v2017 has provided distinct modelling templates for turbocharger, combustion model, diesel particulate filter etc. Moreover, PID controllers for controlling actuators like VGT, egr and throttle valves were useful and discussed in following subsections.

3.8.2 Turbocharger

The turbocharger is a tricky part where flow energy is converted into work by the turbine and then the work is applied on gas to compress it. The interaction of gas and the rotor is hard to simulate accurately in one dimensional modelling approach. A multidimensional model is required however the difficulty of flow simulation is unavoidable [118]. Therefore, turbo mapping from the gas stand was used as a map and the real time operating parameters are interpolated by interpolation method for particular mass flow, pressure ratio and turbine opening positions. Fortunately the ready made template was useful to carry out these operation in GT-Power.

However, getting exact transient behavior resembling the tests is difficult due to following reasons. The interpolation method treats a transient, a series of steady state operations while the flow variables hold different values than a stable steady operations. Therefore the efficiency is needed to be corrected appropriately during the change of state in operation. Moreover, because of thermal inertia of exhaust components, the energy available at the turbine is not the same. The consequences lead to error in the calculation of exhaust pressure and temperature. Furthermore, the control of VGT plays important role in the turbocharger performance. Finding an exact VGT control is very difficult to attain exact boost pressure evolution from the tests.

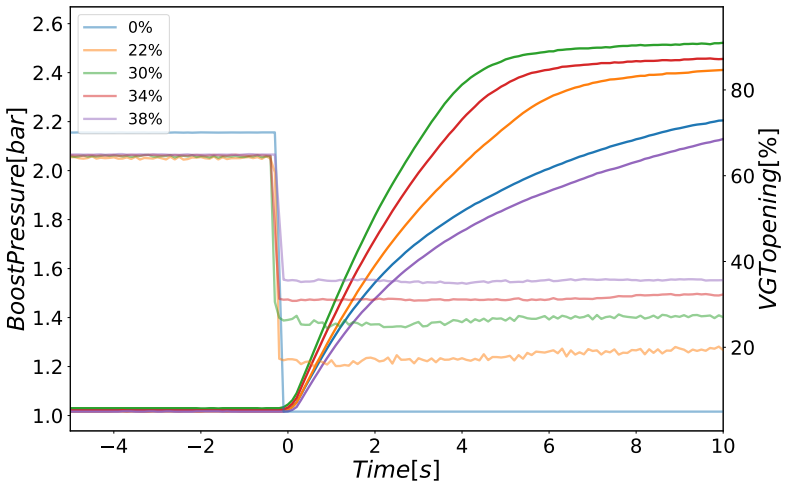

Figure 3.12: Boost pressure evolution with different final VGT positions during a load transient operation at 1500 RPM of engine speed.

The response of turbocharger by changing from one VGT position to another during a change in load is path dependant. The engine response is different with different positions of Variable Geometry turbine after pushing the pedal [119]. The parametric study is carried out with different VGT positions to find the fastest torque and boost pressure evolution, which can be used as reference for the further experiments. The manual PWM signal to close the VGT to 62%, 66%, 70%, 78% and 100% was sent through INCA while performing a transient (from 2 bar BMEP to full load). Figure 3.12 shows the boost pressure with different closing of VGT. Where, closing of VGT up to 70% seems a best solution to provide fastest boost pressure evolution than closing the VGT fully.

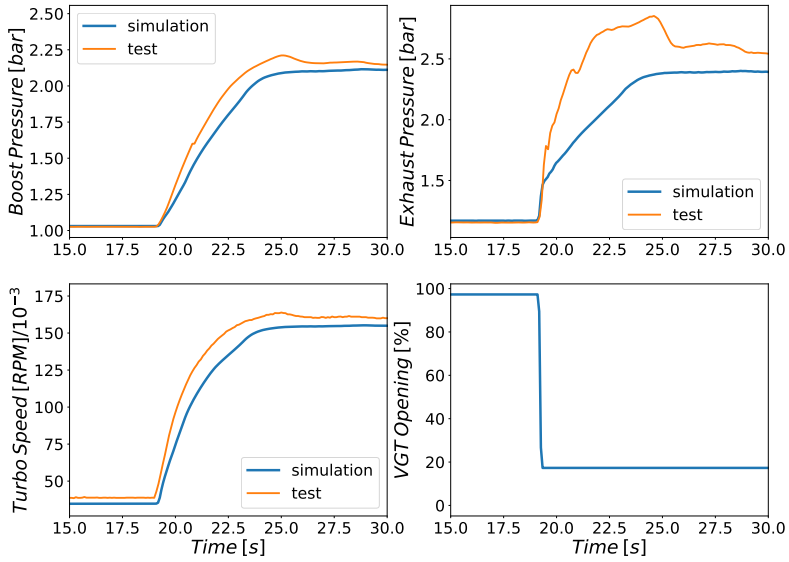

Figure 3.13: Comparison of test and simulated turbocharger performance during a load transient operation at 1500 RPM with the first method of fixing VGT position.

To calibrate the 1D simulation model according to the transient tests performed on the modern engine with VGT control 3 methods have been tested to match with the boost pressure evolution for load transient for different engine speeds. As no information was available for specific VGT control gain implemented in ECU, three methods have been tested to get the targeted boost pressure from the transient tests. First method consists fixing the VGT position for the second state (full load) of transient at the value obtained from the full load steady calculation. A profile of VGT positions (refer to Figure 3.13

bottom-left plot) with respect to time is imposed in the turbocharger model as according to the load change. It contains sharp movement in closing the turbine to a final fixed position as soon as the engine goes through a extreme load change. The turbine efficiency is kept the same as from the maps. Figure 3.13 shows the evolution of turbocharger parameters as a function of time during a load transient from 2bar bmep to full load at 1500 RPM engine speed. The first and final steady part of the transient show the values close to the tests as the VGT positions are taken according to the steady operation. Despite the evolution of boost pressure from the model is underestimated. That means the final position of VGT is not enough to provide power to increase intake pressure though that percentage of opening provides more energy during steady operation. Hence, the VGT right after the change in load should close even more un-till the limit implied in previous parametric study. The same reason can be given for the under estimated turbine speed.

Secondly, the PID controller from GT-Power is implemented to see the evolution of boost pressure during a load transient. The boost pressure profile from tests is given as a target to the controller. The proportional and integral gains are tuned for each engine speed to give the fast and stable response during the change of state. The same load transient from the last method is represented Figure 3.14 with the PID controller. The movement of VGT is rather slow as compared to previous method resulting into the delayed response in all parameters like boost pressure and turbo speed. However after approx. 2 seconds. it manages to attain the target boost pressure and speed of the turbine maintaining it to the final steady state. The control closes the VGT completely resulting into the huge peak in exhaust pressure which could create a back pressure and reduce the engine torque. As a deduction, The VGT movement should be quick after the change of load (when pedal is pushed), and it should take the value providing rapid increase in boost pressure, nonetheless closing fully to even increasing pressure before the turbine.

In the third method, considering the previous approaches and the parametric study performed at the start of this section (Figure 3.12) a new profile is developed. Figure 3.15 (bottom-left plot) shows the new VGT profile as a function of time. According to the new VGT profile, the VGT position is shifted to the 'specific value' for fast response during first few seconds of the transient. This 'specific value' is different for different engine speeds. furthermore, the VGT is shifted to the final optimized state for full load steady state operation from the first method. Importantly, the path that it takes, affects

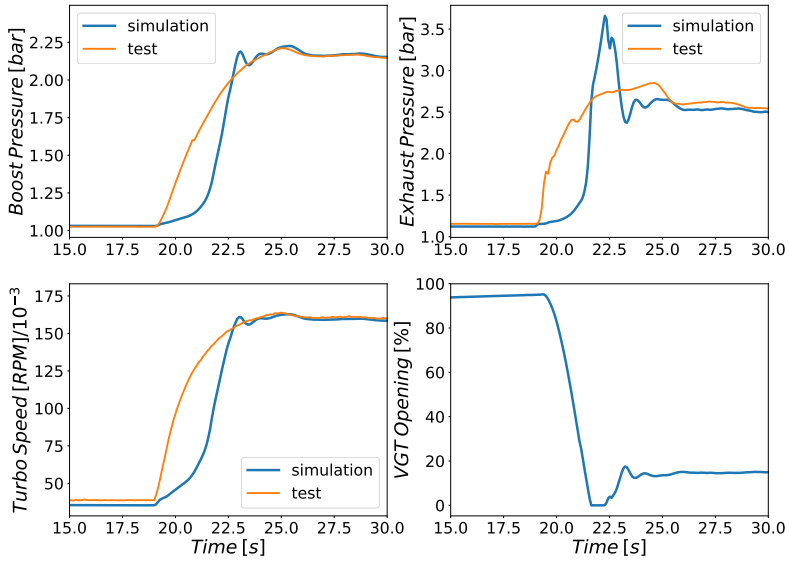

Figure 3.14: Comparison of test and simulated turbocharger performance during a load transient operation at 1500 RPM with the second method of controlled VGT movement by PID controller.

the performance of turbocharger during that small interval of time. The curve is generated from the following equation 3.12,

$$y(t) = y_2 - y_1(e^{-(\frac{t}{\tau})}) + a \tag{3.12}$$

Where, y_2 and y_1 are the first and last values of the VGT positions when the VGT moves to the final steady state value from the optimized position to give fast boost pressure evolution. t is time and τ is the time constant which defines the shape of the curve and eventually the performance of the turbo after the 2-3 seconds of the load change. A is the arbitrary constant added to shift the curve.

The new VGT profile has similar shape to the curve obtained by the PID controller in the previous method. The overshoot in the pressure before turbine is removed with the new profile. The boost pressure evolution and the turbine speed estimation by the model with new profile is quiet closer now to the test results.

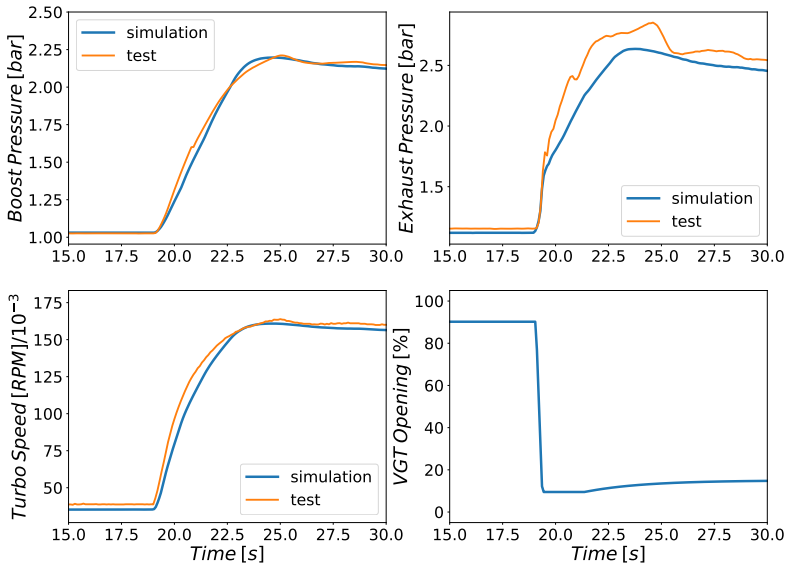

Figure 3.15: Comparison of test and simulated turbocharger performance during a load transient operation at 1500 RPM with the third method of newly developed VGT profile.

3.8.3 Combustion

Due to high complexity, modelling of combustion in diesel engines is challenging task. Usually the measured combustion profiles are imposed in GT-Power for steady state calculations. However, obtaining the accurate burn rate of fuel for certain cycle during transient operation is rather difficult. In-cylinder conditions at certain time of the transient operation can be different from the same fuel injected in steady state conditions [120, 121, 122, 123]. Moreover, there is a variation in the heat release law due to the EGR rate [124, 125]. You need to have the measured combustion data with different intake conditions. For each cycle the heat release rate is chosen from this database interpolated by intake pressure and EGR rate [41]. But this study focuses on the engine and turbocharger performance during load transient operation than emissions in the case of simulations, the effects are neglected. To avoid the creation of the big combustion database, the heat release profile is calculated by interpolating between extreme load profiles and mean indicated pressure. However, GT-Power can not extrapolate the burn rate profile beyond this boundary profiles.

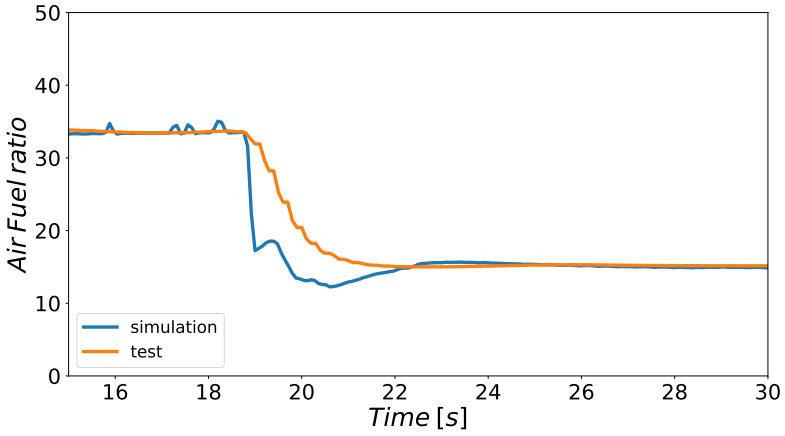

Figure 3.16: Air Fuel ratio comparison between 1 d simulation and test for harsh load transient operation at 1500 RPM.

Lower lambda ratios during load transient operations is common phenomenon due to delay in air mass flow caused by turbo lag. To avoid the soot formation during this kind of situation the λ value should not go below 1. The fuel reduced to cope up with the decreased λ values. This type of control is called as smoke limiter strategy. Similar control was designed in the GT-Power model to cut the fuel as soon as the lambda (λ) value goes below 1 to avoid smoke formation. Figure 3.16 represents air fuel ratio as a function of time measured during a transient test and the one calculated from the 1 d simulation. It shows that the air fuel ratio is maintained above the stoichiometric limit in the absence of air.

3.8.4 Model Validation

As discussed above in the turbocharger section, this study focuses on the engine and turbo performance during load transient operation. The 1D model created in GT-Power is calibrated on most frequently visited engine speeds for harsh load transient operation (see Chapter 2). 1250, 1500, 1750 and 200 RPM engine speeds are added as input in the model. At each engine speed, the engine load has been increased suddenly from 2 bar BMEP situation to full load and back. This is achieved by imposing a fuel flow profile measured during the transient tests on the test bench. Figure 3.17 represents the input

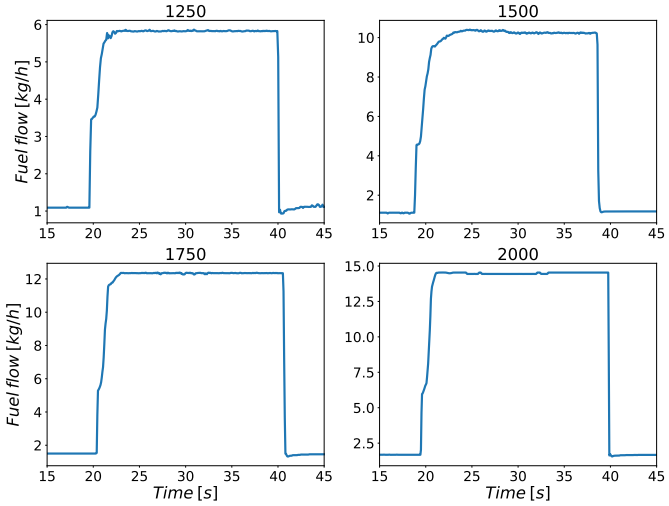

Figure 3.17: Imposed fuel flow profile for load transient simulation for different engine speeds.

profile of fuel injected inside the cylinder representing the harsh load transient operation.

The engine speed is kept constant throughout the transient. The VGT is moved according to newly generated profile as a function of time. The calculated air mass flow is depicted in the Figure 3.18. The intake pressure (Figure 3.19) or boost pressure matches with the test data while the exhaust pressure (Figure 3.20) upstream the turbine fluctuates more in the tests. The reason behind this fluctuation could the sensitivity of exhaust pressure with the change in VGT movement. The VGT profile in simulation is rather smooth and calculated, while the VGT is controlled by a PID controller inside ECU during engine tests. Therefore the final steady values are coinciding well with the recorded data. In addition, turbine efficiency is also not the same as in the tests as it depends on the path through which the transient advances on the turbine map.

The temperature at the intake and exhaust are shown in the Figures 3.21 and 3.22 respectively. The shape of intake temperature curve looks quiet similar to the test results with slightly higher temperature. Equivalently,

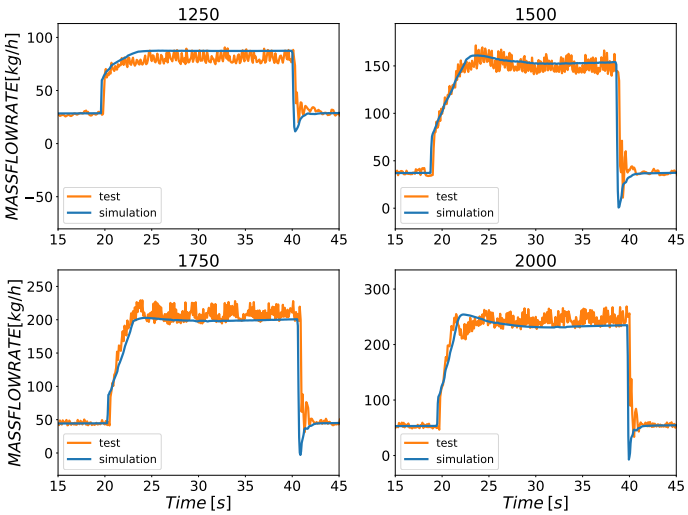

Figure 3.18: Air mass flow comparison between calculated and measured during the harsh load transient operation at different engine speeds.

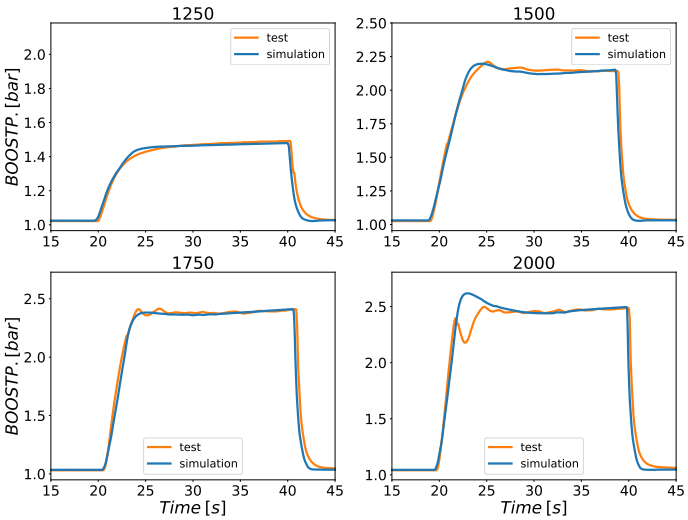

Figure 3.19: Boost pressure comparison between calculated and measured during the harsh load transient operation at different engine speeds.

the exhaust temperature follows the shape of temperature curve measured upstream the turbine. However the values match with the measured data near full load while at low load calculated temperature are higher. This is

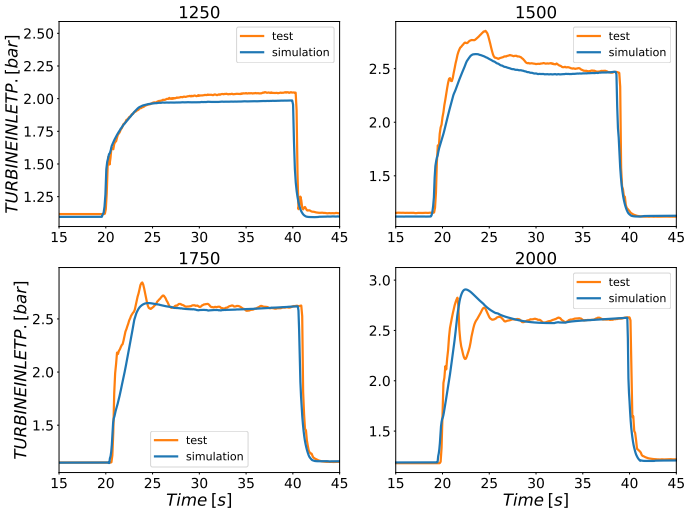

Figure 3.20: Exhaust pressure comparison between calculated and measured during the harsh load transient operation at different engine speeds.

because the turbine efficiency is tuned to the flows at full load operation of the engine, while at low load the efficiency should be more. Likewise, probably the modeling of the combustion process and of the heat transfer along the exhaust ducts is not the same as tests.

Calculated engine torque and the measured on the test bench during transient tests are in perfect agreement as per the Figure 3.23, as the fuel profile is imposed in the model. Mismatch in air flow and boost pressure during the first few seconds is reflected on the torque curve. The back pressure of the overestimated exhaust pressure has seen very little effect on the torque calculated by the model. Retrospectively, the evolution of curves are in conformity with the test results.

Chapter 3 Bibliography

[41] S. Reifarth and H.-E. Ångström. "Transient EGR in a High-Speed DI Diesel Engine for a set of different EGR-routings." *SAE International Journal of Engines* 3(1) (2010), pp. 1071–1078. ISSN: 19463936. DOI: 10.4271/2010-01-1271 (cit. on pp. 11, 73).

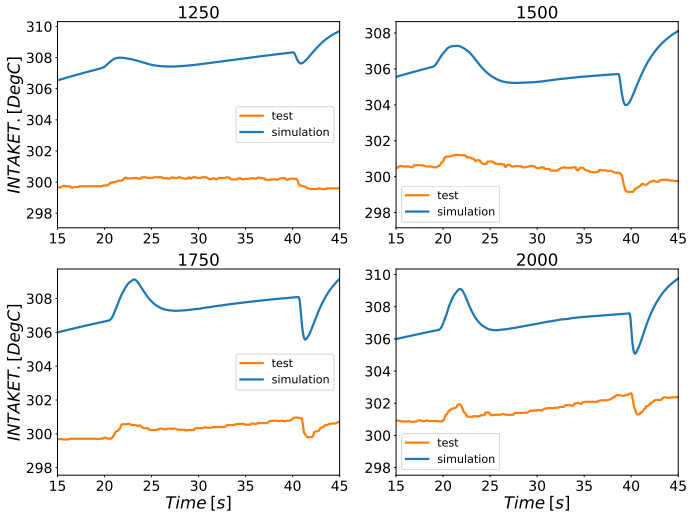

Figure 3.21: Intake temperature comparison between calculated and measured during the harsh load transient operation at different engine speeds.

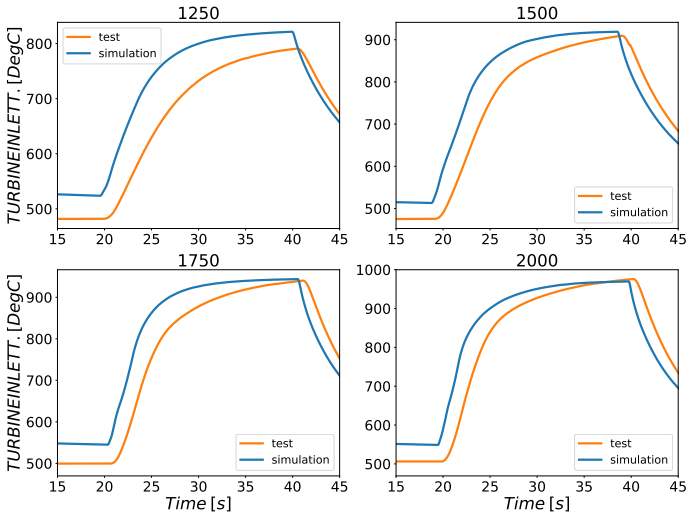

Figure 3.22: Exhaust temperature comparison between calculated and measured during the harsh load transient operation at different engine speeds.

[49] C. D. Rakopoulos and E. G. Giakoumis. "Review of Thermodynamic Diesel Engine Simulations under Transient Operating Conditions." *SAE Technical Paper Series* (2006). ISSN: 0148-7191. DOI: 10.4271/2006-

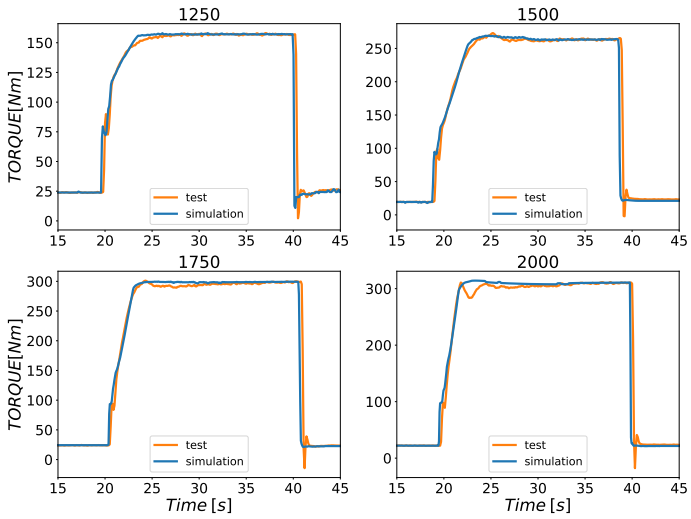

Figure 3.23: Engine torque comparison between calculated and measured during the harsh load transient operation at different engine speeds.

01-0884. URL: http://papers.sae.org/2006-01-0884/https://www.sae.org/content/2006-01-0884/ (cit. on pp. 12, 68).

[55] C. Rakopoulos, A. Dimaratos, E. Giakoumis, and M. Peckham. "Experimental Assessment of Turbocharged Diesel Engine Transient Emissions during Acceleration, Load Change and Starting." *SAE Technical Paper Series* 1 (2010). DOI: 10.4271/2010-01-1287 (cit. on pp. 14, 55).

[73] C. D. Rakopoulos, A. M. Dimaratos, and E. G. Giakoumis. "Experimental Study of Transient Nitric Oxide, Smoke, and Combustion Noise Emissions during Acceleration of an Automotive Turbocharged Diesel Engine." *Proceedings of the Institution of Mechanical Engineers, Part D: Journal of Automobile Engineering* 225(2) (2011), pp. 260–279. ISSN: 09544070. DOI: 10.1243/09544070jauto1493. URL: http://pid.sagepub.com/cgi/content/abstract/225/2/260 (cit. on p. 54).

[74] B. T. McClure. "Characterization of the Transient Response of a Diesel Exhaust-Gas Measurement System." In: *SAE Technical Paper Series*. 1988. DOI: 10.4271/881320 (cit. on p. 54).

[75] J. D. Pakko. "Reconstruction of Time-Resolved Vehicle Emissions Measurements by Deconvolution." *SAE International Journal of Fu-*

els and Lubricants 2(1) (2010), pp. 697–707. ISSN: 1946-3960. DOI: 10.4271/2009-01-1513 (cit. on pp. 54, 67).

[76] C. De Petris, S. Diana, V. Giglio, and G. Police. "Some Problems in the Improvement of Measurement of Transient Emissions." *SAE Technical Paper Series* 1(412) (2010). DOI: 10.4271/941949 (cit. on p. 54).

[77] A. Beaumont. "„Noble, AD and Pilley, AD Signal reconstruction techniques for improved measurement of transient emission." *SAE paper* 900233 (1990) (cit. on p. 54).

[78] S. H. Chan, X. S. Chen, and C. Arcoumanis. "Measurement and Signal Reconstruction of Transient Nitric Oxide Emissions in the Exhaust of a Turbocharged Diesel Engine." *Journal of Dynamic Systems, Measurement, and Control* 119(4) (1997), p. 620. ISSN: 00220434. DOI: 10.1115/1.2802370. URL: http://dynamicsystems.asmedigitalcollection.asme.org/article.aspx?articleid=1407662 (cit. on p. 54).

[79] C. S. Nielsen, A. Ivarsson, and T. Løvås. "Evaluation of Test Bench Engine Performance Measurements in Relation to Vehicle Measurement on Chassis Dynamometer." (ICEF2015-1019) (2015), pp. 1–13 (cit. on p. 54).

[80] J. T. Messer, N. Clark, and D. W. Lyons. "Measurement Delays and Modal Analysis for a Heavy Duty Transportable Emissions Testing Laboratory." In: *SAE Technical Paper Series*. Vol. 1. 1995. DOI: 10.4271/950218. URL: https://www.sae.org/content/950218/ (cit. on pp. 57, 67).

[81] J. M. Luján, H. Climent, V. Dolz, A. Moratal, J. Borges-Alejo, and Z. Soukeur. "Potential of exhaust heat recovery for intake charge heating in a diesel engine transient operation at cold conditions." *Applied Thermal Engineering* 105 (2016), pp. 501–508. ISSN: 13594311. DOI: 10.1016/j.applthermaleng.2016.03.028. URL: https://linkinghub.elsevier.com/retrieve/pii/S1359431116303209 (cit. on p. 57).

[82] P. Bielaczyc and J. Merkisz. "Cold Start Emissions Investigation at Different Ambient Temperature Conditions." In: *SAE Technical Paper Series*. 1998. DOI: 10.4271/980401. URL: https://www.sae.org/content/980401/ (cit. on pp. 57, 67).

[83] J. M. Luján, H. Climent, S. Ruiz, and A. Moratal. "Influence of ambient temperature on diesel engine raw pollutants and fuel consumption in different driving cycles." *International Journal of Engine Research* (2018). DOI: 10.1177/1468087418792353. URL: http://journals.sagepub.com/doi/10.1177/1468087418792353 (cit. on pp. 57, 135).

[84] G Konstantas and A Stamatelos. "Quality assurance of exhaust emissions test data." *Proceedings of the Institution of Mechanical Engineers, Part D: Journal of Automobile Engineering* 218(8) (2004), pp. 901–914. ISSN: 0954-4070. DOI: 10.1243/0954407041581075. URL: http://journals.sagepub.com/doi/10.1243/0954407041581075 (cit. on pp. 57, 67).

[85] C. Sutela, N. Collings, and T. Hands. "Real Time CO2 Measurement to Determine Transient Intake Gas Composition under EGR Conditions." In: *SAE Technical Paper Series*. 2000. DOI: 10.4271/2000-01-2953 (cit. on pp. 58, 61).

[86] D. Tree and K. Svensson. "Soot processes in compression ignition engines." *Progress in Energy and Combustion Science* 33(3) (2007), pp. 272–309. ISSN: 0360-1285. DOI: https://doi.org/10.1016/j.pecs.2006.03.002. URL: http://www.sciencedirect.com/science/article/pii/S0360128506000608 (cit. on p. 58).

[87] D. L. Hofeldt and G. Chen. "Transient Particulate Emissions from Diesel Buses During the Central Business District Cycle." In: *SAE Technical Paper Series*. 2010. DOI: 10.4271/960251 (cit. on p. 59).

[88] E. G. Giakoumis, C. D. Rakopoulos, A. M. Dimaratos, and D. C. Rakopoulos. "Exhaust emissions of diesel engines operating under transient conditions with biodiesel fuel blends." *Progress in Energy and Combustion Science* 38(5) (2012), pp. 691–715. ISSN: 03601285. DOI: 10.1016/j.pecs.2012.05.002. URL: http://dx.doi.org/10.1016/j.pecs.2012.05.002 (cit. on pp. 59, 135).

[89] J. R. Hagena, Z. Filipi, and D. N. Assanis. "Transient Diesel Emissions: Analysis of Engine Operation During a Tip-In." In: *SAE Technical Paper Series*. 2010. DOI: 10.4271/2006-01-1151 (cit. on p. 59).

[90] R. Christian, F. Knopf, A. Jaschek, and W. Schindler. "Eine neue messmethodik der bosch-zahl mit erhöhter empfindlichkeit." *Motortech. Z* 54 (1993), pp. 16–22 (cit. on p. 59).

[91] A. Notes. "Smoke Value Measurement With the Filter-Paper-Method." *AVL, AT1007E, Rev* 2 (2005) (cit. on p. 59).

[92] P. Kirchen, P. Obrecht, K. Boulouchos, and A. Bertola. "Exhaust-Stream and In-Cylinder Measurements and Analysis of the Soot Emissions From a Common Rail Diesel Engine Using Two Fuels." *Journal of Engineering for Gas Turbines and Power* 132(11) (2010), p. 112804. ISSN: 07424795. DOI: 10.1115/1.4001083. URL: http://gasturbinespower.asmedigitalcollection.asme.org/article.aspx?articleid=1429022 (cit. on p. 60).

[93] P. Lakshminarayanan and S. Aswin. "Estimation of Particulate Matter from Smoke, Oil Consumption and Fuel Sulphur." In: *SAE International*. 2017, pp. 1–11. DOI: 10.4271/2017-01-7002. URL: http://papers.sae.org/2017-01-7002/https://www.sae.org/content/2017-01-7002/ (cit. on p. 60).

[94] F. Liu and J. Pfeiffer. "Estimation Algorithms for Low Pressure Cooled EGR in Spark-Ignition Engines." *SAE International Journal of Engines* 8(4) (2015), pp. 1652–1659. ISSN: 1946-3944. DOI: 10.4271/2015-01-1620 (cit. on p. 61).

[95] Z. C. Liu, K. B. Yu, J Tian, Y. Q. Han, S. L. Qi, and P. K. Teng. "Influence of rail pressure on a two-stage turbocharged heavy-duty diesel engine under transient operation." *International Journal of Automotive Technology* 18(1) (2017), pp. 19–29. ISSN: 1229-9138. DOI: 10.1007/s12239-017-0002-z. URL: https://doi.org/10.1007/s12239-017-0002-zhttp://link.springer.com/10.1007/s12239-017-0002-z (cit. on pp. 61, 135).

[96] J. Shutty and J. Shutty. "Control Strategy Optimization for Hybrid EGR Engines." *SAE Technical Paper* (2009). DOI: 10.4271/2009-01-1451 (cit. on p. 61).

[97] P. B. Dickinson, K. Hegarty, N. Collings, and T. Ramsander. "Application of Fast Oxygen Sensors for Investigations into Air-Path Dynamics and EGR Distribution in a Diesel Engine." *SAE Technical Paper Series* 1(x) (2014). DOI: 10.4271/2014-01-1177 (cit. on p. 61).

[98] R. Soltis, J. Hilditch, T. Clark, C. House, M. Gerhart, and G. Surnilla. "Intake Oxygen Sensor for EGR Measurement." *SAE Technical Paper Series* (2016). DOI: 10.4271/2016-01-1070 (cit. on p. 61).

[99] J. Chung, H. Kim, and M. Sunwoo. "Reduction of transient NOx emissions based on set-point adaptation of real-time combustion control for light-duty diesel engines." *Applied Thermal Engineering* 137 (2018), pp. 729–738. DOI: 10.1016/j.applthermaleng.2018.03.082. URL: https://doi.org/10.1016/j.applthermaleng.2018.03.082 (cit. on p. 61).

[100] F. Payri González and J. M. Desantes Fernández. "Motores de combustión interna alternativos." *Colección Académica. Editorial UPV* (2011) (cit. on p. 62).

[101] A. Moratal. "Experimental Analysis of Thermal Management Influence on Performance and Emissions in Diesel Engines At Low Ambient Temperature" (2018) (cit. on p. 62).

[102] J. Benajes, J. M. Lujan, V. Bermudez, and J. Serrano. "Modelling of turbocharged diesel engines in transient operation . Part 1: insight into the relevant physical phenomena." *Journal of automobile engineering* 216 (2002), pp. 431–441. DOI: 10.1243/0954407021529237 (cit. on p. 63).

[103] J. Benajes, J. M. Luján, and J. R. Serrano. "Predictive Modelling Study of the Transient Load Response in a Heavy-Duty Turbocharged Diesel Engine." In: *SAE Technical Paper*. 2000. DOI: 10.4271/2000-01-0583. URL: https://doi.org/10.4271/2000-01-0583https://www.sae.org/content/2000-01-0583/ (cit. on p. 63).

[104] J. R. Serrano, H. Climent, C. Guardiola, and P. Piqueras. "Methodology for characterisation and simulation of turbocharged diesel engines combustion during transient operation. Part 2: Phenomenological combustion simulation." *Applied Thermal Engineering* 29(1) (2009), pp. 150–158. ISSN: 13594311. DOI: 10.1016/j.applthermaleng.2008.02.010. URL: http://dx.doi.org/10.1016/j.applthermaleng.2008.02.010 (cit. on p. 63).

[105] K. Robinson, S. Ye, Y. Yap, and S. T. Kolaczkowski. "Application of a methodology to assess the performance of a full-scale diesel oxidation catalyst during cold and hot start NEDC drive cycles." *Chemical Engineering Research and Design* 91(7) (2013), pp. 1292–1306. ISSN: 02638762. DOI: 10.1016/j.cherd.2013.02.022. URL: http://dx.doi.org/10.1016/j.cherd.2013.02.022 (cit. on p. 67).

[106] M. Kao and J. J. Moskwa. "Turbocharged Diesel Engine Modeling for Nonlinear Engine Control and State Estimation." *Journal of Dynamic Systems, Measurement, and Control* 117(1) (1995), pp. 20–30. ISSN: 00220434. DOI: 10.1115/1.2798519. URL: http://dynamicsystems.asmedigitalcollection.asme.org/article.aspx?articleid=1406784 (cit. on p. 68).

[107] M. Goyal. "SIMULATION OF A TURBOCHARGED DIESEL-ENGINE TO PREDICT THE TRANSIENT-RESPONSE." In: *MECHANICAL ENGINEERING*. Vol. 101. 1. ASME-AMER SOC MECHANICAL ENG 345 E 47TH ST, NEW YORK, NY 10017. 1979, pp. 87–87 (cit. on p. 68).

[108] Y. H. Zweiri, J. F. Whidborne, and L. D. Seneviratne. "Detailed analytical model of a single-cylinder diesel engine in the crank angle domain." *Proceedings of the Institution of Mechanical Engineers, Part D: Journal of Automobile Engineering* 215(11) (2001), pp. 1197–1216. ISSN: 0954-4070. DOI: 10.1243/0954407011528734. URL: http://journals.sagepub.com/doi/10.1243/0954407011528734 (cit. on p. 68).

[109] D. Anguita, F. Rivieccio, M. Canova, P. Casoli, and A. Gambarotta. "A Learning-Machine Based Method for the Simulation of Combustion Process in Automotive I.C. Engines." In: *Proceedings of the ASME 2003 Internal Combustion Engine Division Spring Technical Conference. Design, Application, Performance and Emissions of Modern Internal Combustion Engine Systems and Components*. ASMEDC, 2003, pp. 595–602. ISBN: 0-7918-3678-9. DOI: 10.1115/ICES2003-0682. URL: https://asmedigitalcollection.asme.org/ICES/proceedings/ICES2003/36789/595/295959 (cit. on p. 68).

[110] O. Varnier. "Trends and Limits of Two-Stage Boosting Systems for Automotive Diesel Engines." PhD thesis. 2012 (cit. on pp. 68, 98).

[111] N. Chung, S. Kim, and M. Sunwoo. "Nonlinear Dynamic Model of a Turbocharged Diesel Engine." In: *SAE Technical Papers*. 2005. DOI: 10.4271/2005-01-0017. URL: https://www.sae.org/content/2005-01-0017/ (cit. on p. 68).

[112] M. Canova. "Development and validation of a control-oriented library for the simulation of automotive engines." *International Journal of Engine Research* 5(3) (2004), pp. 219–228. ISSN: 1468-0874. DOI: 10.1243/1468087041549625. URL: http://journals.sagepub.com/doi/10.1243/1468087041549625 (cit. on p. 68).

[113] R. Isermann, S. Sinsel, and J. Schaffnit. "Modeling and Real-Time Simulation of Diesel Engines for Control Design." In: *SAE Technical Papers*. 1998. DOI: 10.4271/980796. URL: https://www.sae.org/content/980796/ (cit. on p. 68).

[114] H. J. Dekker and W. L. Sturm. "Simulation and Control of a HD Diesel Engine Equipped with New EGR Technology." In: *SAE Technical Papers*. 1996. DOI: 10.4271/960871. URL: https://www.sae.org/content/960871/ (cit. on p. 68).

[115] S. Saulnier and S. Guilain. "Computational Study of Diesel Engine Downsizing Using Two-StageTurbocharging." In: *SAE Technical Papers*. 2004. ISBN: 0768013194. DOI: 10.4271/2004-01-0929. URL: https://www.sae.org/content/2004-01-0929/ (cit. on p. 68).

[116] C. Ciesla, R. Keribar, and T. Morel. "Engine/Powertrain/Vehicle Modeling Tool Applicable to All Stages of the Design Process." In: *SAE Technical Papers*. 2000. DOI: 10.4271/2000-01-0934. URL: https://www.sae.org/content/2000-01-0934/ (cit. on p. 68).

[117] G. Technolgies. *Engine/Powertrain/Vehicle Modeling Tool Applicable to All Stages of the Design Process*. 2017 (cit. on p. 68).

[118] N. Winkler. "Reduced models for flows in IC-engines." QC 20110928. PhD thesis. KTH, Internal Combustion Engines, 2011, pp. viii, 120. ISBN: 978-91-7501-107-3 (cit. on p. 69).

[119] N. Winkler and H.-e. Ångström. "Simulations and Measurements of a Two-Stage Turbocharged Heavy-Duty Diesel Engine Including EGR in Transient Operation." *SAE Technical Paper 2008-01-0539* 2008(724) (2008). DOI: 10.4271/2008-01-0539 (cit. on p. 70).

[120] J. Galindo, J. M. Lujan, J. Serrano, and L. Hernández. "Combustion simulation of turbocharger HSDI Diesel engines during transient operation using neural networks." *Applied Thermal Engineering* 25(5-6) (2005), pp. 877–898. ISSN: 13594311. DOI: 10.1016/j.applthermaleng.2004.08.004 (cit. on p. 73).

[121] D. N. Assanis, Z. Filipi, S. B. Fiveland, and M. Syrimis. "A Methodology for Cycle-By-Cycle Transient Heat Release Analysis in a Turbocharged Direct Injection Diesel Engine." *SAE Technical Papers* 109 (2000), pp. 1327–1339. DOI: 10.4271/2000-01-1185. URL: https://www.sae.org/content/2000-01-1185/ (cit. on p. 73).

[122] Y. Cui, K. Deng, and J. Wu. "A direct injection diesel combustion model for use in transient condition analysis." *Proceedings of the Institution of Mechanical Engineers, Part D: Journal of Automobile Engineering* 215(9) (2001), pp. 995–1004. ISSN: 0954-4070. DOI: 10.1243/0954407011528563. URL: http://journals.sagepub.com/doi/10.1243/0954407011528563 (cit. on p. 73).

[123] D. Winterbone and D. Tennant. *The variation of friction and combustion rates during diesel engine transients*. Tech. rep. SAE Technical Paper, 1981 (cit. on p. 73).

[124] G. Zamboni and M. Capobianco. "Influence of high and low pressure EGR and VGT control on in-cylinder pressure diagrams and rate of heat release in an automotive turbocharged diesel engine." *Applied Thermal Engineering* 51(1-2) (2013), pp. 586–596. ISSN: 13594311. DOI: 10.1016/j.applthermaleng.2012.09.040. URL: http://dx.doi.org/10.1016/j.applthermaleng.2012.09.040 (cit. on pp. 73, 89).

[125] A. Maiboom, X. Tauzia, S. R. Shah, and J.-f. Hétet. "Experimental Study of an LP EGR System on an Automotive Diesel Engine , compared to HP EGR with respect to PM and NOx Emissions and Specific Fuel Consumption." *SAE International Journal of Engines* 2(2) (2009), pp. 597–610. ISSN: 19463936. DOI: 10.4271/2009-24-0138 (cit. on pp. 73, 89).

Chapter 4

Hybrid EGR strategies

Contents

4.1 Introduction

In the competitive market of internal combustion engines, diesel engines have always been a participant with a better thermodynamic efficiency as compared to gasoline engines. They provide reduced fuel consumption and pumping losses and better combustion efficiency with lean and un-throttled operations [126]. However, conventional diesel engines with high combustion efficiency, produce high nitrogen oxides and soot, which is hampering the health of our environment and living things. Different governments have taken actions against this emission of pollutants and made emission regulations curbing the pollution in environment. Various automotive manufacturers and researchers have developed different techniques to reduce these harmful gases emissions. They can be classified by the way of treatment as internal and external to the combustion chamber. After treatment techniques downstream the exhaust manifold are external methods applied outside of the combustion chamber. They consist of diesel particulate filter, diesel oxidation catalyst, NO_x trap and SCR as a part of them. But these techniques increase the complexity and penalty of fuel efficiency of an engine. On the other hand, in cylinder pollutant reduction consists forced low temperature combustion strategies like PCCI, MK, RCCI and EGR. These are effective ways to provide pre mixed charge and ignition delay for the combustion, reducing the formation of pollutants inside combustion chamber [127].

EGR is one of those strategies which displaces the amount of air going inside the combustion chamber lowering the lambda and oxygen concentration during combustion. It is a proven method to lower the NO_x formation in the combustion chamber with particular flow rate depending upon the operating point of a diesel and gasoline engine [128, 129] as well as natural gas engines [130]. The circulation of these exhaust gases in higher rates can produce soot as per the NO_x and soot trade-off explained in Chapter 1. Studies have been carried out to reduce the soot formation with higher EGR rates with specific injection duration also called as negative ignition dwell [131]. However, as the EGR rate increases, exhaust gas emissions and thermal efficiency vary with the intake oxygen content rather than with the excess air ratio [132]. Therefore intake oxygen concentration is also required to be monitored. Using an optimized dwell, injection ratio and two-stage injection the UHC and CO emissions can be reduced. However, their values are still high in the ultra-high EGR smokeless regime suggested by [133].

There are various methods/types to inject this exhaust gases to combustion chamber by using a high pressure circuit (HPEGR) just before the intake manifold and low pressure (LPEGR) circuit before the compressor. Both of these EGR types are beneficial at particular operating points depending on the size and components of the engine. Additionally, the internal EGR concept is also useful, which can be implemented by changing the overlap of intake and exhaust valve timing. However, the cooling of these kind of recirculation appears to be impractical [134, 135]. The LPEGR mixes properly with the intake air giving better reduction in NO_x [136, 124]. It increases the mass flow through the compressor increasing the efficiency of the turbocharger and high EGR rates can be achieved and implemented [125, 50]. Besides, there is no transportation of exhaust gases before turbine, the turbine power also increases. On the other hand, HPEGR is faster in response as it reaches to the intake manifold through shorter route which is helpful in the transient operations. Moreover, HPEGR reduces the pressure difference across the intake and exhaust of the engine reducing the pumping losses. Henceforth, it improves the brake specific fuel consumptions (BSFC). Comparatively, HPEGR generally shows better results at low loads while LPEGR offers advantages at high loads [39]. Nonetheless, LPEGR has shown a clear advantage over HPEGR with respect to engine efficiency and NO_x/smoke emissions trade-off in a large part of the engine map. LPEGR in combination with single-stage VGT was found to offer a balanced engine efficiency and emissions trade-off over the entire engine operating area [126]. Cooling of the exhaust gases before sending them to intake of the cylinder reduces the temperature of the intake charge [137, 138, 139]. In deduction, both types of EGR have their advantages depending the operating point of the engine. Most studies have proved that the simultaneous use of both HP and LPEGR with certain proportions are useful for performance and emission specific zones of the engine maps [140, 136]. Researchers even tried to design controllers for the actuators of EGR flow to provide required EGR rate to combustion chamber in steady state and transient operation [141, 142]. However, the proper optimization of this proportion between existing HP and LPEGR is required.

In regards to optimization of various engine output parameters, various numerical methodologies have been used and developed for single and multi objective optimization. Genetic algorithm is the most popular of them. The MOGA is able to collectively find a pareto optimal set using a multi-point search method. It is used on phenomenological models to optimize the fuel economy and emissions by [143, 143, 144]. It is also used to train the neu-

ral networks with the data from CFD models to predict the performance by reducing the time of optimization [145, 146]. Additionally, MOGA is useful in optimizing the piston geometry [147], while Non dominated sorting GA is used for modelling CO and NO_x emissions [148]. In the case of EGR splitting between HP and LPEGR, MOGA is used by [149, 150]. It takes into account the possible range of EGR rates and thermo-mechanical limits of the engine system. However full fledge analysis of impacts of different proportion of HP and LPEGR with single stage turbocharger considering various thermo-mechanical limits is required. The effect of cooling of HPEGR is also needed to be analysed to make a comparative study with LPEGR with variable geometry turbocharger. Moreover, a sophisticated solution is required other than DOE to reduce the calculation time to find the optimum ratio between HP and LPEGR to get the desired output from the engine.

This chapter includes, the parametric study of different split between HP and LPEGR to see the effect on different engine parameters. The designated EGR split index is used to characterized the ratio between both EGR types. The 1D model for engine 2 is created in GT-Power software described in Chapter 3. Various thermo mechanical limits have been set for studying the full potential of the EGR implementation. Moreover to access the advantages of cooled high pressure EGR, coolers have been created and calibrated with the engine test results. Thereafter, a sweep has been performed changing the split index of LP and HPEGR mass flow rate, respecting the total EGR rate with and without HPEGR coolers. Finally, various advantages and penalties are concluded with these various splits ratios on engine parameters like BSFC, PMEP, MEP and compressor efficiency. In the following section, optimization techniques are applied to the ESI by multi objective genetic algorithm. In the end, a new control algorithm is proposed to reduce the time of optimization by using the different modelled controllers in GT Power.

4.2 Engine model

A 1D model is created for engine 2 described in the Chapter 3. It consisted two EGR lines called HPEGR and LPEGR. The HPEGR line (short route) is designed through the intake manifold. The exhaust gases are directed through a solenoid valve and injected before the intake valve through a common rail type structure as shown in Figure 4.1(a). The simplified 1D GT-Power model

of HPEGR system along with the intake manifold and engine is presented in Figure 4.1(b).

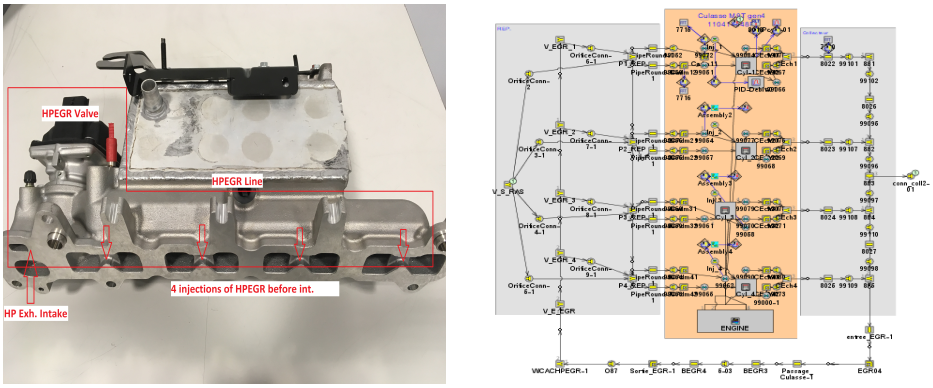

(a) Physical system (b) GT-Power model

Figure 4.1: HPEGR line from the engine and simplified GT-Power model.

LPEGR system normally has very long path connecting the exhaust line after the DPF to intake of compressor. On the engine 2, efforts has been done to reduce the length of LPEGR line to overcome the delays involved in the mass flow rate. Figure 4.2(b) shows the full LPEGR line with compact LPEGR cooler attached downstream of the DPF and LPEGR valve. The low pressure exhaust gases mix with the fresh air before compressor. The 1D model of this LPEGR line is displayed in the Figure 4.2(b). To model the DPF, DOC and SCR, ready made templates from GT-Power have been used and tuned with the test results obtained in steady state for getting the exact back pressure in the exhaust line.

The LPEGR system is not enough to provide high EGR rates even after opening th LPEGR valve fully. This happens due to absence of large pressure difference across the LPEGR valve. Therefore exhaust throttle is used to create the larger pressure difference serving for higher LPEGR rates. An extra PID controller is used to control the exhaust throttle. The controller activates when LPEGR valve reaches to its threshold opening value (90% of maximum open condition). This activates the ET controller closing the throttle to reach higher LPEGR mass flows. Otherwise, when the LPEGR valve is below the threshold, the ET control is deactivated providing output of 100% valve opening.

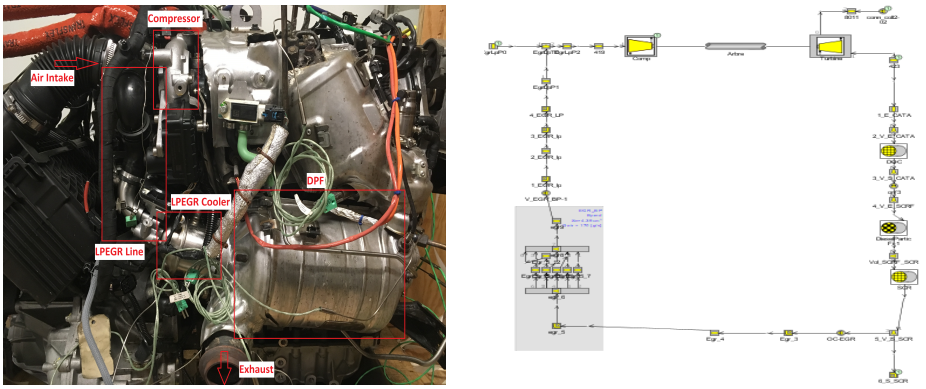

(a) Physical system (b) GT-Power model

Figure 4.2: LPEGR line from the engine 4.2(a) and simplified GT-Power model 4.2(b).

The LPEGR cooler is modelled with the help of a basic volume and surface area from the physical cooler. The effectiveness of the cooler is determined as a function of mass flow rate flowing upstream the LPEGR cooler from the test results. The same corelation is used to calculate the temperature of the low pressure exhaust gases.

$$\epsilon = \frac{q}{q_{max}} = \frac{T_{in} - T_{out}}{T_{in} - T_{coolant}} \tag{4.1}$$

To see the effects of cooled HPEGR, external heat exchanger is added in the model. The characterization of this HPEGR cooler is done with the help of $\epsilon - NTU$ method. Following the equation 4.1, The effectiveness of the counter flow heat exchanger can be calculated by the equation 4.2 (by the $\epsilon - NTU$ analysis) [151, 152].

$$\epsilon = \frac{1 - e^{(-NTU \cdot (1-C))}}{1 - C \cdot e^{(-NTU \cdot (1-C))}} \tag{4.2}$$

Where, C is the dimensionless heat capacity ratio of hot gas and coolant inside the heat exchanger.

$$C = C_{min}/C_{max} \tag{4.3}$$

While, NTU is the number of transfer units (NTU) that is used for heat

exchanger analysis and is defined as,

$$NTU = \frac{U \cdot A}{C_{min}} = \frac{U \cdot A}{mf \cdot c_p} \tag{4.4}$$

Considering the same coolant temperature of around 70-80°C, the C_{max} value goes to infinity formulating the heat capacity ratio equal to zero. Therefore the equation 4.2, substituted with 4.3 and 4.4, can be reduced to a simple governing equation (4.5). Whereas, K stands for a $\frac{U \cdot A}{C_p}$, which can be tuned to get the effectiveness of the heat exchanger corresponding to the test data of LPEGR cooler. Figure 4.3 represents the calculated effectiveness of the HPEGR cooler (with K=0.04), as a function of mass flow rate of high pressure gases going through it. This curve of effectiveness is imposed in the model as input to calculate the HPEGR temperature after the cooler.

$$\epsilon = 1 - e^{(-\frac{K}{m_f})} \tag{4.5}$$

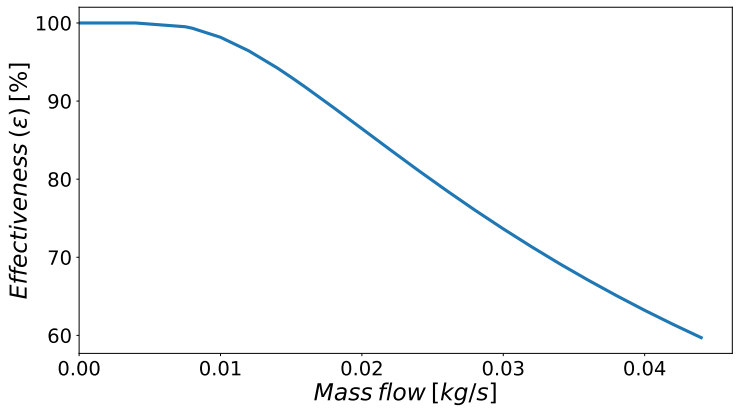

Figure 4.3: Calculated effectiveness of HPEGR cooler imposed in the 1D model during simulations.

To model the combustion, the combustion profiles for full load operations at each engine speed were imposed as a heat release rate in the combustion template of GT-Power. The start of injection (SOI) is positioned to get the indicated mean effective pressure from the tests.

4.3 Model validation

Validation of the above engine model is done on 11 engine operating points spread over the engine map with existing engine calibration in the ECU. Figure 4.4 represents the chosen operating points on the engine map for the model validation and study. According to the current engine calibration, ECU uses LPEGR on the entire operating range except the cold start period. HPEGR is used instead to heat up the engine [1]. Therefore the above GT-Power model is validated with the test results from existing calibration. The coolant temperature is kept above 70°C and LPEGR is used, keeping the HPEGR valve completely closed. The engine speed, fuel injection quantity, boost pressure and EGR rate measured during the tests were inputs to the model. The target boost pressure and EGR rate is achieved by PID controllers actuation of VGT and area of the LPEGR valve respectively.

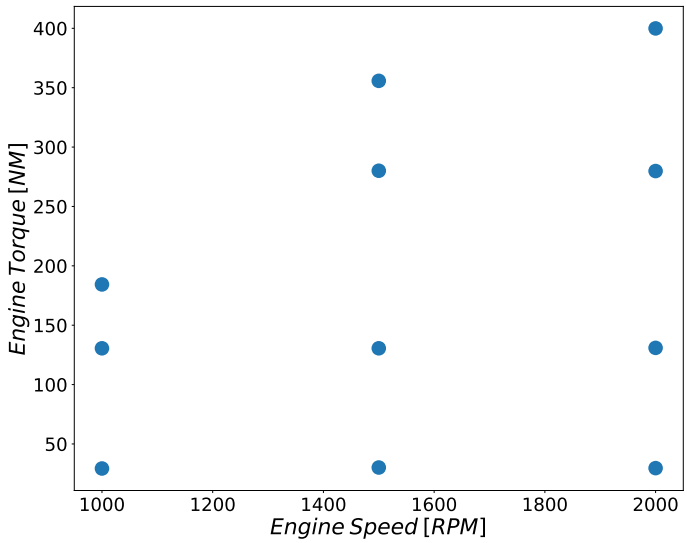

Figure 4.4: 11 steady operating points over the engine map of Engine 2 used for validation of 1D model.

The results obtained from simulation are compared with the test results. The comparison of experimental and modeled data for the intake and exhaust line are presented in Figure 4.5 and 4.6. The simulated results show good

[1]This current calibration of engine regarding EGR rate and NO_x modelling is discussed in Chapter 6

agreement with the experimental data with ±5% of tolerance. The variables names depend on the location on the engin map as follows,

P1,T1 Pressure and temperature before compressor

P2,T2 Pressure and temperature after compressor

P3,T3 Pressure and temperature before turbine

P4,T4 Pressure and temperature after turbine

The difference between experimental and test values for each variable are calculated. Figure 4.5 represents the difference between experimental and simulation values of intake line variables. Figure 4.6 represents the same for exhaust line.

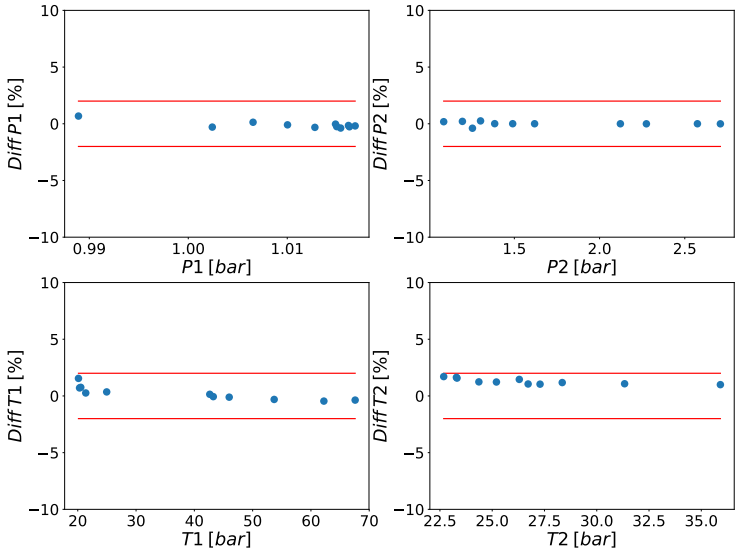

Figure 4.5: Validation of intake line variables of engine model with the tolerance of ±1%.

4.4 EGR Split Index

The proportion of high and low pressure exhaust that is recirculated to the intake of the engine is represented by the index which is called as EGR Split

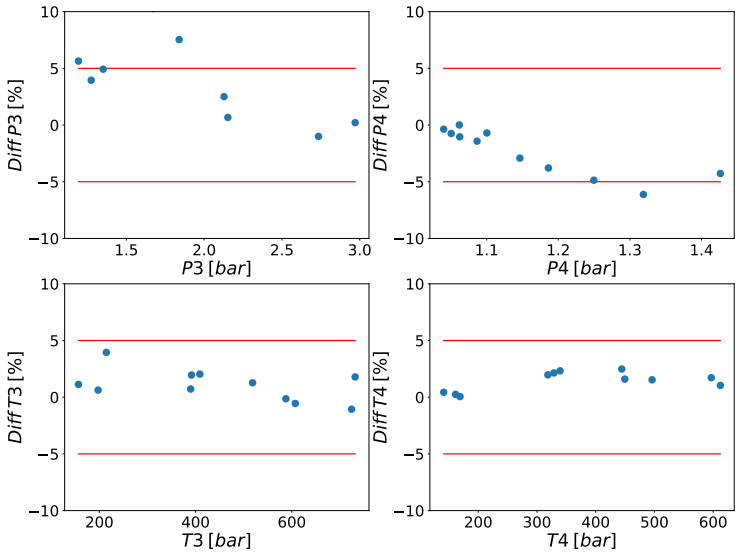

Figure 4.6: Validation of exhaust line variables of engine model with the tolerance of $\pm 5\%$.

Index. It is not just a ratio of exhaust gas flow coming from the high and low pressure line. The ESI for a specific engine operation is actually calculated by the inverse exponential [2] of LP and HPEGR gas fraction (see Equation 4.6). The index has a realistic range of 0 to 1, which is not the case by taking the simple ratio of mass flows of those exhaust gases only.

$$\begin{aligned} ESI &= {}^{1}/_{e^{\left(\frac{P_{lp}}{P_{hp}}\right)}}; \\ where, \quad P_{lp} &= \frac{F_{lp}}{F_{egr}}; \quad P_{hp} = \frac{F_{hp}}{F_{egr}} \end{aligned} \tag{4.6}$$

F_{lp} and F_{hp} are the mass flow rates of LP and HPEGR respectively. While, the F_{egr} is the total EGR rate going inside the cylinder. Inferring to the equation 4.6, ESI takes values from range 0 to 1 representing only LPEGR (ESI=0) to only HPEGR (ESI=1) configuration. The Figure 4.7 represents the amount (in percentage) of LPEGR rate as a function of HPEGR rate for different ESI values obtained by the Equation 4.7 derived from the Equation 4.6 by taking

[2] The inverse exponential benefits the value of function between 0-1 for positive EGR fractions. Positive x axis acts as an asymptote for the curve considering the range of term $\frac{P_{lp}}{P_{hp}}$ varying from 0 to $+\infty$

natural logarithm. The slope of different straight lines is nothing but the natural logarithm of ESI values associated with respective LP and HPEGR rate. The exact equal amount of HP and LPEGR gives the ESI value equal to 0.368 mathematically representing the dotted blue line with 45º of angle with horizontal x-axis.

$$LPEGR = -HPEGR \cdot (\ln(ESI)) \tag{4.7}$$

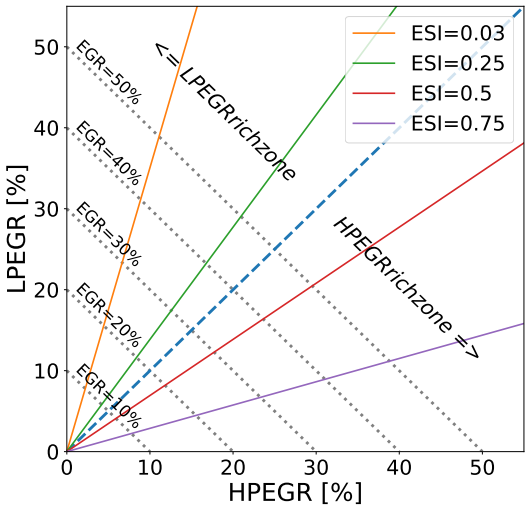

Figure 4.7: EGR split indices used during the simulations with different HP and LPEGR contribution from 10 tp 50% of total EGR rate.

4.5 Methodology

To see the effect of ESI on various engine parameters during the steady state operation, exhaustive simulation campaign has been carried out varying EGR rate and ESI. In the first step, variation of total EGR rate is done on full load operations among above mentioned 11 operating points. The values used for total EGR rates with only LPEGR configuration as per the calibration are 10,20,30,40%. The mass of fuel injected was kept constant for each operating

point while injection settings (Start of injection) are optimized with different LPEGR rates to give maximum BSFC. The second step consisted of variation of ESI values for respective total EGR rates. The ESI values are varied from 0 to 1 by 0.2 while the SOI and air mass flow were tried to be kept constant for each EGR rate [3]. Figure 4.8 displays the SOI and air mass flow for full load point at 1000 RPM with variation of ESI. In second phase, the low load operating points simulated with ~ 25, ~ 50 and $\sim 75\%$ of load. The variations of EGR and ESI is done similar to the full load points.

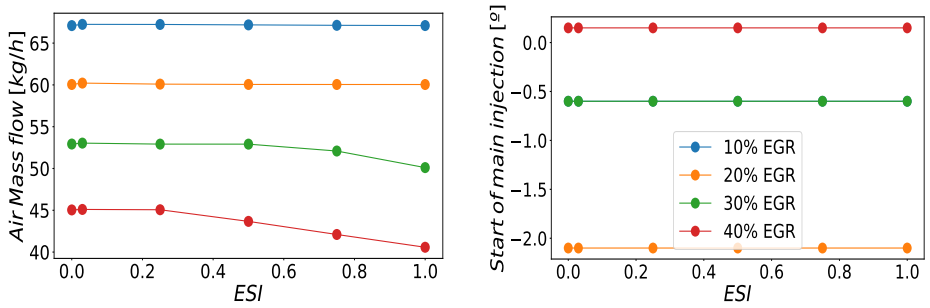

(a) Air flow (b) SOI

Figure 4.8: Air mass flow and SOI settings during the parametric study at full load 1000 RPM engine speed.

Different levels of thermo-mechanical constraints were defined considering the state of art for passenger cars [110]. From the compressor point of view, the outlet compressor temperature is limited to 190ºC to prevent damage of the plastic ducts which compose the intake line and 9% of margin is taken on the maximum turbocharger speed to limit over speed problems in altitude. For the combustion chamber at 1000 rpm the limitation is up to 150 bar for passenger cars. For higher engine speeds, the cylinder pressure is limited to 170 bars. Finally, the maximum permissible exhaust temperature is also limited to prevent turbine and exhaust manifold failures setting the level at 810ºC.

Optimization of the ESI to attain certain objective is done in the third phase. Two methods were used to find the optimum ESI at particular engine operating point. First one involves the genetic algorithm for multi objective pareto optimization. The independent variables like ESI and total EGR rate

[3]For high EGR rates and high ESI values at full load operation, it is difficult to maintain the air mass flow due to absence of turbine power.

Compressor downstream Temp.	190°C
Turbine upstream Temp.	810°C
Max. In-cyl. Pressure(1000rpm)	150bar
Max. In-cyl. Pressure(>1000rpm)	170bar

Table 4.1: Thermo-mechanical limits of the engine part.

are varied to optimize the dependent variables like pumping losses and BSFC. The optimization problem defined by the equation 4.8 represent the function which needs to be minimized with the mentioned thermo-mechanical limits as the constraints.

$$Torque_{req}, BSFC, NO_x = f(ESI, EGR, m_{fuel}) \tag{4.8}$$

The algorithm makes a matrix of various combination of ESI, EGR and m_{fuel} within the specified range for each variable. The selection of operating conditions are selected further to minimize BSFC and NO_x, maintaining the required engine torque. An extra constraint of air to fuel ratio is added considering the smoke limiter strategy mentioned in the Chapter 3. The minimum value of AFR is maintained above stoichiometric value (λ greater than 1) during the optimization.

4.6 Parametric study

This section contains the results of the parametric study of EGR rate and ESI, that is done on the 11 operating points. The full load (first phase) and partial load (second phase) results are presented chronologically. Several engine parameters like boost pressure, intake temperature, PMEP, BSFC etc. are studied with impact from the changes in total EGR rate and ESI.

4.6.1 Full load operations

As stated earlier, the boost pressure (pressure after the compressor) is controlled by the PID controller by changing the VGT positions. Therefore, the pressure values are very much sensitive to VGT positions. From the Figure 4.9,

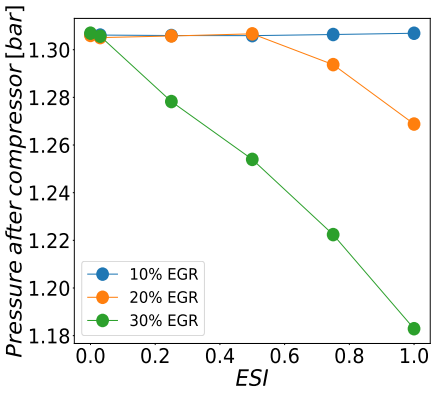

(a) 1000 RPM

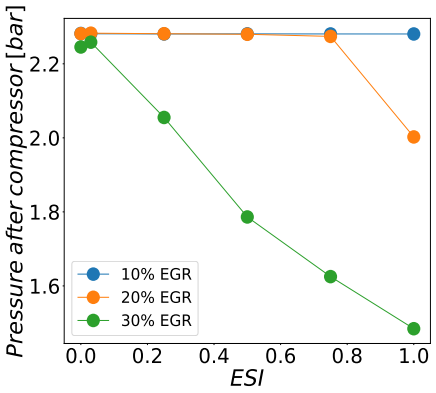

(b) 1500 RPM

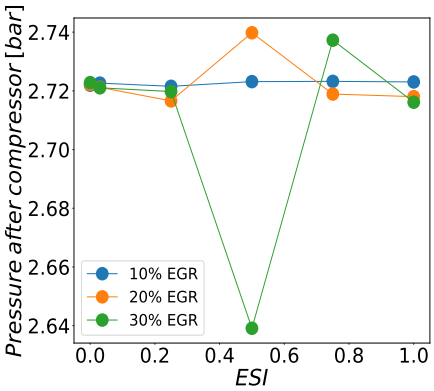

(c) 2000 RPM

Figure 4.9: Boost pressure after the compressor during the parametric study at full load.

it can be seen that, the boost control manages to control the target boost pressure for lower EGR rates. However, for high EGR rates, the boost pressure decreases with the higher ESI values for low engine speeds. Because, the air flow through the compressor decreases with higher proportion of HPEGR flow. Figure 4.10 shows the corresponding VGT positions suggested by the control. It is evident that, even though VGT closes fully (reaching to its minimum limit), in absence of the enough air at lower speeds the turbocharger is not able to maintain the required boost pressure at higher EGR rates. However, at 2000 rpm the availability of air causes the turbocharger to control the boost

pressure very well. The point at 0.5 ESI for 2000 rpm is an outlier as the boost control was not stable for this operating point.

Additionally, opening of HPEGR valve reduces the pressure before turbine, which lowers the energy available for a turbine to drive the turbocharger shaft. Therefore the boost pressure control has to close the VGT fully for those high EGR rates.

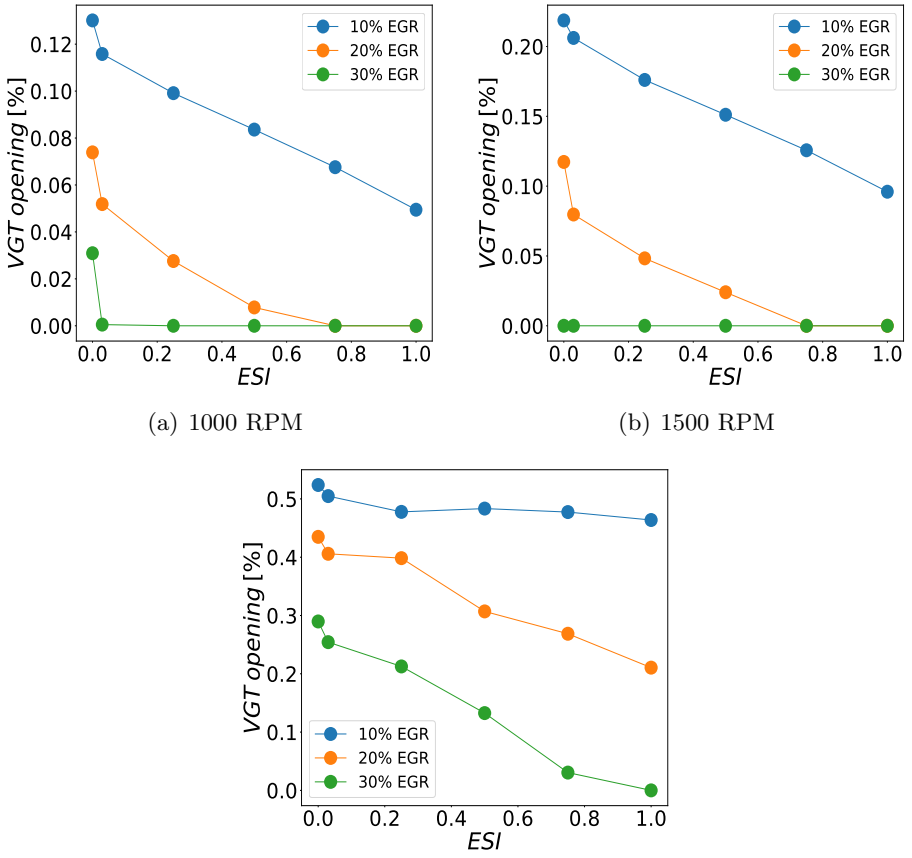

(a) 1000 RPM

(b) 1500 RPM

(c) 2000 RPM

Figure 4.10: Percentage opening of the variable geometry turbine during the parametric study at full load.

Since the compressor outlet temperature was the limiting factor in many situations, the range of application of LPEGR is strongly limited by this tem-

perature limit. The LPEGR configuration increases the temperature downstream of compressor rapidly crossing the threshold of 190°C at full load points (See Figure 4.11). Reduction of hot gases through the compressor with higher ESI values id the cause of low temperature values. Big difference in temperature at ESI=1 with high EGR rates is due to reduced boost pressure and air for example 30% of EGR at 1000 and 1500 RPM of engine speeds. At higher engine speeds, LPEGR causes the temperature after the compressor to reach above the limit where as HPEGR addition can reduce this temperature. Therefore higher ESI values for high speeds are beneficial for compressor outlet temperature.

Figure 4.12 represents the intake manifold temperature. Intuitively, addition of HPEGR should increase the temperature of the intake manifold, but the HPEGR is cooled and injected very close to intake valve of the cylinders. While, in the case of only LPEGR configuration, the hot gases are cooled twice in LPEGR cooler and WCAC. Therefore, no substantial differences are seen for the intake temperature values. Although the intake temperature is same for both LP and HPEGR case, the volumetric efficiency is not the same considering the injection of HPEGR gas is very close to intake valves.

As discussed earlier, the air to fuel ratio is controlled by the smoke limiter strategy. It maintains the value of AFR higher than stoichiometric AFR. In this case, for the diesel combustion, this minimum value was set to 14.7. Therefore, by the definition of lambda [153], the control tries to maintain the lambda higher than one [154, 155, 156]. At full load, higher EGR rates displace the air with exhaust gases leading to lower air to fuel ratios. This situation activates the smoke limiter control, and the fuel is reduced drastically to maintain the AFR value more than 14.7. Therefore, at full load, the EGR rates higher than 10% does not show benefit in torque as a consequence of fuel cutoff. Figure 4.13 represents the AFR values for the full load operations with different EGR rates. For EGR rates higher than 10% the AFR is maintained at 14.7 reducing fuel accordingly. While for 10% EGR rate the value increases with the ESI. That means, the lesser fuel gives sufficient torque output due to lesser losses in pumping.

The MEP is the indicated mean effective pressure without subtracting the pumping losses. The MEP (See Figure4 4.14) increases as you shift the EGR index to LPEGR side. For higher EGR rates, the reduced air mass flow surpasses the threshold for AFR. Therefore, the injected fuel is reduced leading to lower MEP for high total EGR rates. While at 10% EGR rate, the result

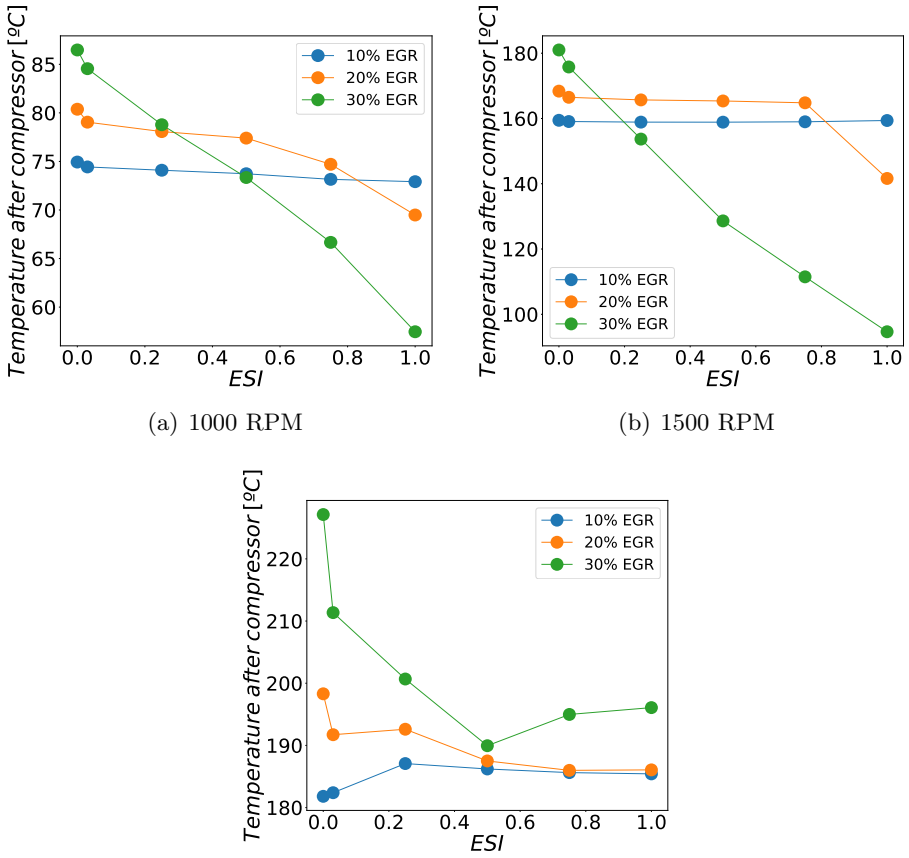

(a) 1000 RPM

(b) 1500 RPM

(c) 2000 RPM

Figure 4.11: Temperature downstream of compressor during the parametric study at full load.

are iso-fuel. For those points, LPEGR configuration is more convenient to obtain high MEP values compared to HPEGR for similar total EGR rates. Moreover, this situation is helpful to reduce the NO_x formation with better mixing of exhaust gases and air. Please note that the combustion parameters are not calibrated to empirical data considering the HPEGR. Secondly, although the HPEGR is cooled effectively (from the Figure 4.16), the LPEGR is cooled twice and has temperature close to 25ºC while high ESI values exhibit more temperature at the intake port (not the manifold). Therefore, this configuration reduces the volumetric efficiency and so the MEP as compared

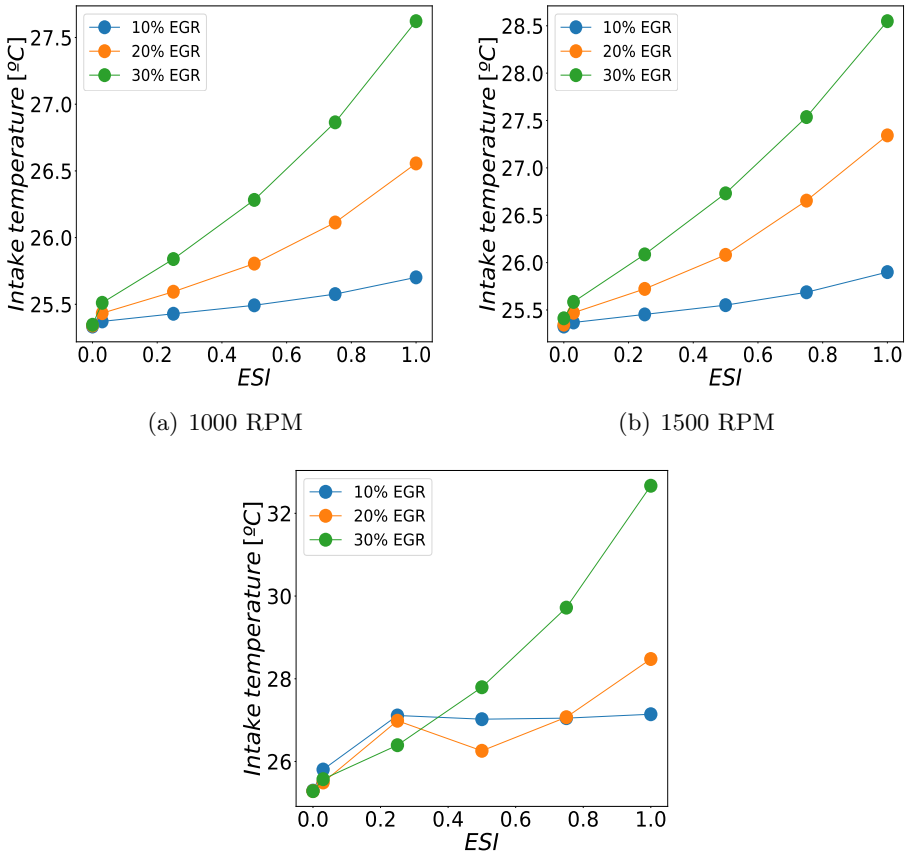

(a) 1000 RPM

(b) 1500 RPM

(c) 2000 RPM

Figure 4.12: Intake manifold temperature during the parametric study at full load.

to LPEGR.

High Pressure EGR line directly connects the exhaust manifold to intake manifold. This reduces the pressure difference (δP) across the intake and exhaust line, reducing the pumping losses caused during the complete 4 stroke engine cycle. But this phenomenon is critically impacted by the area of variable geometry turbine. Fixed area of the turbine geometry facilitates the reduction of pumping losses with HPEGR flows. Reduction in pumping losses is represented by reduction in absolute value of PMEP. However, the Figure 4.14 shows the absolute value of PMEP is increased with higher ESI (more share of

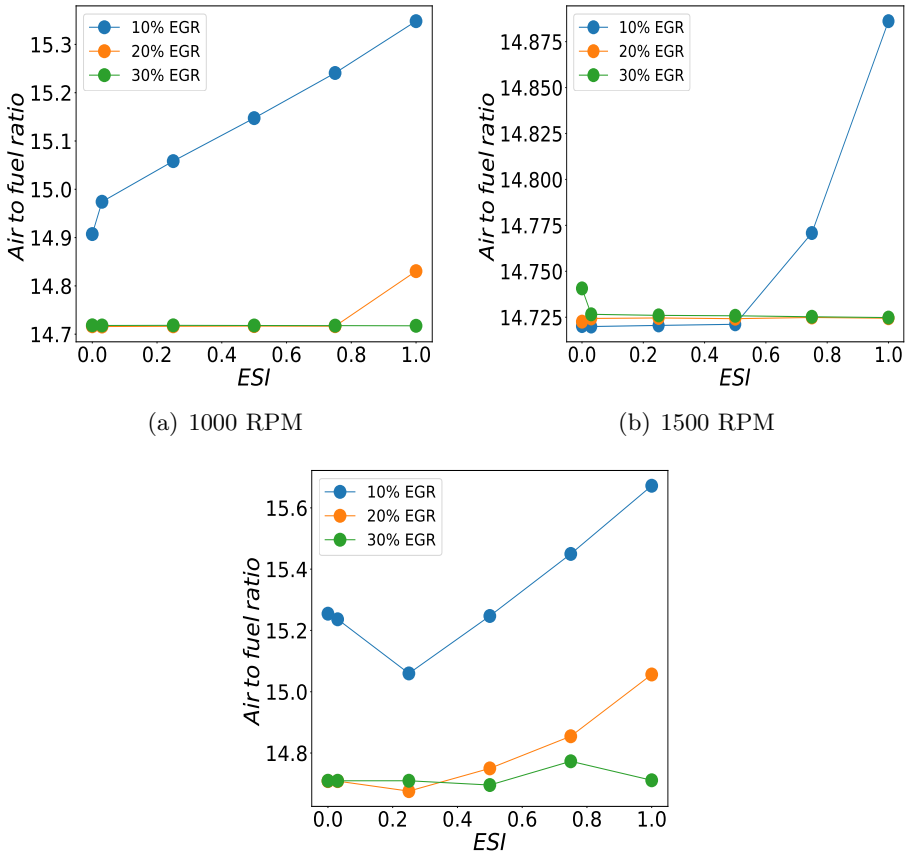

(a) 1000 RPM

(b) 1500 RPM

(c) 2000 RPM

Figure 4.13: Air to fuel ratio during the parametric study at full load.

HPEGR) values. Surely, the reason behind this disagreement can be explained by the VGT movement displayed in Figure 4.10. The given turbocharger is designed according the LPEGR configuration in consideration. HPEGR valve opening stresses the boost pressure control resulting into closure of the VGT. This eventually increases the δP across the cylinder and hence increases the pumping losses. At higher EGR rates (30%), the fuel is limited by smoke limiter causing less energy available at the turbine inlet. In succession to this, VGT is closed fully to meet the boost pressure requirement. Because of this fixed position of VGT, the natural phenomenon of higher ESI (high HPEGR) and then less δP happens as usual. Therefore, absolute PMEP decreases with

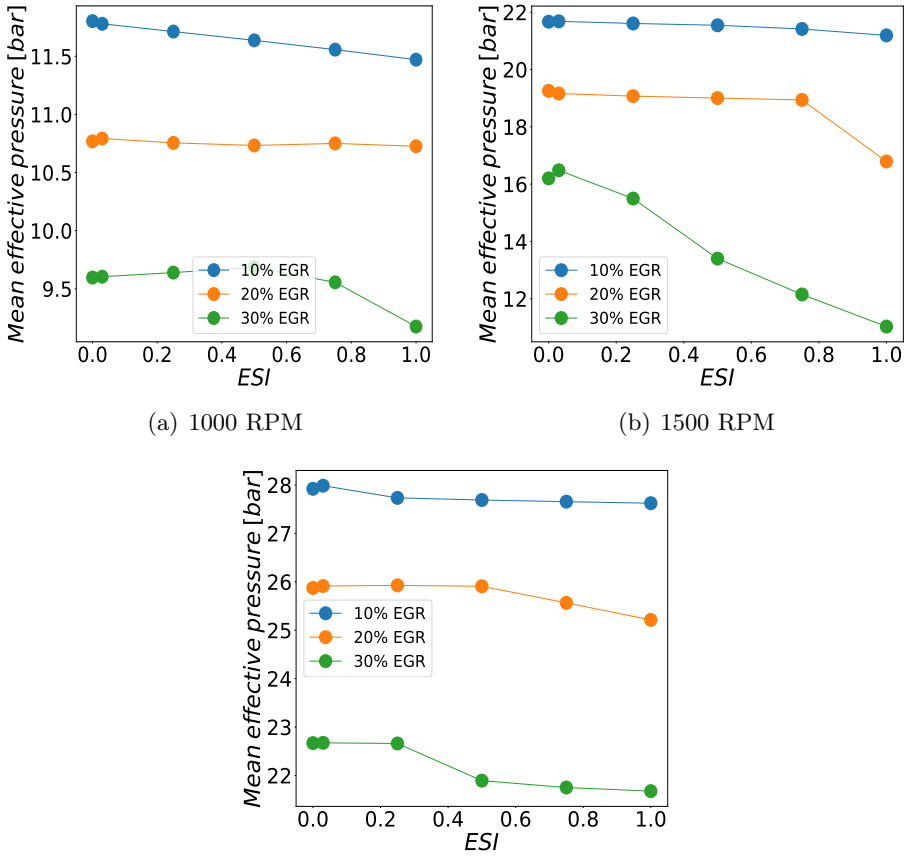

(a) 1000 RPM

(b) 1500 RPM

(c) 2000 RPM

Figure 4.14: Mean effective pressure in cylinder during the parametric study at full load.

ESI.

At higher engine speeds, Figure 4.15(c) shows that with 10% EGR rate, the trend is opposite. This is also explained by the VGT control as the higher flows supplies enough energy before turbine maintaining the VGT positions almost same for all ESIs. Retrospectively, the boost pressure control has major impact on the pumping losses together with the usage of HPEGR setting.

In the case of only LPEGR, higher EGR rate causes higher pumping losses. The effect of LPEGR on pumping losses depends on engine running conditions.

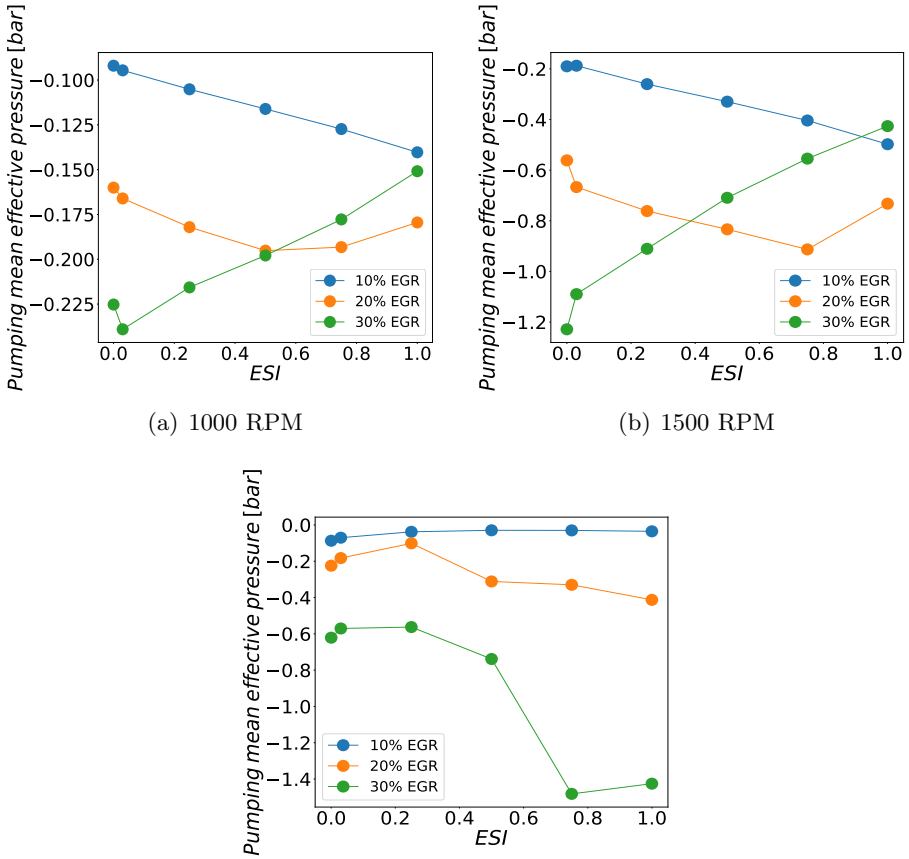

(a) 1000 RPM

(b) 1500 RPM

(c) 2000 RPM

Figure 4.15: Pumping mean effective pressure in cylinder during the parametric study at full load.

During high speeds, when the mass flow is higher the pumping losses with LP EGR increase dramatically because of increase in exhaust pressure. It seems that the optimum point of EGR split index can be found with HPEGR causing minimum pumping losses in the cycle. Therefore HPEGR is preferred with well designed turbine at full load high speeds. Whereas at low speeds, the LP EGR configuration is better with low total EGR rates with enough turbocharger power. The higher total EGR rate (30%) at low speeds, causes 100% closing of VGT meaning the reduction of pumping losses as fixed geometry turbine. Where, direct connection of intake and exhaust manifold reduce the delta P.

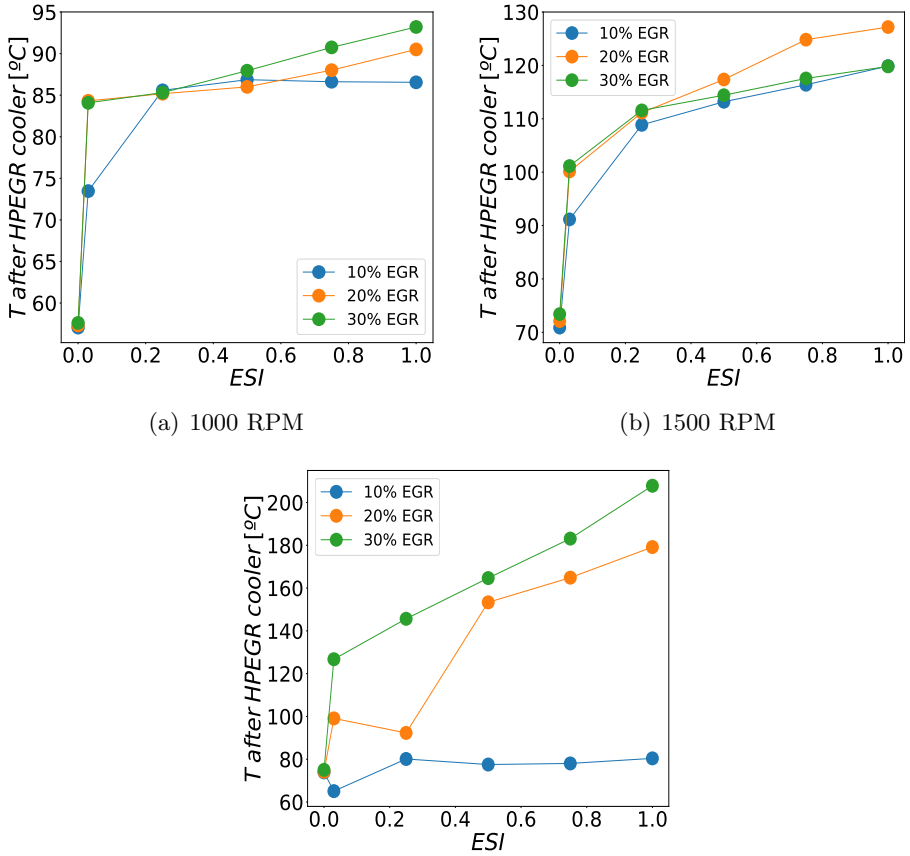

(a) 1000 RPM

(b) 1500 RPM

(c) 2000 RPM

Figure 4.16: Temperature after HPEGR cooler considering the effectiveness curve imposed in the calculations as a function of mass flow rate.

The BSFC depends on the fuel consumption and power output of the engine. Therefore the collective effect of MEP and pumping losses decide the final output of the engine. At 1000 rpm full load, the increase in global EGR rate decreases BSFC due to unavailability of air and thus fuel is reduced to avoid smoke. While at 1500 rpm, high global EGR rates increase the BSFC. As BSFC is the ratio of fuel consumed to the energy available for the application. Therefore, reduction of energy increases the BSFC for higher EGR rates which can be seen in the Figure 4.17(b) at 1500 and 2000 RPM. Collectively, the trade-off between gross IMEP (IMEP-PMEP) and fuel consumption is seen

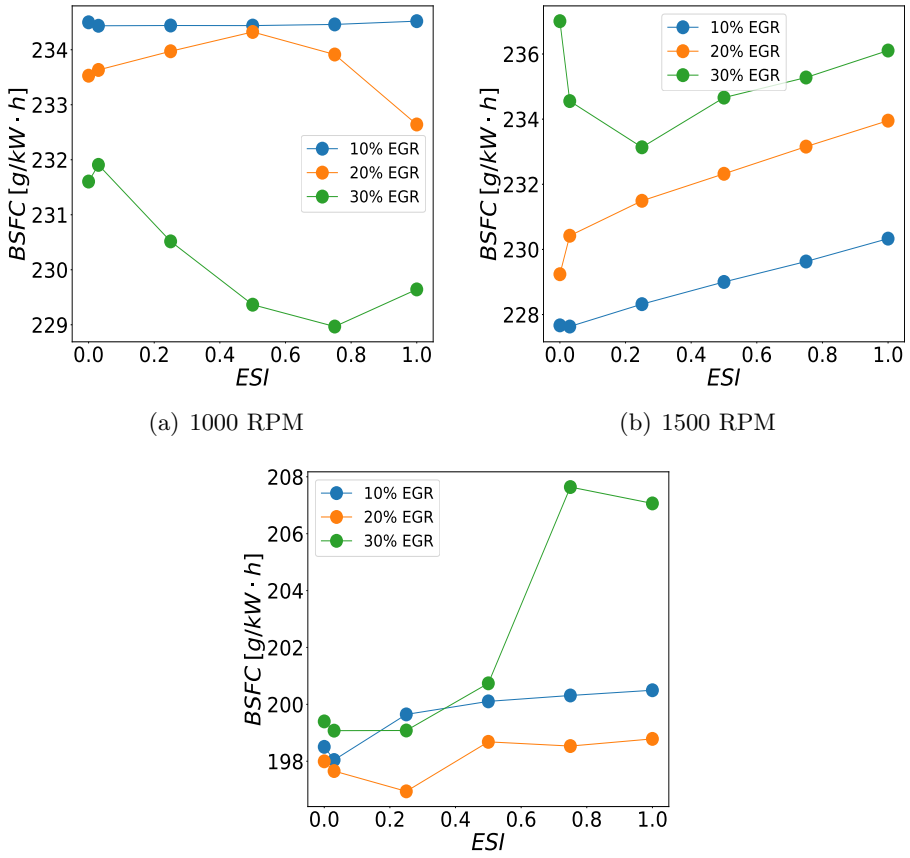

(a) 1000 RPM

(b) 1500 RPM

(c) 2000 RPM

Figure 4.17: Brake specific fuel consumption during the parametric study at full load.

with HP and LPEGR share at particular EGR rate. If the HPEGR can be cooled even more [4], it can increase the volumetric efficiency. Henceforth, in addition to the proper matching of turbocharger, BSFC can be lowered with HPEGR configuration.[157]. And so, it will increase the importance of HPEGR share in ESI.

From the compressor point of view, if above operating points are plotted on the efficiency map of compressor (See Figure 4.18). With only HPEGR configuration, the operating points fall at the lower mass flow side of the

[4] the limit is engine coolant temperature of 70°C

map (Considering the effect of intake temperature, mass flow is corrected by multiplying factor of $\sqrt{\frac{T/T_{ref}}{P/P_{ref}}}$). While with LPEGR, the operating point moves to upper-right side (more mass flow rate and pressure ratio). The temperature of the charge gets increases with LPEGR. It is evident from the Figure 4.18 that, the application of LPEGR moves the operating point of the compressor in higher efficiency zone. As this turbocharger is designed considering the LPEGR flows, this phenomenon is advantageous at the higher engine speeds too. Similarly in case of turbine, HP EGR configuration reduces the mass flow going through the turbine as it is bypassed to intake before entering into the turbine. Whereas, LP EGR configuration increases the flow through turbine.

4.6.2 Partial load operation

The second phase consists of the same study but on partial load points. The approximate load point selection is done for 25%, 50% and 75% of load at each engine speed (from Figure 4.4). The injection settings were obtained with LPEGR configuration and kept constant over the ESI sweep. The fuel is also kept constant to see the performance of engine with different EGR rates and EGR split index. The smoke limiter strategy is activated to keep the minimum air fuel ratio above the stoichiometric AFR. The total EGR rate is changed from 10% to 40% with increment of 10% while the ESI is swept from 0 (only LPEGR) to 1 (only HPEGR) with variation of 0.2.

As usual, the compressor outlet temperature (see Figure 4.19) at partial loads increases with the LPEGR. The limit of maximum temperature is surpassed at higher engine speeds close to full load. On the other hand, high ESI reduces the temperature after compressor as LPEGR flow gets reduced through the compressor. Increasing value of ESI, demands high power for turbine to provide enough energy to compress the intake air. But the minimum limit of VGT restricts this energy transfer. This causes less boost pressure after compressor, changing its operating point. That is why, in only HPEGR configuration, higher total EGR rates reduce the air mass flow and thus the compressor outlet temperature.

Intake temperature in the manifold is not much affected with the use of HPEGR same as in the full load, because of the HPEGR injection system design. This helped to maintain the lower air intake temperature. However,

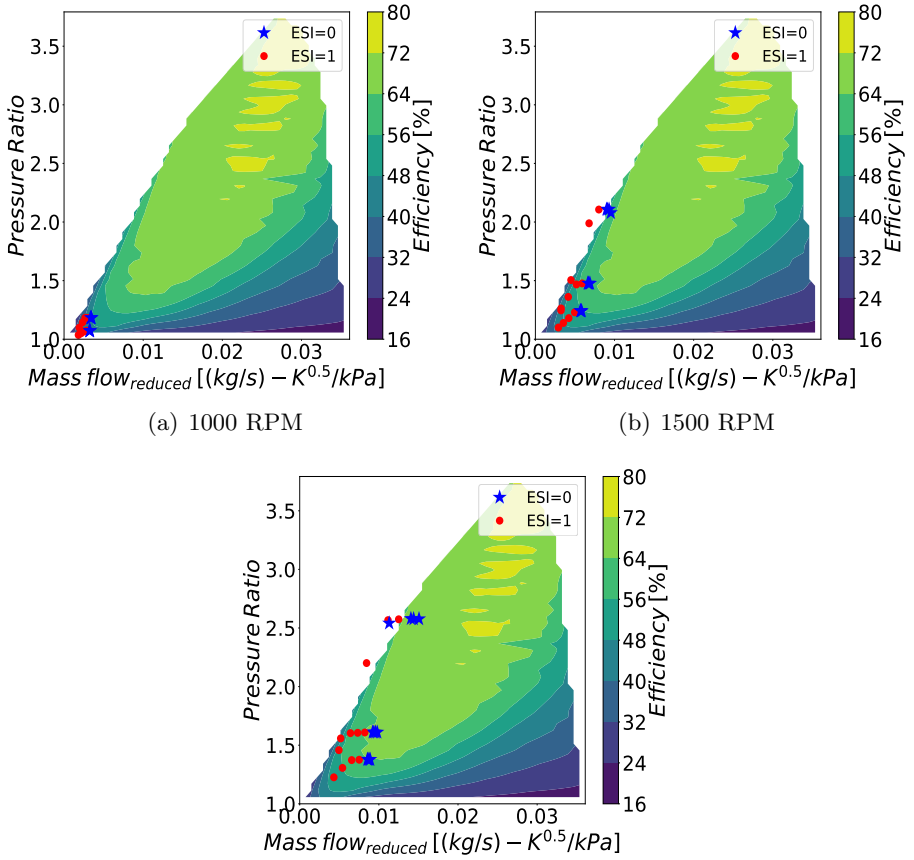

(a) 1000 RPM

(b) 1500 RPM

(c) 2000 RPM

Figure 4.18: Extreme operating points with HP (ESI=1) and LP (ESI=0) on a compressor efficiency map.

as discussed earlier in previous phase of full load operations, the volumetric efficiency of the cylinder gets affected with the HPEGR configuration in this particular engine. Mean effective pressure (see Figure 4.20) increases with the usage of HPEGR at low load points. The supply of high HPEGR rates is simpler, as the δP across the HPEGR valve is readily available. While in the case of LPEGR, the high LPEGR rate is not possible due to unavailability of enough δP across the LPEGR valve. This can be provided by throttling the exhaust gases using exhaust throttle. This causes increase in the back pressure in the exhaust line and eventually reduction in MEP. Therefore, HPEGR con-

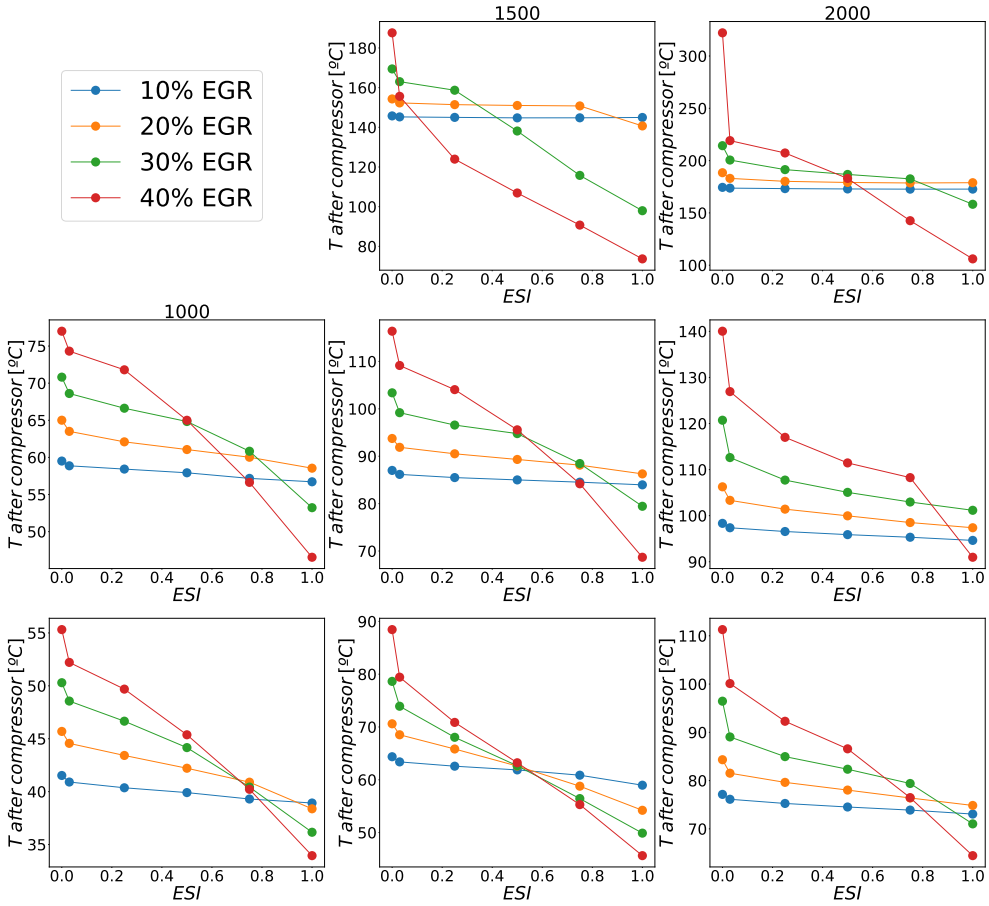

Figure 4.19: Compressor downstream temperature with HP, LP and their combinations at different engine speeds with partial loads. (The loadings are 75%, 50% and 25% from top to bottom.)

figuration is better at low loads providing higher global EGR rates. However, the partial load points (50% and 75%) show the contrary results. As we go to higher load points, higher ESI values reduce the MEP by less volumetric efficiency and also the turbocharger fails to provide enough boost pressure in the intake line.

The impact of global EGR rate on PMEP is less in the case of LPEGR as it is further from the cylinder and recirculates exhaust gases after the turbine. While HPEGR rates affect the PMEP largely as it is directly connected to the

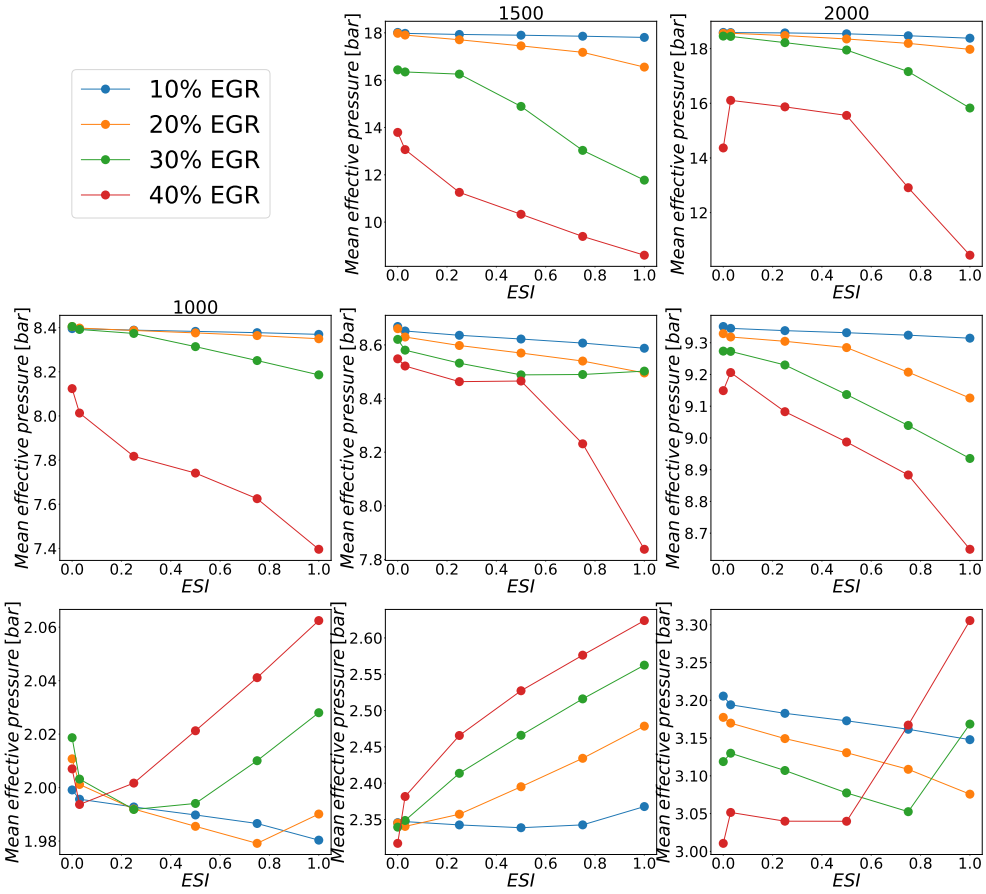

Figure 4.20: Mean Indicated Pressure with HP, LP and combinations. (part load)

intake and exhaust of the cylinder. Hence at low loads it is advantageous to use high ESI configuration for less pumping losses while at high loads LPEGR is useful for lower global EGR rates. Higher global EGR rate also can be pushed to meet the NO_x emission objectives.

Moreover, with ESI=0 configuration, the higher EGR rates requires high pressure drop across the LPEGR valve. This is fulfilled by exhaust throttle in the exhaust line. The increase in exhaust pressure also increases the pumping losses. Similar to full load results for high global EGR rates, LPEGR has more pumping losses compare to HPEGR (Figure 4.21), which can be avoided by higher ESI values. The only difference is the insufficient power of turbo at

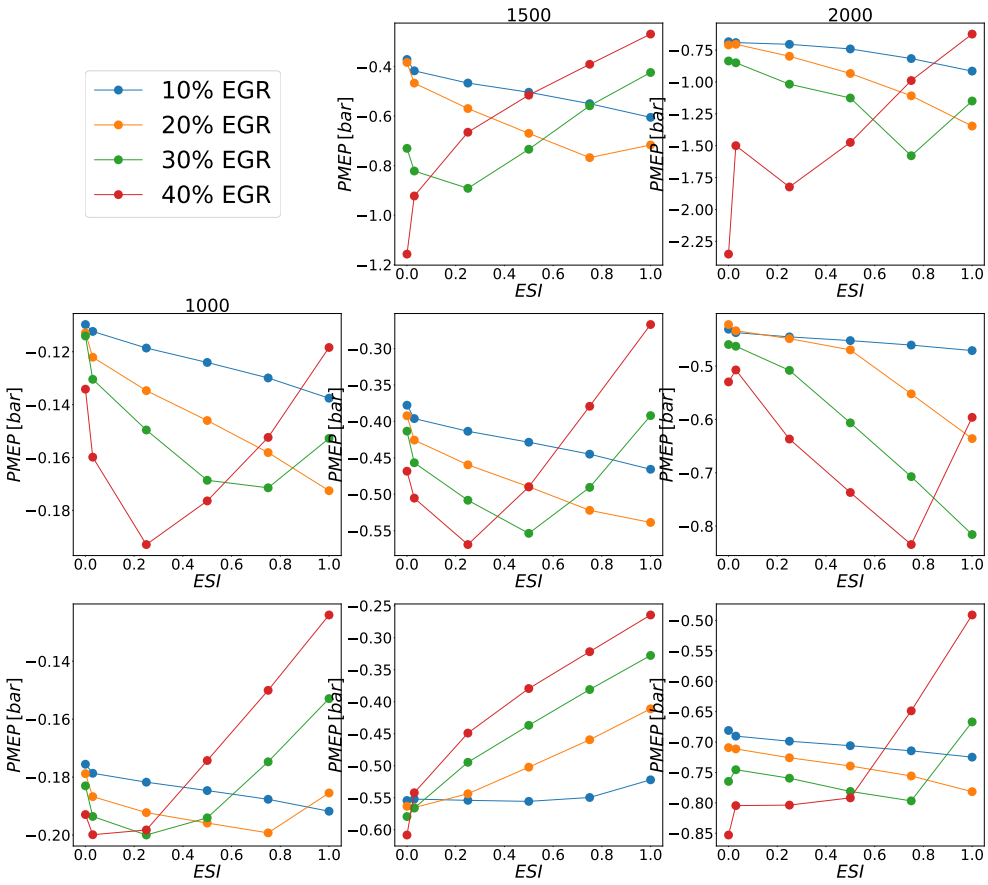

Figure 4.21: Pumping Mean Effective Pressure (PMEP) with HP, LP and combinations (part load).

full load and exhaust throttle control at low load are the origin of these high pumping losses. The partial load points (50% and 75%) needs the optimization for ESI considering the PMEP values depending on the turbocharger operating condition.

As the comparison is made with iso-fuel configuration (which was not possible at full load high EGR rate, due to smoke limiter for AFR), The brake specific fuel consumption for partial loads this comparison holds good for high global EGR rates too. LPEGR configuration shows less BSFC as the MEP is higher for 50% and 75% loads. Whereas, in case of low load (25%), BSFC decreases with the addition of HPEGR in the global EGR due to reduction

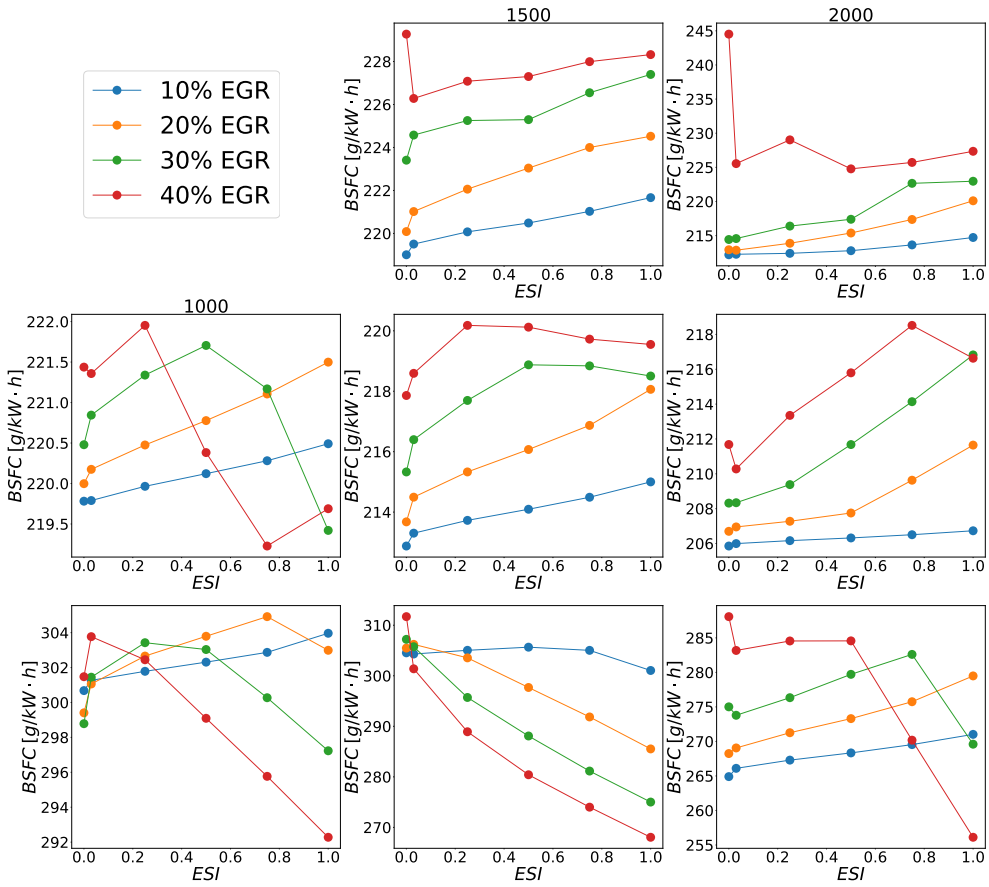

Figure 4.22: Brake Specific Fuel Consumption with HP, LP and combinations (part load).

of pumping losses and bigger MEP values. For 25% load iso-fuel points, the BSFC follows mostly the trend of pumping losses in reverse.

All the above operating points in the simulation were constrained to similar fuel injection quantity. In this way the energy input to the engine was kept almost same for the sweep in the global EGR rate and the EGR split index. That means, the results are needed to be analyzed for maximum torque output with minimum losses. Figure 4.23 represents the torque output of a model with different EGR rates and ESI values. The light areas represent higher torque in the figure. For the selected quantity of fuel, the engine torque is higher

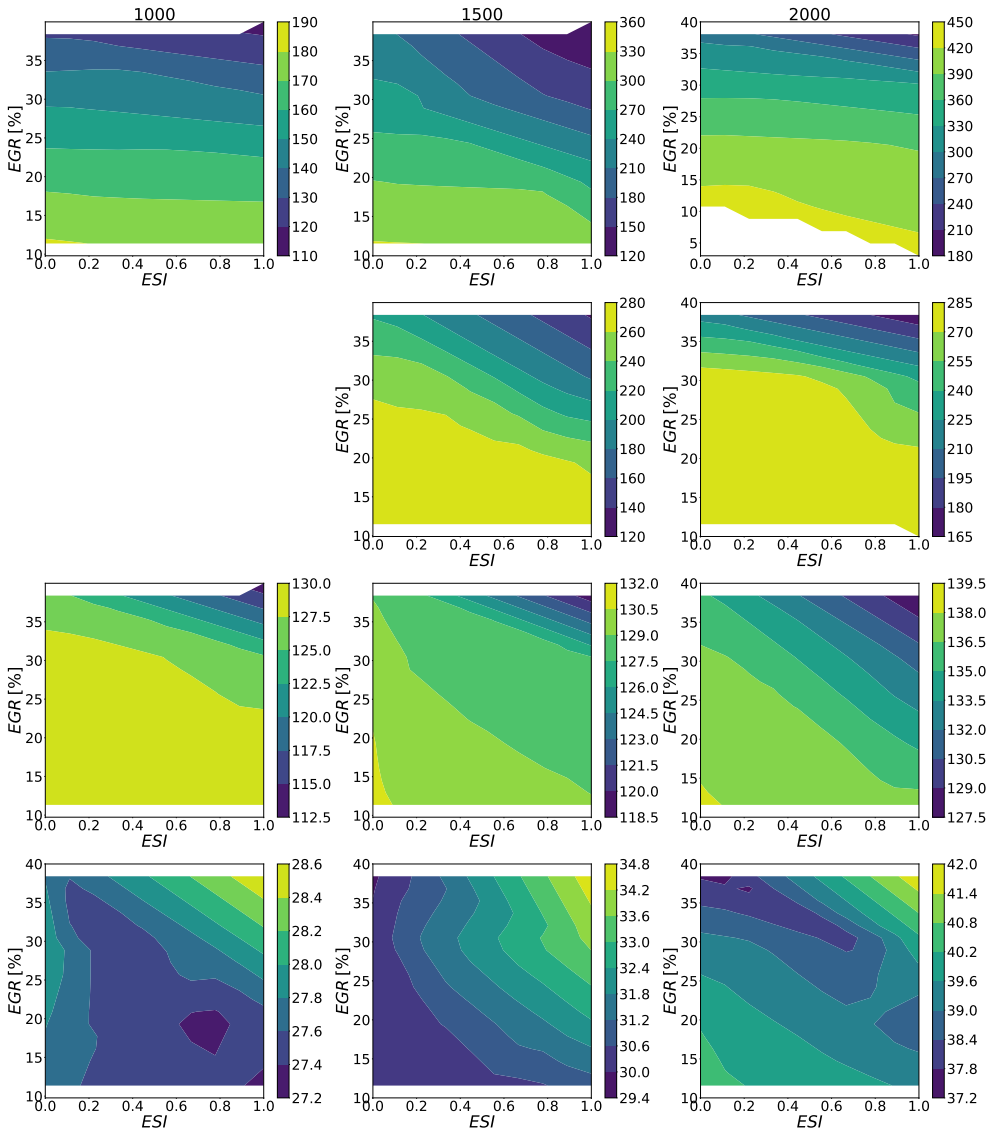

Figure 4.23: EGR and ESI sweep giving the engine torque with the 1D simulation.

with lower EGR rates in general. Mostly, at full load points, the torque is not very sensitive to change in ESI. However, at high EGR rates, lower ESI values show slight advantage. This trend gets prominent while going down the low load points. Low ESI values produce higher torque while pushing bigger

quantities of total EGR rates. Contradictorily, at very low loads, sensitivity of torque on the ESI axis is noticeable. Higher ESI and EGR rates can improve the performance of the engine. Depending on the engine speed, it can be seen that, torque at high speed points are more sensitive to change in ESIs.

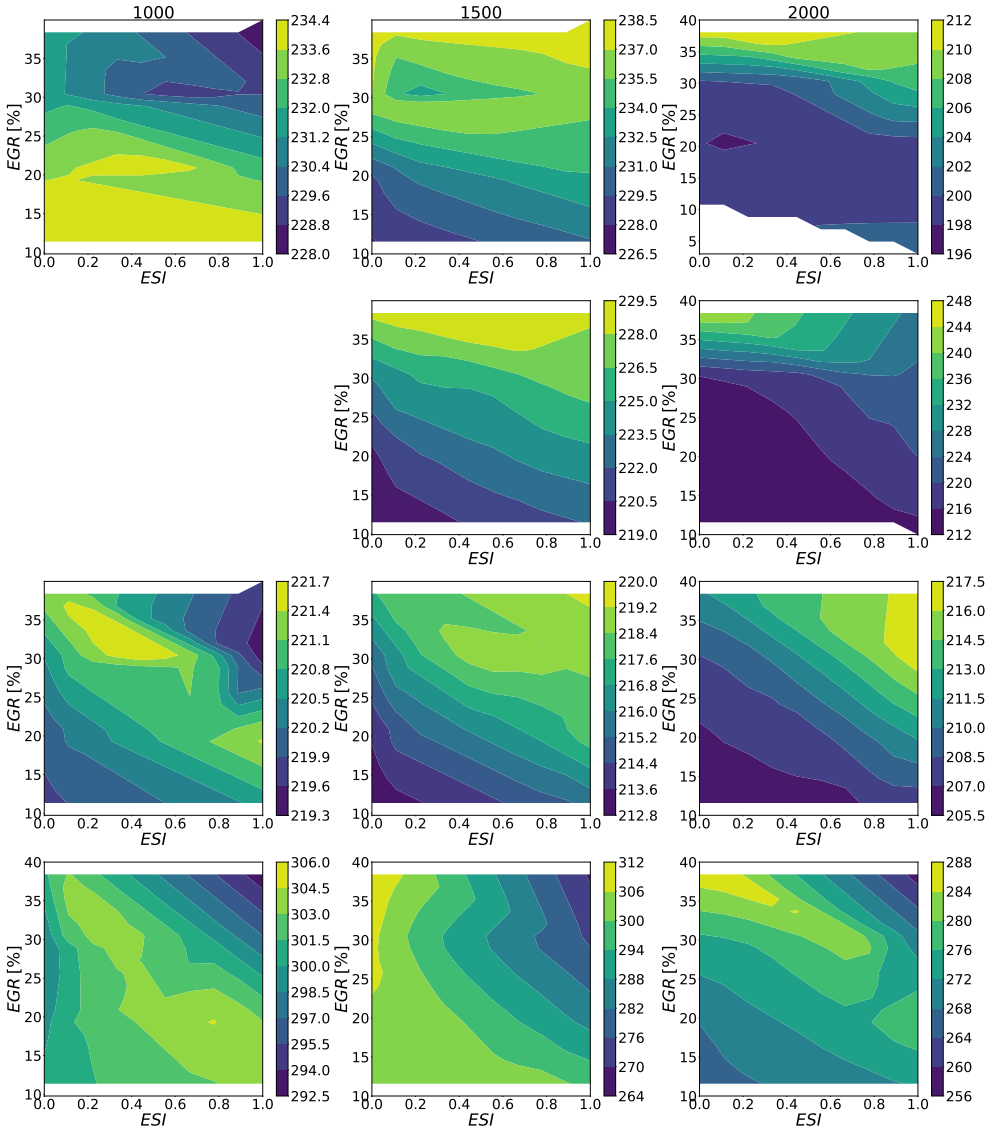

Figure 4.24: EGR and ESI sweep giving the BSFC with the 1D simulation.

It is evident from the Figure 4.24 that, brake specific fuel consumption is more affected by change in ESI as compared to engine torque. The dark areas in the figure show less BSFC. The 1000 rpm engine speed shows contrasting behavior than other engine speeds. At full load, BSFC increases with high total EGR rates and ESI, while at 1000 rpm, it decreases. The lower ESI allows to achieve less BSFC for 50% to 100% load. Retrospectively, at some areas on the map of EGR rates and ESIs there is potential of high torque but BSFC may show different behavior. Therefore it is necessary to find the tradeoff between the engine torque and fuel consumption with minimizing the emissions which can be done by pushing large EGR rates.

4.7 ESI Optimization

The objective of this section is to find the optimum value of split (ESI) between HP and LPEGR within the tradeoff of performance and emissions. Various optimization techniques are discussed in the introduction to find the optimum value of ESI. In this section, two methods of optimization are used. One of them uses the genetic algorithm to optimize the created cost function with multi variable inputs. The second method consists of a new algorithm generated from the control logic in GT Power. The advantages and results of both techniques are compared at the end.

4.7.1 Genetic algorithm

The genetic algorithm (NSGA-III) implemented via the open source JAVA based MOEA framework, is used to create a simulation matrix with dependent and independent variables (see Table 4.2) to generate multi variable pareto. The algorithm selects the operating point with arbitrary input within a specified range of independent variables and minimizes the cost function $f(x)$ by simulating the steady engine operation,

$$f(x) = \begin{bmatrix} BSFC \\ (1 - EGR) \\ \varepsilon_{Torque} \end{bmatrix} \quad ; \quad x = \begin{bmatrix} ESI \\ EGR \\ m_{fuel} \end{bmatrix} \tag{4.9}$$

Basically it finds a solution for minimum BSFC and error in the torque requirement (ε_{Torque}) while maximizing EGR rate (in fraction). The range of

inputs or the independent variables is given in the Table 4.2. The 40 iterations were used for the genetic algorithm for each operating point. This number is the multiplication of the population size and number of generations which depends on the number of independent variables. The population size (n) is calculated from the following expression [158] .

$$n = (number\,of\,"Independent"\,variables) * (number\,of\,active\,cases) \quad (4.10)$$

Dependant Variables	Independent Varibales
BSFC	ESI [0-1]
Total EGR rate	Total EGR [0-60]
Error in torque	Fuel injection [±5%]

Table 4.2: List of dependant and independent variables for optimization problem with genetic algorithm.

The results of simulation with 6 engine operating conditions are mentioned in the Figure 4.25 with variable ESI, EGR and fuel mass to optimize the given cost function. To identify the optimum solution from the pareto points generated from the algorithm, the minimum value of cost function is chosen with respective inputs of independent variables. This point is marked with the circle in the figure 4.25 along with respective value of ESI. The selected solution has minimum BSFC, maximum EGR rate and the torque value close to the requirement at that specific operating point.

This method takes lot of time and resources for the simulation. The number of unnecessary solutions which are not the part of pareto are also simulated increasing the total time of the optimization. Moreover, the accuracy of this method is directly proportional to the number of iterations performed to calculate the pareto solutions. This further increases the time of the calculations upto 10 to 12 hours per operating point. Therefore, a new algorithm is required to optimize the specific variables in less time.

4.7.2 Proposed algorithm

The main objective of finding the split between HP and LPEGR is to minimize the emissions and fuel consumption while maintaining the torque output of

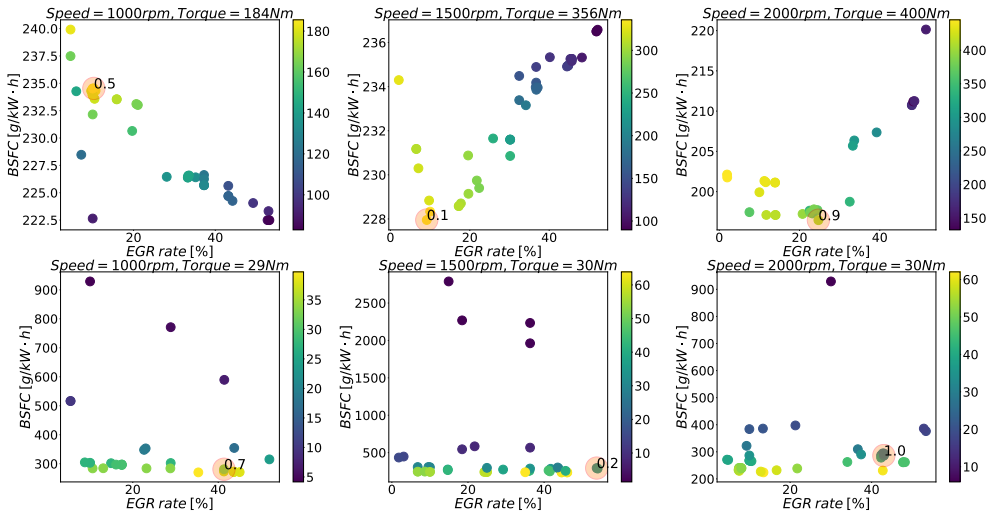

Figure 4.25: 6 operating points simulated with genetic algorithm to find the optimize the given cost function 4.9.

the engine. Therefore, the algorithm should focus on these minimum output variables and reduce the simulation time. The new control algorithm is created with the logical operators and controllers existed in the GT-Power tool. Instead of making entire DOE matrix, the algorithm changes the ESI value in real time by monitoring the variables which are needed to be optimized. Figure 4.26 demonstrates the flow of algorithm in which the optimization variables are BSFC, compressor efficiency and total EGR rate. The ESI value for the respective optimization variable is proposed in real time to maximize or minimize the variable accordingly. The PID opto-controller is used for the prediction of split for each variable. The value selector decides the final ESI values as per the weighted criteria or the average of the proposed ESI. The Total EGR rate is controlled by monitoring an engine torque with a PI controller. The respective value of LP and HPEGR rates are calculated from the ESI and total EGR rate by the expression 4.6. Controller 1,2 and 3 control the HP, LP and ET valve respectively with the target value set by the previous calculations. The exhaust throttle controller 3 is connected with the controller as they share same target. The constraint for controller 3 to be activated depends on the opening on the LPEGR valve. Thant means, when the LPEGR valve reaches to 90% of its limit, controller 3 gets activated to attain the required LPEGR rate.

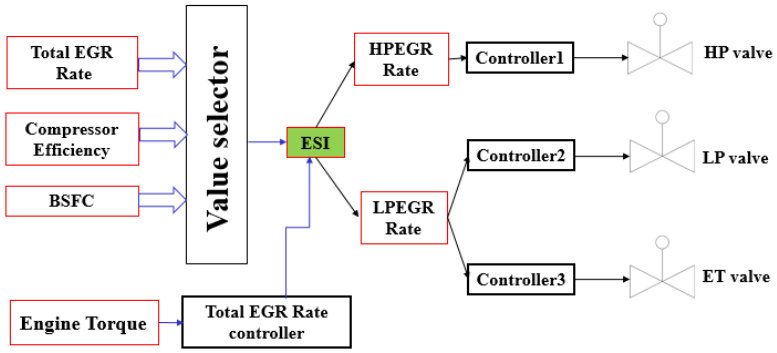

Figure 4.26: Control algorithm to find the optimized ESI value at particular operating point.

Initial value for the ESI is kept 0 (i.e. only LPEGR configuration) and incremented by prescribed fraction at every interval δt (provided by user). A constant feedback of output variables which are needed to be optimized is fed to the controller [5]. The increment is reversed if the feedback of the output variable goes away from the target. For example if the current BSFC with the current ESI of the iteration is higher than the BSFC from the previous iteration with respective ESI, then the ESI value for next iteration is decremented instead of increasing and vice versa. This allows the ESI value to converge to the particular value after some iterations, giving respective optimized split between HP and LPEGR rates (eg. higher BSFC).

To add more than one output variables to monitor, same number of controller are required to be added. Moreover, a weighted logic is also need to be provide to select the appropriate ESI at every iteration, proposed by each controller. The logic could be average or maximum/minimum of all ESI proposed from all controllers. The logic to select the corresponding ESI value for every iteration is provided in the value selector block.

The time required for each operating point is only 2-3 hours which is almost 80% less than the time consumed by the genetic algorithm. The time for genetic algorithm increases more if the number of iteration are increased further.

[5] OptoController from the GT suite library

4.7.3 Comparison

The two algorithms to find the optimized ESI value for the selected operating points are compared with the original calibrated engine model with the only LPEGR strategy. The engine torque output is one of the targets during the optimization study. Therefore, the efforts have been made to maintain the torque from the model during both algorithms. Figure 4.27 depicts the torque outputs from the model during the two algorithms with the original calibrated model. The torque during the new control algorithm is maintained to the original one however the torque from the genetic algorithm has some tolerance of $\pm 5\%$ with the original. This can be improved by increasing the iterations during the genetic algorithm.

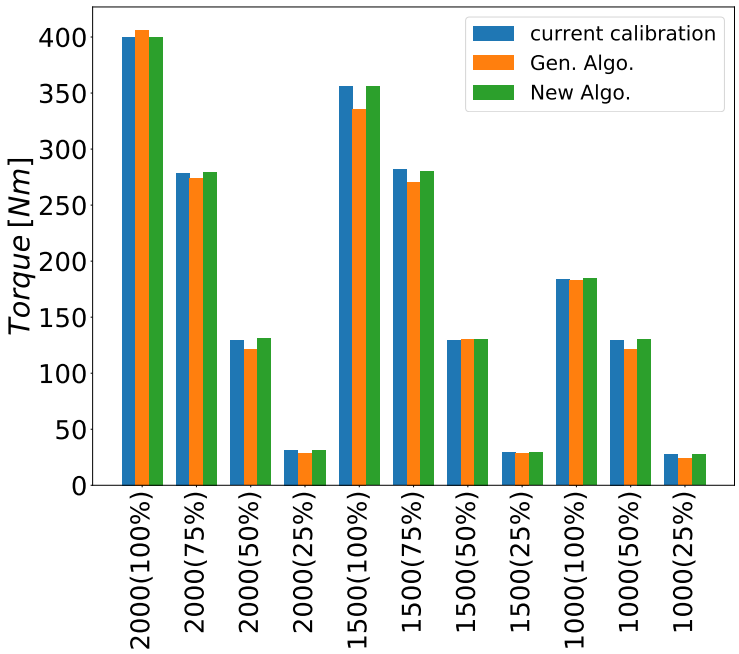

Figure 4.27: Engine torque comparison from current calibration (only LPEGR configuration) with optimized ESI obtained from genetic and new control algorithms.

Concerning the emissions, the maximum EGR rate corresponds to lesser NO_x emissions. Therefore, maximizing the total EGR rate is one of the main objectives of the two algorithms. The total EGR rates that could be pushed in the air system is portrayed in Figure 4.28 in comparison with the one from

original calibration. The higher EGR rates with optimized algorithms are always higher than the original calibration. With the air to fuel limitation for smoke control, higher amount of total EGR rates can be pushed with combination of HP and LPEGR. Even at full load, the total EGR rate is considerably higher. The potential for injecting larger EGR rates is way higher for low loads by new control algorithm, without loosing the engine torque.

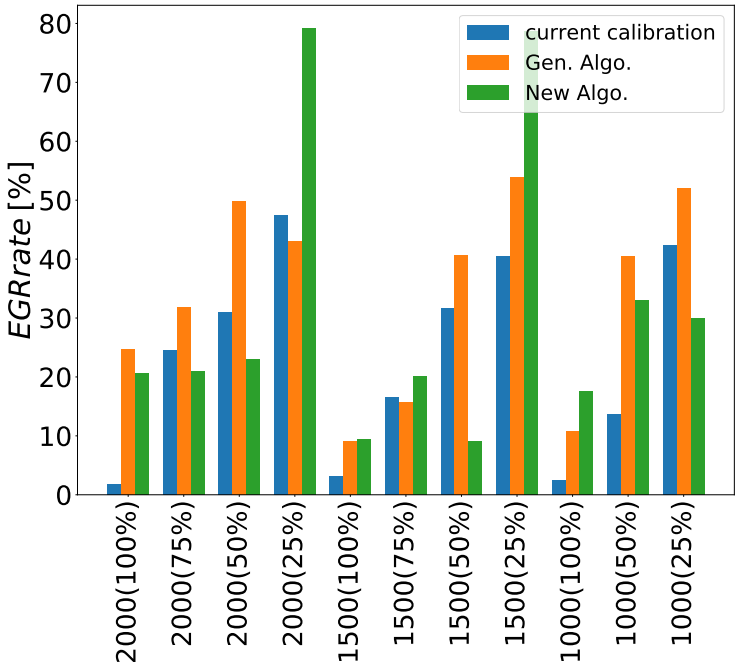

Figure 4.28: Total EGR rate comparison of original calibration (only LPEGR configuration) with optimized ESI obtained from genetic and new control algorithms.

Although, the torque is same, BSFC stays as an important concern. Figure 4.29 shows the BSFC values for all the operating points procured by the two algorithms. The overall change in BSFC is not substantial, however, there is always an improvement with the optimized combination of both types of EGR. Inferring to the torque differences from the genetic algorithm, the inequality is also got reflected on the BSFC values. The new control algorithm predicts the good BSFC results at low load points.

Finally, the splits between the HP and LPEGR obtained from the two algorithms are presented in the Figure 4.30. The original calibration consists

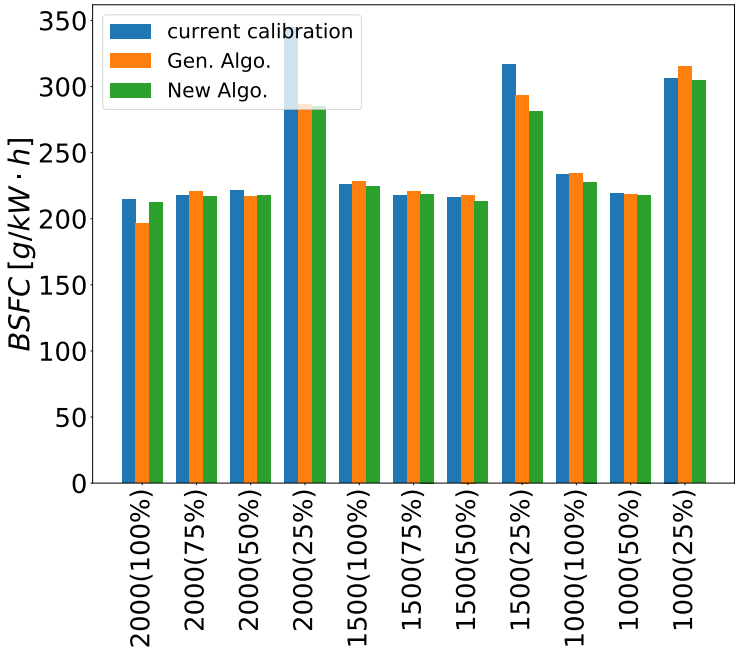

Figure 4.29: BSFC comparison of original calibration (only LPEGR configuration) with optimized ESI obtained from genetic and new control algorithms.

only LPEGR configuration, therefore the ESI values are always 0 (blue lines). As per GA , high engine speeds require higher ESI with bigger share of HPEGR in global EGR rate. The proposed algorithm goes inline with the previous results obtained by the ESI sweep for different engine operating points. The low load points require higher ESI values and it gets close to 0 at higher loads. The logic used in value selector block selects the average of all ESIs proposed by each controller at every iteration. In other words, equal weight is given for BSFC and EGR rate optimization function to find the solution. Because of this reason, at the higher engine speeds, ESI values are lower than genetic algorithm. At low loads, high share of HPEGR requirement is predicted to gain advantages in BSFC.

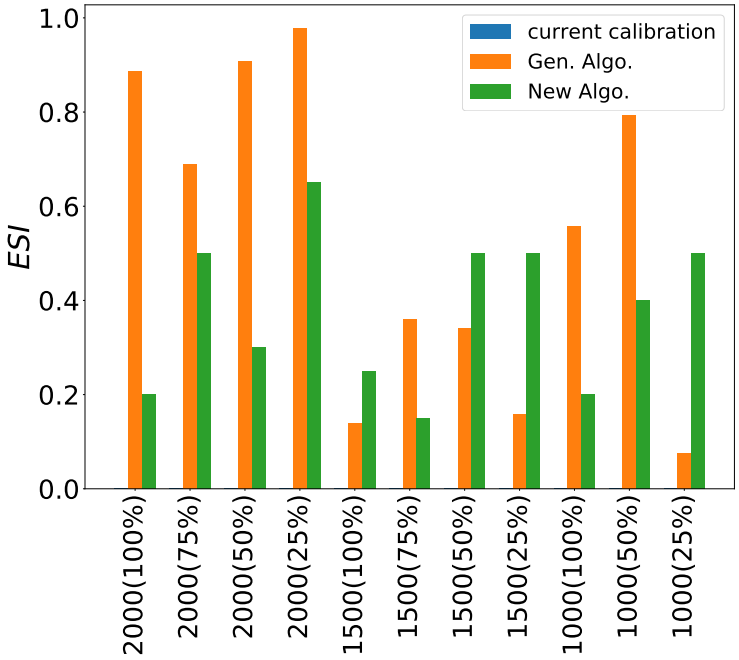

Figure 4.30: BSFC comparison of original calibration (only LPEGR configuration) with optimized ESI obtained from genetic and new control algorithms.

4.8 Conclusion

This chapter gives the insights about using combination of EGR systems on wide operating range of turbocharged diesel engine and its effect on different engine parameters. This study will be useful for the design and calibration of diesel engines with both high and low pressure EGR configuration meeting the upcoming emission regulations. Moreover, the optimization algorithm will be helpful to reduce the simulation time to carry out specific optimization of split between HP and LPEGR.

The temperature downstream of the compressor is very sensitive to the LPEGR only configuration for high EGR rates at full load. On the other hand, cooled HPEGR seems to be advantageous in this area. For the low loads, LPEGR provides less temperature in the intake manifold, but seems useful to utilize only at low speeds considering the problem of pumping losses at high speeds, reducing the mean effective pressure. These requirements can

be fulfilled by cooled HP EGR. HPEGR reduces the pumping losses at low air mass flow and high EGR rates. However, at full load points, pumping losses does not reduce with higher HPEGR rates as the boost pressure control plays the important role. Mostly, at full load points, the torque is not very sensitive to change in ESI. However, at high EGR rates, lower ESI values show slight advantage. Collectively, Lower ESI values produce higher torque allowing bigger quantity of global EGR rates, while torque at high speed points are more sensitive to change in ESIs. BSFC is more affected by change in ESI as compared to engine torque. For the partial loads, BSFC can be lowered with the low ESI except at lowest load points (involving throttling of exhaust gases to drive LPEGR), where high EGR rates can be supplied with reduced BSFC values

The DOE and genetic algorithm method for ESI optimization are easy to set up. However, the number of unnecessary solutions which are not part of pareto are also simulated increasing the total time of the optimization. Moreover, the accuracy of this method directly depends on the number of iterations that are performed, to calculate the pareto solutions. This further increases the time of the calculations. On the other hand, the new control algorithm is faster and reduces around 80% of time over the genetic algorithm.

Chapter 4 Bibliography

[39] M. Van Aken, F. Willems, and D. J. De Jong. "Appliance of high EGR rates with a short and long route EGR system on a heavy duty diesel engine." In: *SAE Technical Papers*. 2007. DOI: 10.4271/2007-01-0906 (cit. on pp. 11, 89).

[50] L. Cornolti, A. Onorati, T. Cerri, G. Montenegro, and F. Piscaglia. "1D simulation of a turbocharged Diesel engine with comparison of short and long EGR route solutions." *Applied Energy* 111 (2013), pp. 1–15. ISSN: 03062619. DOI: 10.1016/j.apenergy.2013.04.016. URL: http://dx.doi.org/10.1016/j.apenergy.2013.04.016 (cit. on pp. 13, 89).

[110] O. Varnier. "Trends and Limits of Two-Stage Boosting Systems for Automotive Diesel Engines." PhD thesis. 2012 (cit. on pp. 68, 98).

[124] G. Zamboni and M. Capobianco. "Influence of high and low pressure EGR and VGT control on in-cylinder pressure diagrams and rate of

heat release in an automotive turbocharged diesel engine." *Applied Thermal Engineering* 51(1-2) (2013), pp. 586–596. ISSN: 13594311. DOI: 10.1016/j.applthermaleng.2012.09.040. URL: http://dx.doi.org/10.1016/j.applthermaleng.2012.09.040 (cit. on pp. 73, 89).

[125] A. Maiboom, X. Tauzia, S. R. Shah, and J.-f. Hétet. "Experimental Study of an LP EGR System on an Automotive Diesel Engine , compared to HP EGR with respect to PM and NOx Emissions and Specific Fuel Consumption." *SAE International Journal of Engines* 2(2) (2009), pp. 597–610. ISSN: 19463936. DOI: 10.4271/2009-24-0138 (cit. on pp. 73, 89).

[126] M. S. Khalef, A. Soba, and J. Korsgren. "Study of EGR and Turbocharger Combinations and Their Influence on Diesel Engine ' s Efficiency and Emissions." *SAE International* (2016). DOI: 10.4271/2016-01-0676.Copyright (cit. on pp. 88, 89, 134).

[127] W. Glewen, C. Meyer, D. Foster, M. Andrie, and R. Krieger. "Sources and Tradeoffs for Transient NO and UHC Emissions with Low Temperature Diesel Combustion." *SAE Technical Paper* (2011-01-1356) (2011). DOI: 10.4271/2011-01-1356 (cit. on p. 88).

[128] N Ladommatos, S Abdelhalim, and H Zhao. "The effects of exhaust gas recirculation on diesel combustion and emissions." *International Journal of Engine Research* 1(1) (2000), pp. 107–126. ISSN: 1468-0874. DOI: 10.1243/1468087001545290. URL: https://doi.org/10.1243/1468087001545290 (cit. on p. 88).

[129] P. Dimitriou, J. Turner, R. Burke, and C. Copeland. "The benefits of a mid-route exhaust gas recirculation system for two-stage boosted engines." *International Journal of Engine Research* 19(5) (2017), pp. 553–569. ISSN: 1468-0874. DOI: 10.1177/1468087417723782. URL: https://doi.org/10.1177/1468087417723782 (cit. on p. 88).

[130] Y Qi, K. K. Srinivasan, S. R. Krishnan, H Yang, and K. C. Midkiff. "Effect of hot exhaust gas recirculation on the performance and emissions of an advanced injection low pilot-ignited natural gas engine." *International Journal of Engine Research* 8(3) (2007), pp. 289–303. ISSN: 1468-0874. DOI: 10.1243/14680874JER02306. URL: https://doi.org/10.1243/14680874JER02306 (cit. on p. 88).

[131] C. a. Idicheria and L. M. Pickett. "Ignition, soot formation, and end-of-combustion transients in diesel combustion under high-EGR conditions." *International Journal of Engine Research* 12 (2011), pp. 376–392. ISSN: 1468-0874. DOI: 10.1177/1468087411399505 (cit. on p. 88).

[132] H Ogawa, T Li, and N Miyamoto. "Characteristics of low temperature and low oxygen diesel combustion with ultra-high exhaust gas recirculation." *International Journal of Engine Research* 8(4) (2007), pp. 365–378. ISSN: 1468-0874. DOI: 10.1243/14680874JER00607. URL: https://doi.org/10.1243/14680874JER00607 (cit. on p. 88).

[133] T Li, M Suzuki, and H Ogawa. "Effect of Two-Stage Injection on Unburned Hydrocarbon and Carbon Monoxide Emissions in Smokeless Low-Temperature Diesel Combustion with Ultra-High Exhaust Gas Recirculation." *International Journal of Engine Research* 11(5) (2010), pp. 345–354. ISSN: 1468-0874. DOI: 10.1243/14680874JER585. URL: https://doi.org/10.1243/14680874JER585 (cit. on p. 88).

[134] J. A. Caton. "A thermodynamic comparison of external and internal exhaust gas dilution for high-efficiency internal combustion engines." *International Journal of Engine Research* 16(8) (2015), pp. 935–955. ISSN: 1468-0874. DOI: 10.1177/1468087414560593. URL: https://doi.org/10.1177/1468087414560593 (cit. on p. 89).

[135] J. Kim and C. Bae. "Emission reduction through internal and low-pressure loop exhaust gas recirculation configuration with negative valve overlap and late intake valve closing strategy in a compression ignition engine." *International Journal of Engine Research* 18(10) (2017), pp. 973–990. ISSN: 1468-0874. DOI: 10.1177/1468087417692680. URL: https://doi.org/10.1177/1468087417692680 (cit. on p. 89).

[136] G. Zamboni and M. Capobianco. "Experimental study on the effects of HP and LP EGR in an automotive turbocharged diesel engine." *Applied Energy* 94 (2012), pp. 117–128. ISSN: 03062619. DOI: 10.1016/j.apenergy.2012.01.046. URL: http://dx.doi.org/10.1016/j.apenergy.2012.01.046 (cit. on pp. 89, 134).

[137] T Alger, J Gingrich, C Roberts, and B Mangold. "Cooled exhaust-gas recirculation for fuel economy and emissions improvement in gasoline engines." *International Journal of Engine Research* 12(3) (2011), pp. 252–264. ISSN: 1468-0874. DOI: 10.1177/1468087411402442. URL: https://doi.org/10.1177/1468087411402442 (cit. on p. 89).

[138] G McTaggart-Cowan, W. K. Bushe, P. G. Hill, and S. R. Munshi. "Nox. reduction from a heavy-duty diesel engine with direct injection of natural gas and cooled exhaust gas recirculation." *International Journal of Engine Research* 5(2) (2004), pp. 175–191. ISSN: 1468-0874. DOI: 10.1243/146808704773564578. URL: https://doi.org/10.1243/146808704773564578 (cit. on p. 89).

[139] G. P. McTaggart-Cowan, S. N. Rogak, P. G. Hill, W. K. Bushe, and S. R. Munshi. "Effect of operating condition on particulate matter and nitrogen oxides emissions from a heavy-duty direct injection natural gas engine using cooled exhaust gas recirculation." *International Journal of Engine Research* 5(6) (2004), pp. 499–511. ISSN: 1468-0874. DOI: 10.1177/146808740400500602. URL: https://doi.org/10.1177/146808740400500602 (cit. on p. 89).

[140] Y. Park and C. Bae. "Experimental study on the effects of high/low pressure EGR proportion in a passenger car diesel engine." *Applied Energy* 133 (2014). ISSN: 03062619. DOI: 10.1016/j.apenergy.2014.08.003 (cit. on p. 89).

[141] S. Chen and F. Yan. "Decoupled, Disturbance Rejection Control for A Turbocharged Diesel Engine with Dual-loop EGR System." *IFAC-PapersOnLine* 49(11) (2016). DOI: 10.1016/j.ifacol.2016.08.090 (cit. on p. 89).

[142] J. Park and J. Choi. "Optimization of dual-loop exhaust gas recirculation splitting for a light-duty diesel engine with model-based control." *Applied Energy* 181 (2016), pp. 268–277. ISSN: 03062619. DOI: 10.1016/j.apenergy.2016.07.128. URL: http://dx.doi.org/10.1016/j.apenergy.2016.07.128 (cit. on pp. 89, 134).

[143] H. Hiroyasu, H. Miao, T. Hiroyasu, M. Miki, J. Kamiura, and S. Watanabe. "Genetic Algorithms Optimization of Diesel Engine Emissions and Fuel Efficiency with Air Swirl, EGR,Injection Timing and Multiple Injections." In: *SAE Technical Papers*. 2003. DOI: 10.4271/2003-01-1853. URL: https://www.sae.org/content/2003-01-1853/ (cit. on p. 89).

[144] T. Hiroyasu, M. Miki, J. Kamiura, S. Watanabe, and H. Hiroyasu. "Multi-Objective Optimization of Diesel Engine Emissions and Fuel Economy using Genetic Algorithms and Phenomenological Model." In: *SAE Technical Papers*. 2002. DOI: 10.4271/2002-01-2778. URL: https://www.sae.org/content/2002-01-2778/ (cit. on p. 89).

[145] M. Costa, G. Bianchi, and C. Forte. "A Numerical Methodology for the Multi-Objective Optimization of an Automotive DI Diesel Engine." In: *SAE Technical Papers*. 2013. DOI: 10.4271/2013-24-0019. URL: https://www.sae.org/content/2013-24-0019/ (cit. on p. 90).

[146] M. Costa, G. M. Bianchi, C. Forte, and G. Cazzoli. "A Numerical Methodology for the Multi-objective Optimization of the DI Diesel Engine Combustion." *Energy Procedia* 45 (2014), pp. 711–720. ISSN: 18766102. DOI: 10.1016/j.egypro.2014.01.076. URL: https://linkinghub.elsevier.com/retrieve/pii/S1876610214000770 (cit. on p. 90).

[147] H.-W. Ge, Y. Shi, R. D. Reitz, D. D. Wickman, and W. Willems. "Optimization of a HSDI Diesel Engine for Passenger Cars Using a Multi-Objective Genetic Algorithm and Multi-Dimensional Modeling." *SAE International Journal of Engines* 2(1) (2009), pp. 2009–01–0715. ISSN: 1946-3944. DOI: 10.4271/2009-01-0715. URL: https://www.sae.org/content/2009-01-0715/ (cit. on p. 90).

[148] S. Lotfan, R. A. Ghiasi, M. Fallah, and M. Sadeghi. "ANN-based modeling and reducing dual-fuel engine's challenging emissions by multi-objective evolutionary algorithm NSGA-II." *Applied Energy* 175 (2016), pp. 91–99. ISSN: 03062619. DOI: 10.1016/j.apenergy.2016.04.099. URL: https://linkinghub.elsevier.com/retrieve/pii/S030626191630561X (cit. on p. 90).

[149] J Park, K. S. Lee, S Song, and K. M. Chun. "Numerical study of a light-duty diesel engine with a dual-loop EGR system under frequent engine operating conditions using the DOE method." *International Journal of Automotive Technology* 11(5) (2010), pp. 617–623. DOI: 10.1007/s12239 (cit. on p. 90).

[150] J. Park, S. Song, and K. S. Lee. "Numerical investigation of a dual-loop EGR split strategy using a split index and multi-objective Pareto optimization." *Applied Energy* 142 (2015), pp. 21–32. ISSN: 03062619. DOI: 10.1016/j.apenergy.2014.12.030. URL: http://dx.doi.org/10.1016/j.apenergy.2014.12.030 (cit. on pp. 90, 134).

[151] P. K. Bansal and B. Purkayastha. "An NTU-ϵ model for alternative refrigerants." *International Journal of Refrigeration* 21(5) (1998), pp. 381–397. ISSN: 01407007 (cit. on p. 92).

[152] H. A. Navarro and L. C. Cabezas-Gómez. "Effectiveness-ntu computation with a mathematical model for cross-flow heat exchangers." *Brazilian Journal of Chemical Engineering* 24(4) (2007), pp. 509–521. ISSN: 0104-6632. DOI: 10.1590/S0104-66322007000400005. URL: http://www.scielo.br/scielo.php?script=sci{_}arttext{\&}pid=S0104-66322007000400005{\&}lng=en{\&}tlng=en (cit. on p. 92).

[153] R. Stone. *Introduction to internal combustion engines*. Springer, 1999 (cit. on p. 102).

[154] J. Macek, V. Dolecek, S. Srinivasan, F. Tanner, and O. Vitek. "Optimization of Engine Control Strategies During Transient Processes Combining 1-D and 3-D Approaches." In: 2010. DOI: 10.4271/2010-01-0783. URL: http://papers.sae.org/2010-01-0783/ (cit. on p. 102).

[155] X. Llamas and L. Eriksson. "Optimal Transient Control of a Heavy Duty Diesel Engine with EGR and VGT." *IFAC Proceedings Volumes* 47(3) (2014), pp. 11854–11859. ISSN: 14746670. DOI: 10.3182/20140824-6-ZA-1003.01520. URL: https://linkinghub.elsevier.com/retrieve/pii/S1474667016435020 (cit. on p. 102).

[156] B. Liu, F. Zhang, C. Zhao, X. An, and H. Pei. "A novel lambda-based EGR (exhaust gas recirculation) modulation method for a turbocharged diesel engine under transient operation." *Energy* 96 (2016), pp. 521–530. ISSN: 03605442. DOI: 10.1016/j.energy.2015.12.097. URL: http://www.scopus.com/inward/record.url?eid=2-s2.0-84958634759{\&}partnerID=tZOtx3y1 (cit. on p. 102).

[157] N. R. Abdullah, H. Ismail, Z. Michael, A. A. Rahim, and H. Sharudin. "Effects of air intake temperature on the fuel consumption and exhaust emissions of natural aspirated gasoline engine." *Jurnal Teknologi* 76(9) (2015), pp. 25–29. ISSN: 01279696. DOI: 10.11113/jt.v76.5639 (cit. on p. 109).

[158] G. Technolgies. *Optimization Manual*. 2016 (cit. on p. 119).

Chapter 5

Transient EGR strategies

Contents

5.1 Introduction

It's been many years that exhaust gas recirculation strategy has been used to lower the temperature of combustion and to reduce NO_x formation on high speed turbocharged diesel engines. Plenty of literature is available regarding effective implementation of both HPEGR (also known as short route) and LPEGR (also known as long route) [126, 159, 160]. Use of HPEGR decreases BSFC of an engine reducing pumping losses, while the homogeneous mixture of LPEGR with air reduces even more cylinder out NO_x concentration comparatively at steady state [136]. LPEGR increases the mass flow rate through the compressor shifting the operating point to a higher efficiency zone along with effective use of variable geometry turbo [161]. Looking at different benefits and drawbacks of these two systems, a hybrid system using both EGR configurations is also studied. For example switching in-between both HPEGR and LPEGR at particular operating conditions [40] or combination of both of them from the last chapter. Specific split in flow between these two architectures has been optimized experimentally and with simulations in steady operations [142, 150]. However, all these studies consist the optimization of all the EGR systems during particular steady state operation. However, increasing challenges of emission regulations with dynamic engine behavior, this system needs an update to match with real world driving conditions. The condition where the engine changes its loads state frequently. Inferring to Chapter 2 the real driving conditions consist of frequent transient operations. On the one hand, various technologies have been developed to curb the emissions during transient operations. Nevertheless, they add the extra cost and weight to the engines [162, 163]. On the other hand, the available EGR lines on production engines can be used conveniently with strategic control to control the emissions during transient operations. It could act as a simple solution to adapt with the new regulations cost effectively rather than new inventions.

PEMS has made measurements of on-road real driving emissions possible from the tail pipe. Therefore the scope of type approval tests is not limited up to the test bench anymore. The traditional driving cycles and emission regulation procedures seem to be replaced by new advanced cycles like WLTC and RDE in near future. Moreover, as a consequence of the diesel gate scandal a lot of data on real driving emissions of Euro 6 cars has become available [164, 165]. It has been mentioned that EURO 6 calibrated vehicles have the more

emissions than the new regulation limits and need high conformity factor to pass the newly developed type approval process [166, 25]. In parallel, dynamic cycles like WLTC are being developed to represent the real driving conditions [72]. Retrospectively, the emissions strategies designed for steady cycles are very much needed to be modified to cope up with the emissions. Various studies have been carried out to see the effect of emissions during new dynamic cycles based on cold intake conditions[83], heated after-treatment system[167]. It has been seen that, the transient operations play major role in the high emissions during the real driving conditions and WLTC cycle. These operations are responsible for sudden NO_x peaks from those Tip-In ans Tip-Out operations [168, 88]. Therefore a in depth study of behavior of engines and emission during transient operations is required. As these operations happening quickly in small interval of time, making large impact nevertheless. They need a dynamic and fast emission measurement systems to measure the NO_x formation inside or close to combustion chamber. [169].

Regarding transient EGR, research has been done on small transient operations up to medium load with LPEGR [32] and mild transients with slow change in load on extra urban part of NEDC cycle [170]. Hybrid EGR technology is also simulated to see the effect on the transient air performance and emissions [171]. Evidently, presence of EGR causes delay in duration of transient operation. Comparatively, HPEGR is quiet fast compared to the LPEGR due to the short length of EGR line. While, LPEGR valve movement with exhaust throttle are quiet sensitive for the overshoot in burned gas mass fraction transport [172]. Some strategies regarding the control of EGR during this transient event has been tested and published. One of the strategies consists of implementation of 'threshold limit' for burned gas mass fraction, to reduce the NO_x peaks during mild transients and air fuel ratio, to reduce the particle matter formation. However, this strategy is not useful when the transient events last up to full load, where the air-to-fuel ratio (AFR) is already close to 1. Moreover the strategy of burned gas mass fraction will reduce the performance of the engine too much [173]. The effect of transportation delay of EGR on NO_x is presented in [174]. Apart from diesel engines, there are some methods that has been developed on gasoline engines, regarding estimation of LPEGR rate considering transportation delays from the EGR valve to intake valve of the cylinder which can be helpful to design the LPEGR control during transients [95]. This study acts as a continuation of above studies in order to find out strategies for better performance and reduced emissions with existing production engine structure. This does not include any cost related

changes or high-tech after treatment system.

This chapter mainly focuses on the load transient operations which are responsible for high NO_x emissions during the dynamic driving cycles discussed in chapter 2. These harsh load transients (from low load to full load) are repeated on dynamic engine test bench to observe the raw emissions. The pollutants are measured with fast response NDIR500 (for CO_2) and CLD500 (for NO_x) measurement system. Application of LPEGR and HPEGR system and their impacts have been presented during these transient and full load operations. A parametric study with the movement of LPEGR valve during Tip-In operation is also carried out to see the tradeoff between emissions and performance of the engine. Moreover, to assess the delays of EGR in the intake line, a typical transient operation, mimicking a roundabout path maneuver is performed with HP and LPEGR combination.

5.2 Methodology

Taking into account certain difficulties in design and instrumentation mentioned in the chapter 3, a methodology is followed to achieve the objective of this study. The identified load transient operations from the cycle analysis section are performed on the engine test bench with various EGR strategies at full load. The implementation of EGR at full load is done first with both HP and LPEGR systems. As the HPEGR measurement was the challenging task specifically for this type of engine,a comparative relation is pre-decided and fixed with both EGR systems. The decided EGR valve positions are further used during harsh load transient operations to quantify the effect on NO_x emissions.

5.2.1 Full load operation with EGR

Before performing different transient operation, a strategy of implementing EGR at full load has to be tested in steady state. According to the original calibration, whenever the engine is hot and comes across any transient operation or goes outside EGR zone, the ECU closes the EGR valves and cuts the EGR going to the combustion chamber [174, 23]. Hence, normally there is no exhaust gas recirculation at full load. So addition of EGR creates a complex

scenario considering the smoke limiter strategy, as the diesel engine already runs with lambda close to 1. This condition is critical for the formation of soot. Moreover, from the control point of view, it will hinder with the close loop control of boost pressure at full load. So, firstly, the EGR valves are controlled manually to find out the position to provide around 5% EGR rate at full load in steady state. Secondly, these valve positions of HP and LP EGR valves are fixed for respective type of strategies, whenever engine operates on full load. Table 5.1 represent the 4 operating points where the EGR valve positions are determined.

Speed [RPM]	**EGR rate [%]**	**LPEGR [% open]**	**HPEGR [% open]**	**Torque [Nm]**
1250	5%	20.84	16.36	268
1500	5.10%	20.84	26.78	342
1750	5.08%	20.84	50.59	390
2000	5.10%	20.84	44.64	393

Table 5.1: Full load steady state points with 5% of EGR from LP and HPEGR system at iso-torque operation.

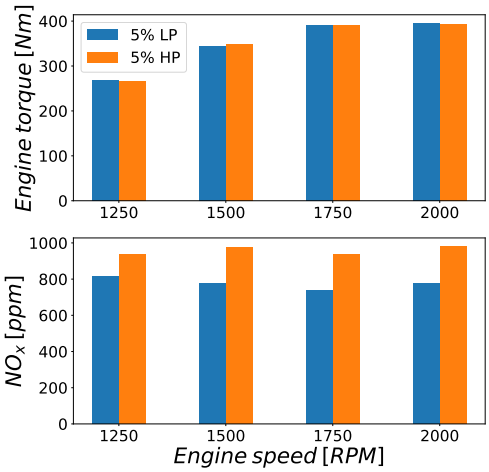

Figure 5.1: Iso-torque engine operation to have same composition of the HPEGR and LPEGR at full load for different engine speeds.

In the case of HPEGR, as said before, due to complexity of the intake manifold, it was difficult to measure the EGR rate. With 5% of LPEGR

conditions at full load, the engine always exceeds the AFR limitations for soot formation. Therefore, the air-fuel ratio value is not a good parameter to determine the same operating condition for comparison of HP and LP configuration. However, HPEGR valve positions giving the same torque values with full load engine running condition as in LPEGR is can be used to see the effect on the emissions with similar performance. The effect of intake manifold temperature variations can be neglected here since the EGR rates are reduced and the air-EGR mixture temperature will not be significantly affected between LP or HP-EGR. Therefore, the HPEGR valve position was found out to deploy 5% of EGR rate giving same torque values as in LPEGR as shown in Figure 5.1

5.2.2 Harsh transient operation with EGR

Finally, the harsh transients were performed on 4 engine speeds covering the high density zones of transients on the engine map of different driving cycles. The selected engine speeds are 1250, 1500, 1750, 2000 RPM. All the Tip-In and Tip-Out operations were performed after the engine is warmed with coolant temperature above 80^{o}C. To assess the worst case behavior during a particular case of Tip-In and Tip-Out operation, the pedal shift was carried out from 2 bar BMEP with around 40% of LPEGR as per the ECU calibration to full load in a time less than a second. At the low load point, LPEGR valve was completely open and the exhaust throttle was used to control the air mass flow to the cylinder inside EGR zone. After remaining for 15 seconds at full load, the pedal was shifted back to original position with 2 bar BMEP. Intake throttle was kept open all the time (as exhaust throttle is best suited to drive LPEGR than intake throttle [32]). The emissions and engine parameters (as explained in the experimental setup) were recorded for these 40 s. Different EGR configurations analyzed during these load transients were as follows are described in the Table 5.2

- Without implementing any EGR at full load (original calibration)
- Fixing valve position of LPEGR (long route) giving 5% of EGR at full load.
- Fixing valve position of HPEGR (short route) giving same torque as in LPEGR at full load.

Engine Speed [RPM]	**Transient load progression**	**EGR at Full Load**
Load transient without EGR at FL		
1250,1500,1750,2000 RPM	2bar-FL-2bar	0%
Load transient with EGR at FL		
1250,1500,1750,2000 RPM	2bar-FL-2bar	5% LP
1250,1500,1750,2000 RPM	2bar-FL-2bar	5% HP
Load transient with LP profiles		
1250,1500,1750,2000 RPM	2bar-FL	Prof5
1250,1500,1750,2000 RPM	2bar-FL	Prof10
1250,1500,1750,2000 RPM	2bar-FL	Prof15
Load transient at roundabout		
1500 RPM	2bar-0bar-FL-2bar	5% LP

Table 5.2: Transient operation studies with different EGR strategies.

5.3 Analysis

A typical transient with the original calibration and different engine parameters for 1500 RPM is shown in Figure 5.2. When pedal is shifted to 100%, leading the operating point outside of EGR zone, LPEGR valve closes completely. The CO_2 concentration just before the intake valve reduces slowly to zero as there are exhaust gases present already in the intake circuit. Due to this, high peak of NO_x in not observed by the fast cambustion system during this kind of load transients. A different type of harsh transient without having burned gas concentration beforehand in the intake line are studied to see the formation of high NO_x peak in the section of roundabout transients. From the perspective of time, thanks to the compact design of LPEGR line, the transportation delay of the burned gases is found to be reduced considerably as discussed in [172]. A trend in the evolution of NO_x can be established during harsh load transient operations. The observed pollutant measurement consists of a three step process where NO_x increases up to a certain value until the CO_2 concentration starts to decrease at the intake valve. Thereafter, CO_2 starts decreasing and NO_x evolves to a next step with higher value where fuel

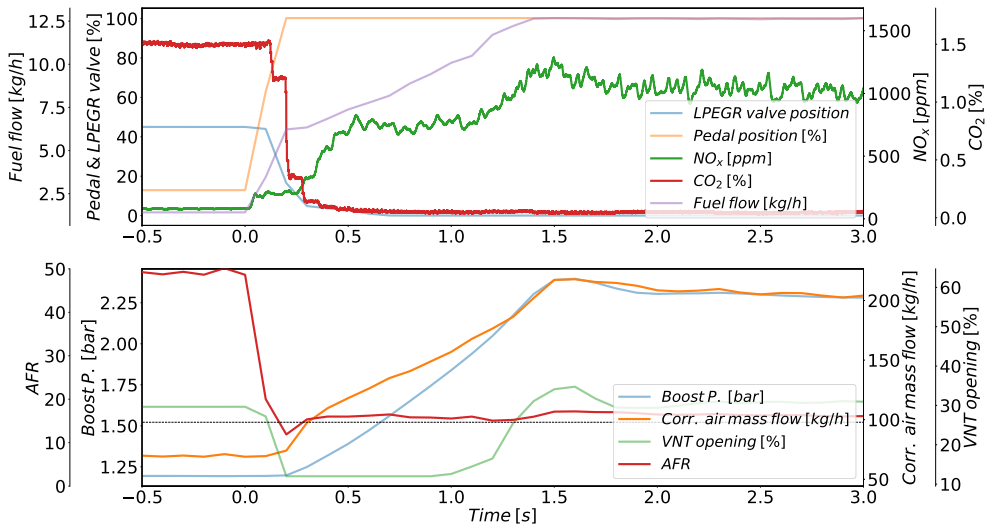

Figure 5.2: Measurements of different engine parameters and emission along with valve actuation during a typical Tip-In operation from low load to full load at 1500 RPM.

is getting limited as the AFR value goes below the smoke limiting value (the black dashed line represents stoichiometric AFR). This part could be coined as a "waiting zone" where fuel is being limited. The fuel starts increasing further as soon as air arrives with the delayed turbo boost and it increases in-cylinder temperature and eventually NO_x formation to even a higher final steady state value.

On the other hand, during the Tip-Out operation from the full load to 2 bar BMEP running conditions, fuel reduces back instantly while the air goes down sluggishly creating high AFR more than 150. Moreover, as the operating point goes back into the EGR strategy zone opening again LPEGR valve, CO_2 concentration in the intake line evolves with a time delay leading to a peak of NO_x for that short period of time as seen in the Figure 5.4. Later, due to combination of LPEGR valve and closing of exhaust throttle, a high flow of LPEGR is recirculated which leads to an important reduction of NO_x [172]. As the EGR rate demand is high, the LPEGR valve opens completely and the flow control of EGR and air flow is transferred to exhaust throttle, which partially closes to increase the pressure in the exhaust line so as to increase the EGR flow at the same time.

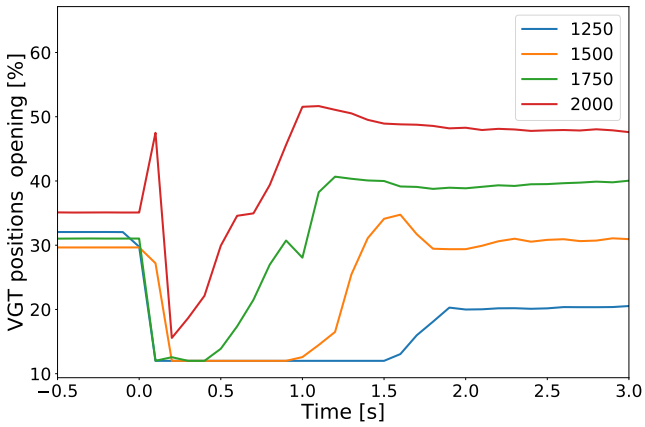

Figure 5.3: Typical turbine geometry movements during a harsh transient operation from low load(2 bar BMEP) to full load

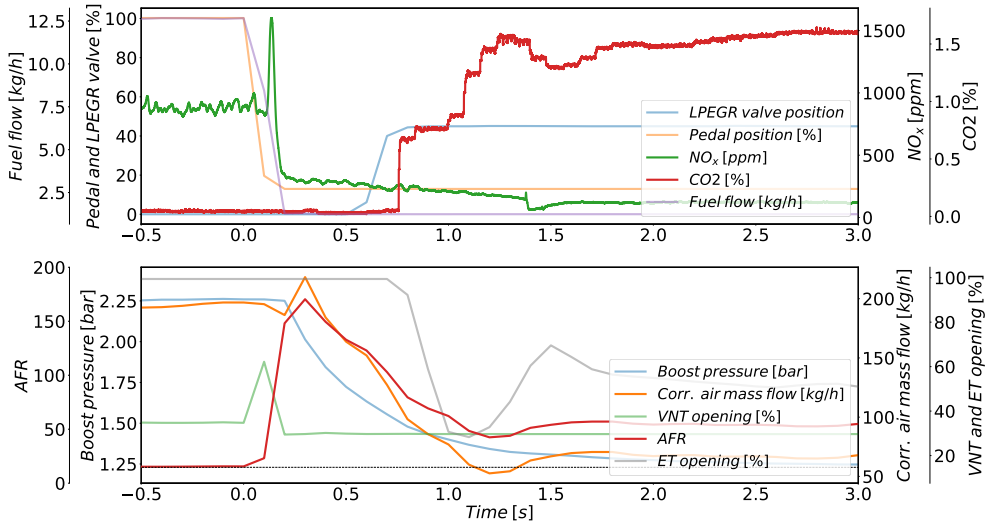

Figure 5.4: Measurements of different engine parameters and emission along with valve actuation during a typical Tip-Out operation from low load to full load at 1500 RPM.

It is important to observe the turbocharger behavior during a transient operation. In the case of Tip-In operation, whenever pedal is pushed at the

start of the operation, the variable geometry turbine closes the vanes reducing the cross sectional area to a value (12% in this case) close to minimum to fulfil the boost pressure demand quickly (see Figure 5.3). As soon as the boost pressure target is achieved, the control moves the turbine positions to higher values regulating intake pressure. The time duration for the turbine to be almost closed is different for different engine speeds as the energy at the turbine inlet and turbine speed are different. This particular time decreases as the engine speed increases and it almost ends along with "waiting zone" as discussed in previous section. The calibrated smoke curbing AFR limit plays an important role for the torque generation during this period while the NO_x is affected by the quantity of air (mainly oxygen) going inside the combustion chamber [175].

5.3.1 Transients with EGR

Recirculation of exhaust gases during transient operation by opening LP or HP EGR valve has a noticeable impact on NO_x emissions. As seen in Figure 5.5, which shows the transient for 1500 RPM, the final steady state NO_x levels at full load is reduced by almost around 50% with LPEGR and 75% with HPEGR configuration. From transient behavioral point of view, NO_x concentration correlates with CO_2 concentration at the intake. The first stage of NO_x evolution remains unchanged despite of any EGR strategy as emptying of exhaust gases in the intake circuit takes time (CO_2 concentration at the intake valve is similar with a configuration without EGR). Thereafter, it reaches to the value for "waiting zone" and then to a final fixed EGR valve (5% rate) steady state concentration. In case of LPEGR, CO_2 concentration reduces slowly with a fixed delay different for engine speeds. Before it reaches to a final value, it has a slight dip representing a start of "waiting zone" (from the point where air starts increasing). This dip gets reflected as a peak in NO_x concentration, which is detected in the middle plot of Figure 5.5. However, in case of HPEGR strategy CO_2 arrives very fast and attains higher values (than expected for 5% EGR rate valve position) due to high amount of EGR flow. Highly scattered values of CO_2 concentration explains the bad dispersion of HPEGR by the fact that exhaust gases and intake air are not properly mixed differing greatly from being homogeneous mixture like LPEGR. Moreover, the location of NDIR500 probe was at the last cylinder just before the intake valve. High amount of HPEGR flow is explained by sudden closure of VGT thereby increasing the pressure before turbine, driving a significant amount

of exhaust gases through the HPEGR valve. Additionally, in the HPEGR case, the time for VGT remaining closed is also increased due to the fact that, the energy upstream the turbine is removed in the form of HPEGR flow and the VGT has to comply with reducing the area of the turbine to provide power to compressor. Clearly, the current turbocharger is not designed to work with HPEGR at full load, and therefore the performance is worse with this configuration.Hence, LPEGR shows advantage over HPEGR giving better performance and comparable reduction in NO_x in transient and also in steady state. Whereas, HPEGR has advantage in case of time due to its fast arrival.

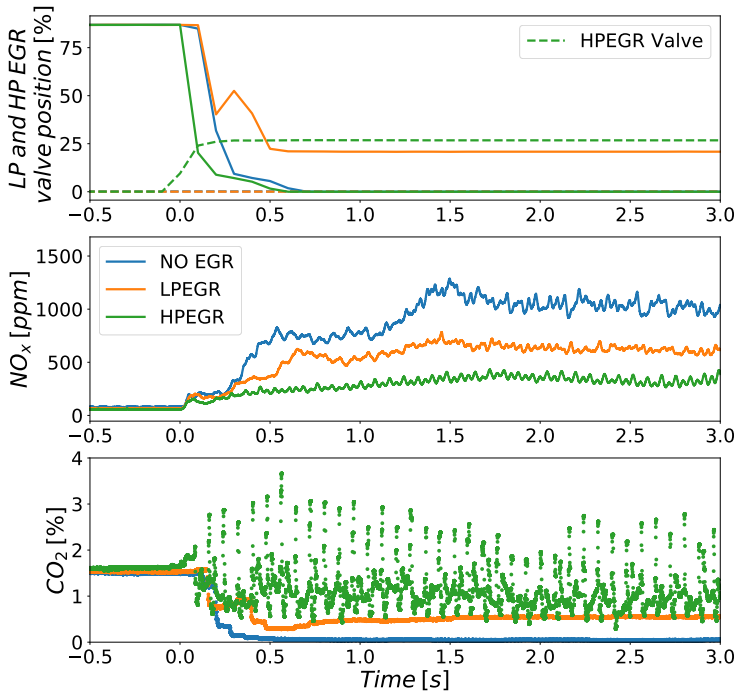

Figure 5.5: High Pressure and Low Pressure EGR valve positions with respective strategy along with the instantaneous NO_x emissions and CO_2 measurement at the intake valve during a harsh transient Tip-In operation at 1500 RPM.

From the performance point of view, HPEGR configuration takes more than 3 seconds to achieve the final boost pressure owing to the energy reduction before turbine even though the VGT is fully closed (see Figure 5.6). As a result, the torque gets diminished due to lack of air and proves that this configuration is not well suited in terms of vehicle dynamics. On the other

hand, comparing with HPEGR configuration, LPEGR shows better results without losing much energy before turbine, which allows to increase the flow through compressor. Figure 5.6 (middle plot) shows LPEGR boost pressure evolution is quiet close to the one with the configuration without EGR. The engine torque (top plot) shows major difference only in the first few seconds of transients (during the "waiting zone") as the final torque is slightly reduced with 5% EGR rate. Hence, performance wise, LPEGR is better than HPEGR. Moreover, we can also deduce that a control design of LPEGR configuration is simpler than HPEGR, for transient operations, with just the difficulty of the slight CO_2 transport delay in the intake line, which should be taken into account.

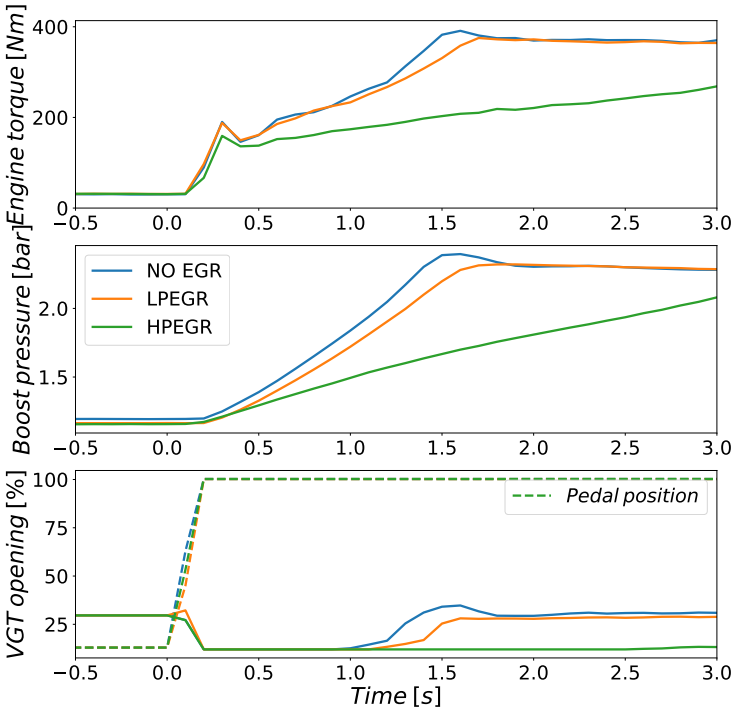

Figure 5.6: The performance of turbocharger and engine during load transient (Tip-In) at 1500 RPM with different EGR strategies.

As stated earlier, the smoke limiting strategy has already been reached with 5% EGR rate for all engine speeds except 1750 RPM. The opacity measurement for 1750 RPM are presented in Figure 5.7. Irrespective to the configuration, the rising part is almost similar while further opacity increases with

the presence of EGR. The comparison with HP and LP EGR is difficult as the quantity of HPEGR in the initial phase is very high. The measured soot concentration for LPEGR strategy is higher than the one without EGR which can be improved by the smoke air-fuel limit.

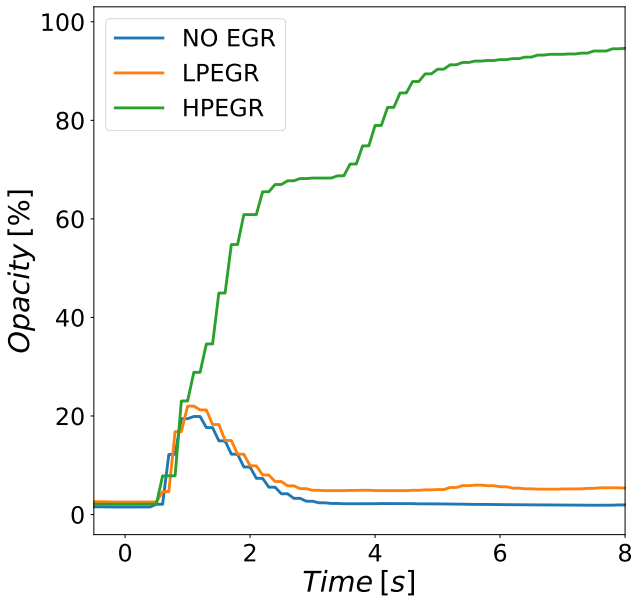

Figure 5.7: Opacity measurement at the exhaust after turbine during a load transient (Tip-In) at 1750 RPM with different EGR strategies.

5.3.2 Transients with different EGR valve profiles

Successful reduction of NO_x with LPEGR strategy without losing significantly the engine performance leaded to another study to reduce those peaks at the start of the "waiting zone", which are results of first dip in CO_2 concentration. Different profiles for LPEGR valve with variation of 5% were used before reaching to the final steady state value prescribed for full load to provide 5% of EGR rate. The profiles are indicated as "prof5", "prof10" and "prof15" for 5%, 10%, and 15% opening of valve respectively for that period. Figure 5.8 shows the arrival of CO_2 at the intake valve during transients for the different valve profiles used for 1750 RPM; "sin" represents the normal configuration without EGR. At this engine speed "prof5" LPEGR valve position has no noticeable

amount of burned gas flowing in the intake circuit. The corresponding engine torque and emission behavior during the above parametric tests are plotted in Figure 5.9.

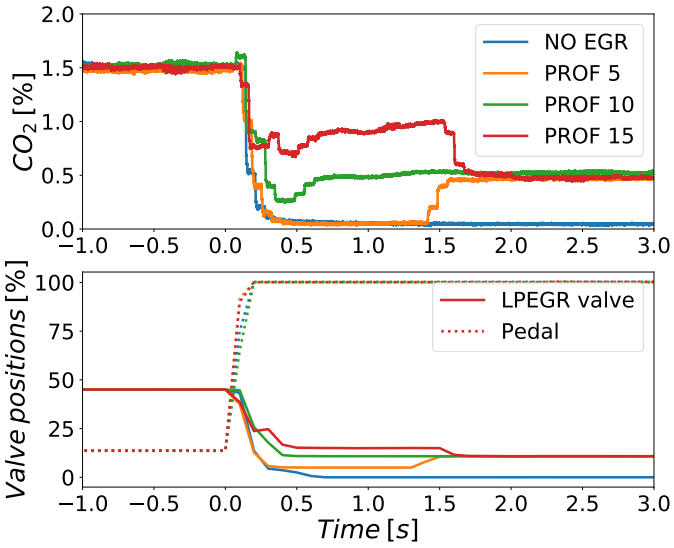

Figure 5.8: The LPEGR valve movement and arrival of CO_2 at the intake valve of engine during a load transient (Tip-In) operation at 1750 RPM with different valve profiles.

Direct effect of change in intake CO_2 concentration can be detected in the "waiting zone" NO_x concentration, while the performance in the form of engine torque is not reduced significantly during the first few seconds. To quantify these losses within these different profiles for the particular period of time during the transient operation, the area under the curve is calculated dividing by the specific time required to stabilize the performance as per the engine speed to obtain the average cumulative performance during respective transient operation. Area under the curve of engine torque after first random ascend introduced by the dynamometer and the acquisition frequency until the end of waiting zone has been calculated and further divided by time interval. The same procedure has been used for emissions until stabilization after the pedal has been pushed. The corresponding time intervals for each engine speed are detailed in the table 5.3.

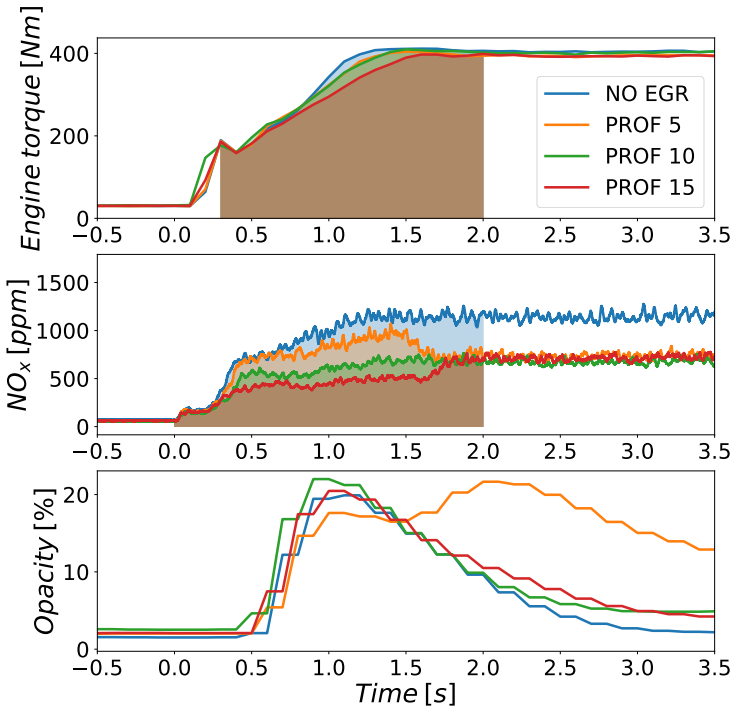

Figure 5.9: Performance and emission evaluation of a load transient at 1750 RPM during first few seconds with different LPEGR valve strategies.

Figure 5.10 shows the breakdown of the NO_x raw emissions, engine torque and opacity change in percentage from the base calibration during transient operation for different engine speeds. Four plots represent each engine speed with the concentration changes for opacity and NO_x prominently with extent of LPEGR valve opening during the first seconds of a transient operation. Increase in valve opening reduces the NO_x proportionally while torque on the other hand has a complex behavior. The torque loss is higher for "prof5" and "prof15" than "prof10" due to the boost control (variable geometry turbine). The VGT closes as soon as pedal is pushed and remains closed for longer period in case of transient EGR compared to without EGR. "Prof10" operation attains the boost pressure set point faster (moving the point to higher efficiency zone on compressor map) than the other 2 profiles. It causes opening of the VGT earlier, releasing the back pressure built up in exhaust manifold and resulting in better torque evolution. A proper value can be find at each engine speed for the LPEGR control to have minimum torque loss and maximum

Speed	1250	1500	1750	2000
Time	3s	2.5s	2s	1.5s

Table 5.3: Evaluation time for performance during transient operation at different engine speeds

reduction in pollutant formation.

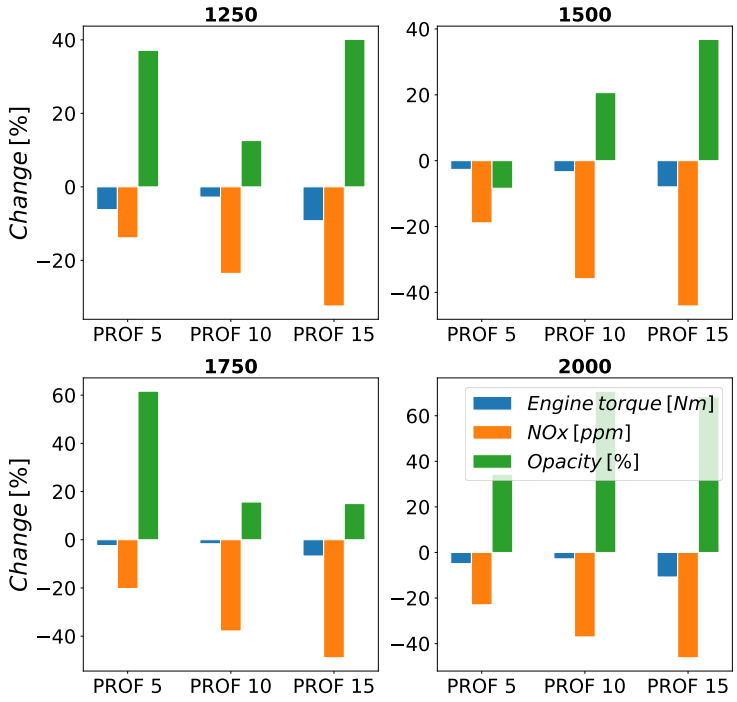

Figure 5.10: Performance and emission trade-off at different engine speeds during first few seconds of a load transient operation.

5.3.3 Transients with EGR at Roundabouts

The typical harsh transient, the engine has to face when a vehicle arrives at a roundabout on conventional roads is also carried out on a dynamic test bench with the same engine. It starts with almost partial load and goes to absolutely no load during the circular phase of the road, where the fuel is cut off for certain period of time and at the roundabout outlet, we have a

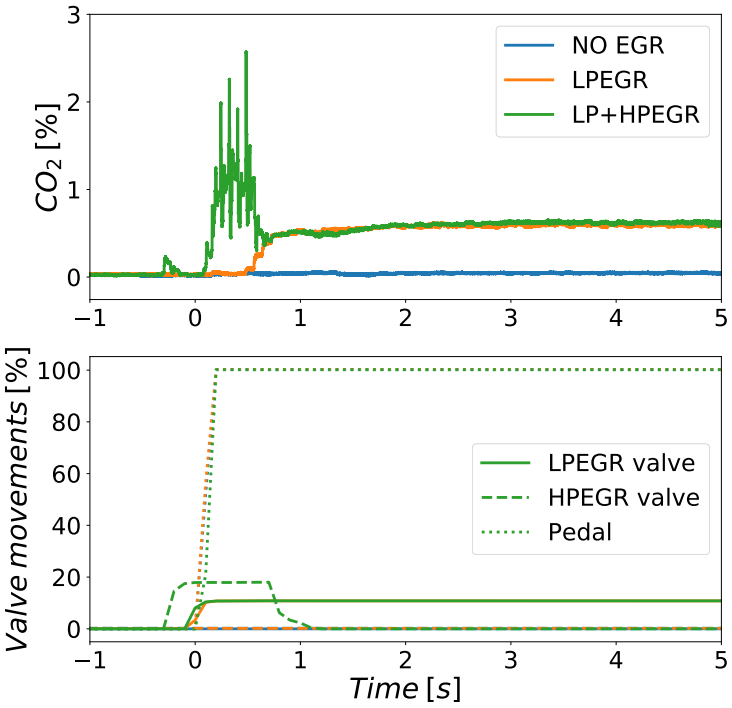

Figure 5.11: The valve actuation and CO_2 at the intake valve of a engine during a typical circular road manoeuvre at 1500 RPM with different EGR strategies.

sudden push of pedal to almost full load. In the testing campaign, these kind of operation were performed with 1500 RPM and the time for the fuel cut-off (engine cracking phase) was around 4 seconds. No matter the EGR valve position or configuration, no burned gas flows in the engine circuits in those 4 seconds. So when pedal is shifted to 100% the flow of gases are not as same as normal Tip-In transient operation described in the previous section. Figure 5.11 shows the valve movements during these types of roundabout transients. As explained above, during cranking the intake line carries only air even in the EGR duct so there is no CO_2 concentration detected (apart from CO_2 in air). When the pedal is pushed, the arrival of CO_2 to the intake manifold is delayed for about half a second in the LPEGR configuration. Although the arrival is delayed, no huge peak of NO_x is observed after turbine. On the contrary, in the case of HPEGR configuration, the arrival is immediate. Therefore, in order to counteract the delay in LPEGR, the HPEGR valve is opened for a second at the same time with LPEGR valve at the start of a transient. This

configuration is called as 'HP-LP' in the figures.

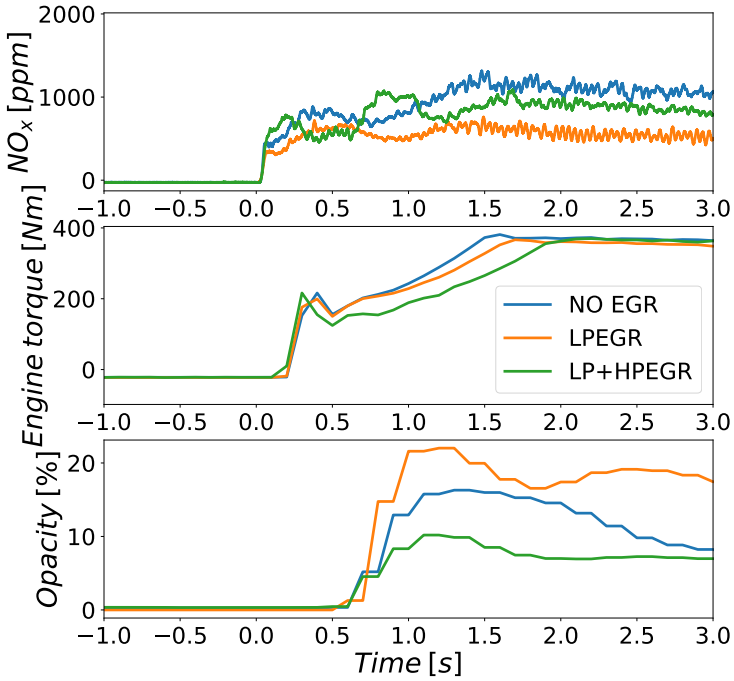

Figure 5.12: Emission and performance of an engine during a typical circular road manoeuvre at 1500 RPM with different EGR strategies.

Several repetitions were performed with the 'LP-HP' configuration. It is seen that, opening of HPEGR valve even for 1 seconds reduces the engine torque without significant reduction of NO_x. Therefore, the only alternative of using LPEGR system during the normal and roundabout load transient operations is remains available.

As the turbocharger is not designed for the energy reduction through HPEGR line flow before the turbine at higher loads, engine performance is heavily reduced with the opening of HPEGR valve for even a short interval of time. The total fuel injection went down with lack of air driven by the turbocharger and that is why the opacity is also seen to be reduced as compared to the basic operation without EGR in Figure 5.12. Moreover, the application of LPEGR at full load reduces the NO_x by 50% during this typical and harsh roundabout transient too where there is no EGR at the start with very limited impact in the engine torque.

5.3.4 Real driving cycles

A specific real driving cycle discussed in the Chapter 2 is used to see the effect of adding new strategies such as EGR at full load and modified valve shift during transient operation. The real driving cycle is separated by the parts called the 'city' and 'highway' driving part. The NO_x measurement is carried out downstream turbine by slow emission measurement systems discussed in the Chapter 3.

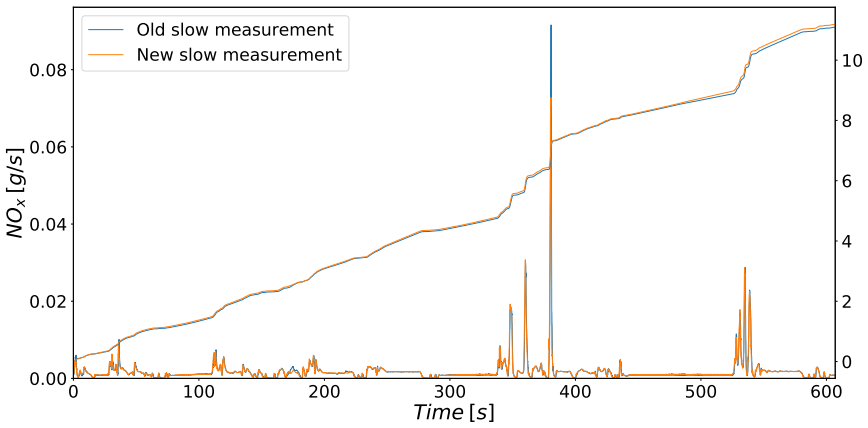

Figure 5.13: comparison of NO_x emission with old and new EGR strategies on city part of the real driving cycle measured by slow emission measurement system.

Figure 5.13 shows the comparison of NO_x measurements done by the slow emission measurement system on the city part of the real driving cycle. Due to the fact that, the engine hardly goes to the full load part (outside of old EGR zone), the NO_x measurement doesn't show much improvement compared to old calibration. Nonetheless, the NO_x peaks captured by high response NO_x measurement, from the transient operation are appeared to be reduced with the new calibration.

Looking at the highway part of real driving cycle, which involves high load points, shows the impressive improvement with the new calibration (see Figure 5.14). Insertion of EGR outside of EGR zone managed to reduce raw NO_x emission effectively. Apart from the peaks captured by fast measurement system, there are certain high load regions where the NO_x measurement shows

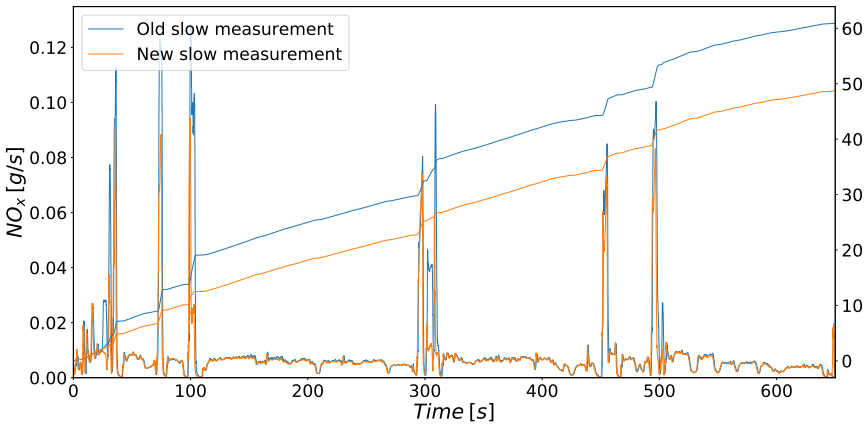

Figure 5.14: comparison of NO_x emission with old and new EGR strategies on highway part of the real driving cycle measured by slow emission measurement system.

lower values compared to previous calibration.

5.4 Conclusions

In this work a 2-liter turbocharged diesel engine with hybrid EGR system is tested in a dynamic test cell. Main instrumentation included a high response time gas analyzer, more useful to measure the NO_x emission during transient operation than the traditional slow analyser. The fast analyzer allows to capture the NO_x peaks resulted from delays in air, fuel and EGR flow. The engine used in this work had a EuroVI calibration, so that, unlike in precedent standards following NEDC, the usage of EGR all over the engine map is necessary. EGR at high loads reduce the NO_x emissions considerably. 5% of EGR at full load has a benefit around 40% reduction in NO_x but a torque penalty of 10%. At full load, LPEGR is more effective in reducing NO_x than HPEGR for the same engine torque. From the control point of view, on the one hand, LPEGR rate is easier to manage during load transients except for the lag in arrival of LPEGR to the intake valve. On the other hand, HPEGR needs proper designing of turbocharger and VGT control during transient operations. As

the movement of VGT has direct impact on the pressure upstream of turbine and thus the HPEGR flow. It has been shown that there is a compromise between performance (torque evolution) and emissions during Tip-Ins. The optimization of LPEGR valve positions (profile) during transient operations (different than steady state operation) is required with specific turbocharger selection to give fast torque evolution, as LPEGR changes the mass flow rate through compressor and hence affecting the boost control which determines the back pressure in the exhaust manifold.

During Tip-Ins no negative effect in NO_x emission is seen with respect to the lag of LPEGR. This is because during the entire transient there is EGR present in the intake system. The worst situation in this regard would be a Tip-In transient with no EGR at the beginning of the maneuver. This is referred in the paper as the "roundabout" transient starting from engine cranking operation without fuel injection up to full load. An EGR strategy to avoid the LPEGR lag is the combination of LPEGR and HPEGR only during the lag time. The tests results show a good control of CO_2 during the transient for this strategy, however they also show a penalty in torque evolution due to the use of HPEGR.

Chapter 5 Bibliography

[23] A. Reig Bernad. "Optimal Control for Automotive Powertrain Applications." PhD thesis. Valencia (Spain): Universitat Politècnica de València, 2017. DOI: 10.4995/Thesis/10251/90624. URL: https://riunet.upv.es/handle/10251/90624 (cit. on pp. 8, 136).

[25] J. M. Luján, V. Bermúdez, V. Dolz, and J. Monsalve-Serrano. "An assessment of the real-world driving gaseous emissions from a Euro 6 light-duty diesel vehicle using a portable emissions measurement system (PEMS)." *Atmospheric Environment* 174 (2018), pp. 112–121. ISSN: 18732844. DOI: 10.1016/j.atmosenv.2017.11.056 (cit. on pp. 9, 135).

[32] S. Reifarth and H.-E. Angstrom. "Transient EGR in a long-route and short-route EGR system." In: *ASME Internal Combustion Engine Division Spring Technical Conference*. 2009, pp. 761–770. ISBN: 978-0-7918-4340-6. DOI: 10.1115/ICES2009-76107 (cit. on pp. 10, 11, 135, 138).

[40] J. M. Luján, C. Guardiola, B. Pla, and A. Reig. "Switching strategy between HP (high pressure)- and LPEGR (low pressure exhaust gas recirculation) systems for reduced fuel consumption and emissions." *Energy* 90 (2015), pp. 1790–1798. ISSN: 03605442. DOI: 10.1016/j.energy.2015.06.138 (cit. on pp. 11, 134).

[72] T. Donateo and M. Giovinazzi. "Building a cycle for Real Driving Emissions." *Energy Procedia* 126 (2017), pp. 891–898. ISSN: 18766102. DOI: 10.1016/j.egypro.2017.08.307. URL: https://doi.org/10.1016/j.egypro.2017.08.307 (cit. on pp. 42, 135).

[83] J. M. Luján, H. Climent, S. Ruiz, and A. Moratal. "Influence of ambient temperature on diesel engine raw pollutants and fuel consumption in different driving cycles." *International Journal of Engine Research* (2018). DOI: 10.1177/1468087418792353. URL: http://journals.sagepub.com/doi/10.1177/1468087418792353 (cit. on pp. 57, 135).

[88] E. G. Giakoumis, C. D. Rakopoulos, A. M. Dimaratos, and D. C. Rakopoulos. "Exhaust emissions of diesel engines operating under transient conditions with biodiesel fuel blends." *Progress in Energy and Combustion Science* 38(5) (2012), pp. 691–715. ISSN: 03601285. DOI: 10.1016/j.pecs.2012.05.002. URL: http://dx.doi.org/10.1016/j.pecs.2012.05.002 (cit. on pp. 59, 135).

[95] Z. C. Liu, K. B. Yu, J Tian, Y. Q. Han, S. L. Qi, and P. K. Teng. "Influence of rail pressure on a two-stage turbocharged heavy-duty diesel engine under transient operation." *International Journal of Automotive Technology* 18(1) (2017), pp. 19–29. ISSN: 1229-9138. DOI: 10.1007/s12239-017-0002-z. URL: https://doi.org/10.1007/s12239-017-0002-zhttp://link.springer.com/10.1007/s12239-017-0002-z (cit. on pp. 61, 135).

[126] M. S. Khalef, A. Soba, and J. Korsgren. "Study of EGR and Turbocharger Combinations and Their Influence on Diesel Engine ' s Efficiency and Emissions." *SAE International* (2016). DOI: 10.4271/2016-01-0676.Copyright (cit. on pp. 88, 89, 134).

[136] G. Zamboni and M. Capobianco. "Experimental study on the effects of HP and LP EGR in an automotive turbocharged diesel engine." *Applied Energy* 94 (2012), pp. 117–128. ISSN: 03062619. DOI: 10.1016/j.apenergy.2012.01.046. URL: http://dx.doi.org/10.1016/j.apenergy.2012.01.046 (cit. on pp. 89, 134).

[142] J. Park and J. Choi. "Optimization of dual-loop exhaust gas recirculation splitting for a light-duty diesel engine with model-based control." *Applied Energy* 181 (2016), pp. 268–277. ISSN: 03062619. DOI: 10.1016/j.apenergy.2016.07.128. URL: http://dx.doi.org/10.1016/j.apenergy.2016.07.128 (cit. on pp. 89, 134).

[150] J. Park, S. Song, and K. S. Lee. "Numerical investigation of a dual-loop EGR split strategy using a split index and multi-objective Pareto optimization." *Applied Energy* 142 (2015), pp. 21–32. ISSN: 03062619. DOI: 10.1016/j.apenergy.2014.12.030. URL: http://dx.doi.org/10.1016/j.apenergy.2014.12.030 (cit. on pp. 90, 134).

[159] G. Zamboni, S. Moggia, and M. Capobianco. "Effects of a dual-loop exhaust gas recirculation system and variable nozzle turbine control on the operating parameters of an automotive diesel engine." *Energies* 10(1) (2017). ISSN: 19961073. DOI: 10.3390/en10010047 (cit. on p. 134).

[160] A. Maiboom, X. Tauzia, and J. F. Hétet. "Experimental study of various effects of exhaust gas recirculation (EGR) on combustion and emissions of an automotive direct injection diesel engine." *Energy* 33(1) (2008), pp. 22–34. ISSN: 03605442. DOI: 10.1016/j.energy.2007.08.010 (cit. on p. 134).

[161] Y. Park and C. Bae. "Experimental study on the effects of high/low pressure EGR proportion in a passenger car diesel engine." *Applied Energy* 133 (2014), pp. 308–316. ISSN: 03062619. DOI: 10.1016/j.apenergy.2014.08.003. URL: http://dx.doi.org/10.1016/j.apenergy.2014.08.003 (cit. on p. 134).

[162] C. A. Lana, K. K., G. Kothandaraman, J. Perfetto K. David, S. C., G. H., and D. K. "Systems and methods for controlling egr flow during transient conditions." Pat. US Patent App. 15/138,892. 2016 (cit. on p. 134).

[163] D. Brookshire and S. D. Arnold. "Dual and hybrid EGR systems for use with turbocharged engine." Pat. US Patent 7,013,879. 2007 (cit. on p. 134).

[164] P. Thunis, W. Lefebvre, M. Weiss, S. Vranckx, A. Clappier, B. Degraeuwe, and S. Janssen. "Impact of passenger car NOX emissions on urban NO2 pollution – Scenario analysis for 8 European cities." *Atmospheric Environment* 171(2) (2017), pp. 330–337. ISSN: 13522310. DOI:

10.1016/j.atmosenv.2017.10.040. URL: http://dx.doi.org/10.1016/j.atmosenv.2017.10.040 (cit. on p. 134).

[165] L. Yang, V. Franco, P. Mock, R. Kolke, S. Zhang, Y. Wu, and J. German. "Experimental Assessment of NOx Emissions from 73 Euro 6 Diesel Passenger Cars." *Environmental Science and Technology* 49(24) (2015), pp. 14409–14415. ISSN: 15205851. DOI: 10.1021/acs.est.5b04242 (cit. on p. 134).

[166] G. Triantafyllopoulos, D. Katsaounis, D. Karamitros, L. Ntziachristos, and Z. Samaras. "Experimental assessment of the potential to decrease diesel NOxemissions beyond minimum requirements for Euro 6 Real Drive Emissions (RDE) compliance." *Science of the Total Environment* 618 (2018), pp. 1400–1407. ISSN: 18791026. DOI: 10.1016/j.scitotenv.2017.09.274. URL: https://doi.org/10.1016/j.scitotenv.2017.09.274 (cit. on p. 135).

[167] R. Daya, J. Hoard, S. Chanda, and M. Singh. "Insulated catalyst with heat storage for real-world vehicle emissions reduction." *International Journal of Engine Research* (2017). ISSN: 1468-0874. DOI: 10.1177/1468087416685470 (cit. on p. 135).

[168] H. Yamada, K. Misawa, D. Suzuki, K. Tanaka, J. Matsumoto, M. Fujii, and K. Tanaka. "Detailed analysis of diesel vehicle exhaust emissions: Nitrogen oxides, hydrocarbons and particulate size distributions." *Proceedings of the Combustion Institute* 33(2) (2011), pp. 2895–2902. ISSN: 15407489. DOI: 10.1016/j.proci.2010.07.001. URL: http://dx.doi.org/10.1016/j.proci.2010.07.001 (cit. on p. 135).

[169] F. C. Leach, M. H. Davy, and M. S. Peckham. "Cyclic NO 2 :NO x ratio from a diesel engine undergoing transient load steps." *International Journal of Engine Research* (2019). ISSN: 20413149. DOI: 10.1177/1468087419833202 (cit. on p. 135).

[170] T Winstanley, P. G. Eastwood, a. M. K. P. Taylor, K Tufail, Y Hardalupas, and J Black. "Diesel engine transient control and emissions response during a European Extra-Urban Drive Cycle (EUDC)." In: *SAE Technical Paper Series*. 2007, pp. 1015–1030. DOI: 10.4271/2007-01-1938 (cit. on p. 135).

[171] D. Heuwetter, W. Glewen, C. Meyer, D. E. Foster, M. Andrie, and R. Krieger. "Effects of Low Pressure EGR on Transient Air System Performance and Emissions for Low Temperature Diesel Combustion."

In: *SAE International*. 2011. DOI: 10.4271/2011-24-0062. URL: http://papers.sae.org/2011-24-0062/https://www.sae.org/content/2011-24-0062/ (cit. on p. 135).

[172] J. M. Luján, H. Climent, F. J. Arnau, and J. Miguel-García. "Analysis of low-pressure exhaust gases recirculation transport and control in transient operation of automotive diesel engines." *Applied Thermal Engineering* 137 (2018), pp. 184–192. ISSN: 1359-4311. DOI: 10.1016/j.applthermaleng.2018.03.085. URL: https://doi.org/10.1016/j.applthermaleng.2018.03.085 (cit. on pp. 135, 139, 140).

[173] A. Darlington, K. Glover, and N. Collings. "A Simple Diesel Engine Air-Path Model to Predict the Cylinder Charge During Transients: Strategies for Reducing Transient Emissions Spikes." In: *SAE International*. 724. 2006, p. 14. DOI: 10.4271/2006-01-3373. URL: https://www.sae.org/content/2006-01-3373/ (cit. on p. 135).

[174] M. S. Peckham, B. W. Campbell, and A. Finch. "Measurement of the effects of the exhaust gas recirculation delay on the nitrogen oxide emissions within a turbocharged passenger car diesel engine." *Proceedings of the Institution of Mechanical Engineers, Part D: Journal of Automobile Engineering* 225(9) (2011), pp. 1156–1166. ISSN: 0954-4070. DOI: 10.1177/0954407011406977. URL: http://pid.sagepub.com/lookup/doi/10.1177/0954407011406977 (cit. on pp. 135, 136).

[175] U. Asad, J. Tjong, and M. Zheng. "Exhaust gas recirculation – Zero dimensional modelling and characterization for transient diesel combustion control." *Energy Conversion and Management* 86 (2014), pp. 309–324. ISSN: 01968904. DOI: 10.1016/j.enconman.2014.05.035. URL: http://dx.doi.org/10.1016/j.enconman.2014.05.035https://linkinghub.elsevier.com/retrieve/pii/S0196890414004464 (cit. on p. 142).

Chapter 6

A quasi-steady prediction of NOx during transients and real driving cycles

Contents

6.1 Introduction

Experimental approach to measure the pollutant emissions like NO_x during transients require highly complicated, sophisticated and costly experimental facility with high response exhaust gas analyzers. The availability of this kind of facility is reasonable for measurement of limited amount of time. Moreover, model based exhaust emission prediction by filling and emptying models or 1-D transient simulation codes lead to higher simulation time which is critical for simulation of driving cycles in whole. Various NO_x estimation models have been proposed in the past including physics based phenomenological models [176][177], empirical models [178][179] and thermodynamic models based on "Zeldovich mechanism" [180, 181] and the artificial neural network [182, 183]. But these models require either too many unavailable inputs or state variables to accurately predict the NO_x formation taking long calculation time. Alternative models based on Local Linear Model Tree (LOLIMOT) structure, Kernel and adapted polynomial methods show more error and require higher memory with lower dimension in the input variables [179]. Real-time NO_x model by the steady measurement and sensitivities calculated from the physical combustion model is also developed by [184]. Querel has classified and compared these different control oriented NO_x models in [185]. A simple and fast method of NO_x prediction is always helpful for the engine manufacturers to design engine with challenging emission constraints on newly developed driving cycles.

In regards to modelling a transient operation, assumption of an engine moving through a series of quasi steady operations is the simple and commonly used methodology for ICEs. The same technique can be used to predict the transient emission by mapping the steady pollutant formation. The model based on this kind of technique is called as a 'Quasi steady model'. These models are simple and require less amount of time and inputs for the estimation of a pollutant during steady and transient operations. Therefore, they are very useful during initial designing phase of an engine, where availability of data and need for detailed emission estimation is limited. Quasi-steady models consist of steady state mapping of an engine parameter as a function of various operating conditions on an engine map. These maps are used to predict the real time emission at any arbitrary operating point using interpolation/extrapolation within the steady operating map. These less complex models have been used to predict CO, HC, NO_x emission from heavy duty diesel engines in [186, 187,

188].

Dynamics during transient operation induces different configuration of gases in the intake system and combustion chamber by change in 'fast' and 'slow' variables as discussed in Chapter 1. It results in different concentration of pollutants than predicted by steady state maps. Therefore, certain correction factors are needed to apply on the estimated emission by quasi steady models. However, these transient correction factors have minor impact on the NO_x prediction as compared to CO and HC [189]. They can be applied for the cumulative estimation [186] or region wise estimation defined earlier on the engine map [190][191].

This chapter speaks about the similar 'Quasi steady model', used for predicting the NO_x emissions during transient operations. Two different models with the difference of number of inputs (2D and 3D) are described and compared to see the effect on the error while predicting the pollutant formation. The effect of an addition of EGR rate as a third input to the proposed model for estimating the NO_x formation is presented at the end.

6.2 NOx mapping

This section consists of the mapping of NO_x emissions from the cylinder as a function of engine operating conditions and EGR rate. The engine 2 from the Chapter 3 is used for mapping this engine out raw NO_x emissions. Various operating points on the engine map were selected to perform the NO_x mapping. The real driving cycle mentioned in the Chapter 2 is used to select the specific points on the engine map. Figure 6.1 represents the same operating points on an engine map along with the points registered from a real driving cycle. The selected operating range for mapping covers maximum part of the cycle. A 2-D map is created with these points to determine the NO_x emission as a function of a engine torque and speed. The EGR rate was kept as per the calibration in ECU

To see the sensitivity and the effectiveness of the quasi-steady NO_x model with the EGR rate, another 3D map is created by varying the EGR rate for every operating point. Figure 6.2 shows the 3D map of new operating points with EGR rate as a third axis.

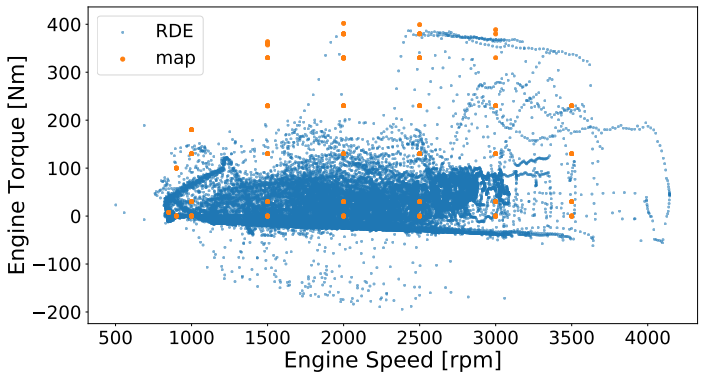

Figure 6.1: Selected engine operating point with the operating range of a real driving cycle (RDE) on a engine map.

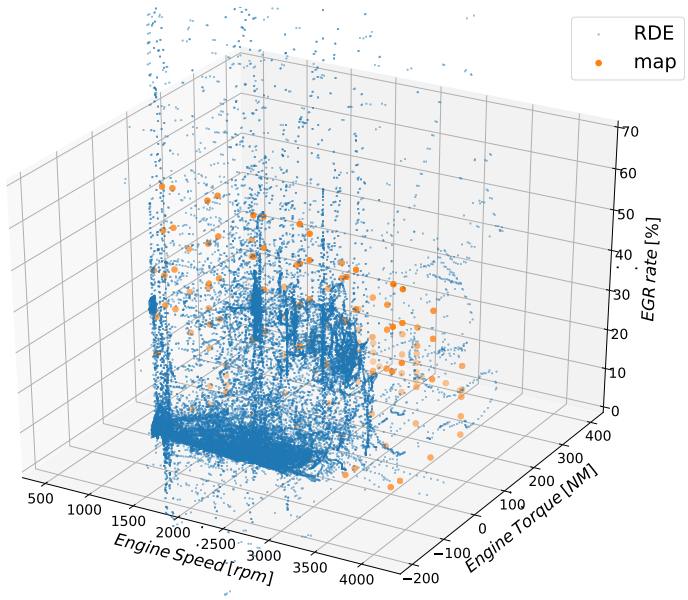

Figure 6.2: Selected engine operating point with the operating range of a real driving cycle (RDE) on a engine map.

6.3 Methodology

Following the maps in the NO_x mapping section, 2 models with different inputs are created to predict the NO_x emission during a transient operations and real driving conditions. The first model with 2 inputs (engine speed and torque) is tested with different interpolation techniques like 'nearest', 'linear' and 'cubic' to see the prediction in harsh load transient operation.

$$NO_x = f(N, \tau) \tag{6.1}$$

Where, τ is the torque and N is the engine speed. Similar study is made with the same model but with 3 inputs.

$$NO_x = f(N, \tau, \xi) \tag{6.2}$$

Where ξ is the total EGR rate going to in the cylinder. The vital part of the model lies in the interpolation technique used to determine the NO_x value among the given selected steady state points. The NO_x values for those operating points lying inside the range of engine speeds and torques are calculated by linear interpolation method. While for the points lying outside the zone of selected operating points, the NO_x prediction is done with the nearest boundary value of the map operating point. The respective models were tested first on the load transient operation from the last chapter. The NO_x measurement done during the Tip-In and Tip-Out operations on the dynamic engine test bench are compared with the 2D and 3D models explained above. Following to the transient comparison, the full cycle NO_x measurement done on the test bench is also compared with the NO_x prediction by the model.

6.4 Load transient prediction

The several repetitions of harsh load transient operation performed on the engine test bench (described in the Chapter 5) are used to compare the NO_x prediction from the NO_x mapping. The typical load transient operation consists of a change of state from 2 bar BMEP to full load and again back to 2 bar BMEP state.

6.4.1 Transient prediction of NO_x by 2D model

Figure 6.3 represents the Tip-IN operation NO_x comparison from the fast measurement system (CLD500) and prediction from the 2D NO_x map at 1000 and 1500 rpm. The NO_x measurement from the rapid response system is corrected from the correction mentioned in the Chapter 3. The interpolation comprises the linear and nearest method as described in the methodology. The steady state NO_x prediction is close to the test measurements while huge error is observed during first few seconds of load transient with the mismatch in the air and fuel flow. Therefore, the prediction is delayed as compared to the fast NO_x measurement by CLD500 system.

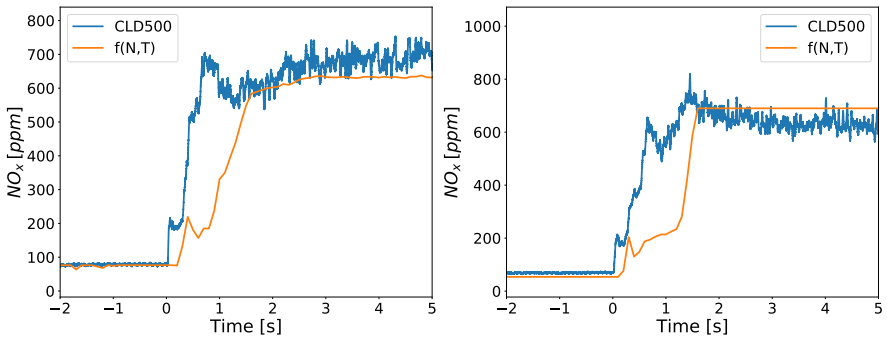

Figure 6.3: Load transient (Tip-In) NO_x prediction from the 2D map at 1000 and 1500 rpm.

Looking at the Tip-Out operation in the Figure 6.4 for the same engine speeds, the NO_x model is unable to predict the peak in the NO_x immediately after the release of pedal. Sudden drop in the fuel and torque leads to under prediction of NO_x during the transient Tip-Out operation. The small peaks and the variation in the NO_x measurement by the CLD500 are not predicted by the 2D model just after the Tip-Out operation.

6.4.2 Transient prediction of NO_x by 3D model

A 3D model is the function of 3 variables. Engine speed and torque from the last 2D model and the third variable is called total EGR rate. The same transient operating conditions with EGR rate values is fed to the model to see the predicted NO_x values during the above transient operations. The EGR rate

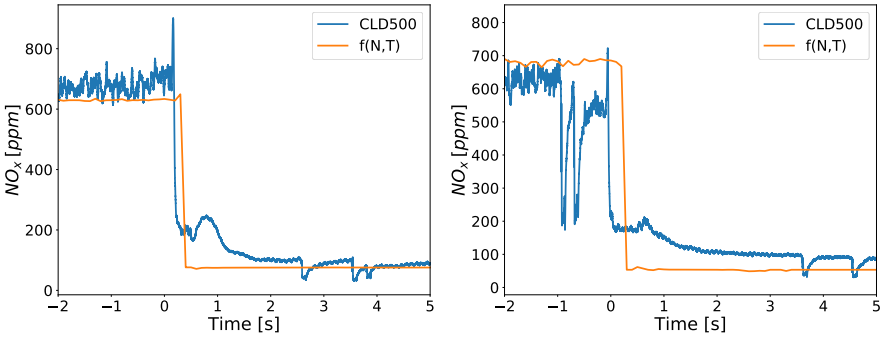

Figure 6.4: Load transient (Tip-Out) NO_x prediction from the 2D map at 1000 and 1500 rpm.

is calculated by the CO_2 concentrations from the intake and exhaust using the Equation 3.5. However, considering the delays in the slow emission measurement system, the NDIR500 system from cambustion is used to measure the CO_2 concentration at the intake port just before the intake valve of the cylinder. On the other hand, due to absence of another NDIR500 sensor the measurement from slow response system is used to calculate the instantaneous EGR rate in the air system. The newly calculated EGR is fed as an input along with engine torque and speed to 3D NO_x model.

Figure 6.5 displays the prediction of NO_x compared with the CLD500 system measurements during Tip-IN operation at 1000 and 1500 rpm. The huge error present in the 2D prediction is minimized with the consideration of EGR rate in the model making NO_x evolution faster. Nonetheless, a little over prediction of NO_x is seen when the transient reaches to full load state, due to error in the calculation of instantaneous EGR rate. The nearest point interpolation method for the points outside of the map range cause some unrealistic prediction of NO_x. This error gets reduce after few seconds at full load steady state.

In the case of Tip-Out operation for the same engine speeds, the sudden drop in NO_x after the release of pedal predicted in the 2D model is also removed. This certainly reduces the error in the predicted and measured NO_x by 3D model.

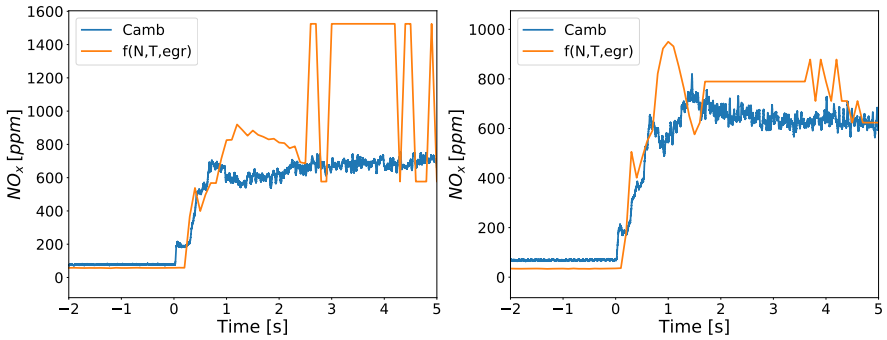

Figure 6.5: Load transient (Tip-Out) NO_x prediction from the 2D map at 1000 and 1500 rpm.

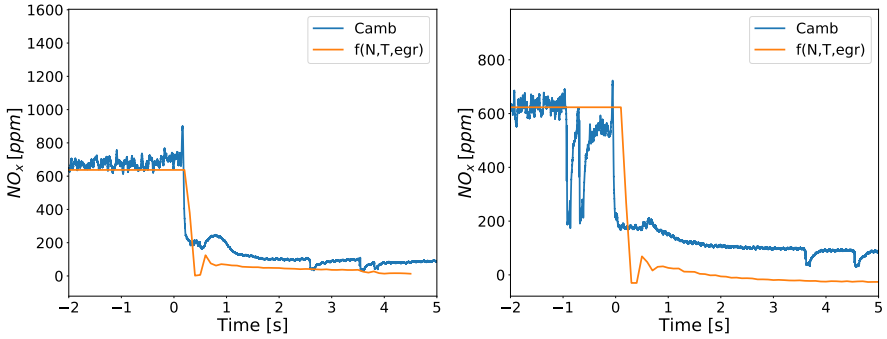

Figure 6.6: Load transient (Tip-Out) NO_x prediction from the 2D map at 1000 and 1500 rpm.

6.5 RDE cycle prediction

The RDE cycle from the Chapter 2 is performed on the engine 2 on dynamic test bench with only LPEGR configuration. The NO_x emission throughout the cycle are recorded with both emission measurement systems mentioned in the Chapter 3. However, the fast system (CLD500) requires bigger memory even though the frequency of acquisition is reduced to 100Hz. Therefore, the RDE cycle is performed in 2 parts. The "city" and the 'highway' part are selected as per the criteria of vehicle velocity. Each part is performed on the dynamically controlled test bench as per the vehicle model mentioned in the Chapter 3. The NO_x measurement is done after the turbine with both fast and slow response system (in ppm), which is then converted into g/s.

The NDIR500 sensor is used at the intake valve to measure the instantaneous CO_2 in the intake line while the CO_2 at the exhaust is measured by the slow response system because the of unavailability of other NDIR500 sensor. The NO_x measurement during the city part from both systems is displayed in Figure 6.7. Both signal from the different systems correspond with each other yet there is a lag between them. The lag of around 1-2 seconds can be seen clearly in the zoomed part of the signals. Similar results are seen with the highway part of the real driving cycle in Figure 6.8. From the both parts, it is evident that, slow system is not able to capture the sudden peaks in NO_x captured by the fast system confirming to the results from previous chapter. There are more peaks of NO_x during the 'highway' part of the cycle than 'city'.

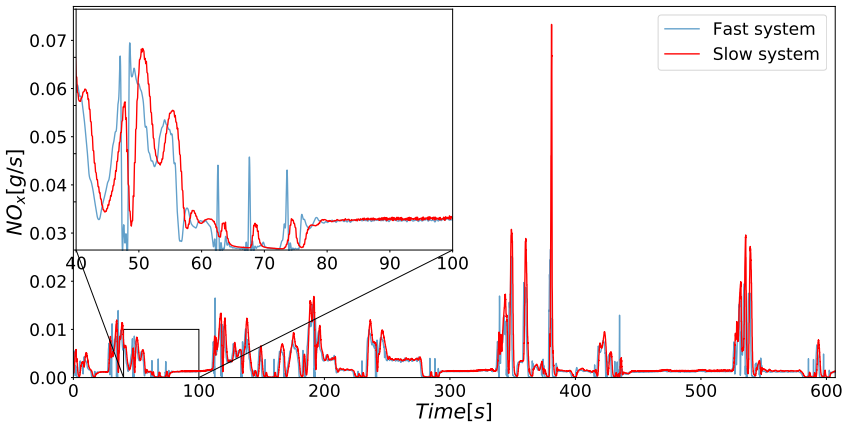

Figure 6.7: RDE cycle 'city' part NO_x measurement with slow and fast response measurements system.

6.5.1 RDE cycle prediction of NO_x by 2D model

The NO_x predicted with the maps consisting engine speed and torque as a inputs for the 'city' and 'highway' parts. Figure 6.9(a) represents the comparison of the NO_x prediction with test measurements. The frequency of error in the prediction in ppm is plotted on the right hand side plot showing the maximum occurred tolerance of ±200ppm.

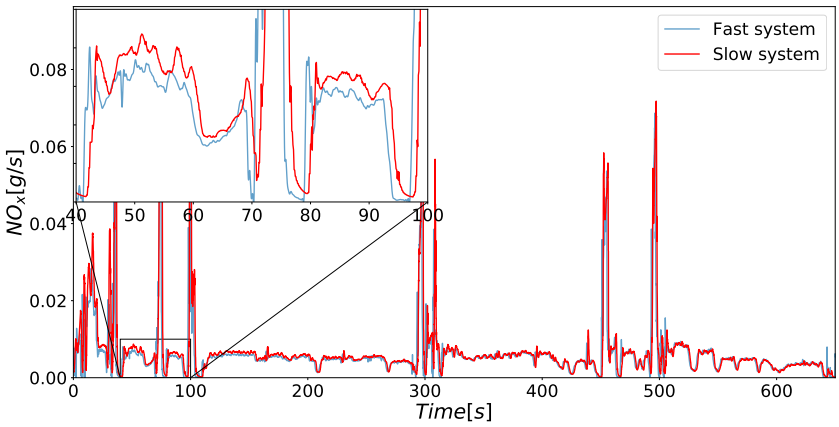

Figure 6.8: RDE cycle 'highway' part NO_x measurement with slow and fast response measurements system.

The temporal prediction of the NO_x with 2D model is plotted in the Figure 6.9(b). The delayed prediction on the time axis as mentioned in the load transient prediction is confirmed on the cycle prediction too. Over estimation of NO_x during the harsh load transient is can be seen with this interpolation method.

On the other hand, the 'highway' part of the real driving cycle shows more error with 2D model compared to 'city' part. The tolerance limits are increased to around ±400ppm on a frequency plot in Figure 6.10(a). The overall tendency of error is inclined to the over estimation of the NO_x on high vehicle speed points.

The NO_x prediction as a function of time for the 'highway' part is presented in the Figure 6.10(b). The huge differences in high values of NO_x are clearly seen which can be explained by the different composition of gases as compared to steady state composition. Extra parameter is required related to the gas composition to match the accurate NO_x prediction during the dynamic condition during the real driving cycles.

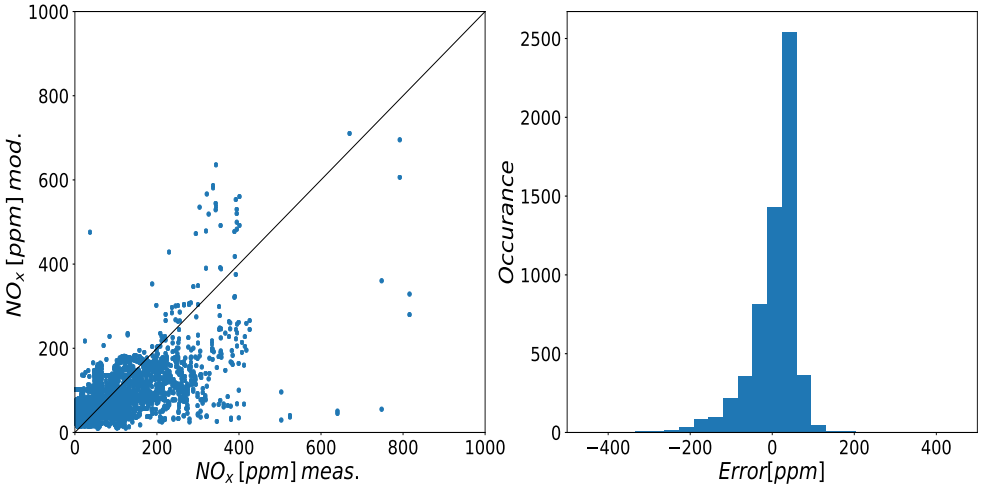

(a) comparison

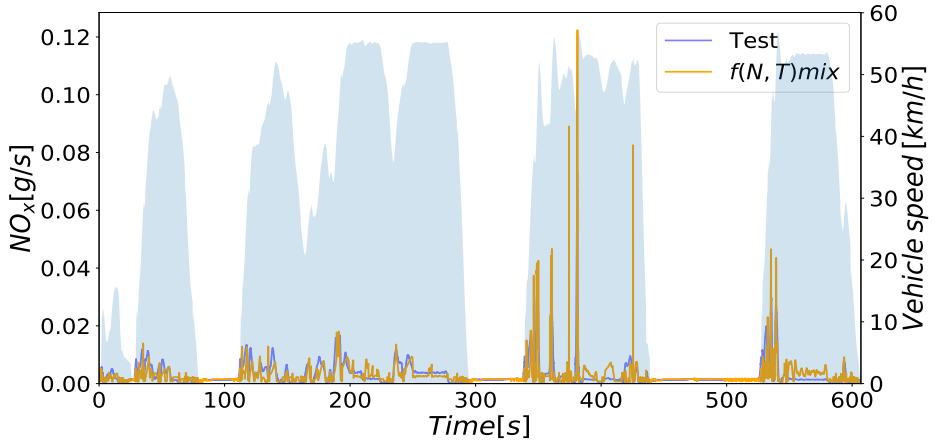

(b) Time response

Figure 6.9: Comparison of NO_x prediction by 2D model with the test measurement on 'city' part of RDE cycle .

6.5.2 RDE cycle prediction of NO_x by 3D model

To match with the correct gas composition as compared to steady state for predicting NO_x, 3D maps with the engine speed, torque and EGR rate as an

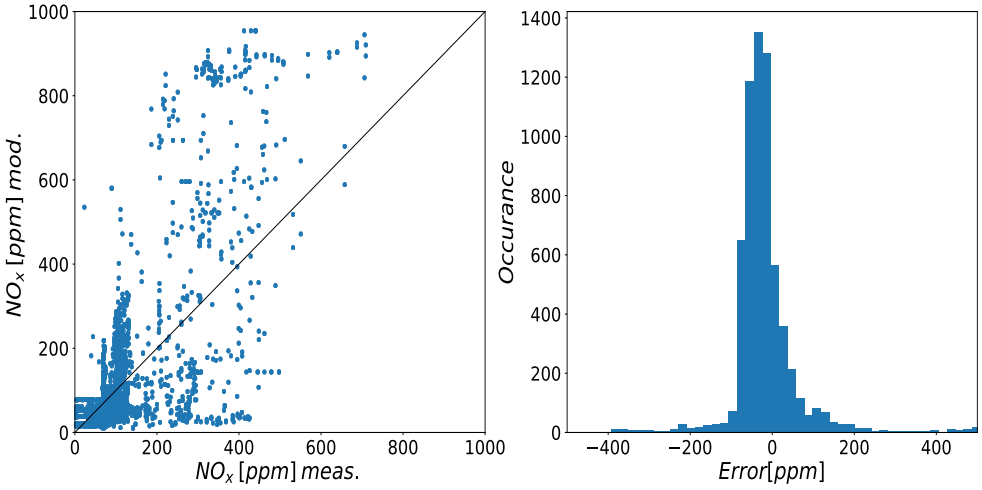

(a) comparison

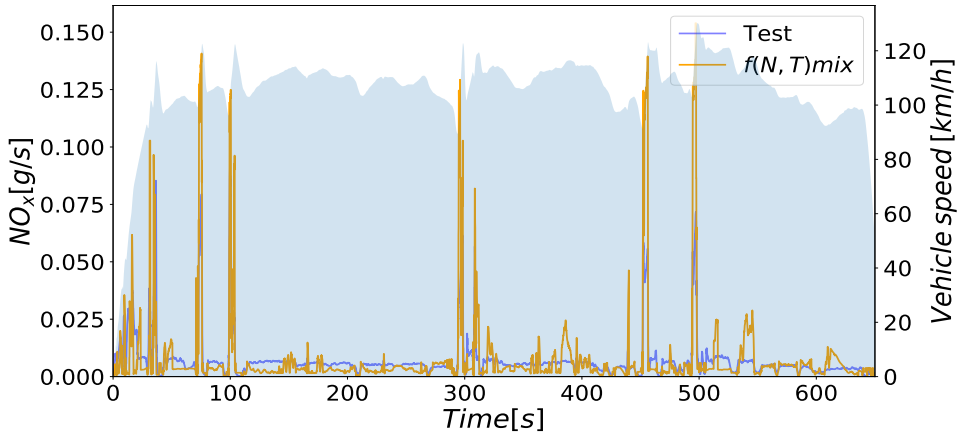

(b) Time response

Figure 6.10: Comparison of NO_x prediction by 2D model with the test measurement on 'highway' part of RDE cycle .

input are used in this section. The instantaneous EGR rate values are calculated by the process mentioned in the prediction for load transient operations. Figure 6.11(a) represents the comparison of NO_x prediction with the measurements. The frequency of error is increased for lower error values. and the

points are more closer to the diagonal line as compared to the 2D prediction of 'city' part. However, the few highly overestimated points as a outcome of the 'nearest' method of interpolation increase the tolerance band to 400ppm. The number of this kind of outliers is less.

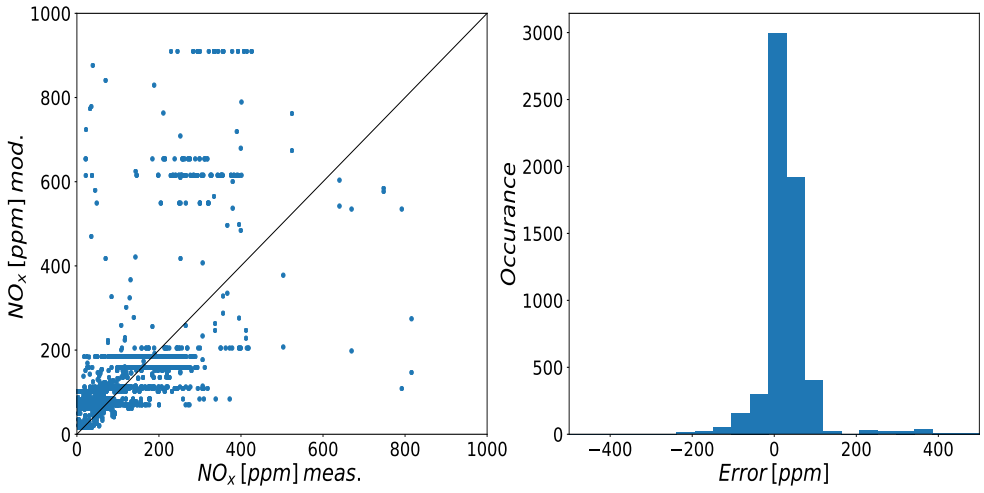

(a) comparison

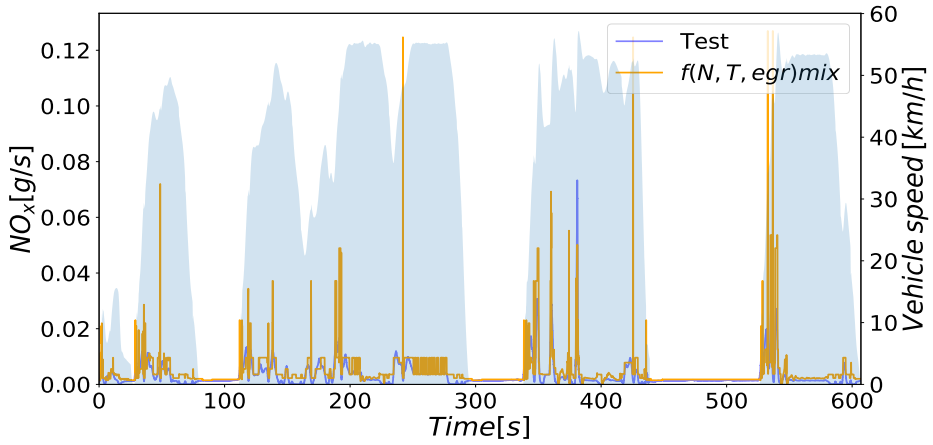

(b) Time response

Figure 6.11: Comparison of NO_x prediction by 3D model with the test measurement on 'city' part of RDE cycle .

The increased accuracy of the 3D model is identified by the temporal prediction in the Figure 6.11(b) excluding the outliers appearing at each Tip-In operation (described in load transient prediction). Moreover, the delays in the NO_x calculation during the transients are removed.

In the case of 'highway' part of RDE cycle, the error is reduced very much comparing with the 2D model. The Figure 6.12(a) shows that, the frequency of less error points is increased reducing the tolerance band. However few outliers are present as referred from the NO_x prediction of 3D model oin 'city' part. This can be explained by the presence of LPEGR as per the calibration for the highway part is higher. Therefore, the prediction of NO_x with 3D map considering EGR rate as an input increases the accuracy

The fast temporal response of the predicted NO_x is evident from Figure 6.12(b). Apart from the over estimation of NO_x close to the load transient area, the model predicts very well. The accurate instantaneous EGR rate measurements can solve this problem.

6.6 Conclusion

A fast predicting quasi-steady model of NO_x is created to roughly predict the pollutant emission during the newly conceptualized highly dynamic real driving conditions on the diesel vehicle. Two fast and slow response NO_x measurement systems are compared on the city and highway part of the RDE cycle. Furthermore, the effect of adding EGR rate as an additional input on the prediction error is assessed.

Additions of EGR rate as an input to the quasi-steady NO_x model can potentially reduce the NO_x prediction error on both city and the highway part of dynamic cycle. The composition of gas in cylinder is important factor to predict the NO_x formation during transient operations. Therefore, accurate measurement of instantaneous EGR rate is required to avoid the over estimation of NO_x during a Tip-In operation.

This type of simple NO_x model is useful to design and calibrate the diesel engine in traditional and hybrid power trains. The required resources and time of calculation is less. Moreover, they can effectively predict the NO_x emission by knowing the operating point on dynamic driving conditions.

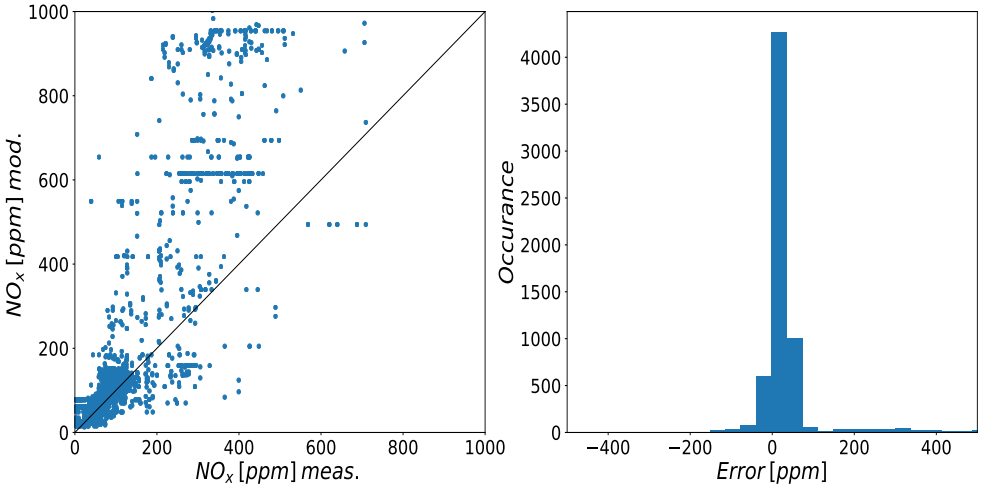

(a) comparison

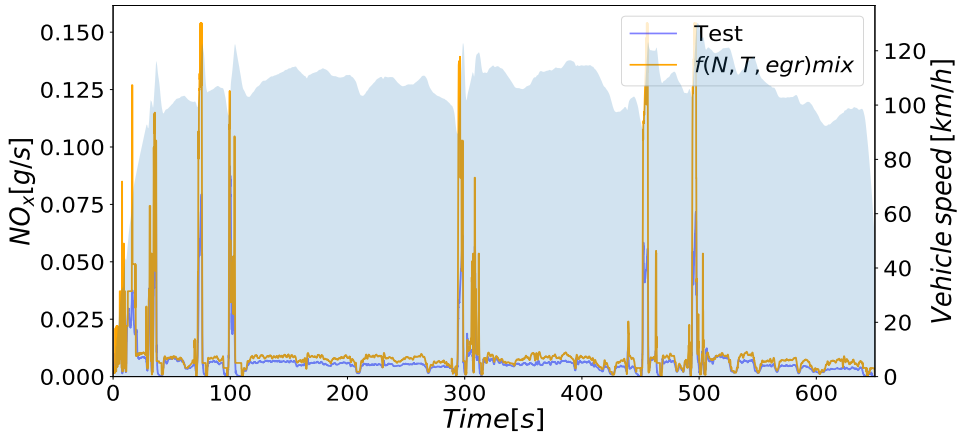

(b) Time response

Figure 6.12: Comparison of NO_x prediction by 3D model with the test measurement on 'highway' part of RDE cycle .

Chapter 6 Bibliography

[176] H. Hiroyasu, T. Kadota, and M. Arai. "Development and Use of a Spray Combustion Modeling to Predict Diesel Engine Efficiency and Pollutant

Emissions : Part 1 Combustion Modeling." *Bulletin of JSME* 26(214) (1983), pp. 569–575. ISSN: 1881-1426. DOI: 10.1299/jsme1958.26.569. URL: http://joi.jlc.jst.go.jp/JST.Journalarchive/jsme1958/26.569?from=CrossRef (cit. on p. 160).

[177] C. Ericson, B. Westerberg, M. Andersson, and R. Egnell. "Modelling Diesel Engine Combustion and NOx Formation for Model Based Control and Simulation of Engine and Exhaust Aftertreatment Systems." In: *SAE Technical Paper Series*. 2006. DOI: 10.4271/2006-01-0687. URL: https://www.sae.org/content/2006-01-0687/ (cit. on p. 160).

[178] M. Hirsch, D. Alberer, and L. Del Re. *Grey-box control oriented engine emissions models*. Vol. 17. 1 PART 1. IFAC, 2008, pp. 8514–8519. ISBN: 9783902661005. DOI: 10.3182/20080706-5-KR-1001.3426. URL: http://dx.doi.org/10.3182/20080706-5-KR-1001.01439 (cit. on p. 160).

[179] H. Sequenz and R. Isermann. *Emission model structures for an implementation on engine control units*. Vol. 44. 1 PART 1. IFAC, 2011, pp. 11851–11856. ISBN: 9783902661937. DOI: 10.3182/20110828-6-IT-1002.03131. URL: http://dx.doi.org/10.3182/20110828-6-IT-1002.03131 (cit. on p. 160).

[180] J. Arrègle, J. J. López, C. Guardiola, and C. Monin. "Sensitivity Study of a NOx Estimation Model for On-Board Applications." In: *SAE Technical Paper Series*. Vol. 1. 724. 2008. DOI: 10.4271/2008-01-0640. URL: https://www.sae.org/content/2008-01-0640/ (cit. on p. 160).

[181] F. Payri, J. Arrègle, J. J. López, E. Mocholí, C.-m. T. Universidad, and P. D. Valencia. "Diesel NOx Modeling with a Reduction Mechanism for the Initial NOx Coming from EGR or Re-entrained Burned Gases." In: *SAE Technical Paper Series*. Detroit, Michigan, 2008 (cit. on p. 160).

[182] O. Obodeh and C. I. Ajuwa. "Evaluation of artificial neural network performance in predicting diesel engine Nox emissions." *Research Journal of Applied Sciences, Engineering and Technology* 33(4) (2009), pp. 642–653. ISSN: 1450-216X (cit. on p. 160).

[183] G. J. Thompson, C. M. Atkinson, N. N. Clark, T. W. Long, and E Hanzevack. "Neural Network Modelling of the Emissions and Performance of a Heavy-Duty Diesel Engine." *Proceedings of the I MECH E Part D Journal of Automobile Engineering* 214(2) (2000), pp. 111–126. ISSN: 00000000. DOI: 10.1243/0954407001527277. URL: http:

//sdj.sagepub.com/lookup/10.1243/0954407001527277 (cit. on p. 160).

[184] A. Schilling, A. Amstutz, C. H. Onder, and L. Guzzella. "Real-time model for the prediction of the NOx emissions in DI diesel engines." In: *EEE International Conference on Control Applications, 2006 IEE*. IEEE, 2006, pp. 2042–2047. ISBN: 0780397967. DOI: 10.1109/CACSD-CCA-ISIC.2006.4776954. URL: http://ieeexplore.ieee.org/document/4776954/ (cit. on p. 160).

[185] C. Quérel, O. Grondin, and C. Letellier. "State of the Art and Analysis of Control Oriented NOx Models." In: *SAE Technical Paper Series*. 2012. DOI: 10.4271/2012-01-0723. URL: https://www.sae.org/content/2012-01-0723/ (cit. on p. 160).

[186] C. Ericson, B. Westerberg, and R. Egnell. "Transient Emission Predictions With Quasi Stationary Models." In: *SAE Technical Paper Series*. Vol. 1. 2005. DOI: 10.4271/2005-01-3852. URL: https://www.sae.org/content/2005-01-3852/ (cit. on pp. 160, 161).

[187] E. Giakoumis and A. Alafouzos. "Study of diesel engine performance and emissions during a Transient Cycle applying an engine mapping-based methodology." *Applied Energy* 87(4) (2010), pp. 1358–1365. ISSN: 03062619. DOI: 10.1016/j.apenergy.2009.09.003. URL: http://dx.doi.org/10.1016/j.apenergy.2009.09.003 (cit. on p. 160).

[188] J. D. Bishop, M. E. Stettler, N. Molden, and A. M. Boies. "Engine maps of fuel use and emissions from transient driving cycles." *Applied Energy* 183 (2016), pp. 202–217. ISSN: 03062619. DOI: 10.1016/j.apenergy.2016.08.175 (cit. on p. 161).

[189] L. Int Panis, C. Beckx, S. Broekx, I. De Vlieger, L. Schrooten, B. Degraeuwe, and L. Pelkmans. "PM, NOx and CO2 emission reductions from speed management policies in Europe." *Transport Policy* 18(1) (2011), pp. 32–37. ISSN: 0967070X. DOI: 10.1016/j.tranpol.2010.05.005. URL: http://dx.doi.org/10.1016/j.tranpol.2010.05.005 (cit. on p. 161).

[190] T. Nüesch, M. Wang, P. Isenegger, C. H. Onder, R. Steiner, P. Macri-Lassus, and L. Guzzella. "Optimal energy management for a diesel hybrid electric vehicle considering transient PM and quasi-static NOx emissions." *Control Engineering Practice* 29 (2014), pp. 266–276. ISSN: 09670661. DOI: 10.1016/j.conengprac.2014.01.020. URL: http://dx.doi.org/10.1016/j.conengprac.2014.01.020 (cit. on p. 161).

[191] D. M. Swain, C. C. Jackson, C. E. Lindhjem, and G. J. Hoffman. "A Method for Comparing Transient NOx Emissions With Weighted Steady State Test Results." In: *SAE Technical Paper Series*. Vol. 1. 724. 1998. DOI: 10.4271/980408. URL: https://www.sae.org/content/980408/ (cit. on p. 161).

Chapter 7

Conclusions and Future Work

Contents

7.1 Introduction

In this chapter main accomplished objectives of the thesis, mentioned at the beginning of thesis, are summarized. The conclusions obtained during the fulfillment of those objectives are presented chapter wise. The whole process of finding a final solution to control the transient emission on turbocharged diesel engine using EGR systems is concluded. Besides, the interesting results and trade-offs obtained from the analysis of the proposed solutions are described. Eventually, the effect of the proposed strategies on the full real driving cycles is presented to improve the overall pollutant emission evolution on real driving cycles. Various future possibilities of continuing this work are listed at the end of this chapter.

7.2 Conclusions

The comparison of different driving cycles (NEDC, WLTC and RDE) presented in the chapter 2 reveals the dynamic nature of the newly developed driving cycles. As these transient operations are an important part of the those dynamic cycles, the need of their improvement is supported evidently. The load transient operations with a load change at particular engine speed are found to be frequent on WLTC and RDE cycles. It is found that, the WLTC cycle has more harsh transient operations per unit time compared to specified RDE cycle in this study. Although engine operating condition during real driving cycles depends on the driving behavior and other road characteristics, it can be seen that load transient operations at same gear/engine speed are way higher than the speed transient operation due to gear change. This condition is also verified on the RDE vehicle speed profiles generated by the external algorithm (by the TNO). The number of harsh Tip-Out operations (with absolute change in BEMP greater than 5 bar) is always higher than harsh Tip-In transients on both WLTC and RDE cycles. Around 85% of Tip-In operations occur in the range of 1000-2000 rpm engine speed. While the same range includes almost 80% of all the Tip-Out operations sharing 60% of them in 1500-2000 rpm. In general Tip-Out operations are more spread over the higher engine speed range than the Tip-Ins. During WLTC, the large number of harsh Tip-Ins/transients occur around 1250 rpm. The similar trend is observed in real driving cycle too, however considerable amount of

load-increasing transients cover the range from 1000 to 2000 rpm compared to WLTC cycle.

The selected range of transient operations like 1250, 1500, 1750 and 2000 RPM are selected from the previous analysis. The harsh transients are performed for these engine speeds individually on the engine test bench in the Chapter 5. Main instrumentation included a high response time gas analyzer which is proved more useful to measure the NO_x emission during transient operation than the traditional slow analyser. The fast analyzer allows to capture the NO_x peaks resulted from delays in air, fuel and EGR flow. The EGR is considered throughout the engine map despite of the EGR zone. Evidently, EGR at high loads reduce the NO_x emissions considerably. 5% of EGR at full load has a benefit around 40% reduction in NO_x but a torque penalty of 10%. At full load, LPEGR is more effective in reducing NO_x than HPEGR for the same engine torque. From the control point of view, on the one hand, LPEGR rate is best option and easier to manage during load transients except for the lag in arrival of LPEGR to the intake valve. On the other hand, HPEGR needs proper designing of turbocharger and VGT control during transient operations. As the movement of VGT has direct impact on the pressure upstream of turbine and thus the HPEGR flow.

A compromise between performance (torque evolution) and emissions during first few seconds of Tip-In using LPEGr strategies is identified. Around NO_x reduction of 20-40% could be achieved in the first few seconds. The penalty in torque for this valve profiles is not more than 5-8%. However, considering this trade-off, the opacity increases in the range of 10-60%. Therefore, the optimization of LPEGR valve positions (actuator profile) during transient operations is required with specific turbocharger selection to give fast torque evolution. The specific control during the transients is different than steady state calibration as the actuator positions are different than steady state full load operation. The turbocharger selection is important here, as LPEGR changes the mass flow rate through compressor and hence affecting the boost control determining the back pressure in the exhaust manifold. During Tip-Ins no negative effect in NO_x emission is seen with respect to the lag of LPEGR. Because, during the entire transient the EGR is present in the intake system. The worst situation in this regard would be a Tip-In transient with no EGR at the beginning of the maneuver. This is referred in the paper as the "roundabout" transient starting from engine cranking operation without fuel injection up to full load. An EGR strategy to avoid the LPEGR lag is the combination

of LPEGR and HPEGR only during the lag time. The tests results show a good control of CO_2 during the transient for this strategy, however they also show a penalty in torque evolution due to the use of HPEGR.

The potential of combining HP and LPEGR systems is assessed through 1D simulations for wide operating range of turbocharged diesel engine in Chapter 4. This study will be useful for the design and calibration of diesel engines with both HP and LPEGR configuration meeting the upcoming emission regulations. Moreover, the optimization algorithm will be helpful to reduce the simulation time to carry out specific optimization of split between HP and LPEGR. The temperature downstream of the compressor is very sensitive to the LPEGR only configuration for high EGR rates at full load. On the other hand, cooled HPEGR seems to be advantageous in this area. For the low loads, LPEGR provides less temperature in the intake manifold, but seems useful to utilize only at low speeds considering the problem of pumping losses at high speeds, reducing the mean effective pressure. These requirements can be fulfilled by cooled HP EGR. HPEGR reduces the pumping losses at low air mass flow and high EGR rates. However, at full load points, pumping losses does not reduce with higher HPEGR rates as the boost pressure control plays the important role. Mostly, at full load points, the torque is not very sensitive to change in ESI. However, at high EGR rates, lower ESI values show slight advantage. Collectively, Low ESI values produce higher torque allowing bigger quantity of global EGR rates, while torque at high speed points are more sensitive to change in ESIs. brake specific fuel consumption is more affected by change in ESI as compared to engine torque. For the partial loads, BSFC can be lowered with the low ESI except at lowest load points (involving throttling of exhaust gases to drive LPEGR), where high EGR rates can be supplied with reduced BSFC values The DOE and genetic algorithm method for ESI optimization are easy to set up. However, the number of unnecessary solutions which are not the part of pareto are also simulated increasing the total time of the optimization. Moreover, the accuracy of this method directly depends on the number of iterations that are performed, to calculate the pareto solutions. This further increases the time of the calculations. On the other hand, the new control algorithm is faster and reduces around 80% of time over the genetic algorithm.

The Chapter 6 gives the potential of using 3D quasi steady model for predicting NO_x emissions during the above transient operations. It can act as a simple resource to predict the instantaneous NO_x formation depending on

the operating condition and the EGR rate. Furthermore, the effect of adding EGR rate as a additional input on the prediction error is assessed. Additions of EGR rate as a input to the quasi-steady NO_x model can potentially reduce the NO_x prediction error on both city and the highway part of dynamic cycle. The composition of gas in cylinder is important factor to predict the NO_x formation during transient operations. Therefore, accurate measurement of instantaneous EGR rate is required to avoid the over estimation of NO_x during a Tip-In operation. This type of simple NO_x model are useful to design and calibrate the diesel engine in traditional and hybrid power trains. The resources and time of calculation is very less and can effectively predict the NO_x emission by knowing the operating point on dynamic driving conditions.

7.3 Future work

There are various aspects related to the objective of the thesis which are not addressed in this work due to lack of time and the resources. In authors opinion, there are various possibilities of future work considering the experimental and simulation part of dynamic operations on diesel engines. Therefore, some suggestions are made which can be the base for the future studies.

7.3.1 Simulation

The transient simulation is complex task and requires more detailed modelling considering the turbocharger response and exhaust pressure calculations. Combustion modelling is required to be refined and corrected taking into account the presence of EGR at full load. Instantaneous air mass flow and EGR measurement is required to know the composition of gases going inside the combustion chamber. This will help in simulating cycle wise combustion accurately. Otherwise, combustion profile database is required to be constructed with air path (slow) variables as inputs with injected fuel to impose a proper in cylinder heat release rate during the transient operations. In regards with the boost control, A fast PID controller is needed for controlling VGT during a load transient operation to replicate the experimental behavior. Following studies can be done with the well equipped 1D model of the turbocharged diesel engine,

- Similar to the steady state optimization of ESI in Chapter 4, the optimization of ESI during transient operations can be done separately to optimize the cumulative torque during 'waiting zone' (defined in Chapter 5) of the load transients;

- Parametric study related to turbocharger response during transients can be carried out to select the appropriate turbocharger for the engine. It consists, study of thermal inertia in the exhaust during transients to simulate accurately exhaust pressure and turbo evolution;

- In reference with quasi-steady NO_x maps from Chapter 6, instantaneous EGR measurement is required to predict the NO_x correctly in dynamic operations. Moreover, considering the hybrid EGR control, a fourth input for the NO_x model can be considered as split between the HP and LPEGR (ESI);

- The dynamic machine learning algorithms with a nonlinear autoregressive exogenous model (NARX) or Recurrent Neural Networks (RNN) can be used to predict the cyclinder out NO_x. The fast models can be trained by real driving cycle data measured on road with the selective inputs like engine torque, speed and EGR rate.

7.3.2 Experimental

With respect to the experimentation part of transients, the similar study with synchronized acquisition system time is obligatory for the comparison of emission and performance. Moreover, more flexible system signalling for actuators is required for valve actuation in synch with the pedal signal. It avoids the mismatch errors which are appeared in this work. Following list of future studies can be considered as the next step in continuation of the experimental part of this thesis,

- The peak of NO_x during a Tip-Out operation due to late arrival of LPEGR requires special attention considering the combined LPEGR and ET control. The delay in the valve actuation and the change of gas concentration in cylinder should be taken into account to design a control in transient operation;

- The ‘speed transients’ are also important part of the real driving cycles which are not as responsible for high emissions as ‘load transients’. However, the gas dynamics and actuator response during speed transients is also needed to improve them like the load transient in this study;
- External air boosting device to provide the required air during the delays of the turbocharged diesel engines (along with EGR) can be useful to avoid the smoke limiter and improve the performance of the engine. The formation of in cylinder NO_x can be monitored with the help of fast emission measurement system;

Global bibliography

[1] R. S. J. Tol. "Comment on 'Quantifying the consensus on anthropogenic global warming in the scientific literature'." *Environmental Research Letters* 11(4) (2016). ISSN: 1748-9326. DOI: 10.1088/1748-9326/11/4/048001. URL: http://stacks.iop.org/1748-9326/11/i=4/a=048001?key=crossref.0b692e0e30f61886b8cfc6904d5e2cbe (cit. on p. 2).

[2] R. S. J. Tol. "CO2 and Greenhouse Gas Emissions." *Our World in Data* (2019) (cit. on p. 2).

[3] R. R. Dickerson. "The Impact of Aerosols on Solar Ultraviolet Radiation and Photochemical Smog." *Science* 278(5339) (1997), pp. 827–830. ISSN: 00368075. DOI: 10.1126/science.278.5339.827. URL: http://www.sciencemag.org/cgi/doi/10.1126/science.278.5339.827 (cit. on p. 3).

[4] R. Atkinson and A. C. Lloyd. "Evaluation of Kinetic and Mechanistic Data for Modeling of Photochemical Smog." *Journal of Physical and Chemical Reference Data* 13(2) (1984), pp. 315–444. ISSN: 0047-2689. DOI: 10.1063/1.555710. URL: http://aip.scitation.org/doi/10.1063/1.555710 (cit. on p. 3).

[5] S. Jungnelius and M. Svartengren. *Hälsoeffekter av trafikavgaser*. Yrkesmedicinska enheten, Karolinska sjukhuset, 2000 (cit. on p. 3).

[6] *Energy, transport and environment indicators*. 2016. ISBN: 978-92-79-60137-8. DOI: 10.2785/138586 (cit. on p. 3).

[7] N. B. o. S. of China. "China statistical yearbook." *Beijing: Chinese Statistical Bureau* (2017) (cit. on p. 3).

[8] S. C. Davis, S. E. Williams, and R. G. Boundy. *Transportation Energy Data Book: Edition 36.1*. 2018. ISBN: 1800553684 (cit. on p. 3).

[9] U.S. Department of Transportation. *Summary of Travel Trends 2001 National Household Travel Survey*. 2001. ISBN: 1800553684 (cit. on p. 3).

[10] Eurostat - Statistical Office of the European Communities. *Energy, transport and environment indicators 2011 edition*. 2011. ISBN: 9789279213847. DOI: DOI10.2785/17571 (cit. on p. 3).

[11] F Payri, J. Luján, C Guardiola, and B Pla. "A Challenging Future for the IC Engine: New Technologies and the Control Role." *Oil & Gas Science and Technology – Revue d'IFP Energies nouvelles* (2015). ISSN: 1294-4475. DOI: 10.2516/ogst/2014002 (cit. on p. 3).

[12] J. B. Heywood. *Internal Combustion Engine Fundementals*. Vol. 21. 1988, p. 930. ISBN: 007028637X. DOI: 10987654 (cit. on p. 5).

[13] J Kahrstedt, A Blechstein, O Maiwald, and J Kabitzke. "Grundlegende Untersuchungen zu Low-NOX-Brennverfahren für PKW-Dieselmotoren unter Nutzung zusätzlicher Variabilitäten, 6." In: *Internationales Stuttgarter Symposium*. 2005 (cit. on p. 6).

[14] J. A. Miller and C. T. Bowman. "Mechanism and modeling of nitrogen chemistry in combustion." *Progress in Energy and Combustion Science* 15(4) (1989), pp. 287–338. ISSN: 03601285. DOI: 10.1016/0360-1285(89)90017-8. URL: https://linkinghub.elsevier.com/retrieve/pii/0360128589900178 (cit. on p. 6).

[15] U. Gärtner. *Die Simulation der Stickoxid-Bildung in Nutzfahrzeug-Dieselmotoren*. na, 2001 (cit. on p. 6).

[16] R. Stone. *Introduction to Internal Combustion Engines*. London: Macmillan Education UK, 1992. ISBN: 978-0-333-55084-7. DOI: 10.1007/978-1-349-22147-9. URL: http://link.springer.com/10.1007/978-1-349-22147-9 (cit. on p. 6).

[17] C. D.Rakopoulos and E. G.Giakoumis. *Diesel Engine Transient Operation*. Vol. 53. 9. 2013, pp. 1689–1699. ISBN: 9788578110796. DOI: 10.1017/CBO9781107415324.004. arXiv: arXiv:1011.1669v3 (cit. on pp. 7, 12).

[18] M. Hirsch, K. Oppenauer, and L. del Re. "Dynamic Engine Emission Models." In: *Lecture Notes in Control and Information Sciences*. 2010, pp. 73–87. DOI: 10.1007/978-1-84996-071-7_5. URL: http://link.springer.com/10.1007/978-1-84996-071-7{_}5 (cit. on p. 7).

[19] O. Park. "Citizens to Preserve Overton Park." *Inc. v. Volpe* 401 (1971) (cit. on p. 8).

[20] A. Faiz, C. S. Weaver, and M. P. Walsh. *Air pollution from motor vehicles: standards and technologies for controlling emissions*. The World Bank, 1996 (cit. on p. 8).

[21] T. J. BARLOW, S Latham, I. McCrae, and P. Boulter. "A reference book of driving cycles for use in the measurement of road vehicle emissions." *TRL Published Project Report* (2009) (cit. on p. 8).

[22] M. Nesbeit, M. Fergusson, A. Colsa, J. Ohlendorf, C. Hayes, K. Paquel, and J.-P. Schweitzer. *Comparative Study on the Differences Between the EU and US Legislation on Emissions in the Automotive Sector: Study*. European Parliament, 2016 (cit. on p. 8).

[23] A. Reig Bernad. "Optimal Control for Automotive Powertrain Applications." PhD thesis. Valencia (Spain): Universitat Politècnica de València, 2017. DOI: 10.4995/Thesis/10251/90624. URL: https://riunet.upv.es/handle/10251/90624 (cit. on pp. 8, 136).

[24] M. Kousoulidou, G. Fontaras, L. Ntziachristos, P. Bonnel, Z. Samaras, and P. Dilara. "Use of portable emissions measurement system (PEMS) for the development and validation of passenger car emission factors." *Atmospheric Environment* 64(x) (2013), pp. 329–338. ISSN: 13522310. DOI: 10.1016/j.atmosenv.2012.09.062. URL: http://dx.doi.org/10.1016/j.atmosenv.2012.09.062 (cit. on p. 9).

[25] J. M. Luján, V. Bermúdez, V. Dolz, and J. Monsalve-Serrano. "An assessment of the real-world driving gaseous emissions from a Euro 6 light-duty diesel vehicle using a portable emissions measurement system (PEMS)." *Atmospheric Environment* 174 (2018), pp. 112–121. ISSN: 18732844. DOI: 10.1016/j.atmosenv.2017.11.056 (cit. on pp. 9, 135).

[26] B. Degraeuwe and M. Weiss. "Does the New European Driving Cycle (NEDC) really fail to capture the NOx emissions of diesel cars in Europe?" *Environmental Pollution* 222 (2017), pp. 234–241. ISSN: 18736424. DOI: 10.1016/j.envpol.2016.12.050 (cit. on p. 9).

[27] N. Hooftman, M. Messagie, J. Van Mierlo, and T. Coosemans. "A review of the European passenger car regulations – Real driving emissions vs local air quality." *Renewable and Sustainable Energy Reviews* 86(March 2017) (2018), pp. 1–21. ISSN: 18790690. DOI: 10.1016/j.

rser.2018.01.012. URL: https://doi.org/10.1016/j.rser.2018.01.012 (cit. on p. 9).

[28] J. Merkisz, P. Lijewski, P. Fuć, Ł. Rymaniak, and A. Ziółkowski. "Measurement of Exhaust Emissions under Actual Operating Conditions with the Use of PEMS: Review of Selected Vehicles." In: *Improvement Trends for Internal Combustion Engines*. InTech, 2018. DOI: 10.5772/intechopen.70442. URL: http://www.intechopen.com/books/improvement-trends-for-internal-combustion-engines/measurement-of-exhaust-emissions-under-actual-operating-conditions-with-the-use-of-pems-review-of-se (cit. on p. 9).

[29] J. Gallus, U. Kirchner, R. Vogt, C. Börensen, and T. Benter. "On-road particle number measurements using a portable emission measurement system (PEMS)." *Atmospheric Environment* 124 (2016). ISSN: 18732844. DOI: 10.1016/j.atmosenv.2015.11.012 (cit. on p. 9).

[30] R. A. Varella, M. V. Faria, P. Mendoza-Villafuerte, P. C. Baptista, L. Sousa, and G. O. Duarte. "Assessing the influence of boundary conditions, driving behavior and data analysis methods on real driving CO2 and NOx emissions." *Science of the Total Environment* 658 (2019), pp. 879–894. ISSN: 18791026. DOI: 10.1016/j.scitotenv.2018.12.053. URL: https://doi.org/10.1016/j.scitotenv.2018.12.053 (cit. on pp. 9, 43).

[31] M. K. Khair and W. A. Majewski. *Diesel Emissions and Their Control*. Warrendale, PA: SAE International, 2006. ISBN: 978-0-7680-0674-2. DOI: 10.4271/R-303. URL: http://books.sae.org/book-r-303 (cit. on p. 10).

[32] S. Reifarth and H.-E. Angstrom. "Transient EGR in a long-route and short-route EGR system." In: *ASME Internal Combustion Engine Division Spring Technical Conference*. 2009, pp. 761–770. ISBN: 978-0-7918-4340-6. DOI: 10.1115/ICES2009-76107 (cit. on pp. 10, 11, 135, 138).

[33] R. Zhang, F. Charles, D. Ewing, J.-S. Chang, and J. S. Cotton. "Effect of Diesel Soot Deposition on the Performance of Exhaust Gas Recirculation Cooling Devices." In: *SAE Technical Papers*. 2004. ISBN: 0768013194. DOI: 10.4271/2004-01-0122. URL: https://www.sae.org/content/2004-01-0122/ (cit. on p. 10).

[34] J. Galindo, H. Climent, O. Varnier, and C. Patil. "Effect of boosting system architecture and thermomechanical limits on diesel engine performance: Part-I—Steady-state operation." *International Journal of Engine Research* 19(8) (2017), pp. 854–872. ISSN: 20413149. DOI: 10.1177/1468087417731654 (cit. on p. 11).

[35] J. Galindo, H. Climent, O. Varnier, and C. Patil. "Effect of boosting system architecture and thermomechanical limits on diesel engine performance: Part-II—Transient operation." *International Journal of Engine Research* 19(8) (2018), pp. 854–872. ISSN: 1468-0874. DOI: 10.1177/1468087417731654. URL: http://journals.sagepub.com/doi/10.1177/1468087417731654 (cit. on pp. 11, 12).

[36] F. Millo, C. V. Ferraro, M. G. Bernardi, S. Barbero, and P. Pasero. "Experimental and Computational Analysis of Different EGR Systems for a Common Rail Passenger Car Diesel Engine." *SAE International Journal of Engines* 2(1) (2009), pp. 527–538. ISSN: 1946-3944. DOI: 10.4271/2009-01-0672. URL: https://www.sae.org/content/2009-01-0672/ (cit. on p. 11).

[37] F. Payri, J. Lujan, H. Climent, and B. Pla. "Effects of the Intake Charge Distribution in HSDI Engines." In: *SAE Technical Papers*. 2010. DOI: 10.4271/2010-01-1119. URL: https://www.sae.org/content/2010-01-1119/ (cit. on p. 11).

[38] G. Lim, Y. Choi, C. Park, and J. Park. "Effects of HPL and LPL EGR Gas Mixed Supply on Combustion and Emissions in Automotive Diesel Engine." In: *SAE Technical Papers*. 2011. DOI: 10.4271/2011-01-1831. URL: https://www.sae.org/content/2011-01-1831/ (cit. on p. 11).

[39] M. Van Aken, F. Willems, and D. J. De Jong. "Appliance of high EGR rates with a short and long route EGR system on a heavy duty diesel engine." In: *SAE Technical Papers*. 2007. DOI: 10.4271/2007-01-0906 (cit. on pp. 11, 89).

[40] J. M. Luján, C. Guardiola, B. Pla, and A. Reig. "Switching strategy between HP (high pressure)- and LPEGR (low pressure exhaust gas recirculation) systems for reduced fuel consumption and emissions." *Energy* 90 (2015), pp. 1790–1798. ISSN: 03605442. DOI: 10.1016/j.energy.2015.06.138 (cit. on pp. 11, 134).

[41] S. Reifarth and H.-E. Ångström. "Transient EGR in a High-Speed DI Diesel Engine for a set of different EGR-routings." *SAE International Journal of Engines* 3(1) (2010), pp. 1071–1078. ISSN: 19463936. DOI: 10.4271/2010-01-1271 (cit. on pp. 11, 73).

[42] P. S. Keller, V. Joergl, O. Weber, and R. Czarnowski. "Enabling Components for Future Clean Diesel Engines." In: *SAE Technical Papers*. 2008. DOI: 10.4271/2008-01-1530. URL: https://www.sae.org/content/2008-01-1530/ (cit. on p. 11).

[43] H.-J. Neusser, J. Kahrstedt, R. Dorenkamp, and H. Jelden. "The EURO 6 engines in the modular diesel engine system of Volkswagen." *MTZ worldwide* 74(6) (2013), pp. 4–10 (cit. on p. 11).

[44] J. M. Desantes, J. M. Luján, B. Pla, and J. A. Soler. "On the combination of high-pressure and low-pressure exhaust gas recirculation loops for improved fuel economy and reduced emissions in high-speed direct-injection engines." *International Journal of Engine Research* 14(1) (2013), pp. 3–11. ISSN: 1468-0874. DOI: 10.1177/1468087412437623. URL: http://journals.sagepub.com/doi/10.1177/1468087412437623 (cit. on pp. 11, 15).

[45] D Jain. "Using and electronically controlled VGT to improve engine transient performance." In: *Proceedings of the IMechE Seminar on Engine Transient Performance*. 1990, pp. 27–30 (cit. on p. 12).

[46] A. Uzun. "Air mass flow estimation of diesel engines using neural network." *Fuel* 117(PART A) (2014), pp. 833–838. ISSN: 00162361. DOI: 10.1016/j.fuel.2013.09.078. URL: http://dx.doi.org/10.1016/j.fuel.2013.09.078 (cit. on p. 12).

[47] K. Min, D. Jung, and M. Sunwoo. "Air system modeling of light-duty diesel engines with dual-loop EGR and VGT systems." *IFAC Proceedings Volumes (IFAC-PapersOnline)* 48(15) (2015), pp. 38–44. ISSN: 14746670. DOI: 10.1016/j.ifacol.2015.10.006. URL: http://dx.doi.org/10.1016/j.ifacol.2015.10.006 (cit. on p. 12).

[48] D. Alberer and L. del Re. "Fast Oxygen Based Transient Diesel Engine Operation." *SAE International Journal of Engines* 2(1) (2009), pp. 2009–01–0622. ISSN: 1946-3944. DOI: 10.4271/2009-01-0622. URL: https://www.sae.org/content/2009-01-0622/ (cit. on pp. 12, 15).

[49] C. D. Rakopoulos and E. G. Giakoumis. "Review of Thermodynamic Diesel Engine Simulations under Transient Operating Conditions." *SAE Technical Paper Series* (2006). ISSN: 0148-7191. DOI: 10.4271/2006-01-0884. URL: http://papers.sae.org/2006-01-0884/https://www.sae.org/content/2006-01-0884/ (cit. on pp. 12, 68).

[50] L. Cornolti, A. Onorati, T. Cerri, G. Montenegro, and F. Piscaglia. "1D simulation of a turbocharged Diesel engine with comparison of short and long EGR route solutions." *Applied Energy* 111 (2013), pp. 1–15. ISSN: 03062619. DOI: 10.1016/j.apenergy.2013.04.016. URL: http://dx.doi.org/10.1016/j.apenergy.2013.04.016 (cit. on pp. 13, 89).

[51] C. D. Rakopoulos, A. M. Dimaratos, E. G. Giakoumis, and D. C. Rakopoulos. "Evaluation of the effect of engine, load and turbocharger parameters on transient emissions of diesel engine." *Energy Conversion and Management* 50(9) (2009), pp. 2381–2393. ISSN: 01968904. DOI: 10.1016/j.enconman.2009.05.022. URL: http://dx.doi.org/10.1016/j.enconman.2009.05.022 (cit. on p. 13).

[52] J. Galindo, J. Luján, J. Serrano, V. Dolz, and S. Guilain. "Description of a heat transfer model suitable to calculate transient processes of turbocharged diesel engines with one-dimensional gas-dynamic codes." *Applied Thermal Engineering* 26(1) (2006), pp. 66–76. ISSN: 13594311. DOI: 10.1016/j.applthermaleng.2005.04.010. URL: https://linkinghub.elsevier.com/retrieve/pii/S1359431105001353 (cit. on p. 14).

[53] C. D. Rakopoulos, E. G. Giakoumis, D. T. Hountalas, and D. Rakopoulos. "The Effect of Various Dynamic , Thermodynamic and Design Parameters on the Performance of a Turbocharged Diesel Engine Operating under Transient Load Conditions." *SAE International* (724) (2004). DOI: 10.4271/2004-01-0926 (cit. on p. 14).

[54] C. Rakopoulos, E. Giakoumis, and D. Rakopoulos. "Cylinder wall temperature effects on the transient performance of a turbocharged Diesel engine." *Energy Conversion and Management* 45(17) (2004), pp. 2627–2638. ISSN: 01968904. DOI: 10.1016/j.enconman.2003.12.014. URL: https://linkinghub.elsevier.com/retrieve/pii/S0196890404000111 (cit. on p. 14).

[55] C. Rakopoulos, A. Dimaratos, E. Giakoumis, and M. Peckham. "Experimental Assessment of Turbocharged Diesel Engine Transient Emissions during Acceleration, Load Change and Starting." *SAE Technical Paper Series* 1 (2010). DOI: 10.4271/2010-01-1287 (cit. on pp. 14, 55).

[56] H. Kang and P. V. Farrell. "Experimental investigation of transient emissions (HC and NOx) in a High Speed Direct Injection (HSDI) diesel engine." *SAE Technical Papers* (724) (2005). ISSN: 26883627. DOI: 10.4271/2005-01-3883 (cit. on p. 14).

[57] S. Park, T. Matsumoto, and N. Oda. *Numerical analysis of turbocharger response delay mechanism*. Tech. rep. SAE Technical Paper, 2010 (cit. on p. 14).

[58] J. Shutty, H. Benali, L. Daeubler, and M. Traver. "Air System Control for Advanced Diesel Engines." In: *Numerical Analysis - Theory and Application*. 2007. DOI: 10.4271/2007-01-0970. URL: https://www.sae.org/content/2007-01-0970/ (cit. on p. 15).

[59] J. Deng, R. Stobart, C. Liu, and E. Winward. "Explicit Model Predictive Control of the Diesel Engine Fuel Path." In: *SAE Technical Papers*. 2012. DOI: 10.4271/2012-01-0893. URL: https://www.sae.org/content/2012-01-0893/ (cit. on p. 15).

[60] F. Tschanz, A. Amstutz, C. H. Onder, and L. Guzzella. "Feedback control of particulate matter and nitrogen oxide emissions in diesel engines." *Control Engineering Practice* 21(12) (2013), pp. 1809–1820. ISSN: 09670661. DOI: 10.1016/j.conengprac.2012.09.014. URL: https://linkinghub.elsevier.com/retrieve/pii/S0967066112001979 (cit. on p. 15).

[61] A. G. Stefanopoulou, I. Kolmanovsky, and J. S. Freudenberg. "Control of variable geometry turbocharged diesel engines for reduced emissions." *Proceedings of the American Control Conference* 3(4) (1998), pp. 1383–1388. ISSN: 07431619. DOI: 10.1109/ACC.1998.707043 (cit. on p. 15).

[62] P. Ortner and L. del Re. "Predictive control of a diesel engine air path." *IEEE Transactions on Control Systems Technology* 15(3) (2007), pp. 449–456. ISSN: 10636536. DOI: 10.1109/TCST.2007.894638 (cit. on p. 15).

[63] B. Haber and J. Wang. "Robust control approach on diesel engines with dual-loop exhaust gas recirculation systems." In: *ASME 2010 Dynamic Systems and Control Conference*. American Society of Mechanical Engineers Digital Collection. 2010, pp. 711–718 (cit. on p. 15).

[64] J. Chauvin, O. Grondin, and P. Moulin. "Control Oriented Model of a Variable Geometry Turbocharger in an Engine with Two EGR Loops." *Oil & Gas Science and Technology – Revue d'IFP Energies nouvelles* 66(4) (2011), pp. 563–571. ISSN: 1294-4475. DOI: 10.2516/ogst/2011103. URL: http://ogst.ifpenergiesnouvelles.fr/10.2516/ogst/2011103 (cit. on p. 15).

[65] D. Alberer and L. del Re. "Optimization of the transient Diesel engine operation." In: *SAE Technical Paper Series*. Vol. 1. 2009. DOI: 10.4271/2009-24-0113. URL: https://www.sae.org/content/2009-24-0113/ (cit. on p. 15).

[66] E. Directive. "90/C81/01,"Emission Test Cycles for the Certification of light duty vehicles in Europe", EEC Emission Cycles, 1999" (). URL: https://dieselnet.com/standards/cycles/index.php (cit. on p. 28).

[67] M. Tutuianu, P. Bonnel, B. Ciuffo, T. Haniu, N. Ichikawa, A. Marotta, J. Pavlovic, and H. Steven. "Development of the World-wide harmonized Light duty Test Cycle (WLTC) and a possible pathway for its introduction in the European legislation." *Transportation Research Part D: Transport and Environment* 40 (2015), pp. 61–75. ISSN: 13619209. DOI: 10.1016/j.trd.2015.07.011. URL: http://dx.doi.org/10.1016/j.trd.2015.07.011 (cit. on p. 28).

[68] European Parliament and Council of the European Union. "Commission Regulation (EU) 2016/427 of 10 March 2016 amending Regulation (EC) No 692/2008 as regards emissions from light passenger and commercial vehicles (Euro 6) (Text with EEA relevance)." *Official journal of the European Union* 82(31/03/2016) (2016), pp. 1–98. URL: http://data.europa.eu/eli/reg/2016/427/oj (cit. on pp. 31, 33).

[69] J. Merkisz and J. Pielecha. "Selected remarks about RDE test." *Cobustion Engines* 166(3) (2017), pp. 54–61. DOI: 10.19206/CE-2016-340 (cit. on p. 32).

[70] R. Fischer, F. Küçükay, G. Jürgens, R. Najork, and B. Pollak. *The Automotive Transmission Book*. Springer Cham Heidelberg New York Dordrecht London, 2015. ISBN: 10.1007/978-3-319-05263-2 (cit. on p. 36).

[71] Q. Gong, S. Midlam-Mohler, V. Marano, G. Rizzoni, and Y. Guezennec. "Statistical analysis of PHEV fleet data." *2010 IEEE Vehicle Power and Propulsion Conference, VPPC* (2010), pp. 1–6. ISSN: 1938-8756. DOI: 10.1109/VPPC.2010.5729224 (cit. on p. 42).

[72] T. Donateo and M. Giovinazzi. "Building a cycle for Real Driving Emissions." *Energy Procedia* 126 (2017), pp. 891–898. ISSN: 18766102. DOI: 10.1016/j.egypro.2017.08.307. URL: https://doi.org/10.1016/j.egypro.2017.08.307 (cit. on pp. 42, 135).

[73] C. D. Rakopoulos, A. M. Dimaratos, and E. G. Giakoumis. "Experimental Study of Transient Nitric Oxide, Smoke, and Combustion Noise Emissions during Acceleration of an Automotive Turbocharged Diesel Engine." *Proceedings of the Institution of Mechanical Engineers, Part D: Journal of Automobile Engineering* 225(2) (2011), pp. 260–279. ISSN: 09544070. DOI: 10.1243/09544070jauto1493. URL: http://pid.sagepub.com/cgi/content/abstract/225/2/260 (cit. on p. 54).

[74] B. T. McClure. "Characterization of the Transient Response of a Diesel Exhaust-Gas Measurement System." In: *SAE Technical Paper Series*. 1988. DOI: 10.4271/881320 (cit. on p. 54).

[75] J. D. Pakko. "Reconstruction of Time-Resolved Vehicle Emissions Measurements by Deconvolution." *SAE International Journal of Fuels and Lubricants* 2(1) (2010), pp. 697–707. ISSN: 1946-3960. DOI: 10.4271/2009-01-1513 (cit. on pp. 54, 67).

[76] C. De Petris, S. Diana, V. Giglio, and G. Police. "Some Problems in the Improvement of Measurement of Transient Emissions." *SAE Technical Paper Series* 1(412) (2010). DOI: 10.4271/941949 (cit. on p. 54).

[77] A. Beaumont. "„Noble, AD and Pilley, AD Signal reconstruction techniques for improved measurement of transient emission." *SAE paper* 900233 (1990) (cit. on p. 54).

[78] S. H. Chan, X. S. Chen, and C. Arcoumanis. "Measurement and Signal Reconstruction of Transient Nitric Oxide Emissions in the Exhaust of a Turbocharged Diesel Engine." *Journal of Dynamic Systems, Measurement, and Control* 119(4) (1997), p. 620. ISSN: 00220434. DOI: 10.1115/

1.2802370. URL: http://dynamicsystems.asmedigitalcollection.asme.org/article.aspx?articleid=1407662 (cit. on p. 54).

[79] C. S. Nielsen, A. Ivarsson, and T. Løvås. "Evaluation of Test Bench Engine Performance Measurements in Relation to Vehicle Measurement on Chassis Dynamometer." (ICEF2015-1019) (2015), pp. 1–13 (cit. on p. 54).

[80] J. T. Messer, N. Clark, and D. W. Lyons. "Measurement Delays and Modal Analysis for a Heavy Duty Transportable Emissions Testing Laboratory." In: *SAE Technical Paper Series*. Vol. 1. 1995. DOI: 10.4271/950218. URL: https://www.sae.org/content/950218/ (cit. on pp. 57, 67).

[81] J. M. Luján, H. Climent, V. Dolz, A. Moratal, J. Borges-Alejo, and Z. Soukeur. "Potential of exhaust heat recovery for intake charge heating in a diesel engine transient operation at cold conditions." *Applied Thermal Engineering* 105 (2016), pp. 501–508. ISSN: 13594311. DOI: 10.1016/j.applthermaleng.2016.03.028. URL: https://linkinghub.elsevier.com/retrieve/pii/S1359431116303209 (cit. on p. 57).

[82] P. Bielaczyc and J. Merkisz. "Cold Start Emissions Investigation at Different Ambient Temperature Conditions." In: *SAE Technical Paper Series*. 1998. DOI: 10.4271/980401. URL: https://www.sae.org/content/980401/ (cit. on pp. 57, 67).

[83] J. M. Luján, H. Climent, S. Ruiz, and A. Moratal. "Influence of ambient temperature on diesel engine raw pollutants and fuel consumption in different driving cycles." *International Journal of Engine Research* (2018). DOI: 10.1177/1468087418792353. URL: http://journals.sagepub.com/doi/10.1177/1468087418792353 (cit. on pp. 57, 135).

[84] G Konstantas and A Stamatelos. "Quality assurance of exhaust emissions test data." *Proceedings of the Institution of Mechanical Engineers, Part D: Journal of Automobile Engineering* 218(8) (2004), pp. 901–914. ISSN: 0954-4070. DOI: 10.1243/0954407041581075. URL: http://journals.sagepub.com/doi/10.1243/0954407041581075 (cit. on pp. 57, 67).

[85] C. Sutela, N. Collings, and T. Hands. "Real Time CO2 Measurement to Determine Transient Intake Gas Composition under EGR Conditions." In: *SAE Technical Paper Series*. 2000. DOI: 10.4271/2000-01-2953 (cit. on pp. 58, 61).

[86] D. Tree and K. Svensson. "Soot processes in compression ignition engines." *Progress in Energy and Combustion Science* 33(3) (2007), pp. 272–309. ISSN: 0360-1285. DOI: https://doi.org/10.1016/j.pecs.2006.03.002. URL: http://www.sciencedirect.com/science/article/pii/S0360128506000608 (cit. on p. 58).

[87] D. L. Hofeldt and G. Chen. "Transient Particulate Emissions from Diesel Buses During the Central Business District Cycle." In: *SAE Technical Paper Series*. 2010. DOI: 10.4271/960251 (cit. on p. 59).

[88] E. G. Giakoumis, C. D. Rakopoulos, A. M. Dimaratos, and D. C. Rakopoulos. "Exhaust emissions of diesel engines operating under transient conditions with biodiesel fuel blends." *Progress in Energy and Combustion Science* 38(5) (2012), pp. 691–715. ISSN: 03601285. DOI: 10.1016/j.pecs.2012.05.002. URL: http://dx.doi.org/10.1016/j.pecs.2012.05.002 (cit. on pp. 59, 135).

[89] J. R. Hagena, Z. Filipi, and D. N. Assanis. "Transient Diesel Emissions: Analysis of Engine Operation During a Tip-In." In: *SAE Technical Paper Series*. 2010. DOI: 10.4271/2006-01-1151 (cit. on p. 59).

[90] R. Christian, F. Knopf, A. Jaschek, and W. Schindler. "Eine neue messmethodik der bosch-zahl mit erhöhter empfindlichkeit." *Motortech. Z* 54 (1993), pp. 16–22 (cit. on p. 59).

[91] A. Notes. "Smoke Value Measurement With the Filter-Paper-Method." *AVL, AT1007E, Rev* 2 (2005) (cit. on p. 59).

[92] P. Kirchen, P. Obrecht, K. Boulouchos, and A. Bertola. "Exhaust-Stream and In-Cylinder Measurements and Analysis of the Soot Emissions From a Common Rail Diesel Engine Using Two Fuels." *Journal of Engineering for Gas Turbines and Power* 132(11) (2010), p. 112804. ISSN: 07424795. DOI: 10.1115/1.4001083. URL: http://gasturbinespower.asmedigitalcollection.asme.org/article.aspx?articleid=1429022 (cit. on p. 60).

[93] P. Lakshminarayanan and S. Aswin. "Estimation of Particulate Matter from Smoke, Oil Consumption and Fuel Sulphur." In: *SAE International*. 2017, pp. 1–11. DOI: 10.4271/2017-01-7002. URL: http://papers.sae.org/2017-01-7002/https://www.sae.org/content/2017-01-7002/ (cit. on p. 60).

[94] F. Liu and J. Pfeiffer. "Estimation Algorithms for Low Pressure Cooled EGR in Spark-Ignition Engines." *SAE International Journal of Engines* 8(4) (2015), pp. 1652–1659. ISSN: 1946-3944. DOI: 10.4271/2015-01-1620 (cit. on p. 61).

[95] Z. C. Liu, K. B. Yu, J Tian, Y. Q. Han, S. L. Qi, and P. K. Teng. "Influence of rail pressure on a two-stage turbocharged heavy-duty diesel engine under transient operation." *International Journal of Automotive Technology* 18(1) (2017), pp. 19–29. ISSN: 1229-9138. DOI: 10.1007/s12239-017-0002-z. URL: https://doi.org/10.1007/s12239-017-0002-zhttp://link.springer.com/10.1007/s12239-017-0002-z (cit. on pp. 61, 135).

[96] J. Shutty and J. Shutty. "Control Strategy Optimization for Hybrid EGR Engines." *SAE Technical Paper* (2009). DOI: 10.4271/2009-01-1451 (cit. on p. 61).

[97] P. B. Dickinson, K. Hegarty, N. Collings, and T. Ramsander. "Application of Fast Oxygen Sensors for Investigations into Air-Path Dynamics and EGR Distribution in a Diesel Engine." *SAE Technical Paper Series* 1(x) (2014). DOI: 10.4271/2014-01-1177 (cit. on p. 61).

[98] R. Soltis, J. Hilditch, T. Clark, C. House, M. Gerhart, and G. Surnilla. "Intake Oxygen Sensor for EGR Measurement." *SAE Technical Paper Series* (2016). DOI: 10.4271/2016-01-1070 (cit. on p. 61).

[99] J. Chung, H. Kim, and M. Sunwoo. "Reduction of transient NOx emissions based on set-point adaptation of real-time combustion control for light-duty diesel engines." *Applied Thermal Engineering* 137 (2018), pp. 729–738. DOI: 10.1016/j.applthermaleng.2018.03.082. URL: https://doi.org/10.1016/j.applthermaleng.2018.03.082 (cit. on p. 61).

[100] F. Payri González and J. M. Desantes Fernández. "Motores de combustión interna alternativos." *Colección Académica. Editorial UPV* (2011) (cit. on p. 62).

[101] A. Moratal. "Experimental Analysis of Thermal Management Influence on Performance and Emissions in Diesel Engines At Low Ambient Temperature" (2018) (cit. on p. 62).

[102] J. Benajes, J. M. Lujan, V. Bermudez, and J. Serrano. "Modelling of turbocharged diesel engines in transient operation . Part 1: insight into the relevant physical phenomena." *Journal of automobile engineering* 216 (2002), pp. 431–441. DOI: 10.1243/0954407021529237 (cit. on p. 63).

[103] J. Benajes, J. M. Luján, and J. R. Serrano. "Predictive Modelling Study of the Transient Load Response in a Heavy-Duty Turbocharged Diesel Engine." In: *SAE Technical Paper*. 2000. DOI: 10.4271/2000-01-0583. URL: https://doi.org/10.4271/2000-01-0583https://www.sae.org/content/2000-01-0583/ (cit. on p. 63).

[104] J. R. Serrano, H. Climent, C. Guardiola, and P. Piqueras. "Methodology for characterisation and simulation of turbocharged diesel engines combustion during transient operation. Part 2: Phenomenological combustion simulation." *Applied Thermal Engineering* 29(1) (2009), pp. 150–158. ISSN: 13594311. DOI: 10.1016/j.applthermaleng.2008.02.010. URL: http://dx.doi.org/10.1016/j.applthermaleng.2008.02.010 (cit. on p. 63).

[105] K. Robinson, S. Ye, Y. Yap, and S. T. Kolaczkowski. "Application of a methodology to assess the performance of a full-scale diesel oxidation catalyst during cold and hot start NEDC drive cycles." *Chemical Engineering Research and Design* 91(7) (2013), pp. 1292–1306. ISSN: 02638762. DOI: 10.1016/j.cherd.2013.02.022. URL: http://dx.doi.org/10.1016/j.cherd.2013.02.022 (cit. on p. 67).

[106] M. Kao and J. J. Moskwa. "Turbocharged Diesel Engine Modeling for Nonlinear Engine Control and State Estimation." *Journal of Dynamic Systems, Measurement, and Control* 117(1) (1995), pp. 20–30. ISSN: 00220434. DOI: 10.1115/1.2798519. URL: http://dynamicsystems.asmedigitalcollection.asme.org/article.aspx?articleid=1406784 (cit. on p. 68).

[107] M. Goyal. "SIMULATION OF A TURBOCHARGED DIESEL-ENGINE TO PREDICT THE TRANSIENT-RESPONSE." In: *MECHANICAL ENGINEERING*. Vol. 101. 1. ASME-AMER SOC MECHANICAL ENG 345 E 47TH ST, NEW YORK, NY 10017. 1979, pp. 87–87 (cit. on p. 68).

[108] Y. H. Zweiri, J. F. Whidborne, and L. D. Seneviratne. "Detailed analytical model of a single-cylinder diesel engine in the crank angle domain." *Proceedings of the Institution of Mechanical Engineers, Part D: Journal*

of Automobile Engineering 215(11) (2001), pp. 1197–1216. ISSN: 0954-4070. DOI: 10.1243/0954407011528734. URL: http://journals.sagepub.com/doi/10.1243/0954407011528734 (cit. on p. 68).

[109] D. Anguita, F. Rivieccio, M. Canova, P. Casoli, and A. Gambarotta. "A Learning-Machine Based Method for the Simulation of Combustion Process in Automotive I.C. Engines." In: *Proceedings of the ASME 2003 Internal Combustion Engine Division Spring Technical Conference. Design, Application, Performance and Emissions of Modern Internal Combustion Engine Systems and Components*. ASMEDC, 2003, pp. 595–602. ISBN: 0-7918-3678-9. DOI: 10.1115/ICES2003-0682. URL: https://asmedigitalcollection.asme.org/ICES/proceedings/ICES2003/36789/595/295959 (cit. on p. 68).

[110] O. Varnier. "Trends and Limits of Two-Stage Boosting Systems for Automotive Diesel Engines." PhD thesis. 2012 (cit. on pp. 68, 98).

[111] N. Chung, S. Kim, and M. Sunwoo. "Nonlinear Dynamic Model of a Turbocharged Diesel Engine." In: *SAE Technical Papers*. 2005. DOI: 10.4271/2005-01-0017. URL: https://www.sae.org/content/2005-01-0017/ (cit. on p. 68).

[112] M. Canova. "Development and validation of a control-oriented library for the simulation of automotive engines." *International Journal of Engine Research* 5(3) (2004), pp. 219–228. ISSN: 1468-0874. DOI: 10.1243/1468087041549625. URL: http://journals.sagepub.com/doi/10.1243/1468087041549625 (cit. on p. 68).

[113] R. Isermann, S. Sinsel, and J. Schaffnit. "Modeling and Real-Time Simulation of Diesel Engines for Control Design." In: *SAE Technical Papers*. 1998. DOI: 10.4271/980796. URL: https://www.sae.org/content/980796/ (cit. on p. 68).

[114] H. J. Dekker and W. L. Sturm. "Simulation and Control of a HD Diesel Engine Equipped with New EGR Technology." In: *SAE Technical Papers*. 1996. DOI: 10.4271/960871. URL: https://www.sae.org/content/960871/ (cit. on p. 68).

[115] S. Saulnier and S. Guilain. "Computational Study of Diesel Engine Downsizing Using Two-StageTurbocharging." In: *SAE Technical Papers*. 2004. ISBN: 0768013194. DOI: 10.4271/2004-01-0929. URL: https://www.sae.org/content/2004-01-0929/ (cit. on p. 68).

[116] C. Ciesla, R. Keribar, and T. Morel. "Engine/Powertrain/Vehicle Modeling Tool Applicable to All Stages of the Design Process." In: *SAE Technical Papers*. 2000. DOI: 10.4271/2000-01-0934. URL: https://www.sae.org/content/2000-01-0934/ (cit. on p. 68).

[117] G. Technolgies. *Engine/Powertrain/Vehicle Modeling Tool Applicable to All Stages of the Design Process*. 2017 (cit. on p. 68).

[118] N. Winkler. "Reduced models for flows in IC-engines." QC 20110928. PhD thesis. KTH, Internal Combustion Engines, 2011, pp. viii, 120. ISBN: 978-91-7501-107-3 (cit. on p. 69).

[119] N. Winkler and H.-e. Ångström. "Simulations and Measurements of a Two-Stage Turbocharged Heavy-Duty Diesel Engine Including EGR in Transient Operation." *SAE Technical Paper 2008-01-0539* 2008(724) (2008). DOI: 10.4271/2008-01-0539 (cit. on p. 70).

[120] J. Galindo, J. M. Lujan, J. Serrano, and L. Hernández. "Combustion simulation of turbocharger HSDI Diesel engines during transient operation using neural networks." *Applied Thermal Engineering* 25(5-6) (2005), pp. 877–898. ISSN: 13594311. DOI: 10.1016/j.applthermaleng.2004.08.004 (cit. on p. 73).

[121] D. N. Assanis, Z. Filipi, S. B. Fiveland, and M. Syrimis. "A Methodology for Cycle-By-Cycle Transient Heat Release Analysis in a Turbocharged Direct Injection Diesel Engine." *SAE Technical Papers* 109 (2000), pp. 1327–1339. DOI: 10.4271/2000-01-1185. URL: https://www.sae.org/content/2000-01-1185/ (cit. on p. 73).

[122] Y. Cui, K. Deng, and J. Wu. "A direct injection diesel combustion model for use in transient condition analysis." *Proceedings of the Institution of Mechanical Engineers, Part D: Journal of Automobile Engineering* 215(9) (2001), pp. 995–1004. ISSN: 0954-4070. DOI: 10.1243/0954407011528563. URL: http://journals.sagepub.com/doi/10.1243/0954407011528563 (cit. on p. 73).

[123] D. Winterbone and D. Tennant. *The variation of friction and combustion rates during diesel engine transients*. Tech. rep. SAE Technical Paper, 1981 (cit. on p. 73).

[124] G. Zamboni and M. Capobianco. "Influence of high and low pressure EGR and VGT control on in-cylinder pressure diagrams and rate of heat release in an automotive turbocharged diesel engine." *Applied Thermal Engineering* 51(1-2) (2013), pp. 586–596. ISSN: 13594311. DOI:

10.1016/j.applthermaleng.2012.09.040. URL: http://dx.doi.org/10.1016/j.applthermaleng.2012.09.040 (cit. on pp. 73, 89).

[125] A. Maiboom, X. Tauzia, S. R. Shah, and J.-f. Hétet. "Experimental Study of an LP EGR System on an Automotive Diesel Engine , compared to HP EGR with respect to PM and NOx Emissions and Specific Fuel Consumption." *SAE International Journal of Engines* 2(2) (2009), pp. 597–610. ISSN: 19463936. DOI: 10.4271/2009-24-0138 (cit. on pp. 73, 89).

[126] M. S. Khalef, A. Soba, and J. Korsgren. "Study of EGR and Turbocharger Combinations and Their Influence on Diesel Engine ' s Efficiency and Emissions." *SAE International* (2016). DOI: 10.4271/2016-01-0676.Copyright (cit. on pp. 88, 89, 134).

[127] W. Glewen, C. Meyer, D. Foster, M. Andrie, and R. Krieger. "Sources and Tradeoffs for Transient NO and UHC Emissions with Low Temperature Diesel Combustion." *SAE Technical Paper* (2011-01-1356) (2011). DOI: 10.4271/2011-01-1356 (cit. on p. 88).

[128] N Ladommatos, S Abdelhalim, and H Zhao. "The effects of exhaust gas recirculation on diesel combustion and emissions." *International Journal of Engine Research* 1(1) (2000), pp. 107–126. ISSN: 1468-0874. DOI: 10.1243/1468087001545290. URL: https://doi.org/10.1243/1468087001545290 (cit. on p. 88).

[129] P. Dimitriou, J. Turner, R. Burke, and C. Copeland. "The benefits of a mid-route exhaust gas recirculation system for two-stage boosted engines." *International Journal of Engine Research* 19(5) (2017), pp. 553–569. ISSN: 1468-0874. DOI: 10.1177/1468087417723782. URL: https://doi.org/10.1177/1468087417723782 (cit. on p. 88).

[130] Y Qi, K. K. Srinivasan, S. R. Krishnan, H Yang, and K. C. Midkiff. "Effect of hot exhaust gas recirculation on the performance and emissions of an advanced injection low pilot-ignited natural gas engine." *International Journal of Engine Research* 8(3) (2007), pp. 289–303. ISSN: 1468-0874. DOI: 10.1243/14680874JER02306. URL: https://doi.org/10.1243/14680874JER02306 (cit. on p. 88).

[131] C. a. Idicheria and L. M. Pickett. "Ignition, soot formation, and end-of-combustion transients in diesel combustion under high-EGR conditions." *International Journal of Engine Research* 12 (2011), pp. 376–392. ISSN: 1468-0874. DOI: 10.1177/1468087411399505 (cit. on p. 88).

[132] H Ogawa, T Li, and N Miyamoto. "Characteristics of low temperature and low oxygen diesel combustion with ultra-high exhaust gas recirculation." *International Journal of Engine Research* 8(4) (2007), pp. 365–378. ISSN: 1468-0874. DOI: 10.1243/14680874JER00607. URL: https://doi.org/10.1243/14680874JER00607 (cit. on p. 88).

[133] T Li, M Suzuki, and H Ogawa. "Effect of Two-Stage Injection on Unburned Hydrocarbon and Carbon Monoxide Emissions in Smokeless Low-Temperature Diesel Combustion with Ultra-High Exhaust Gas Recirculation." *International Journal of Engine Research* 11(5) (2010), pp. 345–354. ISSN: 1468-0874. DOI: 10.1243/14680874JER585. URL: https://doi.org/10.1243/14680874JER585 (cit. on p. 88).

[134] J. A. Caton. "A thermodynamic comparison of external and internal exhaust gas dilution for high-efficiency internal combustion engines." *International Journal of Engine Research* 16(8) (2015), pp. 935–955. ISSN: 1468-0874. DOI: 10.1177/1468087414560593. URL: https://doi.org/10.1177/1468087414560593 (cit. on p. 89).

[135] J. Kim and C. Bae. "Emission reduction through internal and low-pressure loop exhaust gas recirculation configuration with negative valve overlap and late intake valve closing strategy in a compression ignition engine." *International Journal of Engine Research* 18(10) (2017), pp. 973–990. ISSN: 1468-0874. DOI: 10.1177/1468087417692680. URL: https://doi.org/10.1177/1468087417692680 (cit. on p. 89).

[136] G. Zamboni and M. Capobianco. "Experimental study on the effects of HP and LP EGR in an automotive turbocharged diesel engine." *Applied Energy* 94 (2012), pp. 117–128. ISSN: 03062619. DOI: 10.1016/j.apenergy.2012.01.046. URL: http://dx.doi.org/10.1016/j.apenergy.2012.01.046 (cit. on pp. 89, 134).

[137] T Alger, J Gingrich, C Roberts, and B Mangold. "Cooled exhaust-gas recirculation for fuel economy and emissions improvement in gasoline engines." *International Journal of Engine Research* 12(3) (2011), pp. 252–264. ISSN: 1468-0874. DOI: 10.1177/1468087411402442. URL: https://doi.org/10.1177/1468087411402442 (cit. on p. 89).

[138] G McTaggart-Cowan, W. K. Bushe, P. G. Hill, and S. R. Munshi. "Nox. reduction from a heavy-duty diesel engine with direct injection of natural gas and cooled exhaust gas recirculation." *International Journal of Engine Research* 5(2) (2004), pp. 175–191. ISSN: 1468-0874. DOI:

10.1243/146808704773564578. URL: https://doi.org/10.1243/146808704773564578 (cit. on p. 89).

[139] G. P. McTaggart-Cowan, S. N. Rogak, P. G. Hill, W. K. Bushe, and S. R. Munshi. "Effect of operating condition on particulate matter and nitrogen oxides emissions from a heavy-duty direct injection natural gas engine using cooled exhaust gas recirculation." *International Journal of Engine Research* 5(6) (2004), pp. 499–511. ISSN: 1468-0874. DOI: 10.1177/146808740400500602. URL: https://doi.org/10.1177/146808740400500602 (cit. on p. 89).

[140] Y. Park and C. Bae. "Experimental study on the effects of high/low pressure EGR proportion in a passenger car diesel engine." *Applied Energy* 133 (2014). ISSN: 03062619. DOI: 10.1016/j.apenergy.2014.08.003 (cit. on p. 89).

[141] S. Chen and F. Yan. "Decoupled, Disturbance Rejection Control for A Turbocharged Diesel Engine with Dual-loop EGR System." *IFAC-PapersOnLine* 49(11) (2016). DOI: 10.1016/j.ifacol.2016.08.090 (cit. on p. 89).

[142] J. Park and J. Choi. "Optimization of dual-loop exhaust gas recirculation splitting for a light-duty diesel engine with model-based control." *Applied Energy* 181 (2016), pp. 268–277. ISSN: 03062619. DOI: 10.1016/j.apenergy.2016.07.128. URL: http://dx.doi.org/10.1016/j.apenergy.2016.07.128 (cit. on pp. 89, 134).

[143] H. Hiroyasu, H. Miao, T. Hiroyasu, M. Miki, J. Kamiura, and S. Watanabe. "Genetic Algorithms Optimization of Diesel Engine Emissions and Fuel Efficiency with Air Swirl, EGR,Injection Timing and Multiple Injections." In: *SAE Technical Papers*. 2003. DOI: 10.4271/2003-01-1853. URL: https://www.sae.org/content/2003-01-1853/ (cit. on p. 89).

[144] T. Hiroyasu, M. Miki, J. Kamiura, S. Watanabe, and H. Hiroyasu. "Multi-Objective Optimization of Diesel Engine Emissions and Fuel Economy using Genetic Algorithms and Phenomenological Model." In: *SAE Technical Papers*. 2002. DOI: 10.4271/2002-01-2778. URL: https://www.sae.org/content/2002-01-2778/ (cit. on p. 89).

[145] M. Costa, G. Bianchi, and C. Forte. "A Numerical Methodology for the Multi-Objective Optimization of an Automotive DI Diesel Engine." In: *SAE Technical Papers*. 2013. DOI: 10.4271/2013-24-0019. URL: https://www.sae.org/content/2013-24-0019/ (cit. on p. 90).

[146] M. Costa, G. M. Bianchi, C. Forte, and G. Cazzoli. "A Numerical Methodology for the Multi-objective Optimization of the DI Diesel Engine Combustion." *Energy Procedia* 45 (2014), pp. 711–720. ISSN: 18766102. DOI: 10.1016/j.egypro.2014.01.076. URL: https://linkinghub.elsevier.com/retrieve/pii/S1876610214000770 (cit. on p. 90).

[147] H.-W. Ge, Y. Shi, R. D. Reitz, D. D. Wickman, and W. Willems. "Optimization of a HSDI Diesel Engine for Passenger Cars Using a Multi-Objective Genetic Algorithm and Multi-Dimensional Modeling." *SAE International Journal of Engines* 2(1) (2009), pp. 2009–01–0715. ISSN: 1946-3944. DOI: 10.4271/2009-01-0715. URL: https://www.sae.org/content/2009-01-0715/ (cit. on p. 90).

[148] S. Lotfan, R. A. Ghiasi, M. Fallah, and M. Sadeghi. "ANN-based modeling and reducing dual-fuel engine's challenging emissions by multi-objective evolutionary algorithm NSGA-II." *Applied Energy* 175 (2016), pp. 91–99. ISSN: 03062619. DOI: 10.1016/j.apenergy.2016.04.099. URL: https://linkinghub.elsevier.com/retrieve/pii/S030626191630561X (cit. on p. 90).

[149] J Park, K. S. Lee, S Song, and K. M. Chun. "Numerical study of a light-duty diesel engine with a dual-loop EGR system under frequent engine operating conditions using the DOE method." *International Journal of Automotive Technology* 11(5) (2010), pp. 617–623. DOI: 10.1007/s12239 (cit. on p. 90).

[150] J. Park, S. Song, and K. S. Lee. "Numerical investigation of a dual-loop EGR split strategy using a split index and multi-objective Pareto optimization." *Applied Energy* 142 (2015), pp. 21–32. ISSN: 03062619. DOI: 10.1016/j.apenergy.2014.12.030. URL: http://dx.doi.org/10.1016/j.apenergy.2014.12.030 (cit. on pp. 90, 134).

[151] P. K. Bansal and B. Purkayastha. "An NTU-ϵ model for alternative refrigerants." *International Journal of Refrigeration* 21(5) (1998), pp. 381–397. ISSN: 01407007 (cit. on p. 92).

[152] H. A. Navarro and L. C. Cabezas-Gómez. "Effectiveness-ntu computation with a mathematical model for cross-flow heat exchangers." *Brazilian Journal of Chemical Engineering* 24(4) (2007), pp. 509–521. ISSN: 0104-6632. DOI: 10.1590/S0104-66322007000400005. URL: http://www.scielo.br/scielo.php?script=sci{_}arttext{\&}pid=S0104-66322007000400005{\&}lng=en{\&}tlng=en (cit. on p. 92).

[153] R. Stone. *Introduction to internal combustion engines*. Springer, 1999 (cit. on p. 102).

[154] J. Macek, V. Dolecek, S. Srinivasan, F. Tanner, and O. Vitek. "Optimization of Engine Control Strategies During Transient Processes Combining 1-D and 3-D Approaches." In: 2010. DOI: 10.4271/2010-01-0783. URL: http://papers.sae.org/2010-01-0783/ (cit. on p. 102).

[155] X. Llamas and L. Eriksson. "Optimal Transient Control of a Heavy Duty Diesel Engine with EGR and VGT." *IFAC Proceedings Volumes* 47(3) (2014), pp. 11854–11859. ISSN: 14746670. DOI: 10.3182/20140824-6-ZA-1003.01520. URL: https://linkinghub.elsevier.com/retrieve/pii/S1474667016435020 (cit. on p. 102).

[156] B. Liu, F. Zhang, C. Zhao, X. An, and H. Pei. "A novel lambda-based EGR (exhaust gas recirculation) modulation method for a turbocharged diesel engine under transient operation." *Energy* 96 (2016), pp. 521–530. ISSN: 03605442. DOI: 10.1016/j.energy.2015.12.097. URL: http://www.scopus.com/inward/record.url?eid=2-s2.0-84958634759{\&}partnerID=tZOtx3y1 (cit. on p. 102).

[157] N. R. Abdullah, H. Ismail, Z. Michael, A. A. Rahim, and H. Sharudin. "Effects of air intake temperature on the fuel consumption and exhaust emissions of natural aspirated gasoline engine." *Jurnal Teknologi* 76(9) (2015), pp. 25–29. ISSN: 01279696. DOI: 10.11113/jt.v76.5639 (cit. on p. 109).

[158] G. Technolgies. *Optimization Manual*. 2016 (cit. on p. 119).

[159] G. Zamboni, S. Moggia, and M. Capobianco. "Effects of a dual-loop exhaust gas recirculation system and variable nozzle turbine control on the operating parameters of an automotive diesel engine." *Energies* 10(1) (2017). ISSN: 19961073. DOI: 10.3390/en10010047 (cit. on p. 134).

[160] A. Maiboom, X. Tauzia, and J. F. Hétet. "Experimental study of various effects of exhaust gas recirculation (EGR) on combustion and emissions of an automotive direct injection diesel engine." *Energy* 33(1) (2008), pp. 22–34. ISSN: 03605442. DOI: 10.1016/j.energy.2007.08.010 (cit. on p. 134).

[161] Y. Park and C. Bae. "Experimental study on the effects of high/low pressure EGR proportion in a passenger car diesel engine." *Applied Energy* 133 (2014), pp. 308–316. ISSN: 03062619. DOI: 10.1016/j.apenergy.2014.08.003. URL: http://dx.doi.org/10.1016/j.apenergy.2014.08.003 (cit. on p. 134).

[162] C. A. Lana, K. K., G. Kothandaraman, J. Perfetto K. David, S. C., G. H., and D. K. "Systems and methods for controlling egr flow during transient conditions." Pat. US Patent App. 15/138,892. 2016 (cit. on p. 134).

[163] D. Brookshire and S. D. Arnold. "Dual and hybrid EGR systems for use with turbocharged engine." Pat. US Patent 7,013,879. 2007 (cit. on p. 134).

[164] P. Thunis, W. Lefebvre, M. Weiss, S. Vranckx, A. Clappier, B. Degraeuwe, and S. Janssen. "Impact of passenger car NOX emissions on urban NO2 pollution – Scenario analysis for 8 European cities." *Atmospheric Environment* 171(2) (2017), pp. 330–337. ISSN: 13522310. DOI: 10.1016/j.atmosenv.2017.10.040. URL: http://dx.doi.org/10.1016/j.atmosenv.2017.10.040 (cit. on p. 134).

[165] L. Yang, V. Franco, P. Mock, R. Kolke, S. Zhang, Y. Wu, and J. German. "Experimental Assessment of NOx Emissions from 73 Euro 6 Diesel Passenger Cars." *Environmental Science and Technology* 49(24) (2015), pp. 14409–14415. ISSN: 15205851. DOI: 10.1021/acs.est.5b04242 (cit. on p. 134).

[166] G. Triantafyllopoulos, D. Katsaounis, D. Karamitros, L. Ntziachristos, and Z. Samaras. "Experimental assessment of the potential to decrease diesel NOxemissions beyond minimum requirements for Euro 6 Real Drive Emissions (RDE) compliance." *Science of the Total Environment* 618 (2018), pp. 1400–1407. ISSN: 18791026. DOI: 10.1016/j.scitotenv.2017.09.274. URL: https://doi.org/10.1016/j.scitotenv.2017.09.274 (cit. on p. 135).

[167] R. Daya, J. Hoard, S. Chanda, and M. Singh. "Insulated catalyst with heat storage for real-world vehicle emissions reduction." *International Journal of Engine Research* (2017). ISSN: 1468-0874. DOI: 10.1177/1468087416685470 (cit. on p. 135).

[168] H. Yamada, K. Misawa, D. Suzuki, K. Tanaka, J. Matsumoto, M. Fujii, and K. Tanaka. "Detailed analysis of diesel vehicle exhaust emissions: Nitrogen oxides, hydrocarbons and particulate size distributions." *Proceedings of the Combustion Institute* 33(2) (2011), pp. 2895–2902. ISSN: 15407489. DOI: 10.1016/j.proci.2010.07.001. URL: http://dx.doi.org/10.1016/j.proci.2010.07.001 (cit. on p. 135).

[169] F. C. Leach, M. H. Davy, and M. S. Peckham. "Cyclic NO 2 :NO x ratio from a diesel engine undergoing transient load steps." *International Journal of Engine Research* (2019). ISSN: 20413149. DOI: 10.1177/1468087419833202 (cit. on p. 135).

[170] T Winstanley, P. G. Eastwood, a. M. K. P. Taylor, K Tufail, Y Hardalupas, and J Black. "Diesel engine transient control and emissions response during a European Extra-Urban Drive Cycle (EUDC)." In: *SAE Technical Paper Series*. 2007, pp. 1015–1030. DOI: 10.4271/2007-01-1938 (cit. on p. 135).

[171] D. Heuwetter, W. Glewen, C. Meyer, D. E. Foster, M. Andrie, and R. Krieger. "Effects of Low Pressure EGR on Transient Air System Performance and Emissions for Low Temperature Diesel Combustion." In: *SAE International*. 2011. DOI: 10.4271/2011-24-0062. URL: http://papers.sae.org/2011-24-0062/https://www.sae.org/content/2011-24-0062/ (cit. on p. 135).

[172] J. M. Luján, H. Climent, F. J. Arnau, and J. Miguel-García. "Analysis of low-pressure exhaust gases recirculation transport and control in transient operation of automotive diesel engines." *Applied Thermal Engineering* 137 (2018), pp. 184–192. ISSN: 1359-4311. DOI: 10.1016/j.applthermaleng.2018.03.085. URL: https://doi.org/10.1016/j.applthermaleng.2018.03.085 (cit. on pp. 135, 139, 140).

[173] A. Darlington, K. Glover, and N. Collings. "A Simple Diesel Engine Air-Path Model to Predict the Cylinder Charge During Transients: Strategies for Reducing Transient Emissions Spikes." In: *SAE International*. 724. 2006, p. 14. DOI: 10.4271/2006-01-3373. URL: https://www.sae.org/content/2006-01-3373/ (cit. on p. 135).

[174] M. S. Peckham, B. W. Campbell, and A. Finch. "Measurement of the effects of the exhaust gas recirculation delay on the nitrogen oxide emissions within a turbocharged passenger car diesel engine." *Proceedings of the Institution of Mechanical Engineers, Part D: Journal of Automobile Engineering* 225(9) (2011), pp. 1156–1166. ISSN: 0954-4070.

DOI: 10.1177/0954407011406977. URL: http://pid.sagepub.com/lookup/doi/10.1177/0954407011406977 (cit. on pp. 135, 136).

[175] U. Asad, J. Tjong, and M. Zheng. "Exhaust gas recirculation – Zero dimensional modelling and characterization for transient diesel combustion control." *Energy Conversion and Management* 86 (2014), pp. 309–324. ISSN: 01968904. DOI: 10.1016/j.enconman.2014.05.035. URL: http://dx.doi.org/10.1016/j.enconman.2014.05.035https://linkinghub.elsevier.com/retrieve/pii/S0196890414004464 (cit. on p. 142).

[176] H. Hiroyasu, T. Kadota, and M. Arai. "Development and Use of a Spray Combustion Modeling to Predict Diesel Engine Efficiency and Pollutant Emissions : Part 1 Combustion Modeling." *Bulletin of JSME* 26(214) (1983), pp. 569–575. ISSN: 1881-1426. DOI: 10.1299/jsme1958.26.569. URL: http://joi.jlc.jst.go.jp/JST.Journalarchive/jsme1958/26.569?from=CrossRef (cit. on p. 160).

[177] C. Ericson, B. Westerberg, M. Andersson, and R. Egnell. "Modelling Diesel Engine Combustion and NOx Formation for Model Based Control and Simulation of Engine and Exhaust Aftertreatment Systems." In: *SAE Technical Paper Series*. 2006. DOI: 10.4271/2006-01-0687. URL: https://www.sae.org/content/2006-01-0687/ (cit. on p. 160).

[178] M. Hirsch, D. Alberer, and L. Del Re. *Grey-box control oriented engine emissions models*. Vol. 17. 1 PART 1. IFAC, 2008, pp. 8514–8519. ISBN: 9783902661005. DOI: 10.3182/20080706-5-KR-1001.3426. URL: http://dx.doi.org/10.3182/20080706-5-KR-1001.01439 (cit. on p. 160).

[179] H. Sequenz and R. Isermann. *Emission model structures for an implementation on engine control units*. Vol. 44. 1 PART 1. IFAC, 2011, pp. 11851–11856. ISBN: 9783902661937. DOI: 10.3182/20110828-6-IT-1002.03131. URL: http://dx.doi.org/10.3182/20110828-6-IT-1002.03131 (cit. on p. 160).

[180] J. Arrègle, J. J. López, C. Guardiola, and C. Monin. "Sensitivity Study of a NOx Estimation Model for On-Board Applications." In: *SAE Technical Paper Series*. Vol. 1. 724. 2008. DOI: 10.4271/2008-01-0640. URL: https://www.sae.org/content/2008-01-0640/ (cit. on p. 160).

[181] F. Payri, J. Arrègle, J. J. López, E. Mocholí, C.-m. T. Universidad, and P. D. Valencia. "Diesel NOx Modeling with a Reduction Mechanism for the Initial NOx Coming from EGR or Re-entrained Burned Gases." In: *SAE Technical Paper Series*. Detroit, Michigan, 2008 (cit. on p. 160).

[182] O. Obodeh and C. I. Ajuwa. "Evaluation of artificial neural network performance in predicting diesel engine Nox emissions." *Research Journal of Applied Sciences, Engineering and Technology* 33(4) (2009), pp. 642–653. ISSN: 1450-216X (cit. on p. 160).

[183] G. J. Thompson, C. M. Atkinson, N. N. Clark, T. W. Long, and E Hanzevack. "Neural Network Modelling of the Emissions and Performance of a Heavy-Duty Diesel Engine." *Proceedings of the I MECH E Part D Journal of Automobile Engineering* 214(2) (2000), pp. 111–126. ISSN: 00000000. DOI: 10.1243/0954407001527277. URL: http://sdj.sagepub.com/lookup/10.1243/0954407001527277 (cit. on p. 160).

[184] A. Schilling, A. Amstutz, C. H. Onder, and L. Guzzella. "Real-time model for the prediction of the NOx emissions in DI diesel engines." In: *EEE International Conference on Control Applications, 2006 IEE*. IEEE, 2006, pp. 2042–2047. ISBN: 0780397967. DOI: 10.1109/CACSD-CCA-ISIC.2006.4776954. URL: http://ieeexplore.ieee.org/document/4776954/ (cit. on p. 160).

[185] C. Quérel, O. Grondin, and C. Letellier. "State of the Art and Analysis of Control Oriented NOx Models." In: *SAE Technical Paper Series*. 2012. DOI: 10.4271/2012-01-0723. URL: https://www.sae.org/content/2012-01-0723/ (cit. on p. 160).

[186] C. Ericson, B. Westerberg, and R. Egnell. "Transient Emission Predictions With Quasi Stationary Models." In: *SAE Technical Paper Series*. Vol. 1. 2005. DOI: 10.4271/2005-01-3852. URL: https://www.sae.org/content/2005-01-3852/ (cit. on pp. 160, 161).

[187] E. Giakoumis and A. Alafouzos. "Study of diesel engine performance and emissions during a Transient Cycle applying an engine mapping-based methodology." *Applied Energy* 87(4) (2010), pp. 1358–1365. ISSN: 03062619. DOI: 10.1016/j.apenergy.2009.09.003. URL: http://dx.doi.org/10.1016/j.apenergy.2009.09.003 (cit. on p. 160).

[188] J. D. Bishop, M. E. Stettler, N. Molden, and A. M. Boies. "Engine maps of fuel use and emissions from transient driving cycles." *Applied Energy* 183 (2016), pp. 202–217. ISSN: 03062619. DOI: 10.1016/j.apenergy.2016.08.175 (cit. on p. 161).

[189] L. Int Panis, C. Beckx, S. Broekx, I. De Vlieger, L. Schrooten, B. Degraeuwe, and L. Pelkmans. "PM, NOx and CO2 emission reductions from speed management policies in Europe." *Transport Policy* 18(1) (2011), pp. 32–37. ISSN: 0967070X. DOI: 10.1016/j.tranpol.2010.05.005. URL: http://dx.doi.org/10.1016/j.tranpol.2010.05.005 (cit. on p. 161).

[190] T. Nüesch, M. Wang, P. Isenegger, C. H. Onder, R. Steiner, P. Macri-Lassus, and L. Guzzella. "Optimal energy management for a diesel hybrid electric vehicle considering transient PM and quasi-static NOx emissions." *Control Engineering Practice* 29 (2014), pp. 266–276. ISSN: 09670661. DOI: 10.1016/j.conengprac.2014.01.020. URL: http://dx.doi.org/10.1016/j.conengprac.2014.01.020 (cit. on p. 161).

[191] D. M. Swain, C. C. Jackson, C. E. Lindhjem, and G. J. Hoffman. "A Method for Comparing Transient NOx Emissions With Weighted Steady State Test Results." In: *SAE Technical Paper Series*. Vol. 1. 724. 1998. DOI: 10.4271/980408. URL: https://www.sae.org/content/980408/ (cit. on p. 161).